# PROGRESS  IN  RESEARCH

## April 1, 2007 - March 31, 2008

## CYCLOTRON  INSTITUTE

### Texas A&M University

### College Station, Texas

**PROGRESS IN RESEARCH**

**APRIL 1, 2007 - MARCH 31, 2008**

**Prepared By**

**The Cyclotron Institute Staff**

**Texas A&M University**

**College Station, TX 77843-3366**

**Phone: (979) 845-1411**
**Fax: (979) 845-1899**

**Web: http://cyclotron.tamu.edu**

**July 2008**

**TABLE OF CONTENTS**

## SECTION II:  HEAVY ION REACTIONS

## SECTION IV: ATOMIC, MOLECULAR AND MATERIALS SCIENCE

## SECTION V: SUPERCONDUCTING CYCLOTRON, INSTRUMENTATION AND RIB UPGRADE

## SECTION VI:  PUBLICATIONS

## SECTION VII:  APPENDIX

**Introduction**
**April 1, 2007 – March 31, 2008**

Progress in research and operations at the Texas A&M Cyclotron Institute is summarized in this report for the period April, 1, 2007 through March 31, 2008. Sections I through IV contain reports from individual research projects. Operation and technical developments are given in Section V. Section VI lists the publications with Cyclotron Institute authors and the Appendix gives additional information including talks presented by members of the Institute during the past year. Once again, the full volume of this year's Progress in Research is available only on our web site (http://cyclotron.tamu.edu). *Since most of the contributions presented here are truly reports on progress in research, results and conclusions should not be quoted from the report without the consent of the authors.*

We have now completed 3 1/2 years of the Upgrade Project which ultimately will give us accelerated radioactive beams at intermediate energies. The progress on the project continues to be good—we remain close to schedule as of the second quarter of FY08. Last fall, we accelerated a beam in the K150 cyclotron for the first time in 20 years. Beam lines for the refurbished machine are now being installed. During the past year, we had some operational problems with the helium liquifier for the K500 cyclotron that caused some unscheduled maintenance downtime for the program. We have been working hard to catch up with experiments and electronics testing that did not get done during that period.

Institute programs continue to thrive. In the late fall of 2007, Dr. Dan Melconian joined us as an Assistant Professor of Physics and a member of the Cyclotron Institute. Dr. Melconian is developing a new program in experimental physics. In August, 2008, Dr. Cody Folden will join us as a new Assistant Professor of Nuclear Chemistry. He is planning to develop a program in heavy-element research.

Some highlights of work over the past year are given below.

Research highlights:
 (1) Prompted by an anomalous new result for the superallowed decay of $^{46}$V, we have significantly improved our calculations of the nuclear-structure-dependent corrections to all $0^+ \rightarrow 0^+$ superallowed beta transitions. The validity of these improved corrections has been re-enforced by Penning-trap measurements of the Q-values for the superallowed transitions from $^{50}$Mn and $^{54}$Co (experiment performed in collaboration with the University of Jyvaskyla).

 (2) A new detector system has been used to measure the beta-delayed proton decay of $^{23}$Al and $^{31}$Cl. The results provide new information about resonance states that contribute to the proton capture reactions $^{22}$Na(p,γ)$^{23}$Mg and $^{30}$P(p,γ)$^{31}$S.

 (3) Investigations of quantum phase changes in nuclear systems show that near the critical temperature for a second-order phase transition, the quantity I/A=(N-Z)/A behaves as an

order parameter and the difference in chemical potential between the neutrons and protons is its conjugate variable.

(4) We have measured the half-life of $^{198}$Au at 20K and at room temperature. The results are the same within 0.04%, in strong contradiction to a published report claiming a 4% difference. Having tested a beta-minus decay, we are now making a similar measurement on $^{97}$Ru, which decays by electron capture.

(5)  The transverse collective flow of light particles emitted during the reactions of $^{58}$Fe and $^{58}$Ni with $^{58}$Fe and $^{58}$Ni at 35 and 45 MeV/nucleon has been shown to depend on the neutron to proton ratio of the reacting system. Additionally the magnitude of the flow depends on the N/Z ratio of the emitted particle.

(6) High resolution measurements of the spectra of K$\alpha$ x rays originating from excited state configurations having single- and double- K vacancies plus additional L vacancies, produced in heavy ion collisions with argon atoms, have provided a quantitative measure of the effect of inter-atomic transitions on the average fraction of L vacancies remaining at the time of x-ray emission and revealed that they play in increasingly significant role as the number of L vacancies increases.

(7) In the past year, the first measurement of the direct photon-associated jet yields (the "golden probe of energy loss") was performed for heavy-ion collisions at RHIC. The results were presented for the STAR Collaboration at Quark Matter 2008.

(8) The STAR collaboration released new results for the longitudinal double-spin asymmetry, $A_{LL}$, for inclusive jet production in *pp* collisions that provide significant new constraints on the contribution that polarized gluons make to the spin of the proton. These results were identified as one of the highlights of the past five years in the 2007 NSAC Long-Range Plan for Nuclear Science.

(9) The cross section of photon production in deep-inelastic scattering off large nuclei has been calculated in perturbative QCD, re-summing multiple re-scatterings in nuclear matter. This is an important step towards understanding the production of photons from jets in cold nuclear matter and has potential applications at CEBAF and RHIC.

(10) Heavy-quark transport properties have been computed in a Quark-Gluon Plasma (QGP) employing a T-matrix approach based on potentials estimated from lattice QCD. The calculations suggest an intimate connection between a strongly coupled QGP and quark coalescence processes near the phase transition, which is supported by applications to heavy-quark observables at RHIC.

(11) New calculations have constrained the parameters of relativistic mean-field models using the density dependence of nuclear symmetry energy extracted from analyses of experimental

data on isospin diffusion and isotope scaling in intermediate energy heavy ion collisions as well as measured isotope dependence of the giant resonances in even-A Sn isotopes.

(12) Significant advances have been achieved in the theory of the indirect methods in nuclear astrophysics. A new method to estimate direct (n,γ) cross sections via (d,p) reactions has been developed. The half-off-shell R matrix theory of the Trojan Horse method for resonant reactions has been developed and has been applied to measurements in order to obtain information about important CNO cycle reactions.

(13) Results have been finalized for measurements of giant resonance strength in $^{24}$Mg and $^{28}$Si from $^{6}$Li scattering. The results indicate that a $^{6}$Li target will work well to explore giant resonance yields from radioactive beams at K500 energies.

(14) A new energy density functional, which can be consistently employed in calculations of properties of ground states and giant resonances of nuclei within the Hartree-Fock random phase approximation, was developed.

As in the past, Institute scientists remain active in a number of collaborative research efforts around the world. Major programs include: a measurement of Michel parameters in normal $\mu^{+}$ decay at TRIUMF in Vancouver, B.C.; mass measurements using the Penning Traps at Argonne National Laboratory and the University of Jyvaskyla; continued work with STAR collaboration at RHIC; and the measurement of neutron beta decay with the UCNA collaboration.

Once again, I am indebted to Dr. Y.-W. Lui who has managed to assemble this report in a very prompt and efficient manner.

R.E. Tribble
July 16, 2008

# SECTION I

# NUCLEAR STRUCTURE, FUNDAMENTAL INTERACTIONS, AND ASTROPHYSICS

# Giant resonance study of $^{28}$Si and $^{24}$Mg with 240 MeV $^{6}$Li scattering

X. Chen, Y. -W. Lui, H. L. Clark, Y. Tokimoto, and D. H. Youngblood

Inelastic scattering of $^{6}$Li from both $^{28}$Si and $^{24}$Mg excited into the giant resonance region was measured with the spectrometer at 0° and 4° and at 6° for $^{24}$Mg. The folding optical potential obtained with the CDM3Y5 NN interaction and with density **den1** (see Ref.[1] ) were used to analyze the giant resonance data. Sample excitation energy spectra for $^{28}$Si with average center of mass angles 1.3° and 6.4° are shown in Fig. 1 with pink curves representing the continuum choices. Angular distributions of the differential cross sections for the giant resonance peak and continuum are shown in Fig. 2 along with DWBA fits for three energy bins with average excitation energies 10.14 MeV, 20.46 MeV and 29.14 MeV. Sample excitation energy spectra for $^{24}$Mg with average center of mass angles 1.3°, 4.7° and 9.5° are shown in Fig. 3 with pink curves representing the continuum choices. Angular distributions of differential cross sections for the giant resonance peak and continuum for $^{24}$Mg are shown in Fig. 4 along with DWBA fits for three energy bins with average excitation energies 12.94 MeV, 20.08 MeV and 28.75 MeV.



**Figure 1.** Sample spectra for $^{28}$Si at average center of mass angle 1.3° and 6.4°. The pink curves are the continuum chosen for the analysis.

The E0, E1, E2 and E3 strength distributions obtained for $^{28}$Si are shown in Fig. 5 along with those obtained from α scattering. The multipole parameters obtained are summarized and compared with those from α scattering in Table I. The centroid ($m_1/m_0$), rms width and percentage of the EWSR are calculated for the total excitation range measured (~ 8 to 40 MeV), as well as the ranges ~ 8 to 22.4 MeV and ~ 22.4 to 40 MeV.

The E0, E1, E2 and E3 strength distributions obtained for $^{24}$Mg are shown in Fig. 6 and Fig. 7 along with those obtained from two different analyses of α scattering. The multipole parameters obtained for $^{24}$Mg are summarized and compared with those from α scattering and 156 MeV $^{6}$Li scattering in Table II. The centroid ($m_1/m_0$), rms width and percentage of the EWSR are calculated for the total excitation range measured (~ 8 to 40 MeV), as well as for the range ~10 to 20 MeV.

**Figure 3**. Sample spectra for $^{24}$Mg at average center of mass angle 1.3°, 4.7° and 9.5°. The pink curves are the continuum chosen for the analysis. The broad structures pointed by the brown arrow or covered by the brown bracket are from $^6$Li scattering on Hydrogen.
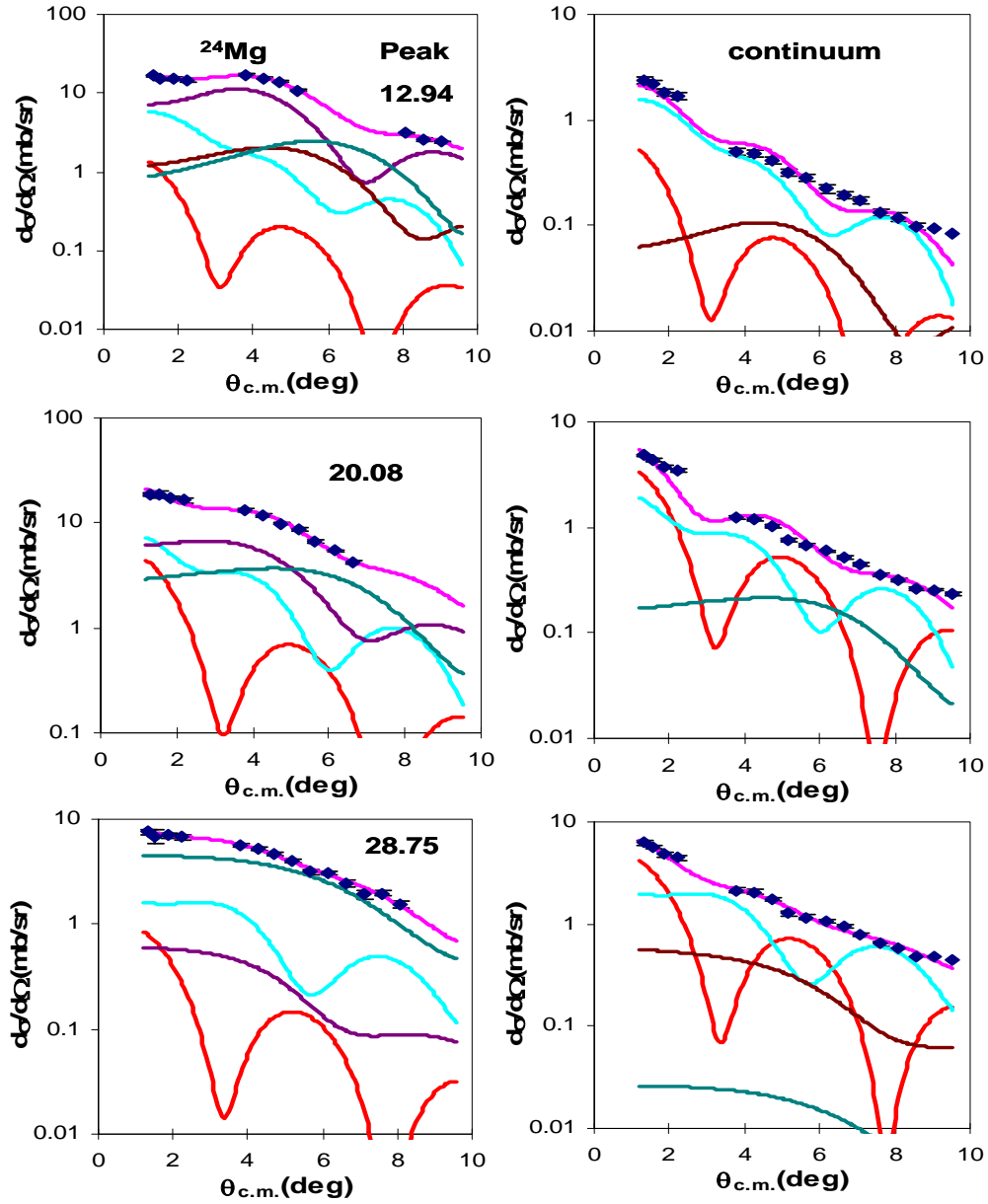
**Figure 4**. Angular distributions of the cross section for inelastic scattering from $^{24}$Mg for 0.8 MeV wide bin centered at $E_x$=12.94, 20.08, 28.75 MeV along with DWBA fits. The left column shows those for the giant resonance peak while the right column shows those for the continuum. The pink lines through the data show the fits. The E0 contribution is shown by the red line, the isoscalar E1 contribution by the light blue line, the E2 contributions by the purple lines, the E3 contributions by the brown lines and E4 contributions by the dark green lines.
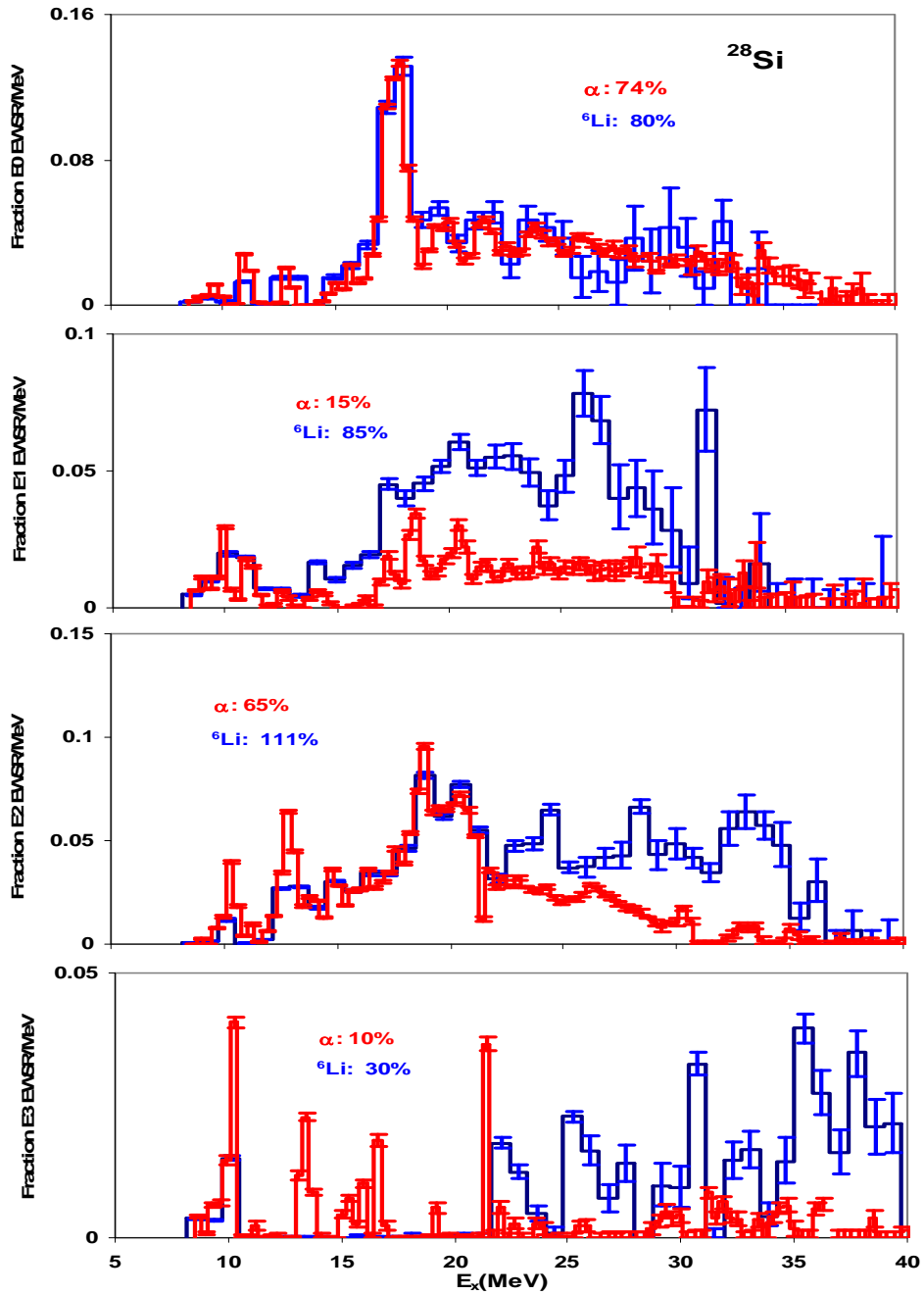
**Figure 5**. The dark blue curves show E0, E1, E2 and E3 strength distributions for $^{28}$Si obtained from analysis of $^6$Li inelastic scattering. The red curves show those obtained with $\alpha$ inelastic scattering [2]. Error bars represent the uncertainty due to the fitting of the angular distributions and different choices of the continuum.
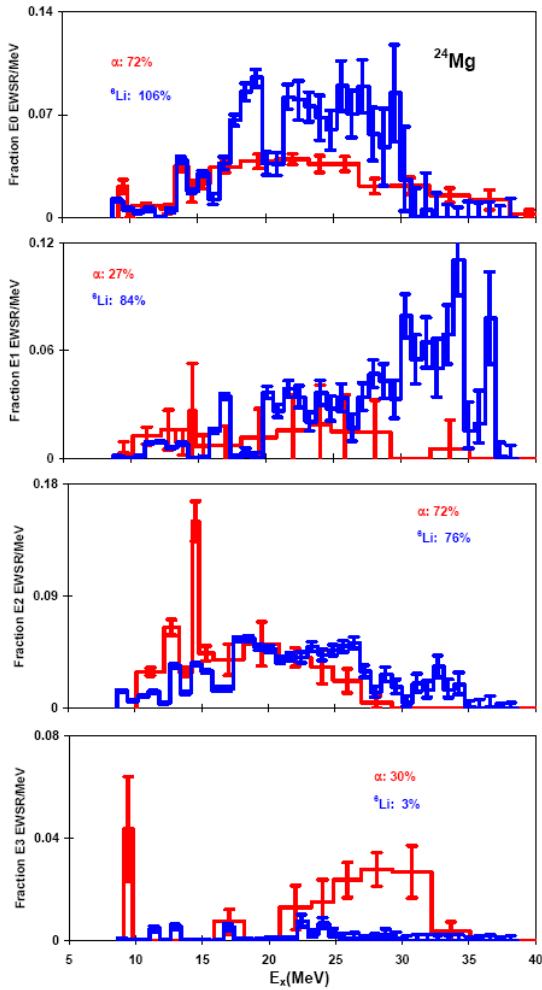
**Figure 6**. The blue curves show E0, E1, E2 and E3 strength distributions for $^{24}$Mg obtained from analysis of $^6$Li inelastic scattering. The red curves show those obtained with α inelastic scattering [3]. Error bars represent the uncertainty due to the fitting of the angular distributions and different choices of the continuum.
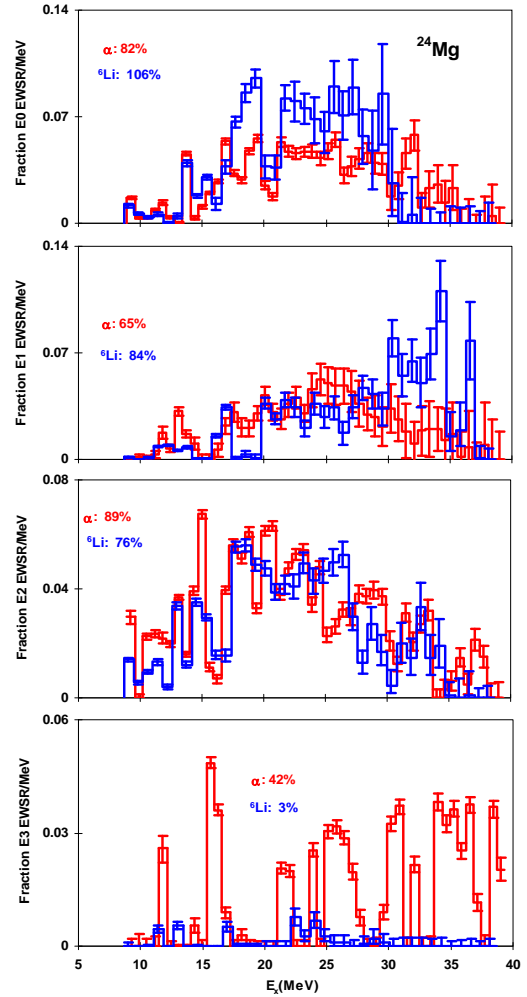
**Figure 7.** The blue curves show E0, E1, E2 and E3 strength distributions for $^{24}$Mg obtained from analysis of $^6$Li inelastic scattering. The red curves show those obtained with new analysis of α inelastic scattering [4]. Error bars represent the uncertainty due to the fitting of the angular distributions and different choices of the continuum.

**Table I.** Multipole parameters obtained for $^{28}$Si in this work compared to those obtained from analysis of α scattering.

| | | This work | | | α scattering [2] | | | |
|---|---|---|---|---|---|---|---|---|
| | $E_x$ range (MeV) | $m_1/m_0$ (MeV) | rms width (MeV) | EWSR (%) | $E_x$ range (MeV) | $m_1/m_0$ (MeV) | rms width (MeV) | EWSR (%) |
| E0 | 8.0-22.4 | 17.60±0.17 | 2.67±0.17 | 48±6 | 8.0-22.5 | 17.27±0.38 | 3.04±0.6 | 38±4 |
| | 22.4-40.0 | $27.72^{+0.73}_{-0.25}$ | $3.21^{+1.34}_{-0.34}$ | $31^{+30}_{-13}$ | 22.5-40.0 | 28.22±0.38 | 3.75±0.6 | 37±4 |
| | 8.0-40.0 | $20.59^{+0.78}_{-0.33}$ | $5.78^{+1.34}_{-0.34}$ | $80^{+35}_{-20}$ | 8.0-40.0 | $21.46^{+0.38}_{-0.38}$ | 6.3±0.6 | 74±10 |
| E1 | 8.0-22.4 | 16.9±0.17 | $3.77^{+0.74}_{-0.19}$ | 40±4 | 8.0-22.5 | 15.3±0.60 | 4.75±0.7 | 8±0.8 |
| | 22.4-40.0 | $27.27^{+0.34}_{-0.20}$ | $2.69^{+0.74}_{-0.19}$ | $38^{+19}_{-10}$ | 22.5-40.0 | 27.56±0.60 | 3.05±0.7 | 7±0.7 |
| | 8.0-40.0 | $21.17^{-0.41}_{-0.24}$ | $5.87^{+0.74}_{-0.19}$ | $84^{+21}_{-11}$ | 8.0-40.0 | 19.27±0.60 | 6.9±0.7 | 15±4 |
| E2 | 8.0-22.4 | 17.25±0.17 | 3.02±0.23 | 47±5 | 8.0-22.5 | 16.59±0.25 | 3.5±0.6 | 47±5 |
| | 22.4-40.0 | $29.22^{+0.20}_{-0.19}$ | 3.81±0.23 | 64±6 | 22.5-40.0 | 27.21±0.25 | 2.98±0.6 | 18±2 |
| | 8.0-40.0 | $22.69^{+0.23}_{-0.20}$ | 6.94±0.23 | 111±16 | 8.0-40.0 | 18.53±0.25 | 4.7±0.6 | 65±9 |
| E3 | 8.0-22.4 | $12.94^{+0.25}_{-0.19}$ | 6.54±0.18 | $4^{+5}_{-1}$ | 8.0-22.5 | 13.31±0.25 | 4.57±0.6 | 7±0.7 |
| | 22.4-40.0 | 32.15±0.17 | 4.48±0.18 | 27±3 | 22.5-40.0 | 33.32±0.25 | 3.48±0.6 | 3±0.3 |
| | 8.0-40.0 | 27.71±0.24 | 8.09±0.18 | $31^{+7}_{-6}$ | 8.0-40.0 | 16.3±0.25 | 9.22±0.6 | 10±1 |

**Table II.** Multipole parameters obtained for $^{24}$Mg in this work compared to those obtained from analysis of α scattering and from previous 156 MeV $^6$Li scattering.

| | | $^6$Li scattering | | | | | α scattering | | | |
|---|---|---|---|---|---|---|---|---|---|---|
| L | Ref. | $E_x$ energy (MeV) | $m_1/m_0$ (MeV) | rms width (MeV) | EWSR (%) | Ref. | $E_x$ range (MeV) | $m_1/m_0$ (MeV) | rms width (MeV) | EWSR (%) |
| 0 | This work | 10.2-20.6 | $16.88^{+0.17}_{-0.17}$ | 2.13 ± 0.17 | 35±5 | [3] | 10.1-20.9 | 16.31±0.6* | 2.62±0.74 | 27±4 |
| | | 8.6-38.6 | $21.35^{+0.37}_{-0.26}$ | $4.98^{+0.68}_{-0.32}$ | $106^{+34}_{-24}$ | | 9.0-41.0 | 21.0±0.6 | 7.3±1.2 | 72±10 |
| | [5] | 10.0-20.2 | 16.66±0.5 | 2.48±0.5 | 34±3** | [4] | 10.2-20.4 | $16.44^{+0.33}_{-0.25}$ | $2.48^{+0.48}_{-0.23}$ | 24±4 |
| | | | | | | | 9.0-41.0 | $21.93^{+0.33}_{-0.25}$ | $6.53^{+0.47}_{-0.23}$ | 82±9 |
| 1 | This work | 10.2-20.6 | $14.75^{+0.20}_{-0.17}$ | 2.29 ± 0.17 | 10±3 | [3] | 10.1-20.9 | 14.68±2.21 | 3.14±0.97 | $12^{+11}_{-5}$ |
| | | | | | | | 9.0-41.0 | 18.8±1.7 | 6.7±1.0 | $27^{+26}_{-11}$ |
| | | 8.6-38.6 | $26.56^{+0.29}_{-0.26}$ | $6.42^{+0.29}_{-0.27}$ | $84^{+24}_{-21}$ | [4] | 10.2-20.4 | $16.12^{+0.23}_{-0.20}$ | $3.33^{+0.68}_{-0.49}$ | 16±5 |
| | | | | | | | 9.0-41.0 | $22.70^{+0.23}_{-0.20}$ | $6.19^{+0.67}_{-0.49}$ | 65±8 |
| 2 | This work | 10.2-20.6 | 15.79±0.17 | 2.58±0.17 | 30±4 | [3] | 10.1-20.9 | 15.07±0.6* | 2.07±0.6* | $51^{+5}_{-8}$ |
| | | | | | | | 9.0-41.0 | 16.9±0.6 | 3.4±0.6 | 72±10 |
| | | 8.6-38.6 | $20.23^{+0.25}_{-0.20}$ | $6.29^{+0.34}_{-0.25}$ | $76^{+14}_{-12}$ | [4] | 10.2-20.4 | 15.56 ± 0.18 | $2.93^{+0.25}_{-0.20}$ | 36±4 |
| | | | | | | | 9.0-41.0 | $19.92^{+0.18}_{-0.18}$ | $7.25^{+0.25}_{-0.20}$ | 89±9 |
| 3 | This work | 8.6-38.6 | $18.54^{+1.40}_{-0.38}$ | $5.85^{+0.28}_{-0.19}$ | $3^{+4}_{-1}$ | [3] | 9.0-41.0 | 25.2±1.0 | 4.5±1.2 | $31^{+9}_{-6}$ |
| | | | | | | [4] | 9.0-41.0 | $25.43^{+0.37}_{-0.23}$ | $8.31^{+0.23}_{-0.22}$ | 42±5 |

* assume the uncertainty is the same as in the total energy range
** The original result from Ref. [5] multiplied by 0.5 (see Ref. [3])

[1] X. Chen, Y. -W. Lui, H. L. Clark *et al.*, *Progress in Research*, Cyclotron Institute, Texas A&M University (2006-2007), p. I-15

[2] D. H. Youngblood, Y. -W. Lui, and H. L. Clark, Phys. Rev. C **65**, 034302 (2002).

[3] D. H. Youngblood, Y. -W. Lui, and H. L. Clark, Phys. Rev. C **60**, 014304 (1999).

[4] D. H. Youngblood (private communication).

[5] H. Dennert, E. Aschenauer, W. Eyrich, *et al.*, Phys. Rev. C **52**, 3195 (1995).

# β-delayed p-decay of proton-rich nucleus $^{31}$Cl

L. Trache, A. Banu, J. C. Hardy, M. McCleskey, E. Simmons, R. E. Tribble, Y. Zhai

A. Saastamoinen,[1] A. Jokinen,[1] T. Davinson,[2] P. J. Woods,[2] L. Achouri,[3] and B. Roeder[3]

[1]*Department of Physics, University of Jyvaskyla, Jyvaskyla, Finland,*

[2] *School of Physics, University of Edinburgh, Edinburgh, United Kingdom,*

[3]*LPC, University of Caen, Caen, France.*

We have continued our recently started series of measurements of the β-delayed proton decay of proton-rich nuclei using a new technique that was proved very successful [1]. This is part of a larger program motivated by nuclear astrophysics. In the first half of 2007 we have measured the β-p decay of $^{23}$Al. We have recently produced and separated $^{31}$Cl using MARS (test run in early October 2007) and have done measurements of its β-γ decay and β-p decay in late November 2007. The interest was generated in the first place by the fact that the reaction $^{30}$P(p, γ)$^{31}$S is one of the most important (if not the most!) stepping stones toward heavier elements created in novae and its currently known rate is affected by a factor 100 uncertainty [2]. The dominant contribution is from resonances. Also, very little is known about the decay of $^{31}$Cl, because of the difficulties encountered in its production and separation. Its half-life and its decay Q-value are known with large uncertainties ($T_{1/2}$=150(25) ms and $Q_{EC}$=11980(50) keV, respectively), while the decay scheme can be at best be characterized as poorly known [3]. β-decay of $^{31}$Cl can populate and give information about the excited states in $^{31}$S above the proton binding energy Sp=6133 keV. These states become resonances in the reaction $^{30}$P(p, γ)$^{31}$S and those within about 1 MeV above threshold are in the Gamow window at novae temperatures and have the largest importance. Precise information about the levels in this region is currently missing or poor [4,5]. The position and the decay widths $\Gamma_p$, $\Gamma_\gamma$ of these states are needed.

Excited states in $^{31}$S above the proton threshold, which are populated in the β-decay of $^{31}$Cl can decay by p, γ, or both. To measure protons with the low energies corresponding to these states, the low-energy efficiency of the detectors is always a problem. We avoid them by implanting the source in the detector. This can be done given the large kinetic energy of our sources produced in inverse kinematics with MARS. The same setup [1] as in the $^{23}$Al experiment was used: one 65-µm thick Si strip detector (p-detector) and one 1 mm thick Si detector (β-detector). This telescope was at 45° to the beam axis to allow for good gamma-ray detection with a 70% HpGe detector situated at 90° outside the small chamber. A variable energy degrader consisting of two Al foils (sum=0.5 mm thick) on a computer controlled rotating feed-through (redesigned after the previous run to give better accuracy) was used to stop the desired source nuclei in the middle of the thin p-detector.

The $^{31}$Cl beam was obtained using a 40 MeV/nucleon $^{32}$S beam from the K500 cyclotron bombarding a cryogenic target containing $H_2$ gas at 2.0 atm. MARS was used to separate $^{31}$Cl (at 34 MeV/nucleon) produced through the $^{32}$S(p,2n) reaction in inverse kinematics. With the momentum acceptance slits set at +/-1.0 cm we had a maximum beam rate of about 2-3000 pps and a purity of 85% on the target detector. The associated momentum spread (+/-0.65%) and angular spread translates into a too large spread of the implantation depths in the p-detector and we had to close the momentum and angle

slits further (to +/-0.27% momentum). We have worked with rates of about 4-500 pps in the p-detector in the actual measurement. This rate proves safe for the detector. Because of the different range in Al (energy degrader)+Si (p-detector) of the accompanying impurities in the beam, the $^{31}$Cl sample that stopped in the p-detector during the measurements was almost 100% pure. In cycles, we pulsed the beam from the cyclotron, implanting the source nuclei (for 0.3 sec.), then switched the beam off and, after a very short delay (1 msec), measured β-p and β-γ coincidences simultaneously (also for 0.3 sec.). Si detectors are sensitive to positrons and protons, and the total signal in the implantation detector is the sum of the proton and beta contributions. That produces an asymmetry on the high-energy side of it and a large background at lower energies. To minimize these effects, the p-detector was taken as thin as possible.

The measurements used the telescope in two different modes:

a) The *implantation control mode*, in which the two detectors worked as a ΔE-E HI telescope. It was used to determine that the implantation was restricted to a central region of the p-detector. The signals in each detector were up to 300 MeV.

b) The *decay study mode*, in which the gain was adjusted to accommodate the detection of low energy protons and betas (up to 4 MeV in the p-detector and 8 MeV in the β-detector).

Gamma-rays in the range $E_\gamma$=0-8 MeV were measured in coincidence with positrons measured by the β-detector.

We have measured the following:

- implantation control in the HI telescope mode for $^{31}$Cl (and later for $^{32}$Cl, $^{29}$S used for calibrations)
- gamma-ray detector calibration with $^{32}$Cl implanted in the p-detector.
- $^{31}$Cl β-delayed p-decay with $^{31}$Cl implanted in the p-detector. β-p and β-γ coincident spectra were measured here to identify the proton peaks and get the proton branchings.
- p-detector calibration with $^{29}$S and $^{32}$Cl implanted in the p-detector.
- off-line Ge detector efficiency calibration with sources ($^{152}$Eu, $^{60}$Co, $^{137}$Cs).

At this time all data have only been preliminarily analyzed. An excellent gamma spectrum following the decay of $^{31}$Cl, far better than existing ones, was obtained and is shown in Fig. 1. A good energy calibration for the whole range up to $E_\gamma$=7 MeV could be made. In particular, four decay cascades from the T=3/2 IAS state of $^{31}$Cl g.s. are identified and the state's excitation energy is well established at E(IAS)=6279.5±0.3(stat)±1.5(syst) keV. From it, and using the IMME equation, we can deduce a more accurate mass for $^{31}$Cl, corresponding to $Q_{EC}$=11980(8) keV. A preliminary decay scheme has also been established. Proton lines in the proton spectra were measured in the 400-2200 keV range.

We intend to extend our studies to nuclei with similar properties and similar importance in explosive H-burning in stars.
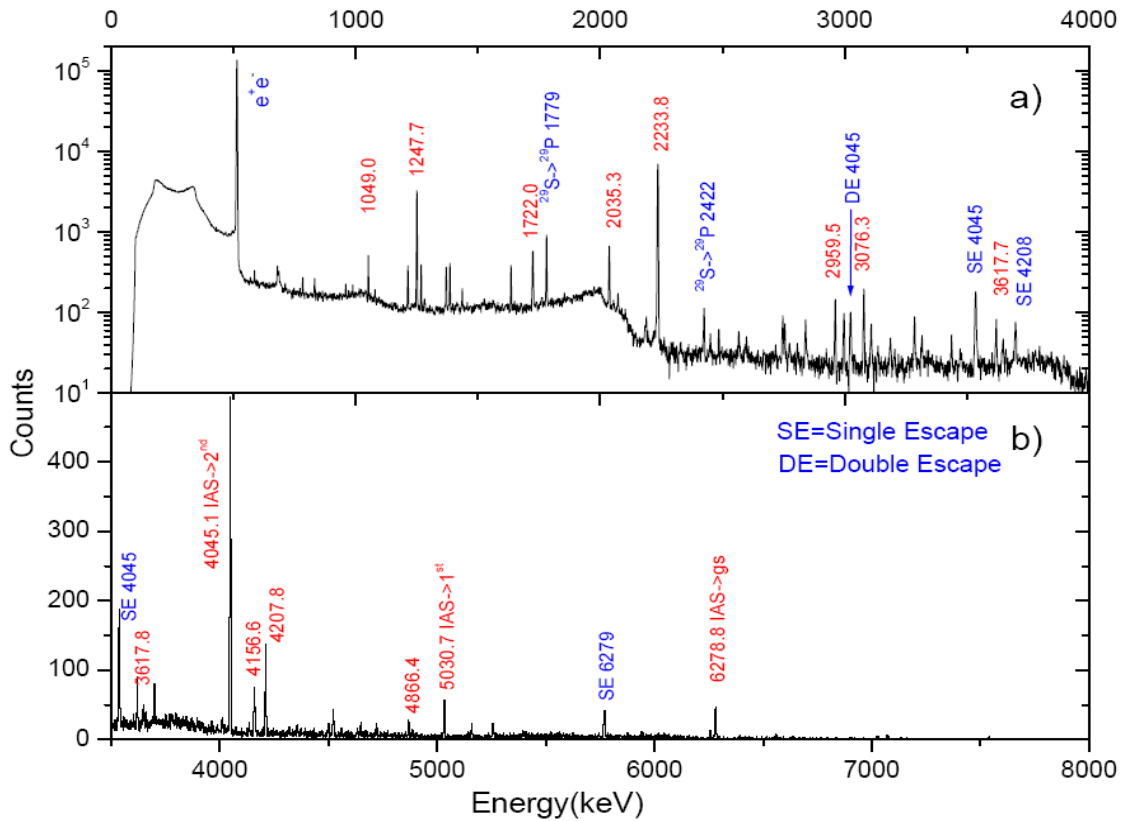
**Figure 1.** The gamma ray spectrum from the decay of $^{31}$Cl implanted in the p-detector.

[1] L. Trache *et al.*, *Progress in Research*, Cyclotron Institute, Texas A&M University (2006-2007), p.I-29; http://cyclotron.tamu.edu/publication.html

[2] A. Coc, in *Proceedings of the 10th International Symposium on Origin of Matter and Evolution of Galaxies (OMEGA07)* (to be published); http://nucl.sci.hokudai.ac.jp/~omeg07/.

[3] A. Kankainen *et al.*, Eur. Phys. J. A **27**, 67 (2006).

[4] D. G. Jenkins *et al.*, Phys. Rev. C **73**, 065802 (2006).

[5] C. Wrede *et al.*, Phys. Rev. C **76**, 052802(R) (2007).

# Determination of the ANC and spectroscopic factor for $^{15}$C from neutron transfer reactions $^{14}$C(d,p)$^{15}$C and $^{13}$C($^{14}$C,$^{15}$C)$^{12}$C

M. McCleskey, A. M. Mukhamedzhanov, R. E. Tribble, L. Trache, E. Simmons,
A. Banu, V. Goldberg, X. F. Chen, and Y. -W. Lui

The neutron capture rate of $^{14}$C is of interest in both inhomogeneous big bang nucleosynthesis and also in CNO cycles that can take place in the neutron-rich environment found in the helium burning region of post main sequence stars [1,2]. The $^{14}$C(n,$\gamma$)$^{15}$C reaction serves as the limiting reaction in this process. Furthermore, $^{14}$C(n,$\gamma$)$^{15}$C is being used as a test case for the indirect determination of neutron capture rates at low energies on neutron-rich nuclei using neutron-transfer reactions at laboratory energies. Our approach combines information from the peripheral reaction of 12 MeV/u $^{14}$C on a thin $^{13}$C target and the non-peripheral reaction of 60 MeV deuterons on a thin $^{14}$C target.

## $^{13}$C($^{14}$C,$^{15}$C)$^{12}$C:

This reaction is peripheral and is being used to determine the ANC for $^{15}$C. The experiment was performed using a radioactive $^{14}$C beam accelerated by the K500 cyclotron which reacted with a thin $^{13}$C target. The reaction products were analyzed by the MDM spectrometer and the MDM detector. A gold target of known thickness was used for calibration. Both the elastic and transfer reactions of $^{14}$C on $^{13}$C were measured. The reaction products are identified by their position in the focal plane of the MDM detector (Fig 1).
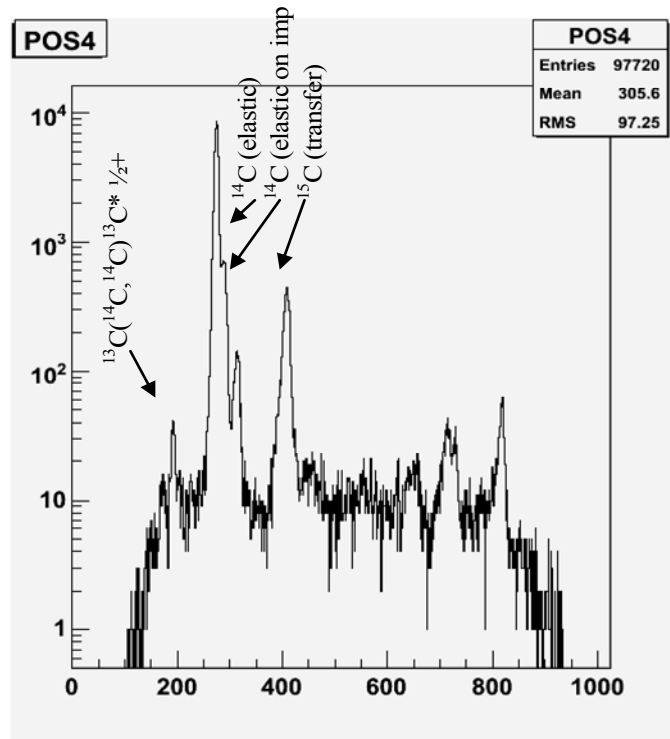


**Figure 1**. Particle identification in the focal plane

## $^{14}$C(d,p)$^{15}$C:

This experiment, performed with a deuteron energy of 60 MeV, will be combined with the previous experiment to determine the spectroscopic factor since at this energy the reaction is not peripheral. The reaction products were analyzed using the MDM spectrometer and the repaired Oxford detector. It was the first (d,p) measurement at this large energy, and detecting the proton with the Oxford

detector was a challenge due to the small energy loss signal. Again both elastic and transfer reactions were measured and elastic scattering on a gold foil was used for calibration. A summary of the preliminary results is shown in Fig. 2. Very good angular and energy resolution were obtained.

[1] A Horvath *et al.*, Astrophys. J. **570**, 926 (2002).
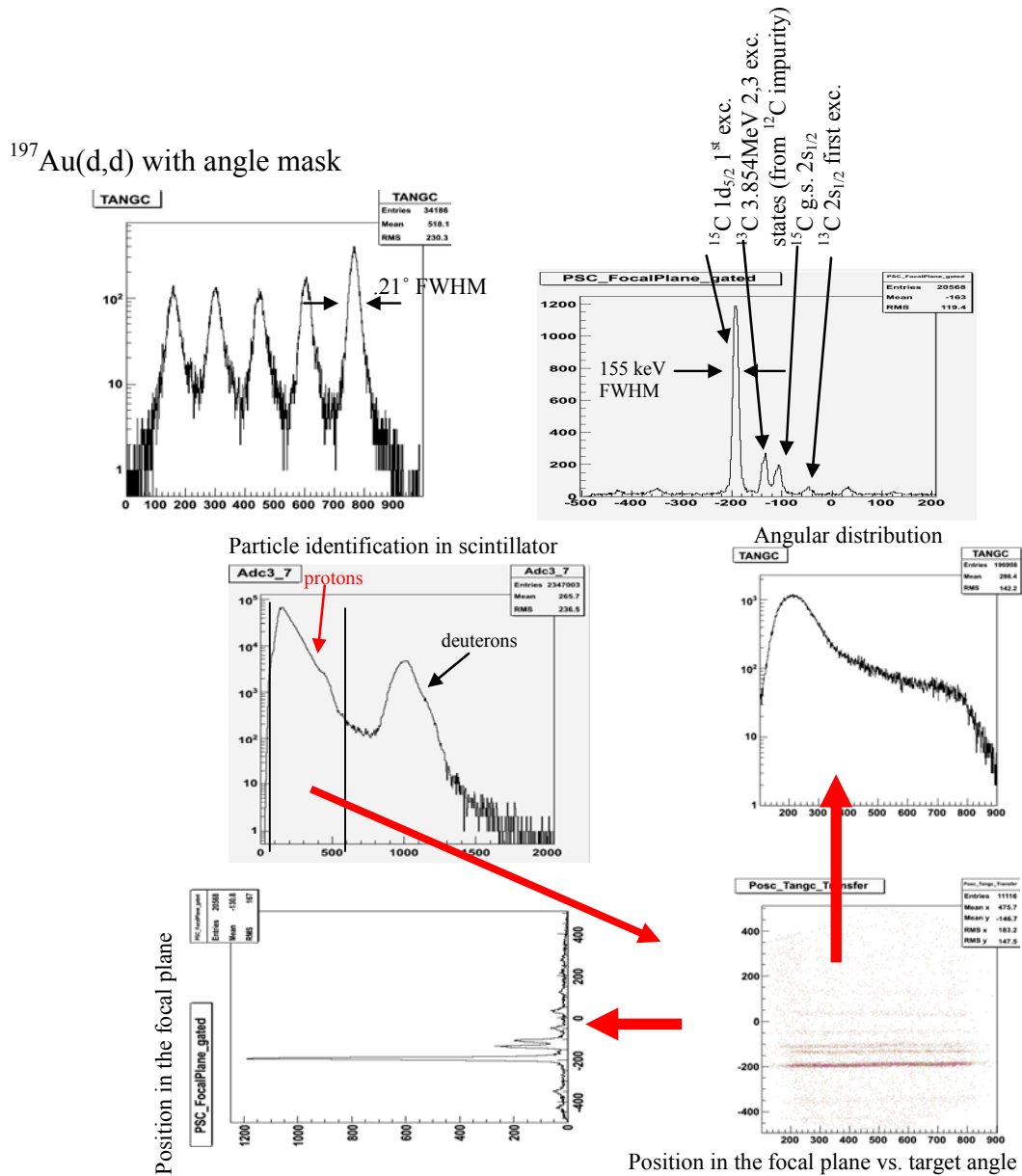


**Figure 2**. Summary of the results of the $^{14}$C(d,p) experiment.

[2] M Wiescher *et al.*, J. Phys. G **25**, R133 (1999).

# Correlated two-proton decay from $^{10}$C*

K. Mercurio,[1] R. J. Charity,[1] R. Shane,[1] L. G. Sobotka,[1] J. M. Elson,[1] M. Famiano,[2] A. Wuosmaa,[2]

A. Banu, C. Fu, L. Trache, R. E. Tribble, and A. M. Mukhamedzhanov

[1]*Washington University, St. Louis, Missouri 63130*

[2]*Western Michigan University, Kalamazoo, Michigan 49008*

Almost 50 years ago Goldansky [1] discussed the issue of correlated two-proton emission. Such decays can be reporters of initial-state correlations, much like α-decay informs us of the importance of α-clusters to the low-density energy-density functional [2]. No clear evidence of correlated two-proton (2p) emission was present in 1997 when Woods and Davids reviewed this subject [3]. Despite the recent flurry of activity near, at, and beyond the proton drip line, there is still no uncontested case of $^1$S correlated 2p emission. The data on the known 2p cases indicate either sequential decay (e.g. $^{12}$O), nearly uniform sampling of the 3-body phase space (e.g. $^6$Be$_{g.s.}$, $^{16}$Ne, and $^{19}$Mg) or 3-body with definite, but not $^1$S, correlations from the parent structure ($^{45}$Fe). In this work we present evidence for a significant $^1$S correlated-2p component in the decay of a state at E* = 6.6 MeV in $^{10}$C. In contrast to this state, we show that a previously known state at E*=5.20 MeV and a previously unknown state at 8.4 MeV decay sequentially, while yet another at E*=5.30 MeV decays by uniformly sampling the 3-body phase space.

Last year, we presented a study of the continuum spectroscopy of $^{10}$C [4]. The data from this (first) experiment provided only a weak suggestion of a 2p correlation in the decay of the state at 6.6 MeV. In the summer of 2007 we repeated this experiment, with an identical experimental set-up, but with 3 times the beam. This was achieved by using enriched Carborane ($C_2[^{10}B_{10}]H_{12}$) as a source material for the primary $^{10}$B beam. The primary beam impinged on a hydrogen gas cell held at a pressure of two atmospheres and kept at liquid-nitrogen temperature. The secondary beam of E/A=10.7 MeV $^{10}$C, with intensity of $2\times10^5$ s$^{-1}$, purity of 99.5%, an energy spread of 3%, and a spot size of 3.5x3.5 mm was produced with the MARS spectrometer. Both 14.1 mg/cm² Be and 13.4 mg/cm² C secondary targets were used.

The two, three and four-body correlations are shown in Fig. 1 as excitation energy spectra (by subtracting the Q-value from the center-of-mass energies.) In addition to the decay paths found in our previous work, a previously unobserved (broad) state at E*=8.4 MeV is found that decays to $^9$B(E*=2.36 MeV). For this report we focus on the correlations between the protons in the decay of both the 5.30 and 6.6 MeV states that 1) bypass the $^9$B$_{g.s.}$ but 2) possess the 2α correlation indicating that $^8$Be$_{g.s}$ was an intermediate. The relative emission angle $\theta_{rel}$ between the two protons in the 2α+2p center of mass and relative energy $E_{rel}$ of the protons are shown in Fig. 2. What is most striking is the symmetry and lack of symmetry about $\theta_{rel}$ =90° for the data from the states at 5.30 and 6.6 MeV, respectively. While angular momentum will generate correlations between successively emitted particles, $\theta_{rel}$ distributions must remain symmetric about $\theta_{rel}$ =90°. The shapes of the $E_{rel}$ distributions are also markedly different for the two cases. The distribution from the 5.30 MeV state is broad with only a weak enhancement at low energy, while the distribution for the 6.6 MeV state is strongly enhanced at low energy.
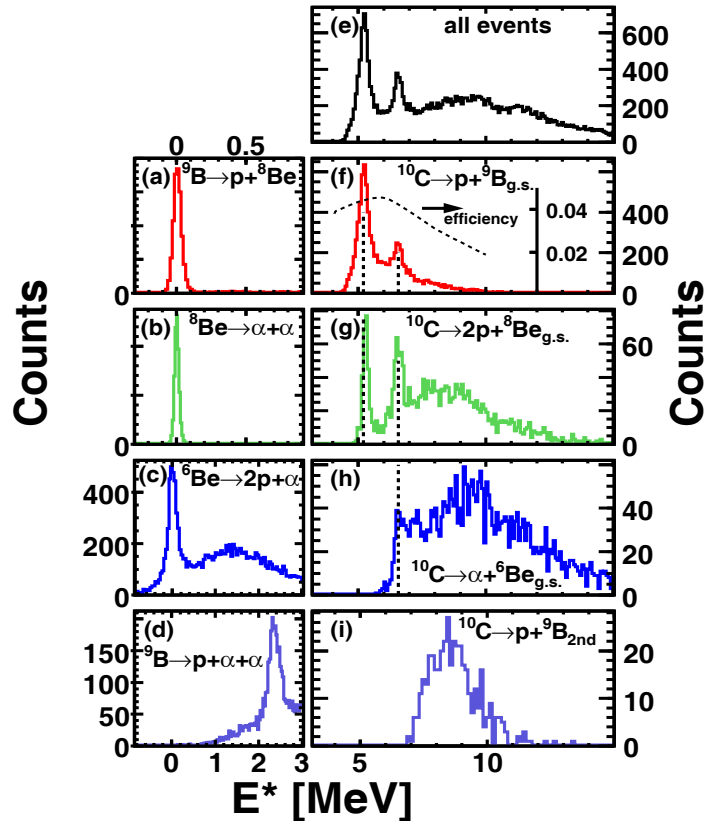
**Figure 1.** (Color online) Reconstructed excitation energies from two and 3-body correlations (left, a-d) and 4-body correlations (right, e-i). Panels (c) and (d) exclude events with the $^8B_{g.s.}$ correlation. The p + $^9B_{g.s.}$ detection efficiency is included, with an internal axis, in panel f.

A number of simulations were performed to evaluate which processes contribute to these decays. The first simulation assumed a sequential two-proton decay passing through the wide E*=1.5 MeV first excited state of $^9$B. In the second simulation, the 3-body phase space of the two protons and the $^8Be_{g.s.}$ fragment is uniformly sampled. The results of these simulations are shown in Fig. 2. Both the sequential and 3-body simulations come close to reproducing the $\theta_{rel}$ and $E_{rel}$ distributions from the 5.30 MeV state, although the 3-body simulation is somewhat better. On the other hand, for the 6.6 MeV state, neither simulation can reproduce either the asymmetry about 90° in $\theta_{rel}$ or the low-energy enhancement observed in the $E_{rel}$ spectrum.

In order to break the symmetry about 90°, we included a 2p correlation, of the type originally imagined by Goldansky, but heretofore never observed. Both an R-matrix scheme, using an $^1$S p-p phase shift for an imagined intermediate, and a Faddeev calculation, where the nuclear p-p scattering amplitude is dominated by the $^2$He resonance, largely reproduce the correlations found between the two protons from the decay of the 6.6 MeV state. It is possible that this is a rotational state built on a single-particle

structure well described as almost pure $(sd)^2$. (Two excited protons alone in the sd shell.) The analog is known in $^{10}$Be, but particle bound.
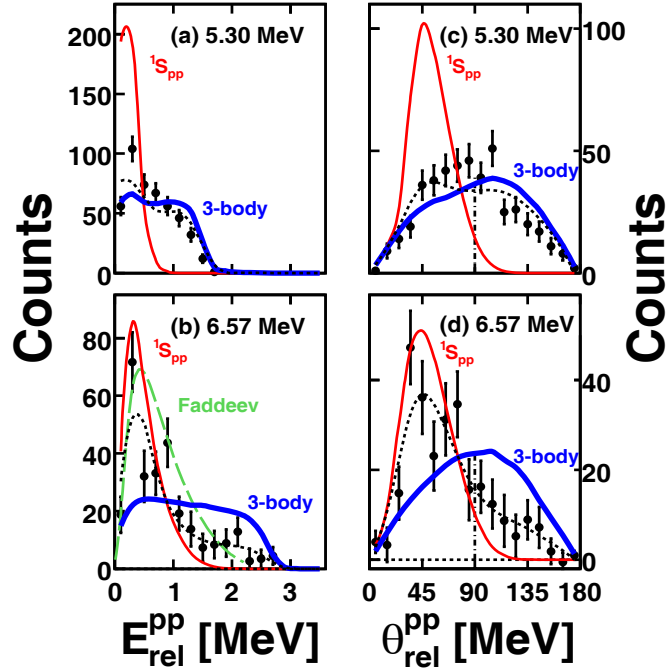


**Figure 2**. Energy (left) and angle (right) p-p correlations for the 5.30 (top) and 6.6 MeV (bottom) structures. The data are the combined data from the present and previous experiments. Simulations for decay uniformily spanning the full 3-body phase space (thick lines) and correlated 2p emission calculated using the R-matrix formalism (thin lines) are shown. The dotted lines are mixtures of 3-body and correlated (85:15 and 35:65 for the 5.30 and 6.6 MeV states, respectively.) The dashed line (b) is a Faddeev calculation.

[1] V. Goldansky, Nucl. Phys. **19**, 482 (1960).

[2] B. Friedman and V. Pandharipande, Nucl. Phys. **A361**, 502 (1981).

[3] R. J. Woods and C. N. Davids, Annu. Rev. Nucl. Part. Sci. **47**, 541 (1997).

[4] R. J. Charity *et al.*, Phys. Rev. C **75**, 051304 (2007).

# Asymptotic normalization coefficient (ANC) of the system $^{13}$O → $^{12}$N + p determined from a ($^{12}$N,$^{13}$O) proton transfer reaction

A. Banu, T. Al-Abdullah, V. Burjan,[1] F. Carstoiu,[2] C. Fu, C. A. Gagliardi, M. McCleskey,
G. Tabacaru, L. Trache, R. E. Tribble, and Y. Zhai
[1]*Institute of Nuclear Physics, Czech Academy of Sciences, Prague, Czech Republic*
[2]*IFIN-HH, Bucharest, Romania*

We report on the determination of the ANC for the system $^{13}$O → $^{12}$N + p. The study was carried out in relation to the radiative proton capture reaction $^{12}$N(p,γ)$^{13}$O for the role that it may play in the hot pp-chain nuclear burning processes possibly occurring in Population III stars [1]. As is generally the case with radiative proton capture reactions, due to the presence of large Coulomb barriers compared to small stellar kinetic energies, the reaction cross sections are in the order of picobarns, too small to be measured directly in the laboratory. Thus, they are studied by indirect methods. For our reaction of interest, we have applied the indirect ANC method [2] by using a ($^{12}$N,$^{13}$O) proton transfer reaction. Details of the experiment are presented elsewhere [3].

The basic of the ANC method is in the fact that the cross section for the radiative proton capture is completely determined by the Asymptotic Normalization Coefficient. This is equivalent with determining the amplitude of the tail of the overlap integral of the ground state wave function of $^{13}$O into the two-body channel $^{12}$N + p. The ANC of the radiative capture of interest is extracted from a peripheral proton transfer reaction in which one of the two reaction vertices is characterized by the same ANC, provided that the other ANC vertex of the transfer reaction is known. In our particular case, the transfer reaction was $^{14}$N($^{12}$N,$^{13}$O)$^{13}$C. Basically, the ANC of interest is extracted by fitting the experimental angular distributions with calculated Distorted Wave Born Approximation (DWBA) cross sections. This is written in the conventional DWBA formalism as:

$$\left(\frac{d\sigma}{d\Omega}\right)^{\exp}(\vartheta) = \sum_{nlj} S_{n_1 l_1 j_1}\left(^{13}O\right) S_{n_2 l_2 j_2}\left(^{14}N\right) \sigma^{DW}(\vartheta)$$

(1)

where *nlj* are the usual quantum numbers that characterize in this case the proton single orbitals involved while $S_{nlj}$ represent the spectroscopic factors of the $^{13}$O (ejectile) ground state wave function and of the $^{14}$N (target nucleus) ground state wave function, respectively. A proton from the $^{14}$N target occupying either the $1p_{1/2}$ or $1p_{3/2}$ orbitals is transferred to the $1p_{1/2}$ in the $^{13}$O nucleus. Thus, using the relation $C_{nlj}^2 = S_{nlj} b_{nlj}^2$ between the asymptotic normalization coefficients of the overlap integral $C_{nlj}$, and the spectroscopic factors and the asymptotic normalization coefficients of the normalized single particle wave functions $b_{nlj}$, Eq. (1) becomes

$$\sigma_{\exp} = \left( C_{p_{1/2}}^{^{13}O} \right)^2 \left\{ \left( \frac{C_{p_{1/2}}^{^{14}N}}{b_{p_{1/2}}^{^{13}O} b_{p_{1/2}}^{^{14}N}} \right)^2 \sigma_{p_{\frac{1}{2}} p_{\frac{1}{2}}}^{DW} + \left( \frac{C_{p_{3/2}}^{^{14}N}}{b_{p_{1/2}}^{^{13}O} b_{p_{3/2}}^{^{14}N}} \right)^2 \sigma_{p_{\frac{1}{2}} p_{\frac{3}{2}}}^{DW} \right\}, \tag{2}$$

where the ANCs for the vertex $^{14}N \rightarrow {}^{13}C + p$ were determined from previous studies [4].

Before presenting the results obtained for the ANC of interest, $C_{p_{1/2}}({}^{13}O)$, we briefly discuss the optical model potential (OMP) parameters used in the DWBA analysis. As one knows, the asymptotic normalization coefficients do not show a strong dependency on the proton binding nuclear potential unlike the spectroscopic factors, however the extracted value for the ANCs depend very much on the OMP parameters. These parameters are determined using measurements of elastic scattering. Instead of a typical elastic data analysis with phenomenological Woods-Saxon shaped optical potentials, we have used an analysis starting from semi-microscopic double-folding optical potentials, a procedure established at TAMU from a wide search for optical potentials to be used in the description of elastic and transfer reactions involving stable loosely bound p-shell nuclei [5]. Applying that procedure we determined the OMP parameters for the measured elastic angular distribution of the entrance channel ($^{12}N$-$^{14}N$) needed in the DWBA analysis of the transfer reaction. For the exit transfer channel ($^{13}O$-$^{13}C$) we assumed the same OMP parameters in the absence of available measured elastic data. As reported in Ref. [3], in our measurements we used a melamine $C_3H_6N_6$ target. The measured elastic angular distribution is compared in Fig. 1 (left) with predicted cross sections computed with double-folding optical potentials. We have found three sets of OMPs which describe reasonably the data for the entire angular range available in the measurements. Details of the elastic analysis are found in Ref. [6]. Here we only summarize those three sets of double-folding OMP parameters [5]:

1. $N_V = 0.37$, $N_W = 1.0$, $t_V = t_W = 1.2$ fm;
2. $N_V = 0.37$, $N_W = 0.80$, $t_V = 1.2$ fm, $t_W = 1.75$ fm;
3. $N_V = 0.37$, $N_W = 0.85$, $t_V = 1.2$ fm, $t_W = 1.75$ fm.

In order to check that we can use the same renormalization ($N_{V(W)}$) and range parameters ($t_{V(W)}$) for $^{14}N$ and $^{12}C$ target nuclei, we conducted a second experiment to measure the elastic scattering of $^{12}N$ on a pure carbon target [3]. Unfortunately, it turned out that the target used had not had the optimum thickness (6.8 mg/cm$^2$). The resulting data had not had the same quality as for the melamine target, smearing the trademark Fraunhofer oscillations, see Fig. 1 (right). Therefore, it was not reasonable to directly subtract them from the melamine data. However, we compared the experimental data on carbon with calculations made with the same potential as discussed above. More details on the results are to be found in Ref. [6].

Combing the results of both elastic measurements on melamine and carbon targets, which are in agreement with previous works [5], we could asses firmly the validity of the double-folding procedure to predict optical model potentials for the use in DWBA calculations.

Following we present the results obtained for the ANC of interest using each of the three aforementioned sets of OMPs:

1. $S^2_{p_{1/2}}({}^{13}O) = 0.58$, ANC $C^2_{p_{1/2}}({}^{13}O) = 2.74$ fm$^{-1}$ with $\chi^2$ (elastic) $= 38.7$;
2. $S^2_{p_{1/2}}({}^{13}O) = 0.53$, ANC $C^2_{p_{1/2}}({}^{13}O) = 2.49$ fm$^{-1}$ with $\chi^2$ (elastic) $= 38.2$;

3. $S^2_{p_{1/2}}(^{13}O) = 0.49$, ANC $C^2_{p_{1/2}}(^{13}O) = 2.33$ fm$^{-1}$ with $\chi^2$ (elastic) $= 43.1$.

Finally, we adopted an average (weighted with the chi-square values of the elastic data) of the above three values, yielding the ANC $C^2_{p_{1/2}}(^{13}O) = 2.53 \pm 0.30$ fm$^{-1}$.
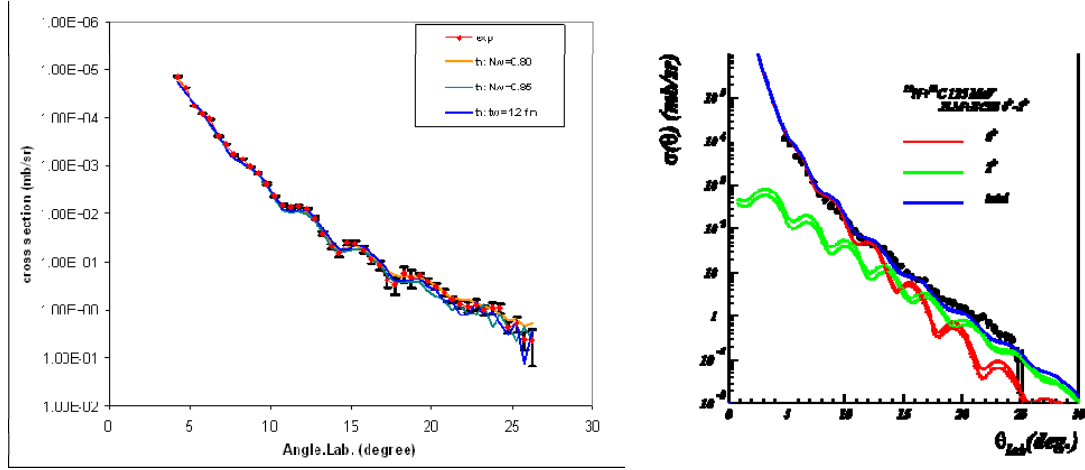


**Figure 1**. (left) Experimental angular distribution in the laboratory frame for elastic scattering of $^{12}$N projectile off $^{14}$N and $^{12}$C nuclei in the melamine target showed in comparison with predicted elastic cross section computed with three sets of double-folding optical potentials (see text for details). The theoretical calculations were smeared in a Monte Carlo simulation of the experiment that included the experimental constrains like finite size of the beam on target, beam divergence and the detector finite resolutions. (right) Experimental angular distribution in the laboratory frame for elastic scattering of $^{12}$N projectile off a 6.8 mg/cm$^2$ thick carbon target compared to theoretical calculations. The inelastic scattering to the first excited $2^+$ state in $^{12}$C could not be disentangled in the experiment from the elastic scattering. We calculated its contribution and included it in a coupled-channel calculation using the code ECIS.

[1] M. Wiescher *et al.*, Astrophys. J. **343**, 352 (1989); G. M. Fuller *et al.*, Astrophys. J. **307**, 675 (1986).

[2] X. M. Xu *et al.*, Phys. Rev. Lett. **73**, 2027 (1994); A. M. Mukhamedzhanov *et al.*, Phys. Rev. C **51**, 3472 (1995); C. A. Gagliardi *et al.*, Phys. Rev. C **59**, 1149 (1999).

[3] A. Banu *et al.*, *Progress in Research*, Cyclotron Institute, Texas A&M University (2006-2007), p. I-14; (2006-2007), p. I-24.

[4] L. Trache *et al.*, Phys. Rev. C **58**, 2715 (1998); P. Bém *et al.*, Phys. Rev. C **62**, 024320 (2000).

[5] L. Trache *et al.*, Phys. Rev. C **61**, 024612 (2000); F. Carstoiu *et al.*, Phys. Rev. C **70**, 054610 (2004).

[6] A. Banu *et al.* (to be published).

# The $^6$Li ($0^+$, T=1) decay of the $^{10}$B states populated in the resonance $^9$Be+p interaction

G. V. Rogachev,[1] V. Z. Goldberg, J. C. Hardy, R. E. Tribble, L. E. Miller,[1] E. D. Johnson,[1] S. Cherubini,[2] M. Gulino,[2] M. La Cognata,[2] L. Lamia,[2] R. G. Pizzone,[2] S. M. R. Puglia,[2] G. G. Rapisarda,[2] S. Romano,[2] M. L. Sergi,[2] C. Spitaleri,[2] W. H. Trzaska,[3] A. Tumino[2]

[1]*Department of Physics, Florida State University, Tallahassee, Florida*
[2]*LNS – INFN and Università di Catania, Catania, Italy*
[3]*University of Jyväskylä, Jyväskylä, Finland*

The T=1 states in $^{10}$B were studied using the $^9$Be(p,α)$^6$Li$^*$(T=1, 3.56, $0^+$) reaction. This reaction was chosen due to its high selectivity with respect to T=1 states with large partial α width, $\Gamma_\alpha$. Angular distributions were measured at 39 different energies, covering an excitation energy range of 8.8 MeV to 12.2 MeV in $^{10}$B. Two prominent resonances have been observed.

**Introduction**

The main motivation for this experiment is to measure the cross section, evaluate background conditions, and determine the best energy regime for a future experiment in which the parity violating α-decay of the T=1, $0^+$ 3.56 MeV  state in $^6$Li will be studied. The branching ratio for this parity-violating decay can be used to evaluate the weak πNN coupling constant, which dominates the isovector term of the parity-violating potential [1]. This potential emerges from the strangeness-conserving, non-leptonic sector of the weak interaction Hamiltonian. It was also pointed out in [2] that the M1 electromagnetic transition of the 3.56 MeV state in $^6$Li into the $^2$H+α continuum is a great tool for exploring the properties of the two-neutron halo ground state of $^6$He. (This is due to the fact that the 3.56 MeV $0^+$ state in $^6$Li is an isobaric analog of the $^6$He g.s.).

However, because the $^6$Li decay of $^{10}$B is accompanied by the α particle, the specific results are related with the α- cluster structure in $^{10}$B. Clustering phenomena in light nuclei represent many interesting and rich problems. The clustering phenomena provide an important insight into the interplay between the mean field and the cluster degrees of freedom. Recent theoretical developments, such as the antisymmetrized molecular dynamics (AMD) approach [3], describe cluster-like and shell-model-like configurations on an equal footing. This allows us to extend our understanding of the cluster degrees of freedom beyond the A=4n nuclei, which had been the main subject of cluster research in the past.

From an experimental perspective information on the cluster degrees of freedom in non-self-conjugate nuclei is scarce. However, there is now strong evidence that the cluster degree of freedom plays a significant role in the structure of light nuclei with A≠4n [4, 5]. In particular, the existence of a molecular-like α:2n:α band in the $^{10}$Be nucleus was suggested in Ref. [3] and three states (at 6.18 MeV ($0^+$), 7.54 MeV ($2^+$) and 10.15 MeV ($4^+$)) were identified as members of this band. Two of the three states mentioned above have had their isobaric analog states identified in $^{10}$B. These are the T=1, $0^+$ at 7.56 MeV and the T=1, $2^+$ at 8.9 MeV [4]. Therefore, one may suggest that these states are members of an isobaric analog, T=1 α:pn:α molecular-like band  in $^{10}$B. If this is the case then there should be a third

member of this band at the excitation energy of ~11.5 MeV. The resonance reaction $^9Be(p,\alpha)^6Li^*$(T=1, 3.56, $0^+$) appears to be an appropriate tool for the search for this state.

**Experiment**

The $^9Be(p,\alpha)^6Li$ excitation functions were measured using inverse kinematics. The experimental setup is shown in Fig. 1. The $^9Be$ beam was provided by the Tandem Van de Graaf accelerator, and polyethylene was used as a proton target. The total energy and scattering angle of $^6Li$ were measured by a resistive-layer, position-sensitive silicon detector with in front a gas ionization chamber for particle identification. Alpha particles were measured in coincidence with $^6Li$ by an array of silicon pin-diode detectors. This coincidence technique allows for the elimination of background and for the process of interest to be identified unambiguously. Measurements were performed at 39 different beam energies.
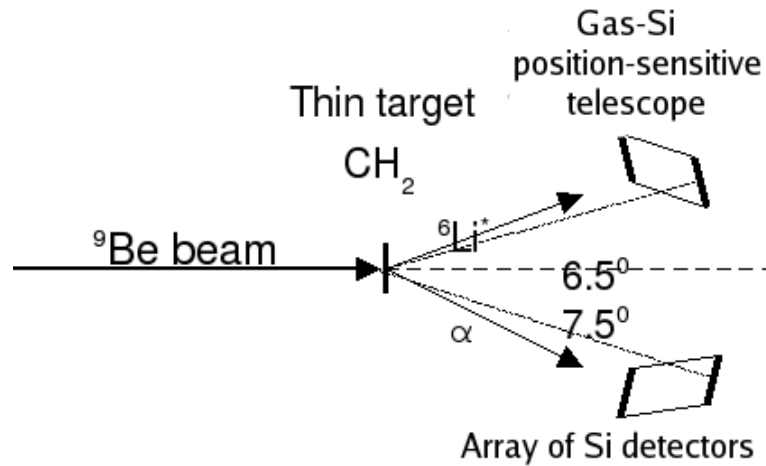


**Figure 1.** Experimental setup. Alpha particles and $^6Li$ from the $^1H(^9Be,\alpha)^6Li$ reaction were measured in kinematical coincidence.

**Results**

The excitation function of the $^9Be(p,\alpha)^6Li^*$(T=1, 3.56 MeV, $0^+$) reaction is shown in Fig. 2. The most obvious feature of the excitation function is the resonance at 8.9 MeV of $^{10}B$ excitation energy. This is the known T=1, $2^+$ state [4]. The angular distribution at this resonance energy is shown in Fig. 3. It is compared with an angular distribution predicted by an R-matrix calculation for the $2^+$ state along with an admixture of the relatively weak T=1, $3^-$ state at 8.9 MeV. Note that the angular distribution for a pure $2^+$ state would be isotropic. It is the admixture of the $3^-$ state that causes the cross section to decrease slightly at higher angles.

A broad peak was observed at an excitation energy of ~11.5 MeV (Fig. 2). It appears at exactly the excitation energy expected from comparison with the isobaric analog $4^+$ state at 10.15 MeV in $^{10}Be$ [3]. The data are still under analysis at present and an angular distribution is not yet available for this state. However, based on the excitation energy of this state and its large partial width in the $\alpha$-$^6Li$ channel,

we can conclude that it could be considered as a good candidate for the isobaric analog of the 4+, 10.15 MeV state in [10]Be.
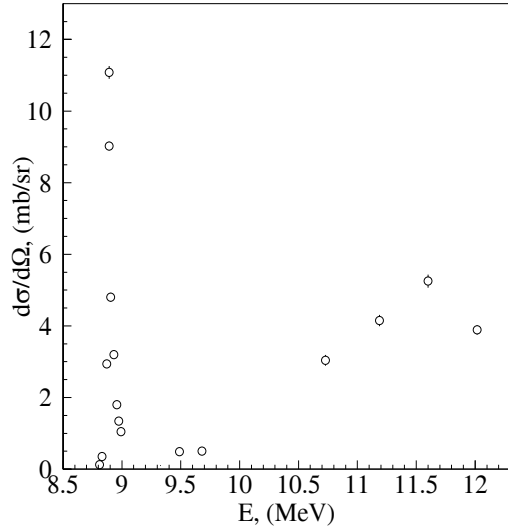


**Figure 2**. Excitation function of the [9]Be(p,α)[6]Li*(T=1, 3.56 MeV, 0+) reaction. X-axis represents excitation energy in [10]B. The low energy part (below 10 MeV) of the excitation function corresponds to 70+/-10 degrees in c.m. and the high energy part corresponds to 140+/-10 degrees in c.m. This is preliminary data and only a fraction of all the data points is shown.
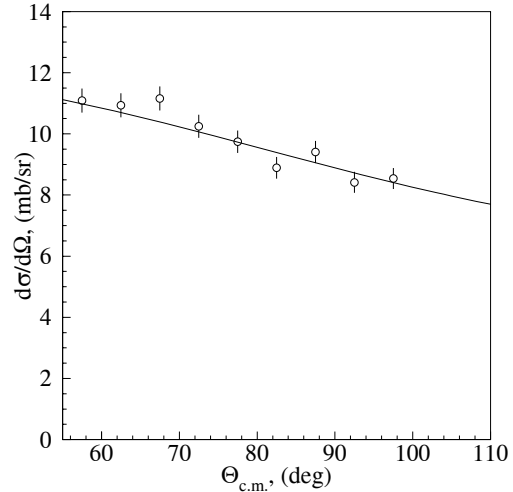
**Figure 3**. Angular distribution of the [9]Be(p,α)[6]Li(3.56) reaction at the resonance energy for the 2+, 8.9 MeV state in [10]B. The solid line is an R-matrix fit, that includes two known resonances [4], the 2+ and 3- both having excitation energy of 8.9 MeV.

Alpha particle partial widths of the observed states can be evaluated from the value of the measured cross section. Both resonances appear to be strong α-cluster states that exhaust significant fractions of the Wigner limit alpha width.

**Conclusion**

The measurement of the [9]Be(p,α)[6]Li*(3.56, T=1) excitation function revealed two states with large α-[6]Li(3.56, T=1) reduced widths at excitation energies of 8.9 and 11.5 MeV. The first is the known 2+ state, and the second is a new state. The spin-parity of this state will be determined from the measured angular distribution. If it is determined  that the spin-parity of this new state is 4+ then both of these resonances could be considered as isobaric analogs of the molecular-like band recently suggested in [10]Be [3] and therefore have an exotic α:pn:α molecular-like structure. Both resonances can be used for the future search of the parity violation in the decay of [6]Li*.

[1] M. J. Ramsery-Musolf *et al.*, Ann. Rev. Nucl. Part. Sci. **56** 1 (2006).
[2] L. Grigorenko *et al*., Phys. At. Nucl. **61** 1472 (1998).

[3] N. Itagaki *et al.*,  Phys. Rev. C **70**, 054307 (2004).

[4] G. Rogachev *et al.*, Phys. Rev. C **64**, 051302 (2001).

[5] M. Freer *et al.*, Phys. Rev. Lett. **96**, 042501 (2006).

[6] D. R. Tilley *et al.*, Nucl. Phys. **A745**, 155 (2004).

# Superallowed beta decay

J. C. Hardy, I. S. Towner, V. E. Iacob, N. Nica, V. V. Golovko, H. I. Park, J. Goodwin,
L. Trache, and R. E. Tribble

Superallowed $0^+ \rightarrow 0^+$ beta decay between T=1 analogue states has been a subject of continuous and often intense study for five decades. The *ft* values of such transitions are nearly independent of nuclear-structure ambiguities and depend uniquely on the vector part of the weak interaction. Their measurement gives us access to clean tests of some of the fundamental precepts of weak-interaction theory, and, over the years, this strong motivation has led to very high precision being achieved in both the experiments and the theory used to interpret them. We have a major program at the Cyclotron Institute to study superallowed beta decay.

To obtain the *ft* value for any transition, three quantities must be measured: the half life of the parent, the $Q_{EC}$ value for the transition of interest and the branching ratio for that transition. We produced a complete survey of existing data on these superallowed decays three years ago [1, 2]. There, all the experimental data for each transition were critically evaluated and final *ft* values obtained; then, small radiative and isospin-symmetry-breaking corrections [3] were applied and a final set of "corrected ft values", denoted $\mathscr{F}t$, were obtained.

In the three years since our review was published, a number of new experimental results have appeared, some from our group and some from a variety of other groups worldwide. Furthermore, the largest radiative correction – the "inner" one – was revisited and its uncertainty reduced by a factor of two [4]; also isospin-symmetry-breaking corrections were improved significantly [5]. Figure 1 shows the raw *ft* values and corrected $\mathscr{F}t$ values for the most precisely known superallowed $0^+ \rightarrow 0^+$ transitions as they are now known in mid 2008. The constancy of the $\mathscr{F}t$ values is evident, their average being 3072.3(8) s, with a normalized $\chi^2$ of 0.3.

There have been important changes in these results since last year. It all began three years ago with our re-measurement of the $Q_{EC}$ value of the $^{46}$V superallowed beta-decay branch [6] using the CPT Penning trap at Argonne National Lab. This was the first time a Penning trap had been used for any of the well-known superallowed transitions and the one chosen was the transition whose $Q_{EC}$ value was least precisely known, with the expectation that it would simply improve the precision of the average. Indeed, it shrunk the error bar but it also changed the result considerably.

This raised the question of whether there could be a systematic difference between on-line Penning-trap and reaction-based measurements. In collaboration with the JYFLTRAP, Penning-trap group at the University of Jyväskylä we settled this issue. We measured the $Q_{EC}$ values for $^{46}$V, $^{42}$Sc and $^{26}$Al$^m$ [7], confirming the Savard *et al.* [6] result for $^{46}$V but finding that the $Q_{EC}$ values for $^{42}$Sc and $^{26}$Al$^m$ agreed well with the survey results, which depended entirely on reaction-based measurements. This demonstrated that there is no systematic shift between Penning-trap and reaction measurements in general.

There still remained the fact that the new corrected $\mathscr{F}t$ value for $^{46}$V was significantly higher than that for any other well known superallowed transition. The most obvious explanation of its unusual value

was that the correction for isospin symmetry-breaking, which depends upon the nuclear structure of the parent and daughter nuclei, was missing some important components, and last year we succeeded in improving our previous calculated corrections [3] by including the effects of core states [5]: *eg.* in the case of $^{46}$V this meant including the *sd*-shell with the *fp*-shell in our configuration space. The new corrections completely removed the anomaly in the $\mathscr{F}t$ value for $^{46}$V but introduced equivalent anomalies for $^{50}$Mn and $^{54}$Co. However the accepted $Q_{EC}$ values for $^{50}$Mn and $^{54}$Co at that time were averages, each with an important contribution from a 30-year-old ($^{3}$He,t) Q-value measurement by Vonach *et al.* [8], which appeared in the same paper in which the newly discredited value for the $^{46}$V $Q_{EC}$ value also appeared. Perhaps their results for $^{50}$Mn and $^{54}$Co were wrong as well.

Last year with the Jyvaskyla Penning trap, we also re-measured the $Q_{EC}$ values for $^{50}$Mn and $^{54}$Co [9]. Our results differ from the values published by Vonach *et al.* [8] by more than 2.5 keV (5 or more of the latter's standard deviations). Evidently, whatever problem these authors had with their measurement of the $^{46}$V $Q_{EC}$ value extended to $^{50}$Mn and $^{54}$Co as well: all three of these values are lower than the modern more-precise values by approximately the same amount. Using our new $Q_{EC}$ values for $^{50}$Mn and $^{54}$Co, we find that the apparent anomaly in their $\mathscr{F}t$ values completely disappears. With the new experimental results and the re-calculated isospin-symmetry-breaking corrections the $\mathscr{F}t$ values are completely consistent with one another as shown in the right panel of Figure 1.
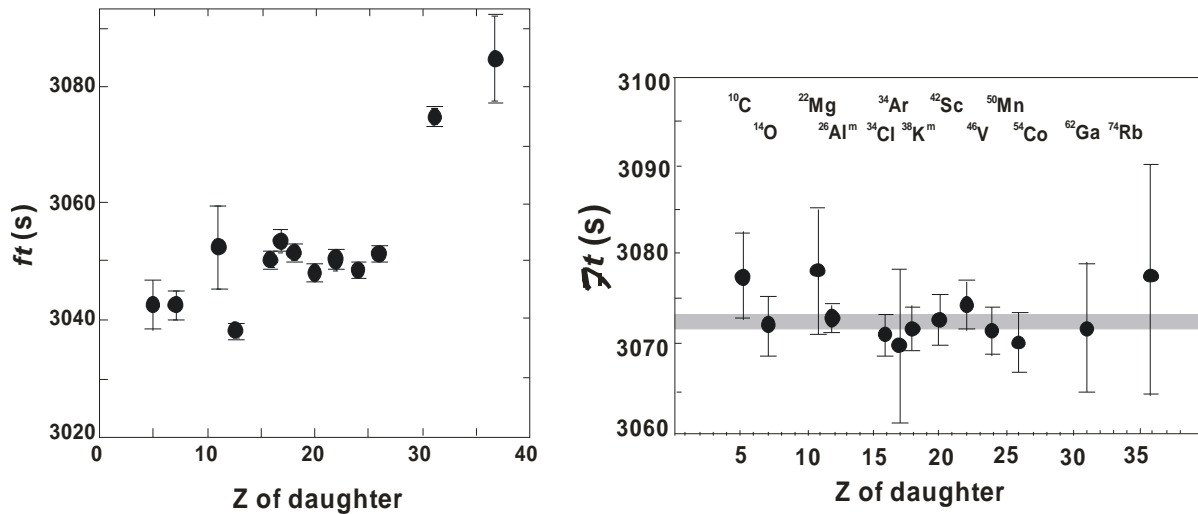


**Figure 1**. Results from the 2005 survey [1] updated with more recent published results. The uncorrected *ft* values for the thirteen best known superallowed decays (left) are compared with the same results after corrections have been applied (right). The grey band in the right-hand panel is the average F*t* value, including its uncertainty.

Since these corrected $\mathscr{F}t$ values are inversely proportional to the square of the vector coupling constant, $G_V$, the constancy of $G_V$ is demonstrated to 1.3 parts in $10^4$. Not only is this an important confirmation of the Conserved Vector Current (CVC) hypothesis but it sets the stage for using the average value of $G_V$ to test a fundamental principle of the electroweak standard model, the unitarity of the

Cabibbo-Kobayashi-Maskawa (CKM) matrix. The up-down quark mixing element of that matrix, $V_{ud}$, is given by $V_{ud} = G_V / G_F$, where $G_F$ is the weak interaction constant for the purely leptonic muon decay. The value of $V_{ud}$ is a key component of the most demanding test available for the unitarity of the CKM matrix, the sum of squares of its top-row elements [1]. Superallowed nuclear beta decays provide by far the most precise and reliable value for $V_{ud}$ and, in fact, that element now is also the most precisely known one in the CKM matrix – by an order of magnitude! Its current value is 0.97402(26)

For several decades, the top-row unitarity sum differed from unity by several standard deviations but, over the past several years, new results from kaon decay have demonstrated that the value of another element of the top row, $V_{us}$, was not correct. There is still some dispute over the exact theoretical correction terms to use in determining $V_{us}$, but the consensus at the moment favors a value for $V_{us}$, which, when combined with the nuclear value for $V_{ud}$, yields a unitarity sum of 0.9997(10). This confirmation of CKM unitarity is not only a significant verification of the standard model but the uncertainty quoted on the sum provides a tight limit on any possible new physics beyond the standard model.

In short, superallowed $0^+ \rightarrow 0^+$ beta decay provides a high-profile application of nuclear-physics measurements to the study of fundamental symmetries, a subject of vital interest to both nuclear and particle physicists. Although much has already been achieved in this field by nuclear physicists, improvements are still possible. Reducing the uncertainty on the unitarity sum – and, with it, the scope for new physics – remains the primary goal of our research program.

The principal difference between the left and right panels of Fig. 1, is the inclusion of the nuclear-structure-dependent corrections, $\delta_{NS}$ and $\delta_C$, in the derivation of the $\mathscr{F}t$ values in the latter. Since these corrections were determined [3,5] completely independently of the superallowed decay data, the consistency of the $\mathscr{F}t$ values is also a powerful validation of these calculated corrections: obviously they act very well to remove the considerable "scatter" that is apparent in the left panel and is effectively absent in the right one.

The 2005 survey [1, 2], which considered a body of world data comprised of more than 125 individual measurements, presented a remarkably consistent picture for the nuclear results. Even so, it is still possible for well selected experiments to make real improvements. For example, the validation of the nuclear-structure-dependent correction terms can be improved by the addition of new transitions selected from amongst those with large calculated corrections. If the $ft$ values measured for cases with large calculated corrections also turn into corrected $\mathscr{F}t$ values that are consistent with the others, then this must verify the calculations' reliability for the existing cases, which have smaller corrections. At TAMU we have just completed a half-life measurement for $^{10}$C decay [10] and are also at the analysis stage of a similar measurement for $^{38}$Ca [11].

We continue to focus on improving and securing our analysis procedures for precise branching-ratio measurements. We have introduced a new laser-based system to determine the source-to-HPGe-detector distance for each sample delivered by our tape-transport system [12]; and we have continued our source measurements and Monte Carlo calculations to thoroughly characterize our beta detector [13-15]. We continue to use $^{34}$Ar decay as a test case to which we apply these improvements [16].

[1] J. C. Hardy and I. S. Towner, Phys. Rev. C **71**, 055501 (2005).

[2] J. C. Hardy and I. S. Towner, Phys. Rev. Lett. **94**, 092502 (2005).

[3] I. S. Towner and J. C. Hardy, Phys. Rev. C **66**, 035501 (2002).

[4] W. J. Marciano and A. Sirlin, Phys. Rev. Lett. **96**, 032002 (2006).

[5] I. S. Towner and J. C. Hardy, Phys. Rev. C **77**, 025501 (2008); *Progress in Research*, Cyclotron Institute, Texas A&M University (2007-2008), p. III-6.

[6] G. Savard, F. Buchinger, J. A. Clark, J. E. Crawford, S. Gulick, J. C. Hardy, A. A. Hecht, J. K. P. Lee, A. F. Levand, N. D. Scielzo, H. Sharma, I. Tanihata, A. C. C. Villari, and Y. Wang, Phys. Rev. Lett. **95**, 102501 (2005).

[7] T. Eronen, V. Elomaa, U. Hager, J. Hakala, A. Jokinen, A. Kankainen, I. Moore, H. Penttilä, S. Rahaman, A. Saastamoinen, T. Sonoda, J. Äystő, J. C. Hardy and V. Kolhinen, Phys. Rev. Lett. **97**, 232501 (2006).

[8] H. Vonach *et al.*, Nucl. Phys. **A278**, 189 (1977).

[9] T. Eronen, V. -V Elomaa, U. Hager, J. Hakala, J. C. Hardy, A. Jokinen, A. Kankainen, I. D. Moore, H. Penttilä, S. Rahaman, S. Rinta-Antila, J. Rissanen, A. Saastamoinen, T. Sonoda, C. Weber and J. Äystő, Phys. Rev. Lett. 100, 132502 (2008); J.C. Hardy, *Progress in Research*, Cyclotron Institute, Texas A&M University (2007-2008), p. I-31.

[10] V. E. Iacob *et al.*, *Progress in Research*, Cyclotron Institute, Texas A&M University (2007-2008), p. I-28.

[11] H. I. Park *et al.*, *Progress in Research*, Cyclotron Institute, Texas A&M University (2007-2008), p. I-30.

[12] V. E. Iacob, V. V. Golovko and J. C. Hardy, *Progress in Research*, Cyclotron Institute, Texas A&M University (2007-2008), p. V-19.

[13] V. E. Iacob, V. V. Golovko and J. C. Hardy, *Progress in Research*, Cyclotron Institute, Texas A&M University (2007-2008), p. V-21.

[14] V. V. Golovko, V. E. Iacob and J. C. Hardy, *Progress in Research*, Cyclotron Institute, Texas A&M University (2007-2008), p. V-29.

[15] V. V. Golovko, V. E. Iacob, J. C. Hardy and D. Melconian, *Progress in Research*, Cyclotron Institute, Texas A&M University (2007-2008), p. V-25.

[16] V. E. Iacob, J. C. Hardy and V. V. Golovko, *Progress in Research*, Cyclotron Institute, Texas A&M University (2007-2008), p. I-29.

# The half Life of $^{10}$C

V. E. Iacob, J. C. Hardy, V. V. Golovko, J. Goodwin, N. Nica, H. I. Park, L. Trache and R. E. Tribble

We have previously reported in detail on progress in our measurement of the half-life of $^{10}$C [1]. This work has now been completed and a paper describing the experiment has been published [2]. We determined the half-life to be 19.310(4) s, a result with 0.02% precision, which is a factor of four improvement over the best previous result. When our result is averaged with all previous results, the resulting half-life is 19.308(4) s and, with the other properties for the superallowed decay of $^{10}$C taken from our 2005 survey [3], the corresponding $ft$ value becomes 3042.4(43) s. This represents a reduction in uncertainty from the previous $ft$ value [3], 3039.5(47) s, now leaving the branching ratio and, to a lesser extent, the $Q_{EC}$ value as the major contributors to the overall uncertainty.

It is interesting to note that our new measurement of the half life increases the $ft$ value for $^{10}$C as well as reducing its uncertainty. Naturally, its corrected $\mathscr{F}t$ value is increased as well, to 3077.4(46) s. This is slightly above the overall average of all well-known superallowed transitions [3] and, if this tendency for $^{10}$C is re-enforced by branching-ratio and $Q_{EC}$-value measurements with improved precision, it could indicate the presence of a small contribution from a scalar current. Clearly, high priority should be attached to the re-measurement of these two quantities with improved precision.

[1] V. E. Iacob *et al.*, *Progress in Research*, Cyclotron Institute, Texas A&M University (2005-2006), p. I-28; *Progress in Research*, Cyclotron Institute, Texas A&M University (2006-2007), p. I-55.
[2] V. E. Iacob, J. C. Hardy, V. Golovko, J. Goodwin, N. Nica, H. I. Park, L. Trache, and R. E. Tribble, Phys. Rev. C **77**, 045501 (2008).
[3] J. C. Hardy and I. S. Towner, Phys. Rev. C **71**, 055501 (2005).

# Improved β branching ratios in $^{34}$Ar

V. E. Iacob, J. C. Hardy, and V. V. Golovko

As part of our program to test the Standard Model *via* the unitarity of the Cabibbo-Kobayashi-Maskawa (CKM) matrix [1] we are re-measuring the branching ratios in the *β* decay of $^{34}$Ar. The experiment has two important motivations: (1) to test our upgraded acquisition system and (2) to increase the precision of the extracted branching ratios.

In this experiment, a $^{35}$Cl beam at 30*A* MeV impinged on a hydrogen gas target, which had a pressure of 2 atm, and was cooled to liquid nitrogen temperature. The $^{34}$Ar ejectiles were then separated in the MARS recoil separator, extracted into air, detected by a thin 0.3-mm plastic scintillator and eventually implanted into a 76-μm-thick mylar tape. The implanted $^{34}$Ar activity had a purity of better then 99.7%. The average $^{34}$Ar beam intensity was about $1.5 \times 10^4$ particles per second. We implanted the $^{34}$Ar ions for 2 s, then the beam was turned off and the collected activity was moved in 0.2 s to the center of a counting station, which consisted of a HPGe detector and a plastic scintillator on opposite sides of the tape. We recorded all *β-γ* coincident events and the total number of *β* singles. The 2 s /0.2 s /2 s collect/move/detect cycle was repeated until sufficient statistics had been acquired. In a one-week experiment we recorded more than $9.5 \times 10^6$ *β-γ* coincident events for $1.3 \times 10^9$ implanted $^{34}$Ar ions.

Although we already reported a rather precise branching ratio for the superallowed decay of $^{34}$Ar in last year's annual report [2], this new experiment should allow us to increase the precision to its ultimate limit, since we now have much better control over the source-to-detector distance at the counting station [3]. The analysis of the experiment is in progress and preliminary values agree with the previously reported value. Even if the final value for the superallowed branching ratio in $^{34}$Ar is not significantly improved, this experiment is an effective test of the upgraded experimental system. If all the tests are passed, we will be able to extend our measurements of accurate branching ratios to nuclei where the ground-state-to-ground-state superallowed branch isn't as favorable as it is in $^{34}$Ar, where it represents about 95% of the total decay strength. In such a case, even a modest 2% error in the sum over the non-superallowed branches is good enough to yield 0.1% precision for the superallowed branch. No other $T_Z$ = -1 superallowed emitter has such a favorable configuration.

[1] I. S. Towner and J. C.Hardy, Phys. Rev. C **77**, 025501 (2008).

[2] V. E. Iacob, *et al.*, *Progress in Research*, Cyclotron Institute, Texas A&M University (2005-2006), p. I-31.

[3] V. E. Iacob, *et al.*, *Progress in Research*, Cyclotron Institute, Texas A&M University (2007-2008), p. V-19.

# High precision half-life measurement of $^{38}$Ca

H. I. Park, J. C. Hardy, V. V. Golovko, V. E. Iacob, N. Nica, A. Banu, L. Trache,
R. E. Tribble, and Y. Zhai

The measured $ft$ values for superallowed $0^+ \rightarrow 0^+$ nuclear $\beta$ decay, can be used to test the unitarity of the Cabibbo-Kobayashi-Maskawa (CKM) matrix. One of the essential elements of this test is accurate calculations of radiative and isospin-symmetry-breaking corrections that must be applied to the experimental data [1]. Some of these corrections depend on nuclear structure and have relatively large uncertainties as a result. However, these uncertainties can, in principle, be reduced by experiment. The efficacy of the nuclear-structure-dependent corrections can be examined, based on how well they convert the scatter in the uncorrected $ft$ values for many transitions into a consistent set of corrected $\mathscr{F}t$ values for all transitions, as required by the Conserved Vector Current (CVC) hypothesis. The decay of $^{38}$Ca is a good candidate to investigate for this purpose since the calculated nuclear-structure-dependent correction for the superallowed transition is larger than that of any of the nine well-known nuclei $^{10}$C, $^{14}$O, $^{26m}$Al, $^{34}$Cl, $^{38m}$K, $^{42}$Sc, $^{46}$V, $^{50}$Mn, and $^{54}$Co [1]. If the measured and corrected $\mathscr{F}t$ values for $^{38}$Ca with its large calculated nuclear-structure-dependent correction is consistent with the average $\mathscr{F}t$ value established from the well-known cases, then it validates the calculation's reliability for the smaller corrections. To extract a meaningful $ft$ value from the experimental data, it is necessary to measure the half-life with a high precision of 0.1%.

We produced $^{38}$Ca via the $^1$H($^{39}$K, $2n$) reaction at a primary beam energy of $30A$ MeV. A 99%-pure $^{38}$Ca beam was obtained at the focal plane of the MARS spectrometer, from which it exited the vacuum system through a 50-μm thick Kapton window, passed through a 0.3-mm thick BC404 scintillator and a stack of aluminum degraders, and finally stopped in the 76-μm thick aluminized Mylar tape of a fast tape-transport system. After $^{38}$Ca was collected on the tape for 0.5 s, the cyclotron beam was interrupted and the collected sample was moved in 196 ms to the center of a $4\pi$ proportional gas counter. Multiscaled signals from the counter were recorded for 15 s into two separate decay spectra, each corresponding to a different pre-set dominant dead-time. This "collect-move-count" cycle was repeated until high statistics were obtained. In this preliminary test run, over 18 million $\beta$ events were recorded under various detecting conditions, with different settings for dominant dead time, bias voltage of the detector, and threshold of the discriminator.

The development of a new data analysis package is in progress. At the current stage, the new analysis package has been successfully tested with simulated data, mimicking the real data obtained from an experiment. By our applying this new analysis package to the real data, the half-life of $^{38}$Ca from this preliminary test run will be extracted soon.

[1] I. S. Towner and J. C. Hardy, Phys. Rev. C **77**, 025501 (2008).

# JYFLTRAP : $Q_{EC}$-values of the superallowed decays of $^{50}$Mn and $^{54}$Co

## J. C. Hardy

We have now completed our second successful measurement of superallowed $Q_{EC}$ values in collaboration with the group at JYFLTRAP, an on-line Penning trap mass spectrometer at the University of Jyväskylä cyclotron facility.   The $Q_{EC}$ values of $^{50}$Mn and $^{54}$Co [1] have now been added to our first results on $^{26}$Al$^m$, $^{42}$Sc and $^{46}$V [2].  Penning-trap measurements of superallowed $Q_{EC}$ values have become particularly interesting since our earlier discovery with the CPT trap [3] that the $Q_{EC}$ value for $^{46}$V was significantly different from a previous reaction measurement.   This was the first Penning-trap measurement of any of the "well known" superallowed transitions.  Until then, all these $Q_{EC}$ values had been determined entirely from reaction measurements, so there arose considerable concern that there might be some undiscovered systematic problem with that type of measurement.

Our repeat measurement [2] of the $^{46}$V $Q_{EC}$ value confirmed the first Penning-trap result [3] but also confirmed earlier reaction results for the $^{26}$Al$^m$ and $^{42}$Sc $Q_{EC}$ values.  This effectively eliminated any concerns about systematic problems with all reaction measurements.  However it left doubts about the 30-year-old ($^3$He,t) Q-value measurement by Vonach *et al.*[4] of seven superallowed transitions, which included the now-discredited value for the $^{46}$V.  Perhaps other results in that publication were wrong as well; in particular, the accepted $Q_{EC}$ values for $^{50}$Mn and $^{54}$Co depended strongly on the Vonach result and their measurement by Penning trap became a priority.

As we did in our earlier experiment at Jyvaskyla, we produced $^{50}$Mn and $^{54}$Co via (p,n)-reactions. A powerful advantage of this approach is that, not only were the superallowed emitters of interest produced in the primary reactions but ions from the target material itself – the beta-decay daughters of these emitters – were also released by elastic scattering of the cyclotron beam. As explained in Refs. [1, 2], with the JYFLTRAP system we can isolate a specific nuclide from the reaction products and measure the cyclotron frequency of its ions in the Penning trap.  For the first time, in this measurement we also employed a fast cleaning procedure to prepare isomerically pure ion samples, and measured part of the data employing the so-called Ramsey excitation scheme [1].  For each determination of a $Q_{EC}$ value, the cyclotron frequency measurements were interleaved: first we recorded a frequency scan for the daughter, then for the mother, then for the daughter and so on. This way, most possible systematic effects could be reduced to a minimum or eliminated.  For each measurement, data were collected in several sets, each comprising ~10 pairs of parent-daughter frequency scans taken under the same conditions.

Our $Q_{EC}$-value results are 7634.48(7) keV and 8244.54(10) keV for $^{50}$Mn and $^{54}$Co respectively. Both results differ from the values published by Vonach *et al.*[4] by more than 2.5 keV (5 or more of the latter's standard deviations).  Evidently, whatever problem Vonach *et al.* had with their measurement of the $^{46}$V $Q_{EC}$ value extended to $^{50}$Mn and $^{54}$Co as well: all three of these values are lower than the modern more-precise values by approximately the same amount.

The new result for $^{46}$V led to its corrected $\mathscr{F}t$ value becoming significantly higher than that for any other well known superallowed transition.  The most obvious explanation of its unusual value was that the correction for isospin symmetry-breaking, which depends upon the nuclear structure of the parent

and daughter nuclei, was missing some important components. We re-examined these calculated corrections and discovered that by including the *sd*-shell with the *fp*-shell in our configuration space, we could remove the shift in the $^{46}$V result but, at the same time, we introduced shifts in the $\mathscr{F}t$ values for $^{50}$Mn and $^{54}$Co as well [5]. With the previously accepted $Q_{EC}$ values for those nuclei, their $\mathscr{F}t$ values became anomalous. Our new measured $Q_{EC}$ values for $^{50}$Mn and $^{54}$Co completely resolve this discrepancy and provide strong confirmation of the new calculated correction terms.

[1] T. Eronen, V. -V Elomaa, U. Hager, J. Hakala, J. C. Hardy, A. Jokinen, A. Kankainen, I. D. Moore, H. Penttilä, S. Rahaman, S. Rinta-Antila, J. Rissanen, A. Saastamoinen, T. Sonoda, C. Weber and J. Äystő, Phys. Rev. Lett. **100**, 132502 (2008).

[2] T. Eronen, V. -V Elomaa, U. Hager, J. Hakala, A. Jokinen, A. Kankainen, I. D. Moore, H. Penttilä, S. Rahaman, A. Saastamoinen, T. Sonoda, J. Äystő, J. C. Hardy and V. Kolhinen, Phys. Rev. Lett. **97**, 232501 (2006).

[3] G. Savard, F. Buchinger, J. A. Clark, J. E. Crawford, S. Gulick, J. C. Hardy, A. A. Hecht, J. K. P. Lee, A. F. Levand, N. D. Scielzo. H. Sharma, K. S. Sharma, I. Tanihata, A. C. C. Villari and Y. Wang, Phys. Rev. Lett. **95**, 102501 (2005).

[4] H. Vonach *et al.*, Nucl. Phys. **A278**, 189 (1977).

[5] I. S. Towner and J. C. Hardy, Phys. Rev. C **77**, 025501 (2008).

# The half-life of $^{97}$Ru: a test for temperature dependence in electron-capture decay

J. R. Goodwin, V. V. Golovko, V. E. Iacob, and J. C. Hardy

This experiment was undertaken to investigate whether the half life of the electron capture decay of $^{97}$Ru in a metallic environment shows any temperature dependence, as has been claimed recently for the electron capture decay of $^{7}$Be [1].

Previous publications claiming to observe a temperature dependence of β-decay half-lives [1 - 3] in a metallic environment have used the so-called "Debye effect" to explain the phenomenon. This Debye-effect theory claims that the conduction electrons, present in a metal, comprise a sort of plasma, referred to as a Debye plasma, which alters the phase space available for beta decay. It is argued that the "Debye plasma" would decrease the phase space for β⁻-decay or electron capture, thus slowing the decay rate and increasing the half-life; and would increase it for β⁺-decay, which would have the opposite effect on the half-life. The theory also indicates that this change in phase space should be enhanced if the sample is cooled to very low temperatures (e.g., ~20 K).

We have already demonstrated that this effect does not, in fact, exist in the case of β⁻-decay by measuring the half-life of $^{198}$Au in gold at room temperature and at 20 K [4]. We are now examining the electron-capture decay of $^{97}$Ru in ruthenium. We have already completed the 20-K portion of the measurement.

We used a ruthenium disc obtained from Goodfellow Corporation. This was a single crystal, 8 mm in diameter, 1 mm thick, with a purity of 99.999%. The crystal was activated in a flux of ~$10^{13}$ neutrons/cm²·s for 10 s irradiation time, at the Texas A&M Triga reactor. For the decay measurement we used the same set-up as we did previously for $^{198}$Au [4]. The activated ruthenium sample containing $^{97}$Ru (and other activities produced from stable ruthenium isotopes) was placed upon the cold head of a CryoTorr 7 cryopump. A 70% HPGe detector was placed directly opposite the sample, and just outside the plate covering the cryopump. A cavity is bored in the cover-plate such that only 3.5 mm of stainless steel remains between the sample and the face of the detector. The detector and cryopump were placed such that the distance between them remained constant throughout the measurement.

Consecutive six-hour γ-ray spectra were acquired and saved for a period of 29 days. All these spectra were collected for an identical, pre-set live time. Throughout the experiment, we synchronized the time, prior to each day's collection, using the signal broadcast from radio station WWVB. We also kept the system's dead time below about 3% for all but the first few days' spectra. Since the TRUMP™ card used in our data collection corrects for dead time losses, our results were nearly independent of dead time losses, but we also made a small additional correction determined empirically [4].

We measured the half-life of $^{97}$Ru via the 216 keV γ-ray in $^{97}$Tc, which follows its β-decay. We used the least-squares peak-fitting program GF3 (in the RADware series [5]), to obtain the peak area in each of the ~115 recorded spectra. Use of this program allowed us to make very accurate determinations of spectral backgrounds and areas. Each peak was analyzed and then corrected for residual, rate-dependent effects, as mentioned above. The decay curves resulting from this analysis were then plotted as a function of time and analyzed, by a maximum-likelihood fit (single exponential), using a code based

on ROOT [6].  We had tested this code previously to a precision of 0.01%, with Monte-Carlo generated data.

From our analysis we have already obtained a preliminary half-life value of $2.8382 \pm 0.0026$ d at 20 K.  We hope to have the room-temperature results available by June 2008.  We expect that the final quoted uncertainties at both temperatures will be less than half the uncertainty now on our preliminary result.  This precision (*i.e.* ~0.07%) will be about the same as we quoted for our completed $^{198}$Au result [4].

[1] B. Wang *et al*., Eur. Phys. J. A **28**, 375 (2006).
[2] B. Limata *et al*., Eur. Phys. J. A **28**, 251 (2006).
[3] T. Spillane *et al*., Eur. Phys. J. A **31**, 203 (2007).
[4] J. R. Goodwin *et al*., Eur. Phys. J. A **34**, 271 (2007); *Progress in Research*,    Cyclotron        Institute, Texas A&M University (2007-2008), p. I-35.
[5] D. Radford, **http://radware.phy.ornl.gov/main.html** (private communication).
[6] R. Brun, and F. Rademakers, Nucl. Instrum. Methods Phys. Res. **A389**, 81 (1997).

# The half-life of $^{198}$Au: high-precision measurement shows no temperature dependence

J. R. Goodwin, V. V. Golovko, V. E. Iacob, and J. C. Hardy

This experiment was undertaken to investigate whether the half life of the β-decay of $^{198}$Au in a metallic environment showed any dependence on temperature as had been claimed in a recent publication [1]. An article describing this experiment has already been published [2].

Previous publications claiming to observe a temperature dependence of β-decay half-lives [1, 3, 4] have invoked the so-called "Debye effect" to explain the phenomenon. Their authors' explanation proceeds as follows: Beta decay involves either the emission of a positron or an electron from the nucleus, or the capture of an electron into the nucleus. Since metals possess large numbers of "conduction" electrons that are basically free to travel within the metal, these electrons are deemed to form a sort of plasma, which is referred to as a "Debye plasma". When a beta-decaying nuclide is placed in a metallic environment, the authors propose that the presence of the Debye plasma alters the phase space available for beta decay. In the case of β$^-$-decay or electron capture decay, they argue that the available phase space is *reduced*, slowing the decay rate and increasing the half-life. For the case of β$^+$-decay, the available phase space is *increased*, having the opposite effect. According to their formulation of this theory, the change in phase space can be enhanced if the host metal is cooled to very low temperatures (e.g., ~20 K).

With an eye to testing both the claimed experimental observation and the model that it generated, we have repeated one of the experiments that claimed to have observed a temperature-dependent effect [1]: a measurement of $^{198}$Au in gold metal. Our experiment was performed to a precision of 0.04%, more precise than the previous work by a factor of 25.

We used gold samples obtained from Goodfellow Corp; these were 10 mm in diameter, 0.1 mm thick, and had a purity of 99.99+%. The foils were activated at a flux of ~$10^{10}$ neutrons/cm$^2$·s, each for 10 s, at the Texas A&M Triga reactor. An activated gold sample, now containing $^{198}$Au, was placed on the cold head of a CryoTorr 7 cryopump. A 70% HPGe detector was placed directly opposite the sample, and just outside the plate covering the cryopump. A cavity had been bored in the cover-plate such that only 3.5 mm of stainless steel remained between the sample and the face of the detector. We used the same set-up for measurements at both room temp and at 20 K, the distance between the detector face and the sample being 4.5 cm.

Consecutive six-hour-long γ-ray spectra, were acquired and saved consecutively, for a period of about one month for each temperature. All spectra were collected for an identical, pre-set live time. Throughout the experiment, we synchronized the time prior to each day's collection, using the signal broadcast from radio station WWVB. We also kept the system's dead time below about 3% for all but the first few spectra. Since the TRUMP$^{TM}$ card used in our data collection corrects for dead time losses, our results were nearly independent of dead time losses. However, to achieve a precision under 0.1%, we performed an additional procedure to allow us to determine the presence of any residual, rate-dependent effects. This procedure involved measuring the 662 keV γ-ray peak from a $^{137}$Cs source, then repeatedly re-measuring this peak in the presence of a $^{133}$Ba source, which was moved nearer and nearer the detector. As the barium source moved closer to the detector, the dead time and the number of chance coincidences

both increased.  By plotting peak areas versus dead time, we found the residual loss to be $(5.5 \pm 2.5) \times 10^{-4}$ per 1% increase in dead time; this small correction was applied to all spectra.

We measured the half-life of $^{198}$Au via the 411-keV γ-ray in $^{198}$Hg, which follows its β-decay. We used the least-squares peak-fitting program GF3 (in the RADware series [5]), to obtain the peak area in each of the ~250 recorded spectra.  Use of this program allowed us to make very accurate determinations of spectral backgrounds and areas.  Each peak was analyzed and then corrected for residual, rate-dependent effects, as mentioned above.  The decay curves resulting from this analysis were then plotted as a function of time.  Following this, the resulting curve was analyzed, by a maximum-likelihood fit (single exponential), using a code based on ROOT [6].  We had tested this code previously to a precision of 0.01%, with Monte-Carlo generated data.

From our analysis we obtained the following half-lives: at 20 K, 2.6953 ± 0.0006 d; at room temperature, 2.6949 ± 0.0005 d (statistical uncertainties only).  The difference between these results is less than 0.0012 d or 0.04%.  This result contradicts the previous claim that there is a 90-times larger difference, 3.6 ± 1.0%, between the half-lives when measured at essentially the same temperatures.

With a provision for systematic error incorporated, our half-lives become 2.6953 ± 0.0009 d (cold), and of 2.6949 ± 0.0008 d (room temperature). These results compare very well with previously published results for room temperature measurements.  Their weighted average (see Ref. [2] for a table) is 2.6950 ± 0.0005 d.

Clearly we see no evidence for the effects of a Debye plasma on the β⁻-decay of $^{198}$Au. Whether these negative results will extend to β⁺-decay or electron capture remains uncertain.  We are currently measuring the half-life of $^{97}$Ru, which decays by pure electron capture. It should provide the answer for that class of decay.

[1] T. Spillane *et al*., Eur. Phys. J. A **31**, 203 (2007).
[2] J. R. Goodwin *et al*. Eur. Phys. J. A **34**, 271-174 (2007).
[3] B. Limata *et al*., Eur. Phys. J. A **28**, 251 (2006).
[4] B. Wang *et al*., Eur. Phys. J. A **28**, 375 (2006).
[5] D. Radford  (private communication); **http://radware.phy.ornl.gov/main.html**.
[6] R. Brun, and F. Rademakers, Nucl. Instrum. Methods Phys. Res. **A389**, 81 (1997).

# Tests of internal-conversion theory with precise γ- and x-ray spectroscopy: the $^{197}$Pt$^m$ case

N. Nica, C. Balonek, J. C. Hardy, M. Hernberg, V. E. Iacob,
J. Goodwin, and M. B. Trzhaskovskaya[1]

[1]*Petersburg Nuclear Physics Institute, Gatchina RU-188300, Russia*

As the next step in a series of precision internal-conversion-coefficient (ICC) measurements [1, 2] designed to test internal-conversion theory, we have proceeded with another interesting case, the 346.5-keV, M4 transition in $^{197}$Pt$^m$. As shown in Figure 1, the previously measured $\alpha_K$ for this transition, 4.02(8) [3], disagrees with modern Dirac-Fock calculations whether or not the atomic vacancy caused by the electron-capture process is incorporated in the theory.
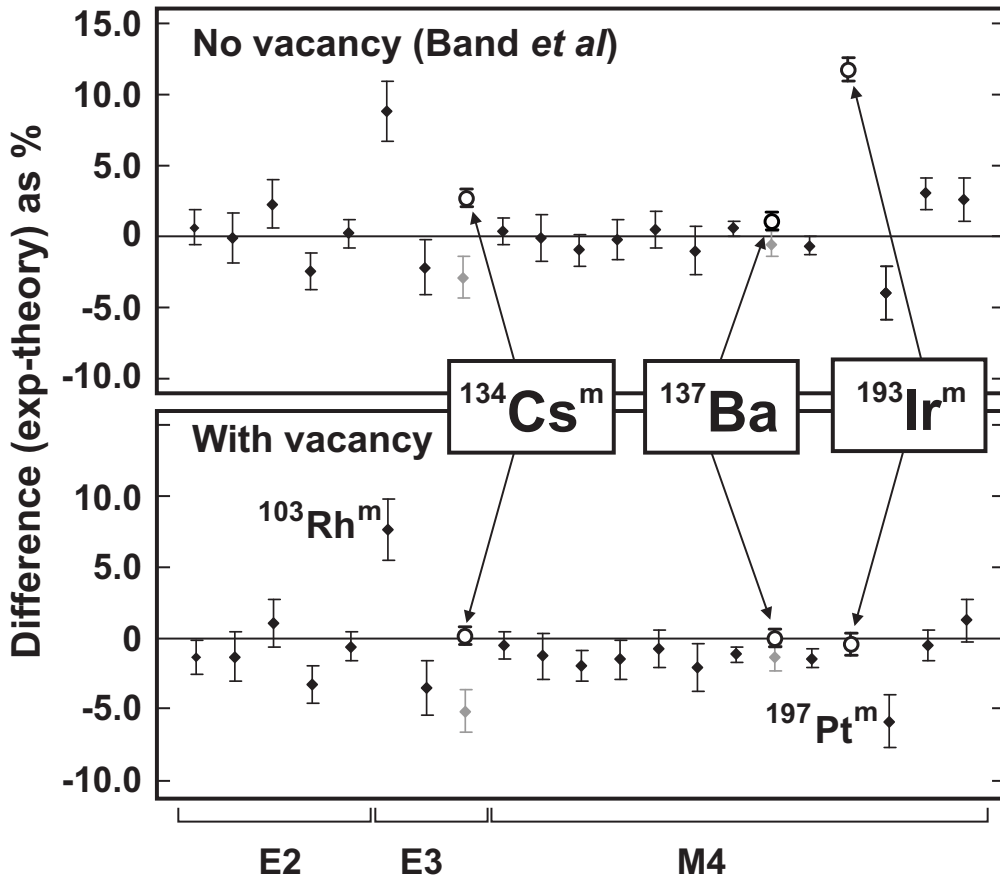


**Figure 1.** Percentage differences between the measured and calculated ICCs for two Dirac-Fock calculations: one (top) is without the atomic vacancy and the other is with it included in the "frozen orbital" approximation. The points shown as solid diamonds in both plots correspond to the twenty cases that have better that 2% precision; as indicated at the bottom, five are for E2 tranditions, three for E3, and the remainder are for M4 transitions. The points shown as open circles correspond to our recently measured $\alpha_K$ values.

The technique we use is to measure the intensity ratio of the K x-ray peaks relative to the γ-ray peak for the transition of interest. Our precision depends on there being no other significant contributors to the x-ray peaks (or to the γ-ray peak). One can easily see that a measurement on the 346.5-keV γ transition presents a number of challenges. We produce $^{197}$Pt$^m$ by neutron activation of enriched $^{196}$Pt, and one of the main difficulties is that the cross section for producing the $^{197}$Pt ground state ($\sigma_{th} = 0.72$ b) is 16-times larger than that for producing the isomer of interest ($\sigma_{th} = 0.044$ b). The $^{197}$Pt ground state β$^-$ decays with a 19.9-hr half-life to states in $^{197}$Au, whose subsequent decays involve internal conversion and give rise to gold K x rays. These x rays are very close in energy to the platinum x rays, whose intensity we need to determine. However, since the half-life of $^{197}$Pt$^m$ is 95.4 min we can use a time analysis of the decay spectra to help with the separation.

Another difficulty comes from the strong 77.4-keV γ ray which is produced by the $^{197}$Pt ground state β$^-$ decay and effectively obliterates the platinum K$_\beta$ peaks (75-78 keV). Moreover, this γ ray creates a scattering "shelf" to lower energies in the γ-ray spectrum, which complicates the background in the region of the platinum K$_\alpha$ x rays. We will again have to make use of the different half-lives to determine the exact shape of this background. These complications will undoubtedly limit our precision.

We prepared our samples at the Cyclotron Institute from 97.4%-enriched $^{196}$Pt as a thin powder held between thin mylar foils. This ensemble was then activated in the Triga reactor at the Nuclear Science Center of Texas A&M University. Because of the low cross section for production of $^{197}$Pt$^m$ by thermal neuron activation (as noted above), both the mass of Pt and the activation time were relatively high. These factors too will affect our ultimate precision.

We measured spectra from the activated source using our very precisely efficiency-calibrated HPGe detector [4]. The full decay of the source was recorded in 17 spectra over about two weeks in order to have sufficient information for multiple decay-curve analysis. A detailed impurity analysis has already been completed, which identified sources of Ir and Hg K x rays; these are relatively weak and can be precisely accounted for by an analysis of their observed γ-rays. A complete analysis is currently in progress.

[1] N. Nica *et al.*, Phys.Rev. C **70**, 054305 (2004); Phys.Rev. C **71**, 054320 (2005); Phys.Rev. C **75**, 024308 (2007); Phys.Rev. C **77**, 034306 (2008).
[2] J. C. Hardy *et al.*, Appl. Radiat. Isot. **64**, 1392 (2006); Appl. Radiat. Isot. **66**, 701 (2008).
[3] I. N.Vishnevsky *et al.*, Bull. Acad. Sci. USSR, Phys.Ser. **51**, 23 (1987).
[4] R. G. Helmer *et al.*, Nucl. Instrum. Methods Phys. Res. **A511**, 360 (2003).

# United States nuclear data program
## evaluated nuclear structure data file (ENSDF) at Texas A&M

N. Nica[1] and J. C. Hardy

[1]*Under contract with Brookhaven National Laboratory*

Since 2005, when we started our data evaluation program at the Cyclotron Institute, Texas A&M University has become an important participant in the nationwide United States Nuclear Data Program (USNDP), to which we contribute about 10% of the total effort. Our work continued in 2007 with the A=147 mass-chain evaluation [1]: this encompassed all publications since 1992, when this mass chain was last fully evaluated [2].

The A=147 mass chain is a massive one, composed of 16 different elements (Xe, Cs, Ba, La, Ce, Pr, Nd, Pm, Sm, Eu, Gd, Tb, Dy, Ho, Er, Tm); it contained 63 datasets[1] in 1992 [2], and the new evaluation, when published, will contain 85 [1]. As well, the number of lines in the database files[2] will be 20,000, about twice what it was before. Figure 1 shows a detailed comparison for each nucleus, where one can see impressive amounts of new data for Nd, Pm, Sm, Eu, Gd and Tb; in particular, $^{147}$Gd and
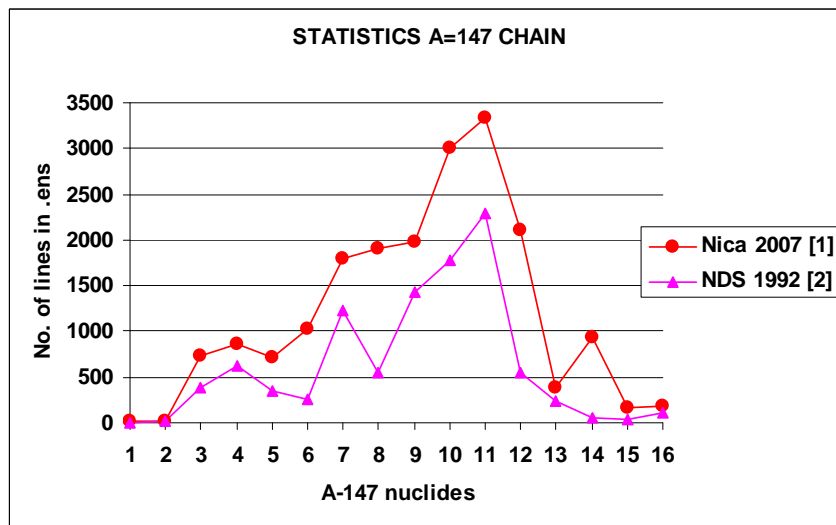


**Figure 1.** Comparison of the new evaluation [1] with the previous one [2], showing the number of database lines for each of the 16 nuclei in the A=147 mass chain. The nuclides appear from left to right in the same order as they are listed in the text.

---

[1] A dataset collects the data for one nucleus as measured in a particular decay or reaction, frequently by several independent experiments. The "Adopted Levels, Gammas" dataset, one for each nucleus, is built from the decay and reaction datasets for that nucleus. It gives the best and most extensive data for each nucleus.

[2] The database file (.ens file), one for each dataset, is written in the special ENSDF data format where one line (sometimes extended) contains typical data for a nuclear level, a particular nuclear transition, or other types of data, as well as comment lines.

$^{147}$Eu contain more than 3,000 lines, largely from high-spin data. There is also a significant increase in the number of publications, about 450 now compared to 350 before[3]. From Fig. 2 one can see that A=147 will be in the group of five largest mass chains.

While the complexity of an evaluation is usually unnoticed by the data consumer, it can have a major impact on the quality of the evaluated data[4]. Each single datum does not exist in isolation but rather is usually interconnected with a wide variety of related data. Often there are significant inconsistencies and conflicts among the existing measurements, and the evaluator must try to reconcile these differences. Obviously, difficult decisions have to be made, often with very little to base them on beyond educated guesswork. Continuity and an experienced evaluator are essential to this process.

In this context, the establishment of an evaluation center at the Cyclotron Institute is becoming desirable. While evaluation now is located predominantly in national laboratories, we have demonstrated that this activity can be done successfully in a university environment at lower costs. Furthermore, at a university some evaluation work can be done with the help of students. Thus, in addition to its intrinsic value for the community, evaluation could also become a tool for teaching nuclear physics.
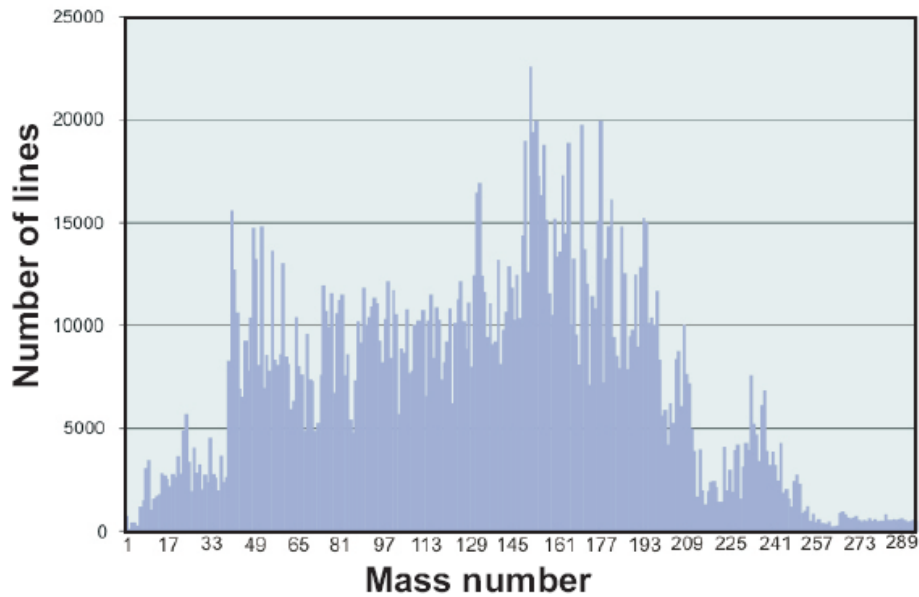


**Figure 2.** The number of .ens lines for each mass chain in ENSDF on March 2007. One can see that while the average number is about 7,000 lines, there are very few near or above 20,000 lines, where A=147 now lies.

[1] N. Nica, Nucl. Data Sheets (to be published).
[2] E. Der Mateosian and L. K. Peker, Nucl. Data Sheets **66**, 705 (1992).

---

[3] Only about 2/3 of the added references were published since 1992.
[4] While A=147 is particularly big, the discussion that follows is valid for ENSDF evaluations in general.

# The UCN-A experiment: measuring the β asymmetry using ultra-cold neutrons

D. Melconian for the UCNA collaboration[1]

Ultra-cold neutrons (UCN) are loosely defined as neutrons which have kinetic energies below a few hundred neV. Certain materials, like $^{58}$Ni, are able to efficiently transport and bottle UCN because the Fermi potential is larger than $E_{UCN}$ so the UCN will undergo complete internal reflection when interacting with the material walls. In addition, they are strongly influenced by magnetic fields and so are easily polarized. UCN therefore offer the opportunity to measure properties of the neutron and its β-decay with unprecedented precision. At Los Alamos National Laboratory's LANSCE facility, a source of UCN has been developed [2] where neutrons are produced via proton spallation from a Tungsten target and then converted into UCN by phonon downscattering within a solid deuterium "superthermal" moderator. These UCN are then guided through 12 m of shielding to the experimental area where the neutrons are polarized and observed in a very clean environment.

Currently, there is an inconsistency between measurements of $A_\beta$ [1], the β-asymmetry parameter which describes the correlation between the neutron's spin and the decay electron's momentum. The goal of the UCN-A experiment is to resolve the issue by measuring $A_\beta$ with a precision four times better than in previous experiments.

The β spectrometer of the UCN-A experiment is shown schematically in Fig. 1: it is a five meter long superconducting solenoid with Multi-Wire Proportional Chambers (MWPC) and plastic scintillator detectors at each end to observe the decay electrons. At the end of 2006, we produced the first measurement of UCN β decay with a counting rate of ≃ 2 Hz. Through 2007, the production and transmission of UCN were improved resulting in a 10× increase in the detection rate, the signal-to-noise ratio was improved to 21:1 (see Fig. 2) and the neutron polarization was shown to be greater than 99%.

We have shown our system is able to perform a high precision measurement of the β asymmetry. With the expected ≃ 8× further increase in rate for 2008, we will be
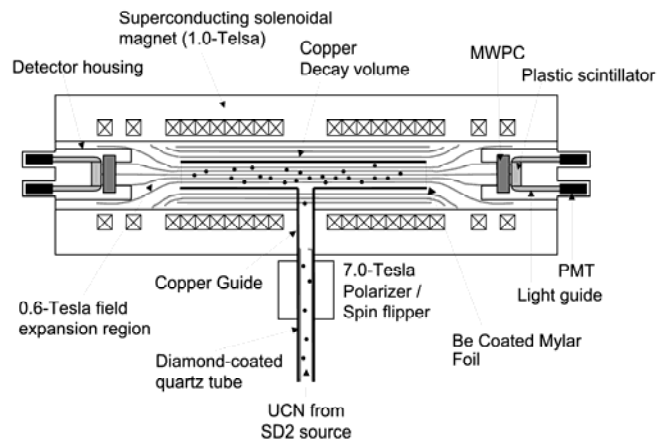


**Figure 1.** Schematic diagram of the β spectrometer for the UCN-A experiment at Los Alamos.

---

in a position to acheive our goal of measuring $A_\beta$ to 0.2%.
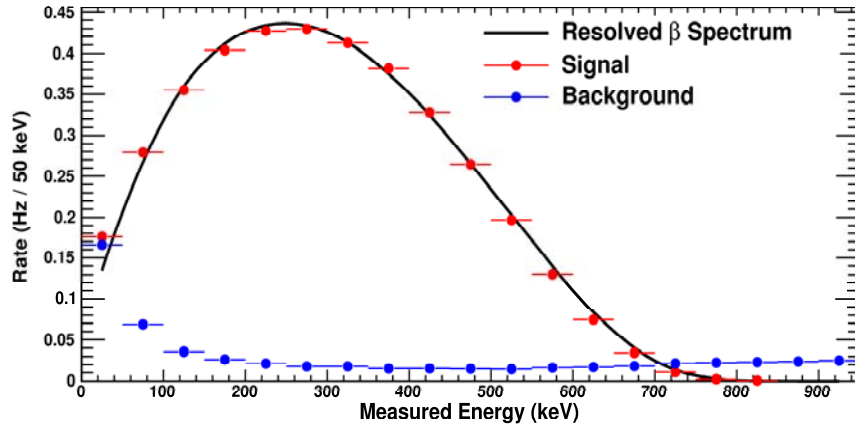


**Figure 2.** UCN $\beta$ spectrum taken at the end of 2007 in one of the UCN-A detectors.

[1] A. Saunders *et al.*, Phys. Lett. B **593**, 55 (2004).
[2] W. -M. Yao *et al.* (Particle Data Group), J. Phys. G **33**, 1 (2006) and 2007 partial update for the 2008 edition.

# *ft* value of the superallowed β-delayed proton decay of $^{32}$Ar

D. Melconian, E. G. Adelberger,[1] M. Bhattacharya,[1,2] A. García[1] and S. Triambak[1,3]

[1]*Physics Department, University of Washington, Seattle, WA 98195*
[2]*Brookhaven National Laboratory, P.O. Box 5000, Upton, NY 11973-5000*
[3]*Department of Physics, University of Guelph, Guelph, Ontario N1G 2W1, CANADA*

The *T*=2 superallowed decay of $^{32}$Ar is an interesting case to study because the isospin breaking correction, $\delta_C$, is predicted [1] to be 3× larger than the cases where the *ft* value has already been measured to the best precision [2]. By measuring this theoretical correction in a case where it is large enough to observe, we will be able to provide experimental confirmation of the calculations applied to the other cases when testing fundamental physics (confirming the conserved vector current hypothesis, unitarity of the CKM mass-mixing matrix, weak scalar and right-handed currents, etc.).

We counted the number of $^{32}$Ar ions produced at NSCL by implanting them in the middle of a 500 mm thick Si detector ($D_3$ in Fig. 1). The β-delayed protons were observed in the same detector, and γs were detected by the surrounding HPGe detectors. Fig. 2 shows our proton spectrum as well as a fit to a Monte Carlo simulation based on an R-matrix parameterization of the decay. Our result for the total superallowed branch is $b^{\beta}_{SA}$ = (22.71±0.16)%. Combining this with the known $^{32}$Ar half-life [3] and energy release [3, 4], we find the *ft* value of the superallowed decay is *ft* = 1552±12 s. If we use the corrected $\mathscr{F}t$ value extracted from the nine precisely known *T*=1 superallowed decays, we find $\delta_c^{\text{exp}}$ = (2.1±0.8)% [5] which can be compared to a theoretical calculation $\delta_C$ = (2.0±0.4)% [1]. In order to produce a stringent test of the theory, an improved version of the experiment is being considered and we hope more detailed calculations of $\delta_C$ and $\delta_{NS}$ will be performed.

As by-products of this work, we determined the γ and proton branches for the decay of the lowest *T*=2 state of $^{32}$Cl, made a precise determination of the total proton branch and relative intensities of proton groups
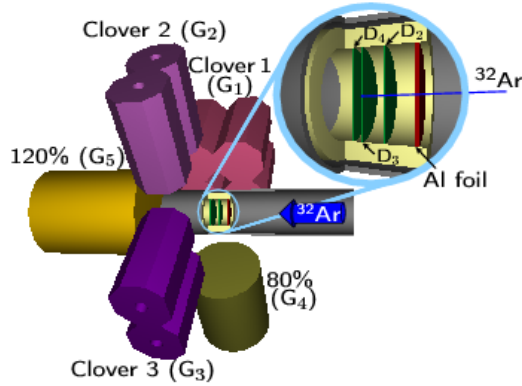


**Figure 1.** Detector setup of the $^{32}$Ar experiment.
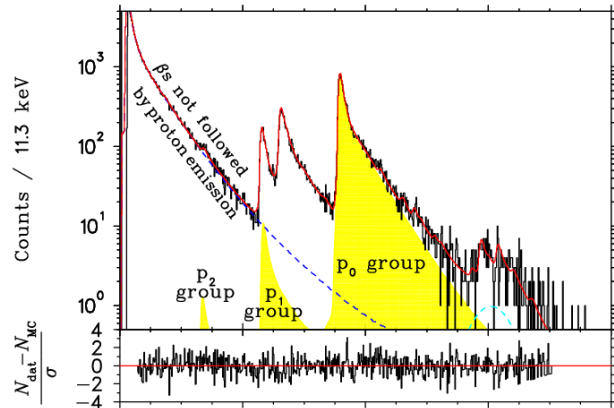


**Figure 2.** β-delayed proton spectrum of $^{32}$Ar (top) and residuals of the fit (bottom). The filled areas represent the proton groups following the superallowed β decay; other peaks arise from Gamow-Teller transitions.

that leave $^{31}$S in its first excited state, and deduced a value for the $^{32}$Cl mass with 1.6 keV uncertainty.

[1] B. A. Brown (private communication).

[2] J. C. Hardy, *Progress in Research*, Cyclotron Institute, Texas A&M University (2007-2008), p.I-24.

[3] A. García *et al.* (to be published).

[4] K. Blaum *et al.*, Phys. Rev. Lett. **91**, 260801 (2003).

[5] M. Bhattacharya *et al.*, Phys. Rev. C (in press).

# [100]Tc electron capture branching ratio

D. Melconian, S. K. L. Sjue,[1] I. Ahmad,[2] A. Algora,[3] J. Äystö,[4] K. S. Dryckx,[1] T. Eronen,[4] A. García,[1]
S. A. Hoedl,[1] A. Jokinen,[4] I. D. Moore,[4] H. Penttilä,[4] S. Rahaman,[4] J. Saastamoinen,[4]
H. E. Swanson,[1] S. Triambak[1,5] and C. Weber[4]

[1]*Department of Physics, University of Washington, Seattle, WA 98195*
[2]*Argonne National Laboratory, Argonne, IL 60439*
[3]*IFIC CSIC-University, Valencia, Spain*
[4]*Department of Physics, University of Jyväskylä, Jyväskylä, Finland*
[5]*Department of Physics, University of Guelph, Guelph, Ontario N1G 2W1, Canada*

The motivation to measure the electron-capture (EC) branch of [100]Tc is two-fold: [100]Mo is a neutrinoless double-β decay (0νββ) candidate [1, 2] for which the [100]Tc EC branch is needed for matrix element calculations; and inverse EC on [100]Mo has been proposed [2] as a potential detector for observing charged-current neutrinos from the pp chain. The main motivation at this time, however, is 0νββ because there is no concrete plans to develop [100]Mo as a neutrino detector due to the large mass ($\simeq$ 3 tons) which would be required. To date, only one measurement of the EC branching ratio has been published which has a 50% uncertainty on its value: $(1.8\pm0.9)\times10^{-5}$ [3].

A schematic diagram of the setup we used at the IGISOL facility in Jyväskylä, Finland is shown in Fig. 1. Using the Penning-trap system JYFLTRAP, contaminants in the beam (most notably ^{99}Tc and [100]Ru) were removed. The purified [100]Tc beam was collimated before entering a cylindrical cavity bored into a cube of plastic scintillator to ensure all the activity was implanted onto a foil near the opposite end of the cube. Imposing a veto from signals in the scintillator allowed us to suppress the dominant ($\simeq$ 99.999%) β⁻ decay branch to [100]Ru by >90%. A planar Ge detector observed the x-rays following the EC of [100]Tc with very little attenuating material between it and the activity (3 mm of scintillator and 120 μm of Be). A preliminary x-ray spectrum from the



**Figure 1.** Schematic diagram of the detector setup at the end of the IGISOL/JYFLTRAP beamline.

experiment is shown in Fig. 2. The dominant peak at 19.2 keV originates from $K_\alpha$ x-rays following the decay to [100]Ru; without the β veto, this peak would overwhelm the small [100]Mo x-ray peak at 17.4 keV. We calculate the EC branching ratio based on the ratio of the area of this small – but clearly resolved – peak to that of the 540 keV γ ray which follows the β⁻ decay. Although analysis of the data continues, preliminary results indicate a branch of $1\times10^{-5}$ with an uncertainty of $\simeq$ 20%. The dominant sources of

uncertainty are expected to be statistics in the [100]Mo peak and our understanding of the relative efficiency of the Ge detector between 17 keV and 540 keV.
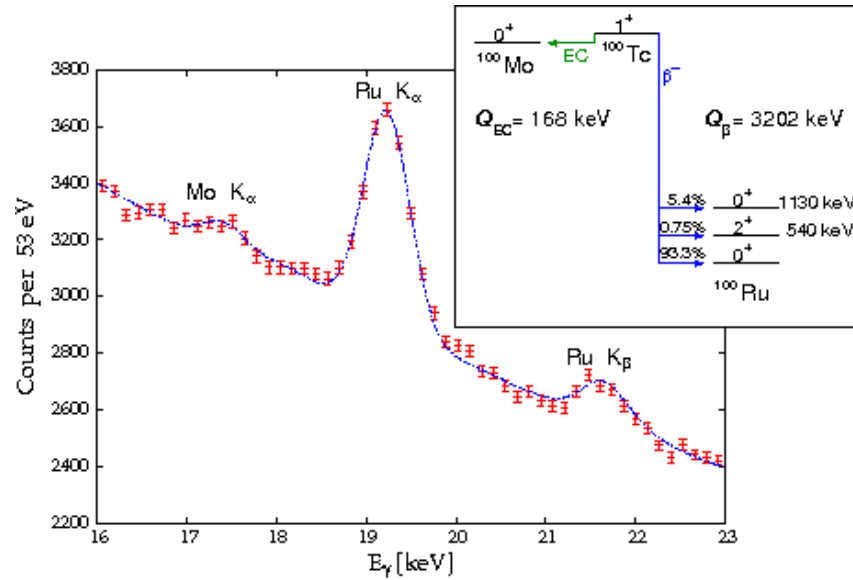


**Figure 2.** Simplified decay scheme (inset) and x-ray spectrum from [100]Tc decay.

[1] R. Arnold *et al.*, Phys. Rev. Lett. **95**, 182302 (2005).
[2] H. Ejiri *et al.*, Phys. Rev. Lett. **85**, 2917 (2000).
[3] A. García *et al.*, Phys. Rev. C **47**, 2910 (1993).

# Spin and low-*x* physics with STAR at RHIC

J. L. Drachenberg, C. A. Gagliardi, L. Huo, M. Sarsour, R. E. Tribble,
and the STAR Collaboration

During the past year, we have continued our focus on the analysis of STAR inclusive jet data from longitudinally polarized p+p collisions to determine the contribution that gluons make to the proton spin. We completed the analysis of the data that were recorded during 2005. As described in last year's progress report, our group, together with R. Fatemi (now at University of Kentucky), developed a new analysis procedure that accounts for most of the distortions that are introduced in the $A_{LL}$ measurement by the STAR detector. This allowed us to perform a quantitative comparison of our measured $A_{LL}$ results to global fits of polarized deep-inelastic scattering (DIS) data within the GRSV framework for various fixed values of $\Delta G$ [1]. The primary results are shown in Fig. 1. The data exclude models where the gluon polarization makes a large positive contribution to the nucleon spin. The data also disfavor models where the gluon polarization is maximally negative. A paper describing this work has been submitted to Physical Review Letters [2]. M. Sarsour is one of the six principal authors of that paper and served as a member of the god-parent committee.
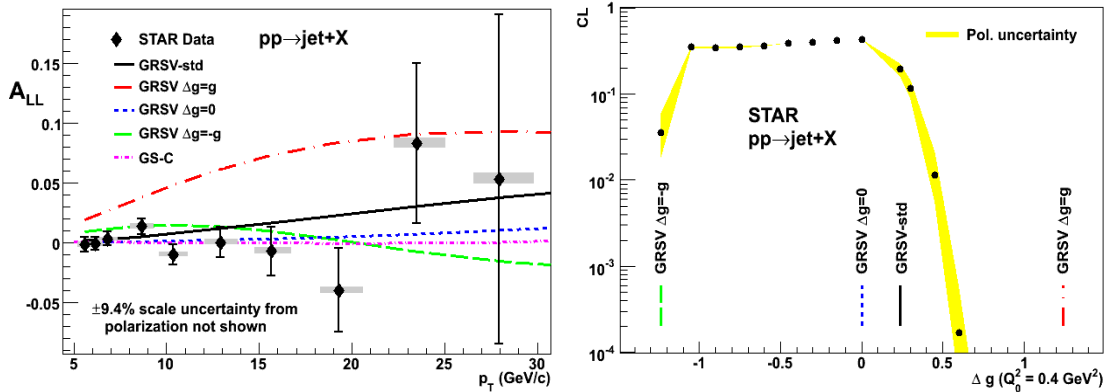


**Figure 1.** The left panel shows $A_{LL}$ versus $p_T$ for inclusive jets from data recorded in 2005, together with predictions from five previous global analyses of polarized DIS data. The right panel shows the confidence level (CL) for comparisons of the $A_{LL}$ measurements to predictions from fits to the polarized DIS data within the GRSV framework for various fixed values of $\Delta G$ [1]. Both figures are from [2].

In parallel, we have now analyzed the inclusive jet data that were recorded during 2006 to determine $A_{LL}$ with higher precision. The analysis procedures were similar to those we developed for the 2005 analysis. However, the increased calorimeter coverage during Run 6 allowed us to increase the jet cone radius from 0.4 to 0.7. We also improved the treatment of several of the systematic uncertainties, especially those due to beam-gas and pile-up backgrounds. M. Sarsour gave the first public presentation of the preliminary 2006 results in a talk at the DNP meeting in Newport News. (The same talk also included the first public presentation of the final 2005 results described above.) Figure 2 shows the

results. The statistical uncertainties in $A_{LL}$ are a factor of 3 to 4 smaller at high $p_T$. The increased precision leads to significantly more stringent constraints on gluon polarization models. We find that the gluon polarization must be small or negative, or the momentum-dependence of the gluon polarization must be more complex than has been assumed in most recent global analyses. The 2007 NSAC Long-Range Plan for Nuclear Science identified the STAR preliminary 2006 inclusive jet $A_{LL}$ results, in conjunction with preliminary 2006 inclusive $\pi^0$ measurements from PHENIX, as one of the highlights of the past five years.
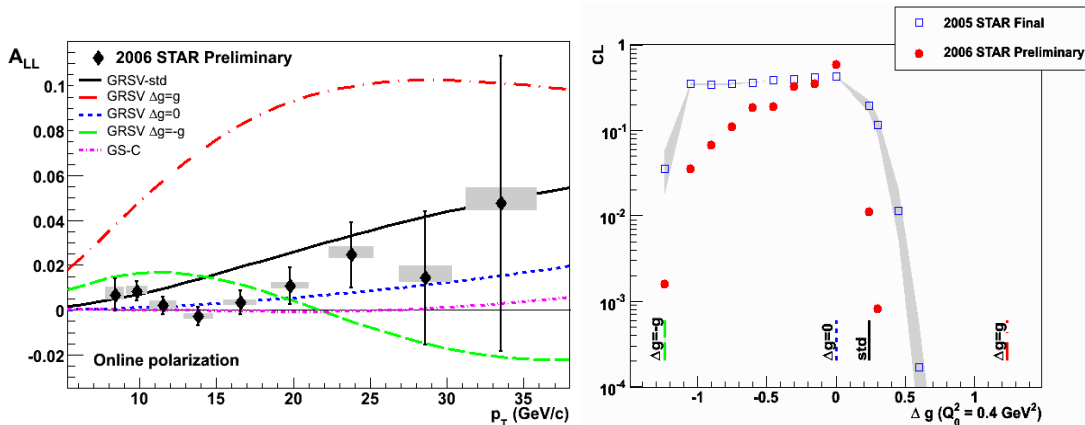


**Figure 2.** The left panel shows the preliminary 2006 STAR results for $A_{LL}$ versus $p_T$ for inclusive jets, together with predictions from five previous global analyses of polarized DIS data. The right panel shows the CL for comparisons of the $A_{LL}$ measurements to predictions from fits to the polarized DIS data within the GRSV framework for various fixed values of $\Delta G$ [1].

Since the DNP meeting, we have made a few additional improvements in the 2006 data analysis. We have also applied all of the improvements that we developed during the 2006 analysis to the 2005 data. Meanwhile, collaborators at UCLA have learned how to use the program of Jager *et al*. [3] to perform next-to-leading-order calculations of $A_{LL}$ for inclusive jet production using essentially any set of polarized parton distribution functions. This allows us to calculate confidence levels for global analyses outside the GRSV framework, and we have done this with our 2005 results. The 2005 and 2006 $A_{LL}$ measurements cannot be combined in the conventional way because the two analyses utilize different jet cone radii. Therefore, we are currently modifying our CL code so that it will perform a simultaneous fit to the results from both years. Once that is complete, we will be ready to write up the results for publication.

The STAR Forward Meson Spectrometer (FMS) is a new addition to the STAR electromagnetic calorimetry, providing complete coverage over the pseudorapidity region $2.5 < \eta < 4$, which is the deuteron forward direction when RHIC studies d+A collisions, and nearly complete EMC coverage over the range $-1 < \eta < +4$. The FMS enables STAR to search for mono-jet production in d+Au collisions. It will also facilitate measurements of gluon polarization in the proton at low-$x$ and detailed studies of the dynamics that underlie the significant single-spin asymmetries that have been seen in forward $\pi^0$

production at RHIC.  J. Drachenberg assisted with the final construction and commissioning of the FMS this past year.  The FMS was then used in Run 8 to take data during the d+Au and polarized p+p runs.  J. Drachenberg will analyze the FMS data that were recorded during the p+p run to determine $A_N$ for inclusive jets at forward rapidity.  This will provide a clean way to distinguish between the initial-state ('Sivers effect') and final-state ('Collins effect') explanations for the large $\pi^0$ single-spin asymmetries, because only the Sivers effect can produce a non-zero $A_N$ for inclusive jets.

We also carried administrative responsibilities in STAR.  This past year, Dr. Gagliardi served as Deputy Spokesperson of the STAR Collaboration.  Dr. Gagliardi also served on the STAR Advisory and Trigger Boards, and Drs. Gagliardi and Tribble participated on several STAR god-parent committees.

[1] M. Gluck *et al*., Phys. Rev. D **63**, 094005 (2001) ; M. Stratmann and W. Vogelsang (private communication).
[2] B.I. Abelev *et al*. (STAR Collaboration), arXiv:0710.2048 [hep-ex].
[3] B. Jager, M. Stratmann, and W. Vogelsang, Phys. Rev. D **70**, 034010 (2004).

**TWIST:  measuring the space-time structure of muon decay**

C. A. Gagliardi, R. E. Tribble, and the TWIST Collaboration

This past year, TWIST completed improved measurements of $\rho$ and $\delta$ based on the analysis of data that were recorded during 2004.  We find $\rho = 0.75014 \pm 0.00017(\text{stat.}) \pm 0.00044(\text{syst.}) \pm 0.00011(\eta)$ and $\delta = 0.75067 \pm 0.00030(\text{stat.}) \pm 0.00067(\text{syst.})$.  Both results are consistent with the Standard Model expectations of ¾, and represent a factor of ~2 improvement in precision compared to the original TWIST measurements [1,2].   When these new results are included in a global analysis of muon decay measurements [3], they lead to improved limits on right-hand muon couplings.  The results are currently being written up for publication.  Dr. Robert MacDonald of the University of Alberta performed the analysis as part of his Ph.D. research. One of us (CAG) assisted Dick Mischke and Art Olin of TRIUMF in advising Dr. MacDonald during his analysis.

TWIST completed its data taking in Summer, 2007, and the TWIST spectrometer has subsequently been disassembled.  We anticipate the final precisions for the Michel parameters $\rho$ and $\delta$ will be approximately $\pm 0.0003$.  The final precision for $P_\mu \xi$ should be $\pm 0.001$ or better.

[1]  J. R. Musser *et al*. (TWIST Collaboration), Phys. Rev. Lett. **94**, 101805 (2005).

[2]  A. Gaponenko *et al*. (TWIST Collaboration), Phys. Rev. D **71**, 071101R (2005).

[3]  C. A. Gagliardi, R. E. Tribble, and N. J. Williams, Phys. Rev. D **72**, 073002 (2005).

# Toward understanding relativistic heavy-ion collisions with the STAR detector at RHIC

M. Cervantes, R. Clarke, M. Codrington, A. Hamed, S. Mioduszewski,
and the STAR Collaboration

We are studying relativistic heavy-ion collisions with two different probes: bottomonium and γ-jet.

## I. Bottomonium (Y) Measurement

The bottomonium measurement is important to disentangle competing effects, dissociation in the deconfined plasma vs. $q\bar{q}$ recombination, both possibly playing a role in the production of charmonium in heavy-ion collisions. During the past year, we developed the tools for mass reconstruction of the Y(b $\bar{b}$), measured via its decay to an electron-positron pair in the STAR detector. STAR presented a preliminary Y mass peak from the Year-7 Au+Au data set at QM 2008 [1], from the UC Davis group, who is also working on this analysis. Prior to this, Y had not been measured in heavy-ion collisions. Because of the low statistical significance of the measurement, it is important to have systematic cross-checks. We are doing an independent analysis to compare with and provide such systematic checks for the parallel analysis effort by the UC Davis group. In particular, there are 2 fronts on which we are investigating systematics. First, we have been looking at the effect of the Barrel Preshower (BPRS) detector for electron identification. Second, we have used an alternate determination of the combinatorial background, in which tracks from different events are combined ("event-mixing") rather than combining only like-sign pairs from within an event. This alternate method reduces the statistical uncertainty on the background subtraction because the event-mixing can be performed over many events, while the number of like-sign pairs is similar in magnitude to the number of unlike-sign pairs within a single event (i.e. the foreground).

Fig. 1 shows the invariant mass distribution of $e^+e^-$ pairs, together with the combinatorial background distribution generated from mixed-events. Fig. 2 shows the
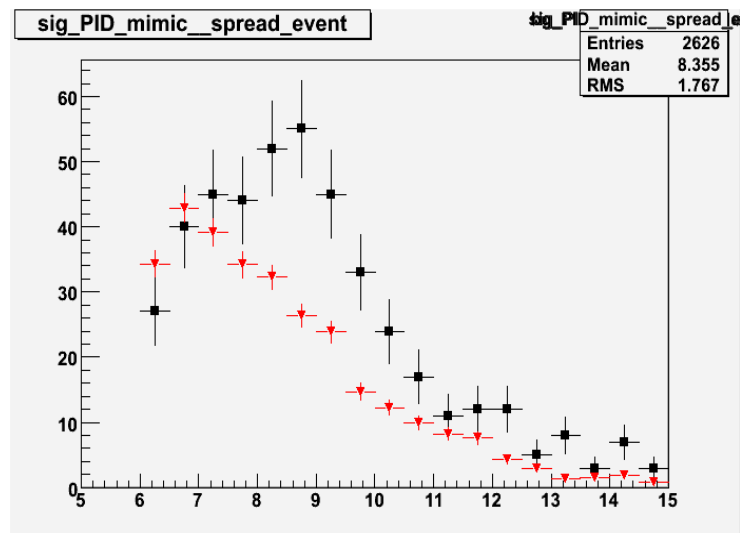


**Figure 1**. Reconstructed mass calculated from $e^+e^-$ pairs (black squares), and from pairs from mixed events (red triangles) normalized by $\sqrt{(2N_{++}N_{--})}$ from the real events.

background-subtracted mass distributions with and without a cut on the BPRS signal, as electron identification for the lower-energy track. The peak loses approximately 20% of its counts when the cut is applied, as expected from the number of bad BPRS channels.
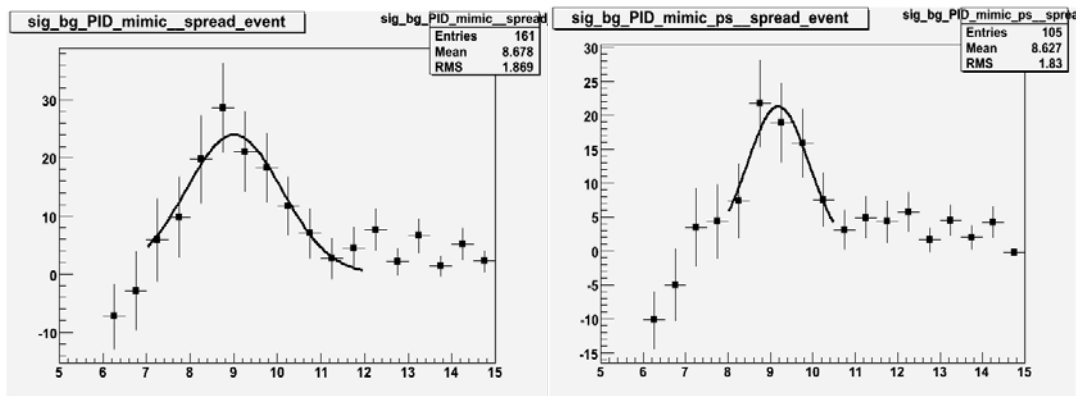


**Figure 2.** Background-subtracted invariant mass distributions, shown without a cut on the BPRS signal (left) and with a cut on the BPRS for electron identification (right).

## II. Gamma-Jet Measurement

In order to measure the medium-induced parton energy loss as a function of the parton's original energy, one must measure photon-hadron correlations (γ-jet) [2]. The idea is to trigger on a "direct" photon, which originates directly from a hard scattering and does not interact strongly with the medium, and measure the jet on the away-side which does suffer from parton energy loss. In order to distinguish direct photons from photons from high-$p_T$ $\pi^0$ decays, we used the Barrel Shower Maximum (BSMD) detector to discriminate between the shower profile of a single photon and that of two close photons. Fig. 3 shows a quantity, derived from the distribution of energy in 15 BSMD strips, on which the discrimination cut was made.
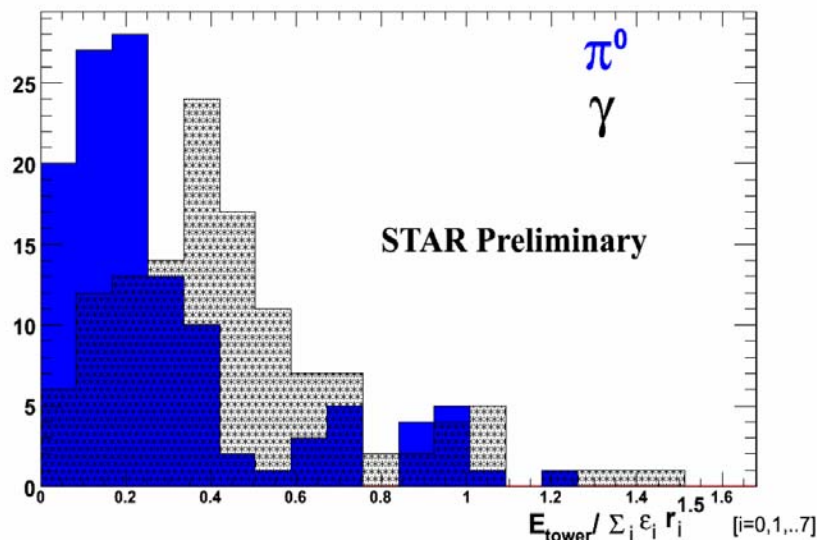


**Figure 3**. A quantity related to the transverse-shower profile, as measured by the BSMD, used to discriminate between direct photons and two photons from high-$p_T$ $\pi^0$ decays. The solid blue histogram is from simulated $\pi^0$ and the hashed black is simulated photons, both embedded into real events.

With a pure sample of $\pi^0$ triggers and a sample of direct photon-rich triggers, the correlation function of each is constructed by calculating $\Delta\Phi$ for each charged hadron, within a given momentum range, with respect to the trigger particle. The flat background in the resulting distribution is subtracted. Since direct photons should have no associated yield at leading order, any remaining yield on the near-side is assumed to originate from $\pi^0$ triggers. Then the direct-photon associated yields can be obtained using the following prescription,

$$Y_{\gamma direct+h} = (Y^a_{\gamma rich+h} - RY^a_{\pi0+h}) / (1-R),$$

where $R = Y^n_{\gamma rich+h} / Y^n_{\pi0+h}$, $Y^n$ represents the near-side yield, and $Y^a$ represents the away-side yield.

We analyzed the Year-7 Au+Au data, and presented first results at Quark Matter 2008 [3], on behalf of the STAR Collaboration. The results are shown in Fig. 4.
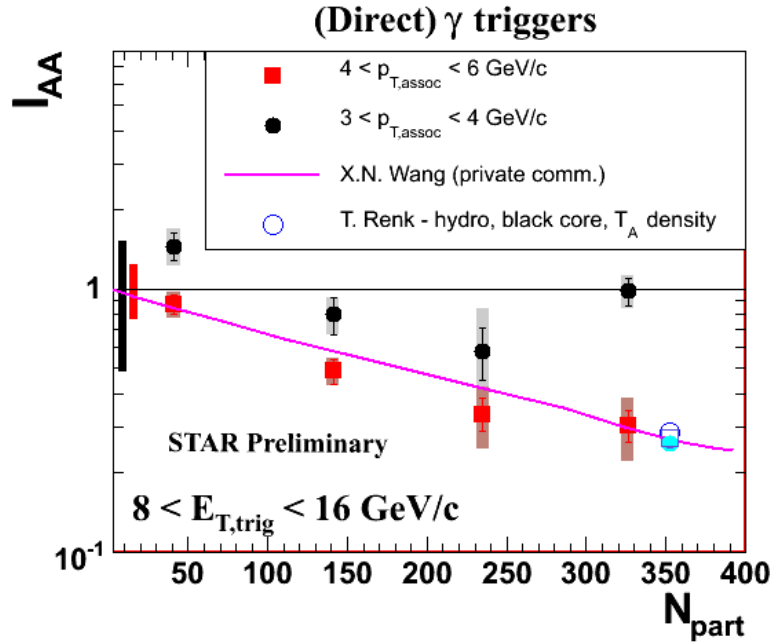


**Figure 4**. Ratio of associated yields for a direct-photon trigger measured in Au+Au collisions to that measured in p+p collisions, as a function of centrality.

[1] D. Das *et al.* (STAR Collaboration), in Proceedings of the 20th International Conference on Ultrarelativistic Nucleus-Nucleus Collisions (Quark Matter 2008), Jaipur, India, 2008.
[2] X. -N. Wang, Z. Huang, and I. Sarcevic, Phys. Rev. Lett. **77**, 231 (1996).
[3] A. Hamed *et al.* (STAR Collaboration), in Proceedings of the 20th International Conference on Ultrarelativistic Nucleus-Nucleus Collisions (Quark Matter 2008), Jaipur, India, 2008.

# SECTION II

# HEAVY ION REACTIONS

# Light particle clusterization in nuclear matter at very low density

L. Qin,  J. B. Natowitz, G. Roepke,[1] K. Hagel, R. Wada, Z. Chen, P. Sahu, S. Kowalski,[2]

C. Bottosso , S. Shlomo, M. Barbui,[3] D. Fabris,[3] M. Lunardon,[3] S. Moretto,[3]

G. Nebbia,[3] S. Pesente,[3] V. Rizzi,[3] G. Viesti,[3] M. Cinausero,[4]

G. Prete,[4] T. Keutgen,[5] Y. El Masri,[5] and Z. Majka[6]

[1]*University of Rostock, FB Physik, Rostock, Germany*

[2]*Institute of Physics, Silesia University, Katowice, Poland*

[3]*Dipartamento di Fisica dell'Universita di Padova and INFN Sezione di Padova, Italy*

[4]*INFN Laboratori Nazionali di Legnaro, Italy*

[5]*Universit´e Catholique de Louvain, Louvain-la-Neuve, Belgium,*

[6]*Smoluchowski Institute of Physics, Jagiellonian University, Krakow, Poland*

Reliable understanding of the nuclear EOS over a range of densities remains a very important requirement in nuclear astrophysics. Several extensive calculations and existing tabulations, based on various models have been pursued,   Recently, Horowitz and Schwenk have reported the development of a Virial Equation of State (VEOS) for low density nuclear matter [1]. At sufficiently low densities, this equation of state, derived from experimental observables should be "model-independent, and therefore set a benchmark for all low density nuclear equations of state. The importance of understanding low density nuclear matter  in both nuclear physics and in the physics of the neutrinosphere in supernovae is emphasized in the VEOS paper [1] as well as in a recent paper by Sumiyoshi *et al.* [2].

At low densities and high temperatures strong alpha clustering of the matter is predicted. Such clusterization can be expected in low density nuclear matter, whether it be gas or the low density surface of an expanded high temperature nucleus. We recently adapted our investigations of the nucleon and light cluster emission that occurs in near Fermi energy heavy ion collisions to probe the properties of the low density participant matter produced in such collisions [3].  The reactions of 35 MeV/nucleon $^{64}$Zn projectiles with $^{92}$Mo and  $^{197}$Au target nuclei were studied.  The data provide experimental evidence for a large degree of alpha clustering resulting from nucleon coalescence in this low density matter.  For nuclear gases with average proton fraction, Yp ~0.44, and densities at and below 0.05 times normal nuclear density and varying temperatures experimental symmetry energy coefficients  have been derived using the isoscaling method.

The resultant symmetry energy coefficients are plotted against density in Fig. 1 where they are compared to those which are predicted by the Gogny effective interaction and to the $31.6 \times (\rho/\rho_0)^{1.05}$ dependence suggested by a recent analysis of isospin diffusion data [4]. These symmetry energies reported in Fig. 1 are far above those obtained in common effective interaction calculations and reflect cluster formation, primarily of alpha particles, not included in such calculations.  Stimulated by these data, Schwenk and his collaborators have since improved the VEOS model with the addition of $^3$H and $^3$He cluster coefficients [5].
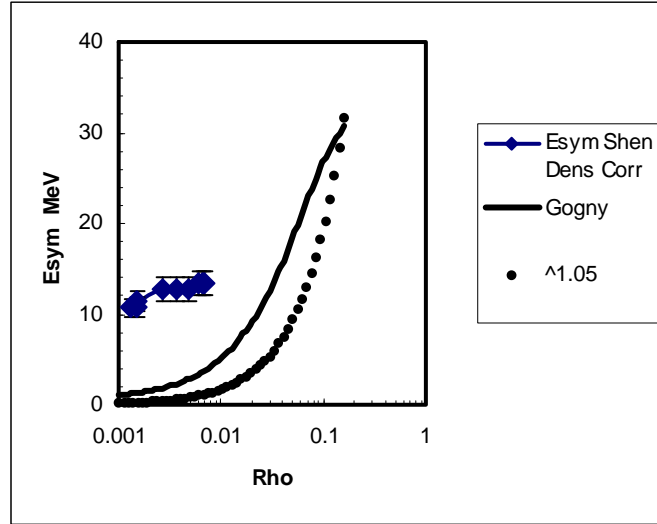
**Figure 1**. Derived symmetry energy coefficients as a function of baryon density. Solid diamonds indicate experimental results. Solid line indicates the variation predicted by the Gogny interaction. The dotted line represents the function 31.6 x $(\rho/\rho_0)^{1.05}$ .

Our original analysis has assumed that at such low density the chemical equilibrium model of Albergo *et al.* should be applicable. Extracting information at higher densities is clearly desirable but requires a more sophisticated analysis. This is made clear from a number of theoretical results [6-8]. For example, in Fig. 2 we present results of Roepke *et al.* who have calculated the in-medium binding energies of clusters as a function of temperature and density. As seen in Fig. 2 for a temperature of 10
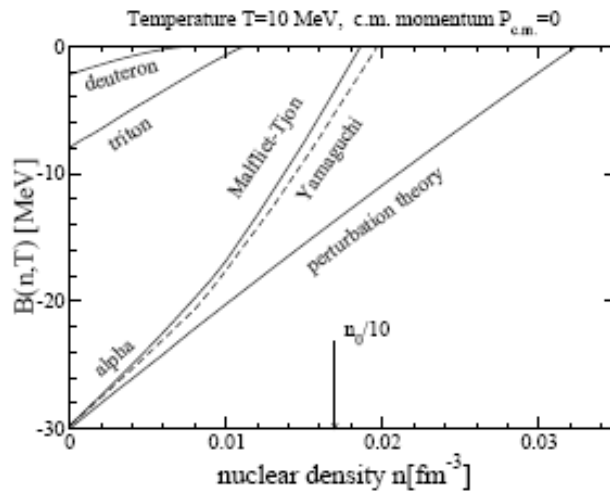


**Figure 2**. In medium binding energies of light clusters

MeV, the free binding energies of the clusters (at 0 on the density axis) decrease with increasing density and reach 0 at a point known as the Mott density. Using this model, G. Roepke has made calculations of the low density symmetry energy for comparison to our experimental results [8].

In order to pursue this effort of taking the in medium modifications into account and broaden the density range over which the symmetry energies are experimentally determined we have now carried out a series of experiments in which the reactions of $^{112}$Sn and $^{124}$Sn with a wide range of projectiles, ranging from p to $^{64}$Zn, all at the same energy per nucleon, 47Mev/u, could be studied. The systems chosen for this study, the PhD thesis of LiJun Qin, were : $^{4}$He, $^{10}$B, $^{20}$Ne, $^{40}$Ar and $^{64}$Zn projectiles with $^{112}$Sn and $^{124}$Sn targets. In this series of experiments different collision systems should lead to different average densities, the analysis is nearing completion. As an example of our results, Fig. 3 presents preliminary results in which our experimental results for alpha mass fractions in low density nuclear matter with T = 5 MeV are compared to the results of various calculations as indicated in the label box.
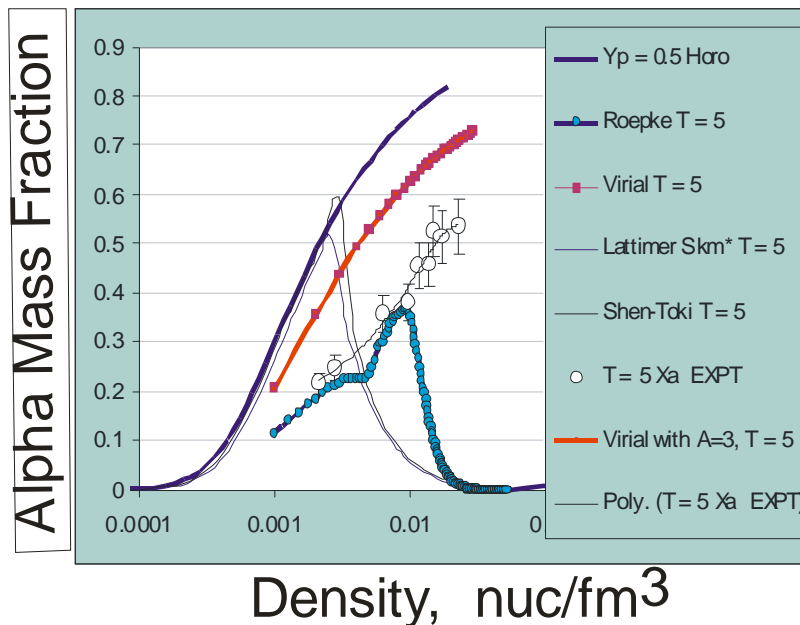


**Figure 3**. Alpha mass fraction in low density matter. See text.

[1] C. J. Horowitz and A. Schwenk, Nucl. Phys. A **776**, 55 (2006).

[2] K. Sumiyoshi and G Roepke , arXiv:0801.0110

[3] S. Kowalski *et al.*, Phys.Rev. C **75**, 014601 (2007).

[4] L. -W. Chen *et al.*, Int. J. Mod. Phys. **E15**, 1385 (2006).

[5] E. O'Connor *et al.*, Phys. Rev. C (to be published); arXiv:nucl-th/0702044.

[6] M. Beyer *et al.*, Phys.Lett. **B488**, 247 (2000).

[7] M. Beyer *et al.*, Eur.Phys .J. **A22**, 261 (2004).

[8] G. Roepke (private communication).

# A new order parameter for IMF isotope distributions

Z. Chen, R. Wada, A. Bonasera, T. Keutgen, K. Hagel, J. Wang, L. May,
L. Qin, J. B. Natowitz, T. Materna, S. Kowalski, and P. K. Sahu

An experiment was performed with beams of $^{64}$Zn, $^{70}$Zn and $^{64}$Ni at 40 AMeV bombarding targets of $^{58}$Ni, $^{64}$Ni, $^{112}$Sn, $^{124}$Sn, $^{197}$Au and $^{232}$Th. Emphasis was placed upon obtaining high quality isotopic identification and high statistics for isotopes with Z between 3 and 18, for all the systems. Using a Si telescope, consisting of four quadrant Si detectors (129, 300, 1000 and 1000μm thick with area of 5cm x 5cm), isotopes of $^{6}$LI to $^{9}$Li, those of $^{7}$Be to $^{12}$Be and 6 to 8 isotopes for Z>4 were clearly separated and identified above an energy threshold ranging from 5 A MeV for Li isotopes to 10 A MeV for Si isotopes. In order to get the angle integrated yield of each isotope, the energy spectra observed at θ= 17.5$^{o}$and 22.5$^{o}$ in different quadrants of the telescope were fit using a moving source parameterization.

From the Fisher model [1], the following relation is obtained between the yield of an isotope, Y, and physical constants;

$$Y = y_0 A^{-\tau} e^{-\beta \Delta \mu A}, \qquad (1)$$

Where $y_0$ is a normalization constant, τ is the exponent of the mass distribution, β is the inverse temperature and Δμ is the difference in chemical potential between neutrons and protons, i.e., the Gibbs free energy per particle, *F(I/A)*, near the critical point, where I=N-Z, is the difference between neutrons and protons in a given isotope. We can compare all systems on the same basis by normalizing the yields and factoring out the power law term. For this purpose we have chosen to normalize the yield data to the $^{12}$C yield with τ =2.3, we define a ratio:

$$R = \frac{Y A^{\tau}}{Y(^{12}C)12^{\tau}}, \qquad (2)$$

In Figure (1) the quantity *F/T = - ln(R)/A* versus (I/A) is shown. I/A indicates the neutron to proton concentration in the emitting source. As one can see, the ratios for all isotopes are well distributed along a bell shaped function. This indicates that I/A, the neutron to proton concentration, is an good order parameter to govern the isotope distribution. All isotope yields measured in each reaction showed very similar distributions. The centroid of the distribution depends on the N/Z ratio of the reaction system, though the width is very similar from system to system.

An attempt was made to fit the distribution, using the Landau model [2,3]. In this approach the ratio of the free energy to the temperature is written in terms of an expansion:

$$\frac{F}{T} = \frac{1}{2}am^2 + \frac{1}{4}bm^4 + \frac{1}{6}cm^6 - m\frac{H}{T} \qquad (3)$$

Where $m = (I/A)$ is an order parameter, $H$ is its conjugate variable and $a$-$c$ are fitting parameters. If we force the parameter $c$ to be 0 in eq. 3, i.e. we reduce the Landau free energy to fourth order. Fitting the data of Fig. 1 we obtain $a = 19.2$ and $b = -130.73$. This result is unphysical since it implies that the free energy is negative for large $m$. A fit using eq.3 gives the following values for the $^{64}Ni$ + $^{58}Ni$ ($^{64}Ni$ + $^{232}Th$): $a = 23.5(18.86)$, $b = -413.8(-260.3)$, $c = 2848.3(1408.1)$ and $H/T = 0.79(1.06)$ and is displayed in Fig. 1(long dashed line). This case corresponds to a 'classical' second-order phase transition.

For first-order phase transitions, the following relation between parameters should hold,

$$b = -4\sqrt{ca/3} \qquad (4)$$

Using the values of a and c given above we get b=-597.5 (-376.3) which is close to the fitted values given above. In particular if we substitute eq.(4) into eq.(3) and perform the fit, we obtain a result shown by the short-dashed line. In the case of the first-order transition the fit bends up for large (positive) m, however the data do not distinguish between the two cases. Further study and discussion on the relation between the isotope distribution and the order parameter are now underway.
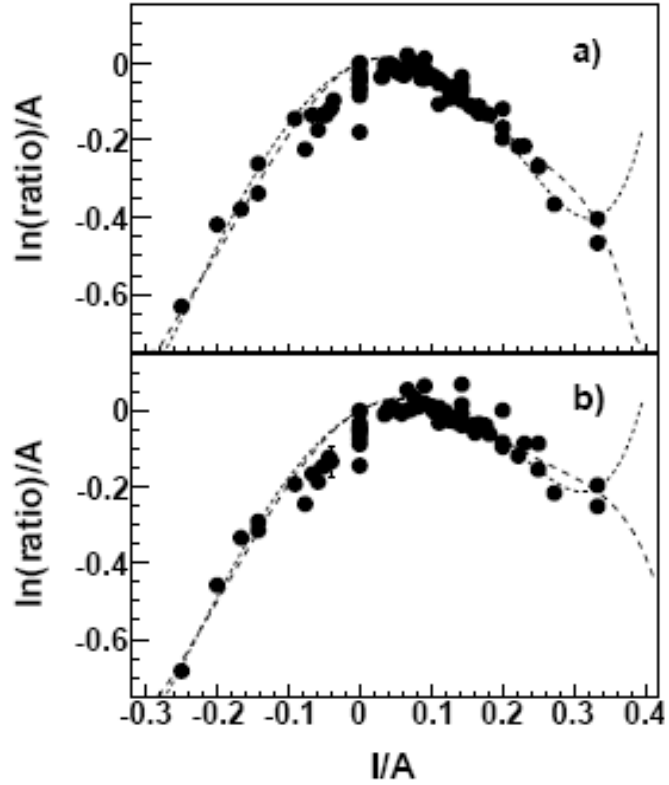


**Figure 1**. The negative of the free energy versus symmetry term for the case $^{64}Ni+^{58}Ni$ (upper panel) and $^{64}Ni+^{232}Th$ at 40 MeV/nucleon (lower panel). The dashed lines are fits based on Landau O($m6$) free energy either for a second-order(long-dashed) or first-order (short-dashed) phase transition (see text).

[1] A. Bonasera *et al.*, Rivista Nuovo Cimento **23**, 1 (2000).
[2] K. Huang, *Statistical Mechanics*, *2nd edition* (J. Wiley and Sons, New York, 1987), Ch.16-17; A. Hosaka and H. Toki, *Quarks, Baryons and Chiral Symmetry* (World Scientific, Singapore, 2001).
[3] L. D. Landau and E. M. Lifshitz, *Statistical Physics*, *3rd edition* (Pergamon press, New York, 1989).

# Lithium production in heavy ion reactions at 47 MeV/u

C. Bottosso, R. Wada, K. Hagel, J. B. Natowitz, L. J. Qin, T. Keutgen, Z. Chen, and P. K. Sahu

In the past few years many efforts have been carried out to investigate the characteristics of the emitting source created at the early stage of various heavy ion collisions using light particles of $Z = 1$ and $Z = 2$. Quantities such as density, temperature and symmetry energy have been studied to better understand the reaction processes [1]. To extend this work, we now perform an analysis to examine the influence of heavier particles on our earlier analysis. For this purpose, we have analyzed the energy spectra of $^6Li$ and $^7Li$ emitted in various reactions using $^{10}B$, $^{20}Ne$, $^{40}Ar$, $^{64}Zn$ as projectiles and $^{112}Sn$ and $^{124}Sn$ as targets, all at the same incident energy of 47 MeV/u. This work, as the previous one, was done using NIMROD [2].

The energy spectra have been studied as a function of the violence of the collision which is correlated to an increase in excitation energy and leads to an increase of the charged particle and neutron multiplicity. We have divided the total multiplicity spectrum (given by the sum of light charged particle and neutron multiplicity) into four regions and have assumed that the most violent events, given by the top 30% multiplicity window, correspond to the more central collisions. We label these four regions Bin1, the most peripheral collisions to Bin 4 the most central. For each multiplicity window we have obtained differential lithium multiplicity spectra and we have performed moving source fits with three sources. In this way we were able to approximately separate the contributions from the projectile like fragment source (PLF), the intermediate velocity source (NN) and the target like fragment source (TLF). The three source fitting allows us to have a schematic picture of the emission process.

An example of the $^6Li$ multiplicity spectra for $^{64}Zn + ^{112}Sn$ system is shown in Fig. 1. As we can see, the most forward angles (q = 4.31 and q = 6.41) are dominated by the PLF contribution for which the velocity is fixed, by definition, near the beam velocity. On the other hand at the most backward angles the fit indicates that most of the Lithium ions originate from the target like source.

In addition this technique allows to estimate velocities, emission barriers, temperatures and particle multiplicities for each source, providing an idea of the evolution of the system. The parameters extracted from the fit for $^6Li$ for the $^{64}Zn + ^{112}Sn$ spectra are shown in Table I.

**Table I**. Multiplicity, temperature, Coulomb energy and source velocity for NN, PLF and TLF functions given by the fit for $^{64}Zn + ^{112}Sn$.

|  | Multiplicity | Temperature | Coulomb barrier | Velocity |
|---|---|---|---|---|
| **NN** | $0.0470 \pm 0.0011$ | $16.00 \pm 0.02$ | $11.000 \pm 0.046$ | $4.884 \pm 0.049$ |
| **PLF** | $0.0040 \pm 0.0012$ | $12.00 \pm 0.02$ | $10.000 \pm 0.347$ | $7.967 \pm 0.045$ |
| **TLF** | $0.0028 \pm 0.0045$ | $3.00 \pm 0.04$ | $4.000 \pm 3.622$ | $0.001 \pm 0.074$ |
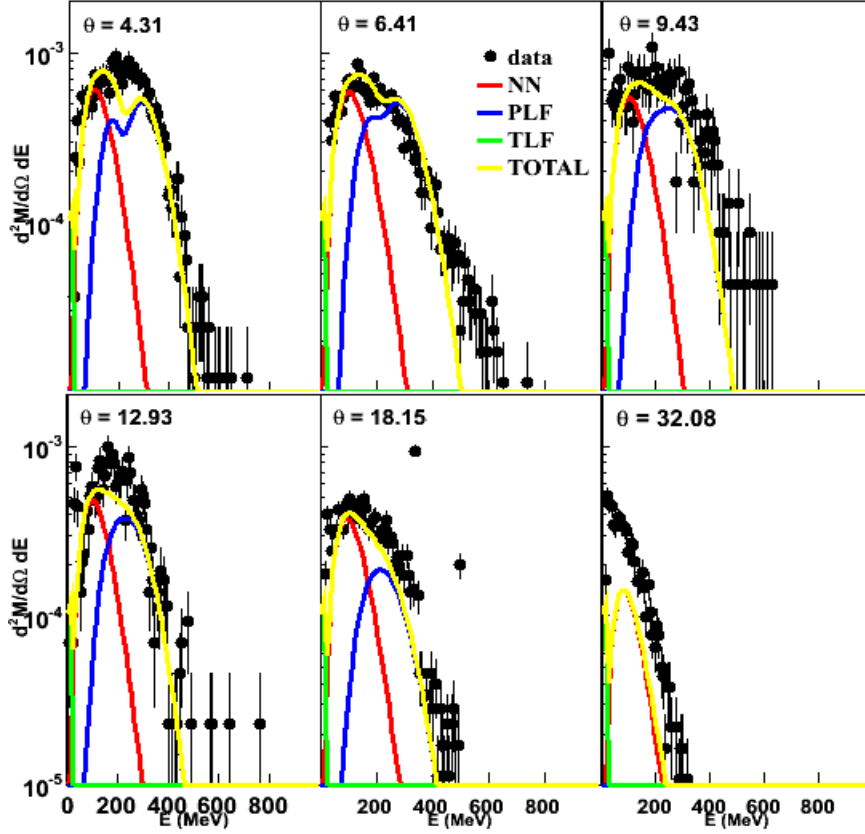
**Figure 1**. Multiplicity spectra for $^6$Li in $^{64}$Zn + $^{112}$Sn system. Black dots are experimental data, fit with PLF function (blue line), NN function (red line) and TLF function (green line). The yellow line represents the total function, given by the sum of the previous three.

To the first approximation extracted source velocities come near expected values. In fact the calculated velocity in the NN source turns to be 4.77 cm/ns, which is close to the half of beam velocity, while it is 8.58 cm/ns for the PLF, which is about 90% of beam velocity. This gives us confidence in the quality of the fit.

To study the evolution of our data with collision violence, we show in Fig. 2 the $^6$Li and $^7$Li NN multiplicity for $^{64}$Zn + $^{112}$Sn system as a function of the centrality.
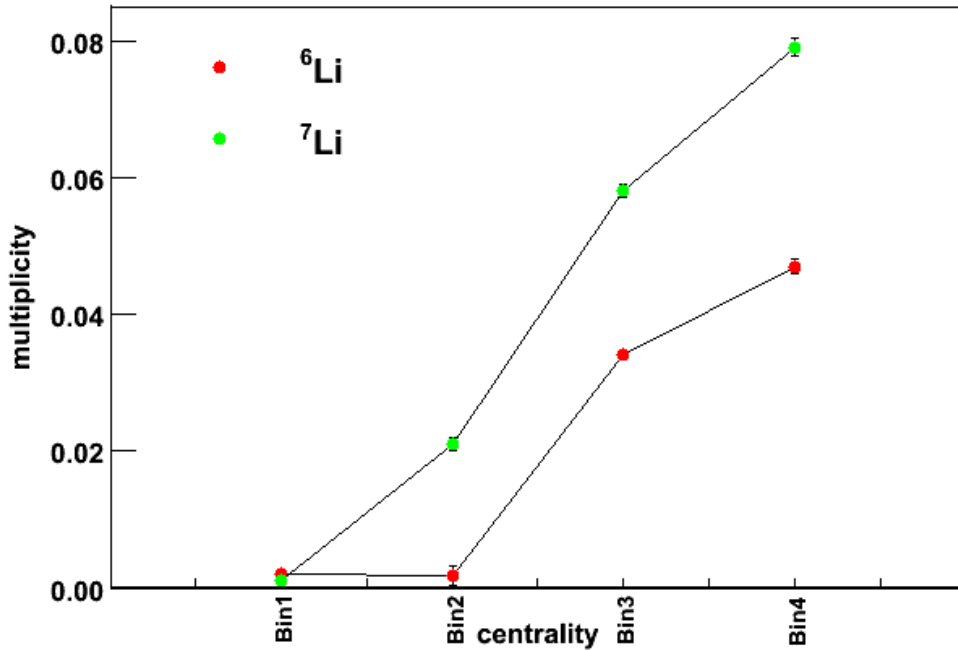
**Figure 2**. Lithium multiplicity in $^{64}$Zn + $^{112}$Sn system sorted by bin. Red dots represent $^{6}$Li multiplicity values, green dots $^{7}$Li.

We note that the number of lithium ions emitted after the collision increases with the collision violence but, in general, the absolute multiplicity is very small compared to values obtained for a particles. For example, in the case of most central collision, the multiplicity for NN component a particles is 2.009±0.230 as compared to the $^{7}$Li multiplicity of 0.0470±0.0011.

This analysis has been done for every reaction system and leads similar results. That allows us to conclude that lithium makes only a very small contribution and does not significantly change the characteristics of the emitting source.

[1] L. J. Qin *et al., Progress in Research,* Cyclotron Institute, Texas A&M University (2006-2007), p. II-5

[2] S. Wuenschel *et al., Progress in Research,* Cyclotron Institute, Texas A&M University (2006-2007), p. II-34

# Progress in BRAHMS

K. Hagel, R. Wada, J. B. Natowitz, and the BRAHMS Collaboration

The p + p measurements at RHIC provide both a baseline measurement for the $R_{AA}$, information of the Single Spin Asymmetry using the polarization information from RHIC, as well as information on the soft physics of p + p collisions. Our analysis of BRAHMS data at the Cyclotron Institute in the past year has concerned generating transverse momentum ($p_t$) hadron spectra resulting from p + p collisions at $\sqrt{s_{nn}} = 200$ GeV in order to analyze the yields of produced particles.

An example of the spectra we have generated is shown in Fig. 1 where we show proton and anti-proton spectra. The points represent the data. The spectra range from mid-rapidity to y~3.5 as noted in the legend. Each spectrum is divided by a successive factor of 10 except for the break between
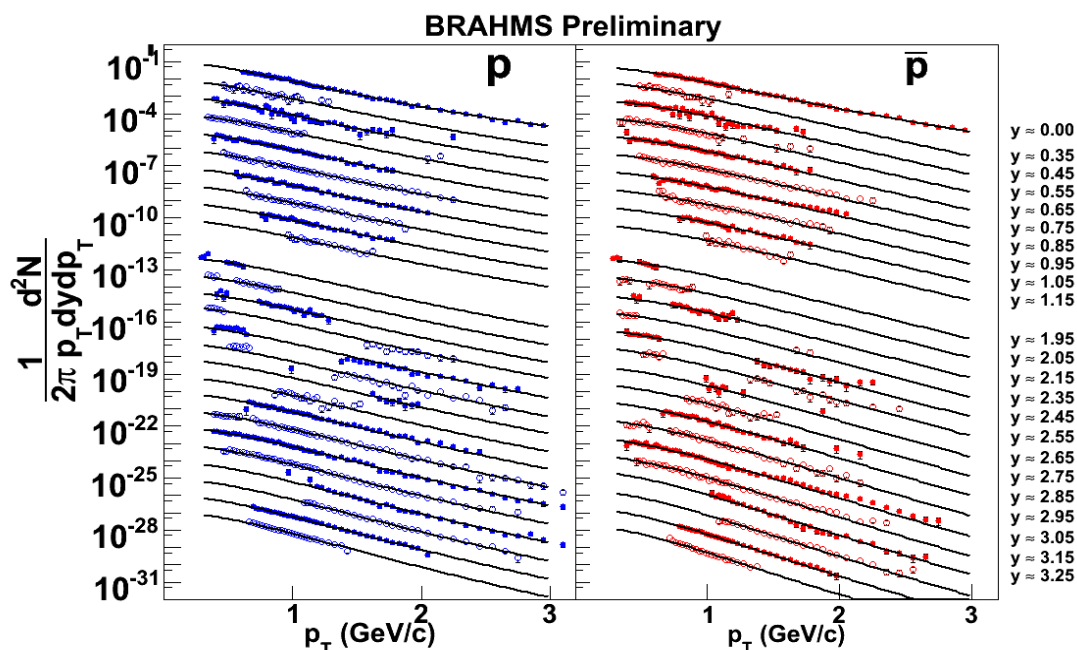


**Figure 1.** Proton and anti-proton $p_t$ spectra from mid-rapidity to y~3.5. The lines indicate the results of a global fit to a Levy function.

measurements with the mid-rapidity spectrometer and the forward spectrometer where there is a factor of 100 between them.

The solid lines represent fits to the data with a Levy function given by:

$$\frac{1}{2\pi p_T} \frac{d^2N}{dydp_T} = \frac{1}{2\pi} \frac{dN}{dy} \frac{(n-1)(n-2)}{nT\big(nT+m_0(n-2)\big)} \left(1 + \frac{(m_T - m_0)}{nT}\right)^{-n}$$

where $m_T^2 = m_0^2 + p_T^2$, and dN/dy, n and T are parameters. A global fit was performed over the entire rapidity range using $T = T_0 + ay + a_2 y^2$, $n = n_0 + by + b_2 y^2$ where the fitting parameters are dN/dy, $T_0$, a, $a_2$, $n_0$, b, $b_2$.

An interesting quantity used to study baryon transport is nuclear stopping. The BRAHMS collaboration has published information on stopping for Au + Au at $\sqrt{s_{nn}} = 200\,\text{GeV}$ [1]. We have started a similar analysis where we examine the net – proton distributions obtained from subtracting the
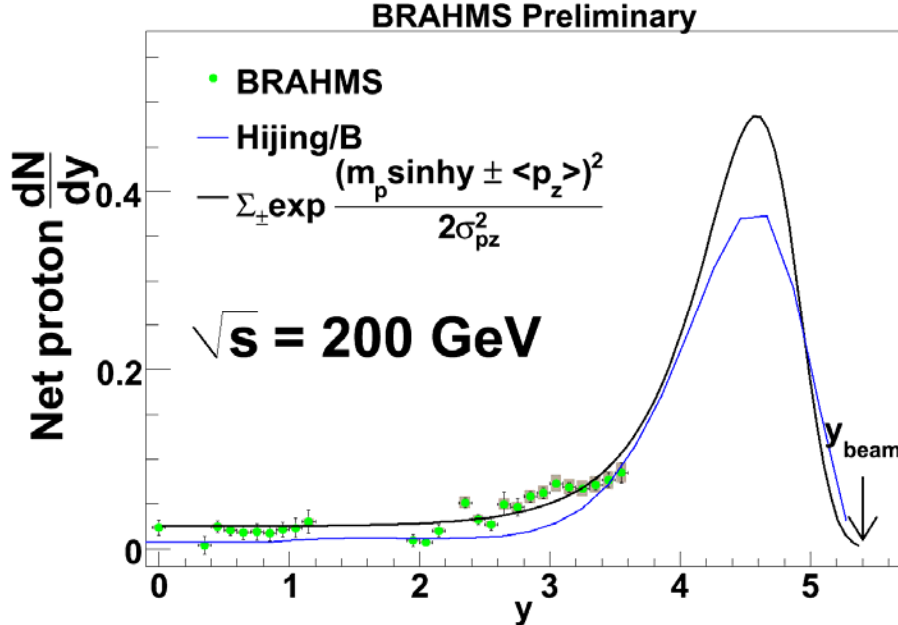


**Figure 2**. Net proton dN/dy. The blue curve indicates the prediction of Hijing/B and the black curve represents a fit to a symmetric sum of two Gaussians in momentum space.

proton and anti-proton dN/dy parameters from the fits. In principle $\langle\delta y\rangle$ should be calculated using the net-baryon distribution. However, the corrections from net-proton to net-baryon are expected to be relatively constant over the rapidity range that we have measured. The net-proton dN/dy is shown in figure 2 where the green points represent the data. We note a relatively flat distribution from mid-rapidity to y~2 and then a slight increase. In fact, we do not, as we did not in Au + Au [1], measure the bulk of the yield. We do, however, have significant information because of baryon conservation. The Hijing/B calculation (also shown in Fig. 2) indicates a net proton integral of about 0.6 in the forward region. The Hijing/B calculation indicates an average proton transport of $\langle\delta y\rangle \sim 1.2$. Allowing Hijing/B to guide us, we make a fit to a Bjorken inspired symmetric sum of two Gaussians in momentum space [2] constraining the area under the curve to be 0.6. Such a fit results in a mean momentum of 46 GeV/c with a spread of 17 GeV/c. The black curve shown in Fig. 1 shows the result of the fit and the resultant parameters indicate $\langle\delta y\rangle \sim 1.5$.

We plan to complete this analysis of this data in the coming months and publish the results of this interesting study.

[1] I. G. Bearden *et al.*, Phys. Rev. Lett. **93**, 102301 (2004).
[2] J. D. Bjorken, Phys. Rev. D **27**, 140 (1983).

# Isospin effects observed in the transverse flow of isotopically resolved fragments below the balance energy

Z. Kohley, E. Bell, K. Hagel, R. Wada, S. Soisson, A. L. Keksis, D. V. Shetty, G. A. Souliotis,
S. Wuenschel, B. Stein, S. Galanopoulos, L. W. May, L. Qin, J. B. Natowitz,
S. J. Yennello, and the NIMROD Collaboration

In heavy-ion collisions (HIC) below the balance energy an enhanced particle emission is observed in the reaction plane due to collective flow and rotation. The examination of the in-plane transverse momentum of the particles provides an opportunity to study these collective effects. The transverse flow observed in HIC allows for the investigation of properties of nuclear matter at temperatures and density away from that of cold nuclei. Collective flow, among other observables, has been used to constrain the compressibility of the nuclear EoS [1-4]. Furthermore, the transverse flow has been suggested to be sensitive to the asymmetric part of the EoS [5-8]. In particular, differences between the transverse flow of neutrons and protons have been predicted to be sensitive to the density dependence of the symmetry energy [5,6]. However, at this time it remains a difficult task to measure the flow of neutrons. Using a BNV (Boltzmann-Nordheim-Vlasov) microscopic transport code, Scalone $et$ $al.$, have shown that a comparison of the flow parameter for $^3$H and $^3$He light clusters would exhibit a similar dependence on the parameterization of the symmetry energy as the neutron and proton flows [7,8].

In this study, the transverse flow of isotopically resolved fragments has been examined in the $^{58}$Fe+$^{58}$Fe and $^{58}$Ni+$^{58}$Ni systems at 35 MeV/u and 45 MeV/u. The K500 Superconducting Cyclotron at the Texas A&M University Cyclotron Institute was used to produce the $^{58}$Fe and $^{58}$Ni beams. The NIMROD array (ca. 2000) was used to obtain the experimental data. Further experimental details can be found in Ref. [9]. In order to determine the in-plane transverse
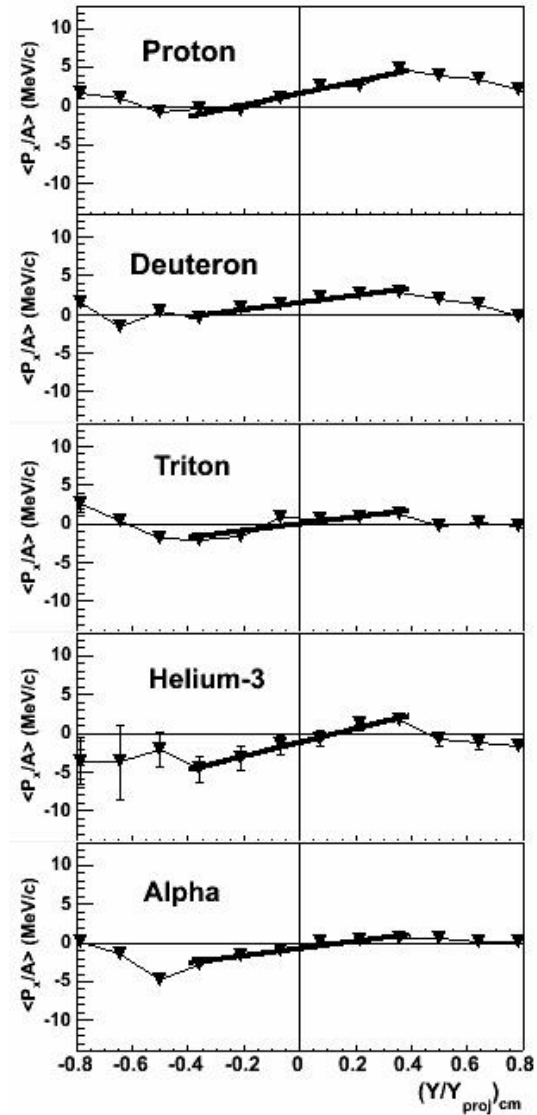


**Figure 1**. The average in-plane transverse momentum per nucleon, $<p_x/A>$, is shown as a function of the reduced rapidity for 45 MeV/u $^{58}$Ni+$^{58}$Ni system.

flow the reaction plane had to be reconstructed for each event. The Azimuthal Correlations Method by Wilson *et al.* was used to determine the reaction plane [10]. The Transverse Momentum Analysis of Danielewicz and Odyniec was used to determine the forward flow side of the reaction plane [11].

The flow parameter was extracted for proton, deuteron, triton, helium-3, and alpha particles. The flow parameter is defined as the slope of the average in-plane transverse momentum, $\langle p_x \rangle$, over the mid-rapidity region. Fig. 1 shows the average in-plane transverse momentum plotted as function of the reduced rapidity, $(Y/Y_{proj})_{cm}$ for the 45 MeV/u $^{58}$Ni+$^{58}$Ni system.. The flow parameters were extracted from linear fits, as shown in Fig. 1, over the range of -0.4 to 0.4 $(Y/Y_{proj})_{cm}$. The resulting flow parameters are shown in Fig. 2 for each system. The flow parameters for the particles from the 35 MeV/u systems are consistently larger than that of the 45 MeV/u systems due to the increased distance from the balance energy. The results in Fig. 2 also present an isospin dependence of the fragment flows on the N/Z of the compound system. As shown in Fig. 2, there is an enhancement in the fragment flow parameters for the more neutron rich $^{58}$Fe+$^{58}$Fe at both energies. This difference is best seen in the flow of the deuteron and triton fragments. This enhancement of the transverse flow with the $(N/Z)_{cs}$ has been previously observed for inclusive Z=1, 2 and 3 particles [12,13]. An isospin dependence on the N/Z of the particle of interest was also observed in comparing the flow parameters of the $^{3}$H and $^{3}$He isobars. Fig. 2 allows for the comparison of $^{3}$H and $^{3}$He for each of the 4 systems. The results show an increased flow for the helium-3 fragments in comparison to the triton fragments for each system, however the error bars for the 45 MeV/u $^{58}$Fe + $^{58}$Fe system do overlap. This difference in the transverse flow between the $^{3}$He and $^{3}$H isobars is significant because it has been predicted to be sensitive to the density dependence of the
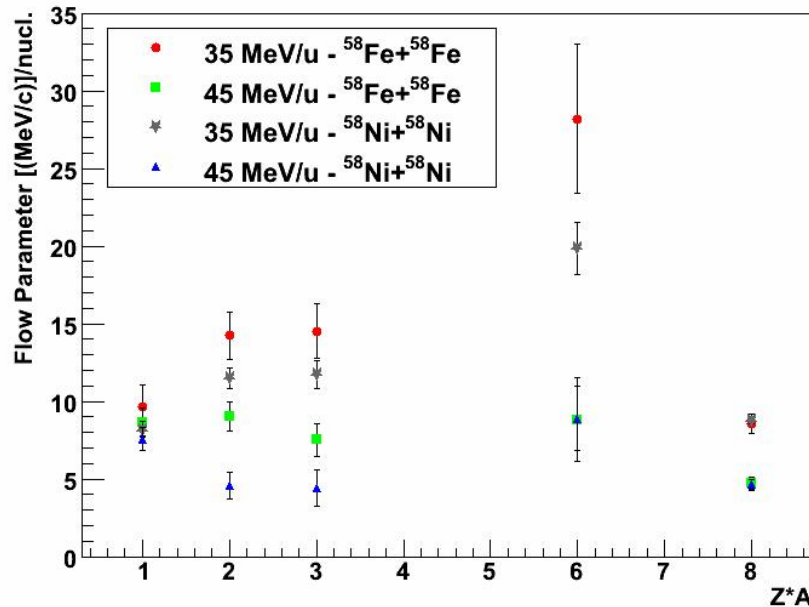


**Figure 2**. The extracted flow parameters for the protons, deuterons, tritons, helium-3 and alpha particles are shown as a function of the mass times charge (Z*A) of the fragment. Results are presented from the $^{58}$Ni + $^{58}$Ni and $^{58}$Fe + $^{58}$Fe systems at 35 MeV/u and 45 MeV/u.

symmetry energy. The observation of an increased $^3$He, in comparison to the $^3$H flow, for the $^{58}$Fe + $^{58}$Fe systems is in qualitative agreement with an "asy-stiff" calculation of Scalone *et al.* for a 55 MeV/u $^{58}$Fe + $^{58}$Fe system.

Overall, the results presented above demonstrate an isospin dependence of the transverse flow on both the N/Z of the compound system and the N/Z of the particle of interest. The observed differences in the triton and helium-3 flow suggest a possible observable which may be sensitive to the density dependence of the symmetry energy. It should be noted that the energy calibrations for this data require corrections and these results should be seen as preliminary. Further experiments to investigate these isospin dependences of the transverse flow with the NIMROD-ISIS array have been planned for the summer of 2008.

[1] P. Danielewicz, R. Lacey and W.G. Lynch, Science, **298**, 1592 (2002).
[2] S. D. Gupta and G. D. Westfall, Phyiscs Today **46**, 34 (1993).
[3] W. Reisdorf and H.G. Ritter, Annu. Rev. Nucl. Part. Sci. **47**, 663 (1997).
[4] N. Herrmann, J.P. Wessles and T. Wienold, Annu. Rev. Nucl. Part. Sci. **49**, 581 (1999).
[5] V. Baran, M. Colonna, V. Greco and M. Di Toro, Phys. Rep. **410**, 335 (2005).
[6] B.A. Li, C.M. Ko and W. Bauer, Int. J. Mod. Phys. E **7**, 147 (1998).
[7] M. Di Toro, S.J Yennello and B.A. Li, Eur. Phys. J. A **30**, 153 (2006).
[8] L. Scalone, M. Colonna and M. Di Toro, Phys. Lett. B **461**, 9 (1999).
[9] E. Bell, Ph.D. Thesis, Texas A & M University, 2005.
[10] W. K. Wilson, R. Lacey, C. A. Ogilvie and G. D. Westfall, Phys. Rev. C **45**, 738 (1992).
[11] P. Danielewicz and G. Odyniec, Phys. Lett. **157B**, 146 (1985).
[12] R. Pak *et al.*, Phys. Rev. Lett. **78**, 1026(1997).
[13] R. Pak *et al.*, Phys. Rev. Lett. **78**, 1022 (1997).

# Isoscaling and nuclear temperature studies of reconstructed quasiprojectiles from peripheral and semiperipheral collisions in the Fermi energy regime

S. Galanopoulos, G. A. Souliotis, A. L. Keksis, M. Veselsky, M. Jandel, D. V. Shetty,
Z. Kohley, S. Soisson, B. Stein, S. Wuenschel, and S. J. Yennello

One of the important observables in heavy – ion collisions is the isotopic composition of the detected fragments investigated in the isoscaling approach [1]. In this approach, the nuclear symmetry energy effects are isolated in the fragment yields allowing us to study the symmetry energy in the formation of hot fragments [2,3]. The isoscaling effect refers to an exponential relation between the yields of a given fragment (N,Z) from two reactions which differ in the isospin asymmetry N/Z [4] of the primary hot fragments and is expressed by the relation

$$R_{21}(N,Z) \equiv \frac{Y_2(N,Z)}{Y_1(N,Z)} = C\exp(\alpha N + \beta Z) \tag{1}$$

where $Y_2$, $Y_1$ are the fragment yields from a neutron rich and a neutron deficient system respectively, $\alpha$ and $\beta$ are the scaling parameters and C is an overall normalization factor. In the present work, the isoscaling effect is investigated for the case of fragments emitted during the de-excitation of quasi-projectiles (QPs), in different $(N/Z)_{QP}$ zones of the same reaction. In this way, the isoscaling parameter $\alpha$ is determined as a function of the excitation energy. The systems studied in this work are $^{40}$Ca+$^{112,124}$Sn and $^{48}$Ca+$^{112,124}$Sn at the beam energy of 45 MeV/u. The measurements were performed at the K500 Cyclotron accelerator of Texas A&M University and the projectile fragments were detected using a forward array for particle detection (FAUST) [5] and A.L. Keksis *et al.*, during his PhD dissertation [6].

The experimental determination of the QPs for each reaction can be obtained from the plots of the atomic number Z of the reconstructed events as a function of the parallel component of their velocities
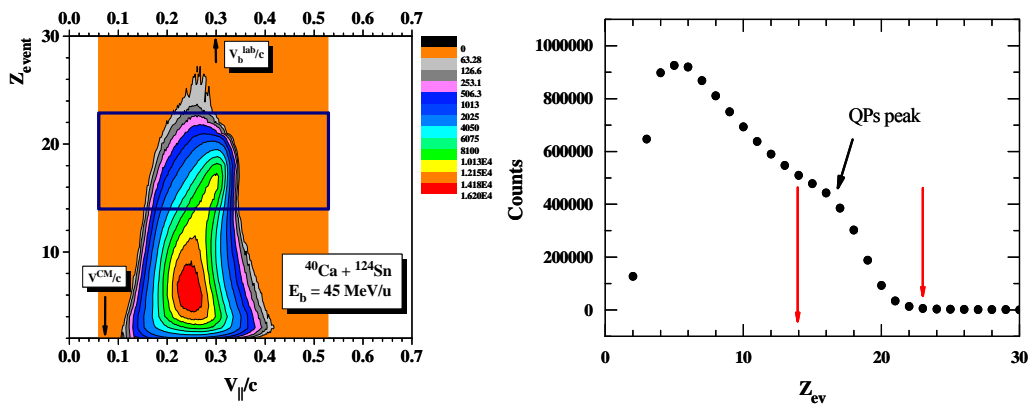


**Figure 1.** (Color online) Left panel: Selection of the reconstructed QPs from Z-$V_z$/c contour plot for the reaction $^{40}$Ca+$^{124}$Sn at 45 MeV/u. Right panel: Charge distribution of the reconstructed events. The quasiprojectiles are characterized by $Z_{QP}$=14-23 (red arrows).

with respect to the beam axis at the beam energy of 45 MeV/u. QPs are also characterized by velocities greater than the velocity of the center of mass system, $V_{QP} > V_{cm}$. The charge of the reconstructed events of the reaction $^{40}Ca+^{124}Sn$ is plotted as a function of the parallel component of their velocity with respect to the beam axis in Fig. 1 (left panel). To display better the reconstructed QPs peak, the same plot is presented in three dimensions (right figure). From plots like this in Fig. 1, one defines the Z gate for the QPs. Similar behaviour was noted for the other reactions under study.

Since the charge numbers of the QPs are known, it is possible to get the region of the N/Z ratios for the QPs as a function of the excitation energy. A typical plot of the $(N/Z)_{QP}$ ratios versus the excitation energy is shown in Fig. 2, where characteristic zones of different $N/Z_{QP}$ ratios are observed.
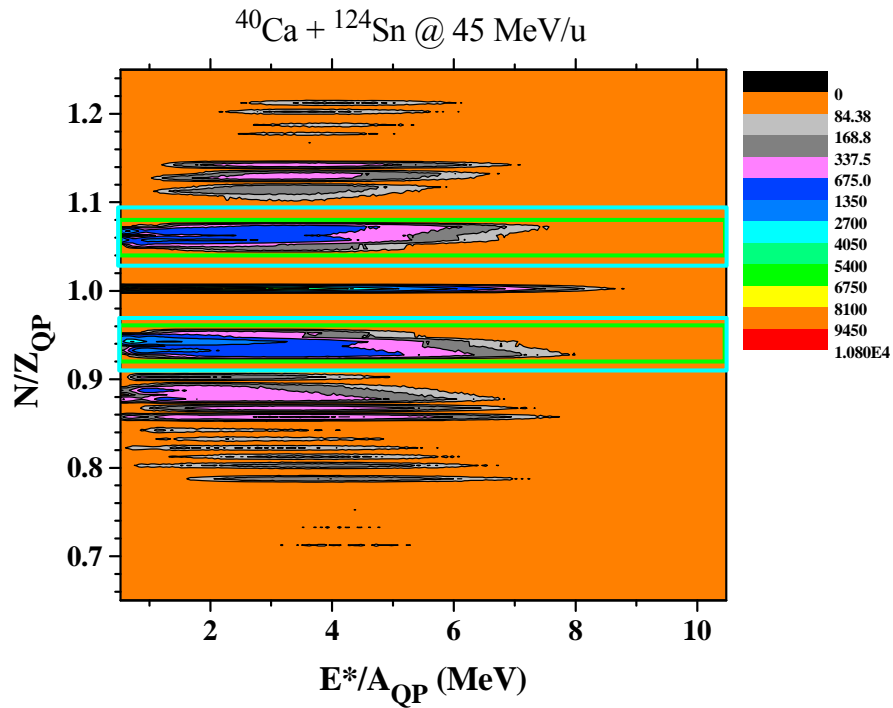


**Figure 2.** (Color online) N/Z ratio of the quasiprojectiles as a function of the excitation energy. The two green rectangulars represent the N/Z regions (0.92 – 0.96 and 1.04 – 1.08) used in the isoscaling. The same procedure was repeated for a wider $(N/Z)_{QP}$ range 0.91 – 0.97 and 1.03 – 1.09 light (blue rectangles)

To get the isoscaling parameter α for each excitation energy and for each element, two different $N/Z_{QP}$ zones were selected and the yields ratio $R_{21}$ for the isotopes obey, in logarithmic form, the expression

$$R_{21}(N) \propto \exp(\alpha N) \tag{2}$$

Applying eq. (2) for the detected isotopes of each element up to Oxygen (which was the heaviest element could be isotopically identified) and for each excitation energy region up to 8 MeV/u, we were able to extract the parameter α values as a function of the excitation energy, as implied by eq. (2), performing a linear fit to the experimental yield ratios for each element. Typical yield ratios of projectile fragments along with the straight line fits to the data points at the excitation energy window 3.5 – 4.5 MeV/u is shown in Fig. 3.
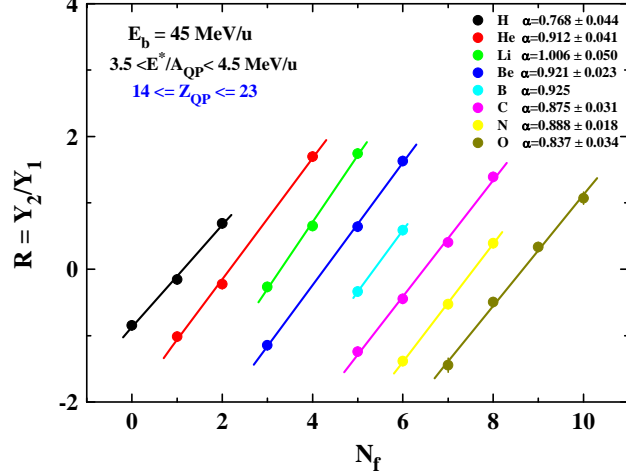


**Figure 3.** (Color online) Yield ratios $R=Y_2(N,Z)/Y_1(N,Z)$ of projectile fragments from primary fragments (QPs) with N/Z ratios $(N/Z)_2=1.04 - 1.08$ and $(N/Z)_1=0.92 - 0.96$ taken from the reaction $^{40}Ca+^{124}Sn$ at the energy of 45 MeV/u.

To further examine the sensitivity of the isoscaling parameters to the selection of two different $(N/Z)_{QP}$ regions, the observable $\xi = \langle \alpha \rangle / \Delta$ used, where $\Delta = (Z/A)_1^2 - (Z/A)_2^2$ was determined from the experimental data. In Fig. 4, it is shown that the ratio $\langle \alpha \rangle / \Delta$ is independent on choice of $(N/Z)_{QP}$ region and its value decreases as the excitation energy increases.

The isoscaling parameter α, the nuclear temperature T and the difference in proton fraction squared of the sources Δ as a function of the excitation energy are related with the symmetry energy coefficient $C_{sym}$ [4] via the expression $\alpha T = 4C_{sym}\Delta$. It is thus
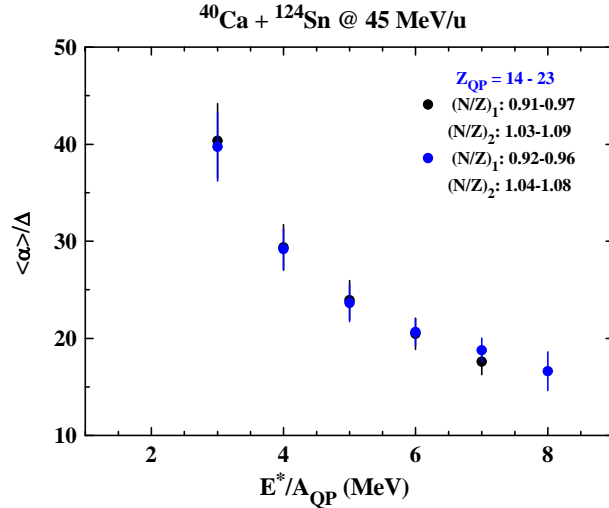


**Figure 4.** $\langle \alpha \rangle / \Delta$ measurements for different $(N/Z)_{QP}$ regions (blue and black dots) as a function of the excitation energy for the reaction system $^{40}Ca+^{124}Sn$ at the beam energy of 45 MeV/u (see text).

important to investigate the excitation energy dependence of the nuclear temperature. The experimental

determination of the nuclear temperatures was carried out using the double isotope ratios method. The isotope yield ratio thermometer requires the yields of four isotopes and is obtained from [7]

$$T = \frac{B}{\ln(\alpha \cdot R)} \tag{3}$$

where, B is a binding energy parameter, $\alpha$ is the statistical factor that depends on the statistical weights of the spins of nuclei involved in the calculation and R is the isotope yield ratio given by the expression

$$R = \frac{Y(A_1, Z_1)/Y(A_1 + 1, Z_1)}{Y(A_2, Z_2)/Y(A_2 + 1, Z_2)} \tag{4}$$

Using the eqs. (3) and (4) and different isotope pairs in the denumerator of eq. (3), namely d, t and $^{12}$C, $^{13}$C, the nuclear temperature was determined as a function of the excitation energy. It is important to note
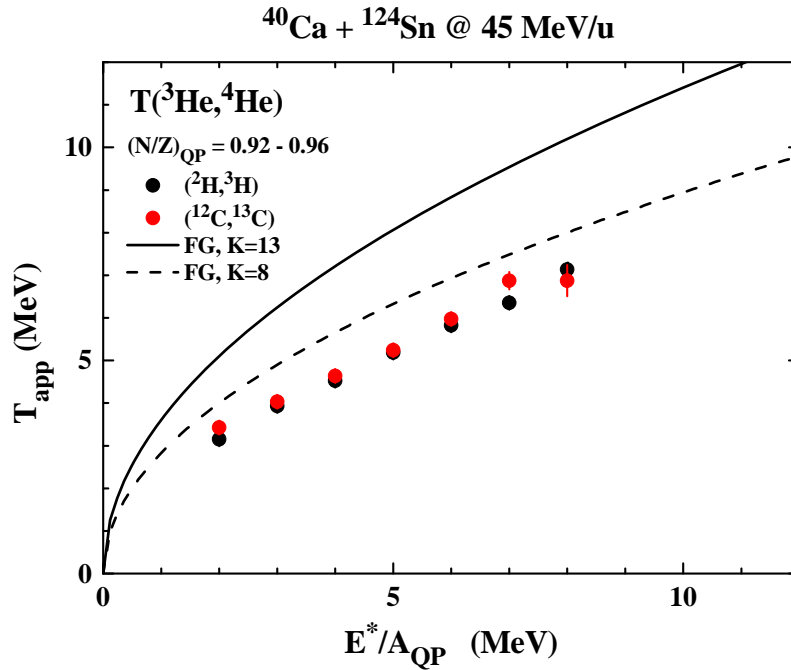


**Figure 5.** (Color online) Apparent isotope temperatures T($^3$He,$^4$He) derived from ($^2$H,$^3$H) and ($^3$He,$^4$He) isotope pairs as a function of the excitation energy for the (N/Z)$_{QP}$ region 0.92 – 0.96. The agreement between the two thermometers (black and red dots) is obvious. The solid and dashed lines are the predictions of the Fermi-gas model with inverse level density parameter K=13 and 8 respectively. Similar behaviour is observed for the other reactions under study.

at this point that the measured temperatures in Fig. 5 are not corresponding to the temperature of the

source (quasi-projectiles), since corrections for sequential decay of the quasi-projectiles have not taken into account yet.

We plan to investigate the relation among the isoscaling parameter α, nuclear temperatures T and the symmetry free energy $F_{sym}$. Moreover, statistical and dynamical codes will be used and comparisons with the data will be made.

[1] M. B. Tsang *et al*., Phys. Rev. Lett. **86**, 5023 (2001).

[2] G. A. Souliotis *et al.*, Phys. Rev. C **75**, 011601(R) (2007).

[3] D. V. Shetty *et al.*, Phys. Rev. C **75**, 034602 (2007).

[4] A. S. Botvina *et al*., Phys. Rev. C **65**, 044610 (2002).

[5] F. Gimeno-Nogues *et al*., Nucl. Instrum. Methods Phys. Res. **A399**, 94 (1997).

[6] A. L. Keksis, PhD Thesis, Texas A&M University, 2007.

[7] S. Albergo *et al.*, Nuovo Cimento A **89**, 1 (1985).

# Semiclassical simulations of peripheral heavy-ion collisions at Fermi Energies and the sensitivity to the density dependence of the nuclear symmetry energy

G. A. Souliotis, D. V. Shetty, S. Galanopoulos, and S. J. Yennello

During the last several years we have undertaken a systematic study of heavy residues formed in quasi-elastic and deep-inelastic collisions near and below the Fermi energy. The original motivation of these studies was the understanding and the optimization of the production of very neutron-rich rare isotopes in these collisions [1,2,3]. In parallel, we became motivated to pursue these studies further in hopes of extracting information on the properties of the nuclear effective interaction as manifested in the mechanism of nucleon exchange and the course towards N/Z equilibration [4].

Recently, we focussed our interest on the possibility of extracting information on the isospin part of the nuclear equation of state (EOS) by comparing our heavy residue data to detailed calculations using microscopic models of heavy-ion collisions at these energies [5]. After some initial efforts with transport-type codes (BUU, BNV), we turned our attention to the quantum molecular dynamics approach (QMD). We have performed detailed calculations using the recent version of the constrained molecular dynamics code CoMD of A. Bonasera and M. Papa [6,7]. This code is especially designed for reactions near and below the Fermi energy. It



**Figure 1**. Density dependence of the nuclear symmetry energy $C_{sym}(\rho)$ corresponding to the choices of the nucleon-nucleon symmetry potential in the CoMD code: blue (asy-soft), red: (asy-stiff), green (super asy-stiff) and grey line (no-symm). The black line represents the form $31.6(\rho/\rho_0)^{0.69}$ consistent with the isoscaling analysis of IMFs from central heavy-ion collisions [8].

implements an effective interaction corresponding to a nuclear-matter compressibility of K=200 (soft EOS) with several forms of the density dependence of the nucleon-nucleon symmetry potential (Fig. 1) [8]. While not using antisymmetrized N-body wave functions, CoMD imposes a constraint in the phase space occupation for each nucleon, effectively restoring the Pauli principle at each time step of the

collision. This constraint preserves the fermionic nature of the interacting nuclei in a satisfactory manner [6]. The latest version (CoMD-II) also fully preserves the total angular momentum along with linear momentum and energy [7].

Results of the calculations and comparisons with our residue data are shown in Figs. 2-5. Fig. 2 shows the calculated average quasiprojectile angle (upper panel) and excitation energy per nucleon (lower panel) as a function of the mass of the (primary) quasiprojectiles. The black line corresponds to the prediction of the deep-inelastic transfer (DIT) code of Tassan-Got that has been extensively used in our studies of quasiprojectile formation near the Fermi energy [9]. The light blue curve shows the prediction of the heavy-ion phase-space exploration (HIPSE) model [10]. The remaining four lines are the results of CoMD calculations with symmetry potential options referred to as: "asy-soft" (blue line), "asy-stiff" (red line), "super asy-stiff" (green line) and "no-symm" (grey line). The first three forms correspond to a dependence of the symmetry-potential $V_{symm}$ on the ½, 1 and 2 power of the density, respectively, whereas in the last case ("no-symm") this potential is set to zero - thus, only the kinetic part of the symmetry energy plays a role in this case (see, also Fig. 1). The CoMD calculation was stopped at t=300 fm/c. We observe differences between the predictions of DIT, HIPSE and CoMD that we will try to further investigate and understand in the near future. Regarding CoMD,



**Figure 2**. Mean quasiprojectile angle (upper panel) and excitation energy per nucleon (lower panel) as a function of quasiprojectile mass for the reaction $^{86}$Kr(25MeV/nucleon) + $^{124}$Sn. Black line: DIT. Light-blue line: HIPSE. Blue (asy-soft), red (asy-stiff), green (super asy-stiff) and grey (no-

despite the observed fluctuations of the mean values, we may tentatively conclude that the mean quasiprojectile angle is not sensitive to the choice of the symmetry potential. However, the mean excitation energy shows some sensitivity in the choice that deserves further exploration.

In Fig. 3, the distributions of the mean angle, mean velocity and yield as a function of the mass of the (final) observable fragments are shown. The deexcitation of the primary fragments was done with the sequential decay code GEMINI [11]. The meaning of the curves is as before: black line: DIT, coloured lines: CoMD. The top panel shows, along with the calculations, the angular acceptance of the MARS separator $\Delta\theta$=3$^o$-6$^o$ for our measurements (dashed horizontal lines). In the middle and lower panels, the MARS data [1] are shown with solid symbols. The calculations in both cases are filtered with the angular
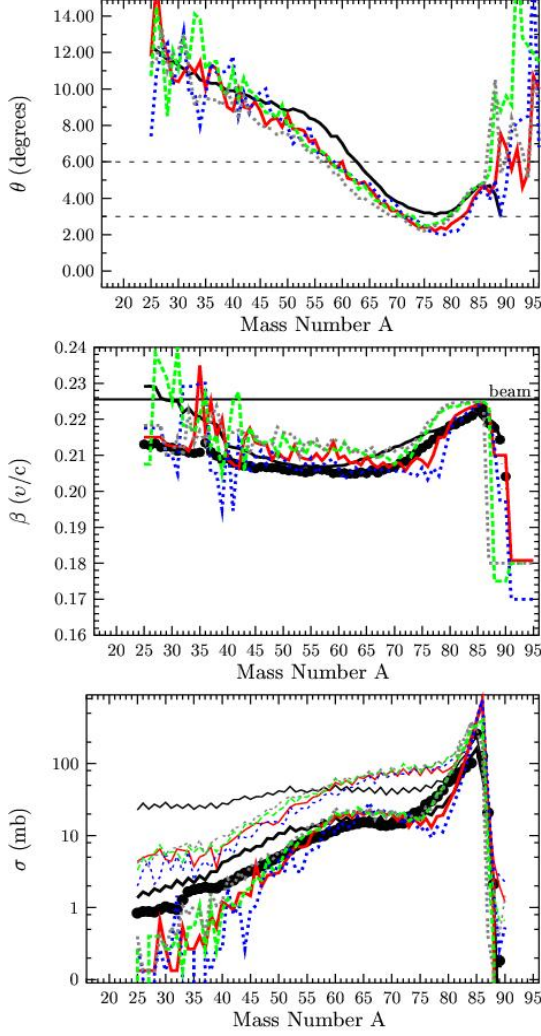
**Figure 3**. Mean angle (upper panel), mean velocity (middle panel) and yield (lower panel) as a function of projectile residue mass for the reaction $^{86}$Kr (25MeV/nucleon) + $^{124}$Sn. Black line: DIT. Blue (asy-soft), red (asy-stiff), green (super asy-stiff) and grey (no-symm): CoMD calculations (see text). Black points: MARS data [1]

acceptance of the separator. Additionally, in the lower panel, the thin lines show the calculations of the total residue yields. We observe an overall satisfactory agreement of the CoMD calculations with the data and again, in the CoMD calculations, an insensitivity to the choice of the symmetry potential. The situation is similar for the
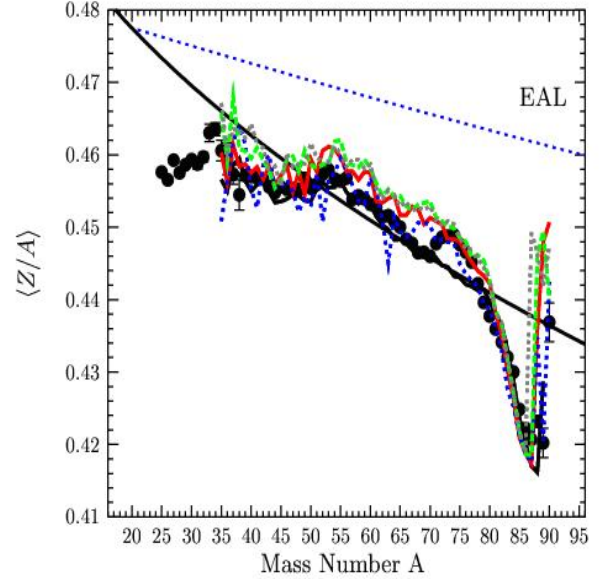


**Figure 4**. Mean projectile residue Z/A as a function of residue mass for the reaction $^{86}$Kr(25MeV/nucleon) + $^{124}$Sn. Black line tracing the data: DIT. Blue (asy-soft), red (asy-stiff), green (super asy-stiff) and grey (no-symm): CoMD calculations (see text). Black points: MARS data [1]. Black line: line of stability.

comparison of the mean Z/A values of the observed residues with the CoMD calculations shown in Fig. 4.

In Fig. 5, upper panel, we show the calculated mean $(Z/A)^2$ of the primary quasiprojectiles as a function of the excitation energy per nucleon. The meaning of the curves is as in Fig. 2. The upper set of curves is for the $^{86}$Kr(25MeV/nucleon) + $^{112}$Sn reaction and the lower set is for the $^{86}$Kr(25MeV/nucleon)+$^{124}$Sn reaction. The solid horizontal line corresponds to the $(Z/A)^2$ of the projectile, whereas the upper and lower dashed lines give the $(Z/A)^2$ of the fully equilibrated systems in the two cases. In the lower panel of the figure we show the difference of the calculated mean $(Z/A)^2$ values, along

with our data (solid and open points) from the heavy-residue isoscaling analysis of [4]. It is interesting to note that the CoMD calculations show sensitivity in the choice of the symmetry potential. However, this observation may be subject to the inherent uncertainty in the determination of the excitation energy of the quasiprojectiles. In the present calculations, the excitation energy has been determined from the difference of the binding energy of the (hot) quasiprojectiles as given by the CoMD code and the corresponding binding energy taken from mass tables. We have investigated the issues of the excitation energy determination and we believe that, except for very peripheral collisions (essentially corresponding to direct reactions) the CoMD code provides a reliable estimate of the excitation energies of the quasiprojectiles. The comparison presented in Fig. 5 suggests a rather stiff dependence of the symmetry energy on density (Fig. 1) in overall agreement with other studies, as presented in Ref. [7] (and references therein).



**Figure 5**. Upper panel: Mean $(Z/A)^2$ of quasiprojectiles as a function of excitation energy per nucleon for the 25 MeV/nucleon reactions: $^{86}Kr+$ $^{112}Sn$ (upper set of curves) and $^{86}Kr+$ $^{124}Sn$ (lower set of curves). Black lines DIT. Blue (asy-soft), red (asy-stiff), green (super asy-stiff) and grey (no-symm): CoMD calculations (see text). Lower panel: Difference in quasiprojectile mean $(Z/A)^2$ . Lines as above.

As part of our detailed consistency checks of the CoMD model framework, we report in Fig. 6 the predicted neutron skin of the $^{86}Kr$ nucleus using the four options of the symmetry potential. The values of the skin show a small sensitivity to the density dependence of the symmetry potentials and are in agreement with expectations from microscopic SHF or Thomas-Fermi calculations. In the same vein, Fig. 7 presents the giant dipole resonance (GDR) spectrum of the $^{86}Kr$ nucleus obtained from the Fourier transform of the spatial oscillation of the neutron vs proton spheres within the CoMD model. The symmetry potentials employed seem to give reasonable values for the GDR energy centroids (although somewhat lower that the value 16.8 MeV expected from empirical systematics [12,13]) and widths ~ 4 MeV in very good agreement with expectations for near ground-state nuclei [12].

Finally, we plan to explore the N/Z equilibration process (e.g., Fig. 5) in greater detail via comparisons of CoMD calculations with our new experimental data from 15 MeV/nucleon [40]Ar and [86]Kr projectiles on [64,58]Ni and [124,112]Sn targets that are currently under analysis.
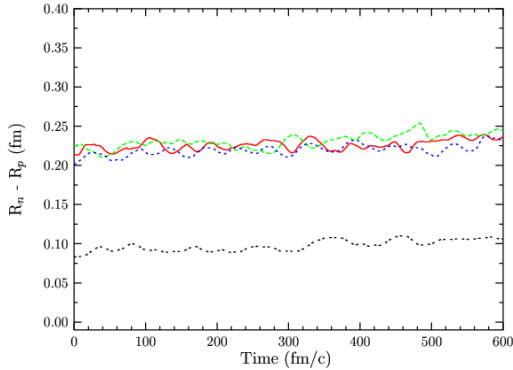


**Figure 6**. Time evolution of the neutron skin of an isolated [86]Kr nucleus predicted by CoMD. Blue (asy-soft), red (asy-stiff), green (super asy-stiff) and gray line (no-symm): choices of the nucleon symmetry potential (see text).
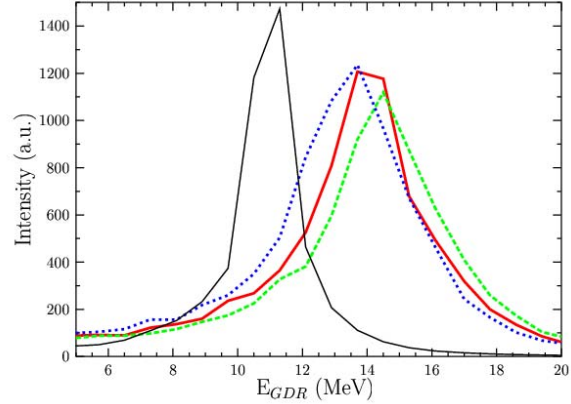


**Figure 7**. Giant dipole resonance (GDR) response of an isolated [86]Kr nucleus predicted by CoMD. Blue (asy-soft), red (asy-stiff), green (super asy-stiff) and black line (no-symm): choices of the nucleon symmetry potential (see text). The expected value of the energy according to the empirical GRD systematics is 16.8 MeV (see text) [12,13].

[1] G. A. Souliotis *et al.*, Phys. Rev. Lett. **91**, 022701 (2003).

[2] G. A. Souliotis *et al.*, Nucl. Instrum. Methods Phys. Res. **B204**, 166 (2003).

[3] M. Veselsky and G. A. Souliotis, Nucl.Phys. **A765**, 252 (2006).

[4] G. A. Souliotis *et al.*, Phys. Lett. B **588**, 35 (2004).

[5] A. Ono and J. Randrup, Eur. Phys. J. A **30**, 109 (2006).

[6] M. Papa *et al.*, Phys. Rev. C **64**, 024612 (2001).

[7] M. Papa *et al.*, J. Comp. Phys. **208**, 403 (2005).

[8] D. V. Shetty, S. J. Yennello, and G. A. Souliotis, Phys. Rev. C **76**, 024606 (2007).

[9] L. Tassan-Got and C. Stephan, Nucl. Phys. **A524**, 121 (1991).

[10] D. Lacroix  *et al.*, Phys. Rev. C **69**, 054604 (2004).

[11] R. Charity *et al.*, Nucl. Phys. **A483**, 391 (1988).

[12] D. Santonocito and Y. Blumenfeld, Eur. Phys. J. A **30**, 183 (2006).

[13] L. Trippa, G. Colo, and E. Vigezzi, [nucl-th] arXiv:0802.3658 (2008).

# An empirical relation for studying the nuclear symmetry energy as a function of excitation energy in various mass regions

D. V. Shetty, G. A. Souliotis, S. Galanopoulos, Z. Kohley, S. N. Soisson, B. C. Stein,
S. Wuenschel, and S. J. Yennello

Information on the symmetry energy is crucial for understanding nuclei that can be produced in extreme conditions of density, excitation energy and $N/Z$ asymmetry. Currently, there exists no detailed understanding of how the symmetry energy evolves with the excitation energy of hot nuclei over a large range of nuclear masses. In this work, we report an empirical relation for studying the symmetry energy in various mass regions.

The symmetry energy of finite nuclei at saturation density is often extracted by fitting ground state masses with various versions of the liquid drop mass formula. However, real nuclei are cold ($T \sim 0$ MeV), nearly symmetric ($N \sim Z$) and found at equilibrium density ($\rho_o \sim 0.16$ fm$^{-3}$). Also, one needs to decompose the symmetry term of the liquid drop into bulk (volume) and surface terms along the lines of the liquid droplet model, and identify the volume symmetry energy coefficient as the symmetry energy derived from infinite nuclear matter at saturation density. In a previous work [1], we had shown how a constraint on the density dependence of the symmetry energy of infinite nuclear matter can be obtained from multifragmentation studies. Following the expression for the symmetry energy of finite nuclei at normal nuclear density by Danielewicz [2], and using the constraint obtained from our work on the symmetry energy of infinite nuclear matter, one can write the symmetry energy of a finite nucleus of mass $A$, as,

$$S_A(\rho) = \alpha(\rho/\rho_o)^\gamma / [1 + (\alpha(\rho/\rho_o)^\gamma / \beta A^{1/3})] \tag{1}$$

where, $\alpha$ = 31 - 33 MeV, $\gamma$ = 0.55 - 0.69 and $\alpha/\beta$ = 2.6 - 3.0. The quantities $\alpha$ and $\beta$ are the volume and the surface symmetry energy at normal nuclear density. At present, the values of $\alpha$, $\gamma$ and $\alpha/\beta$ remain unconstrained. The ratio of the volume symmetry energy to the surface symmetry energy ($\alpha/\beta$), is closely related to the neutron skin thickness [2]. Depending upon how the nuclear surface and the Coulomb contribution is treated, two different correlations between the volume and the surface symmetry energy have been predicted [3] from fits to nuclear masses. Experimental masses and neutron skin thickness measurements for nuclei with $N/Z > 1$ should provide further constraint on the above parameters.

Fig. 1 shows the symmetry energy as a function of excitation energy obtained from the above empirical relation, Eq. 1, for $A$ = 40, 150 and 197. These are shown by the dashed curves in top three panels of Fig. 1. The calculation was done with the parameters, $\alpha$ = 31.6 MeV, $\gamma$ = 0.69 and $\alpha/\beta$ = 2.6. The figure also shows the experimentally determined symmetry energy from our multifragmentation studies of $^{58}$Ni + $^{58}$Ni, $^{58}$Fe + $^{58}$Ni and $^{58}$Fe + $^{58}$Fe reactions. These are shown by the solid circles and inverted triangle symbols for mass $A \sim 150$. The solid squares in the figure correspond to the data measured in a previous study [4] at lower excitation energies. One observes that the result of the empirical relation is in good agreement with the experimentally deduced symmetry energy as a function of excitation energy.

In order to compare the empirical relation with a more formal calculation, we also show in the figure the results of the Thomas Fermi calculation [5] for $A = $ 40, 150 and 197. These are shown by the solid blue curves in the top three panels of Fig. 1. To be consistent with the Thomas-Fermi calculation, the excitation energy dependence of the density of the expanding nucleus, assumed in Eq. 1, were the same as those obtained from the Thomas-Fermi calculation. The excitation energy dependence of the density assumed in Eq.1 are shown by solid curves in the bottom most panel of Fig. 1 for nuclear masses of $A = $ 40, 150 and 197. Also shown in this plot are the densities obtained from our multifragmentation studies (solid circles and inverted triangles) and those from Ref. [6] (star symbols). The comparison shows that the numerical values obtained from Eq. 1 agrees very well with the Thomas Fermi calculation over a wide range of nuclear mass and excitation energy. The empirical relation can be used to obtain a quick estimate of the symmetry energy as a function of excitation energy in future measurements for very light and heavy nuclei.
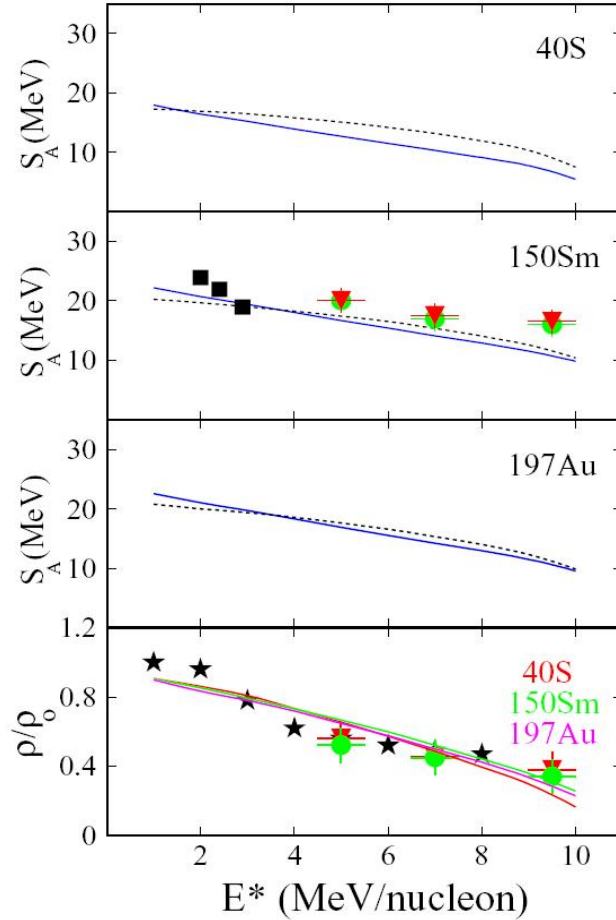


**Figure 1.** Top three panels: Symmetry energy as a function of excitation energy for $A = $ 40, 150 and 197. The solid blue curve corresponds to the Thomas-Fermi calculation and the dotted curve to the empirical relation, Eq. 1. Bottom panel: Density as a function of excitation energy. The curves are from the Thomas-Fermi calculation. The star symbols are data from Ref. [6]. The solid circle and inverted triangle symbols are from Ref. [1]. The solid squares are from Ref.. [4].

[1] D. V. Shetty, S. J. Yennello and G. A. Souliotis, Phys. Rev. C **75**, 034602 (2007).

[2] P. Danielewicz, Nucl. Phys. **A727**, 233 (2003).

[3] A. W. Steiner, M. Prakash, J. M. Lattimer, and P. J. Ellis, Phys. Rep. **411**, 325 (2005).

[4] G. A. Souliotis *et al*., Phys. Rev. C **73**, 024606 (2006).

[5] S. K. Samaddar, J. N. De, X. Vinas, and M. Centelles, Phys. Rev. C **76**, 041602 (2007).

[6] J. B. Natowitz, K. Hagel, Y. Ma, M. Murray, L. Qin, S. Shlomo, R. Wada, and J. Wang, Phys. Rev. C **66**, 031601 (2002).

# A new method of point-to-curve distance calculations

L. W. May, S. Wuenschel, B. Stein, and S. J. Yennello

One method of particle identification in heavy ion collisions is ΔE vs. E. These plots are often analyzed by linearization as described in [1]. This requires the determination of distance between any given data point and a curve of known form. A new method was developed for determining the exact distance between a point and a curve and is outlined below.

Three other methods of distance determination have been previously used: horizontal distance, vertical distance and distance along a 45-degree line. The challenge lies in that a method is needed that works over the whole range of a line of extreme curvature. The development of the new Point-to-Curve method is an attempt to reach a more accurate determination of distance globally over all regions. The horizontal and vertical methods simply take distances along paths parallel to the axes that intersect the curve, while the 45-degree method does the same, but tracks along a path that occurs at the angular bisection of the two axes.

There is a mathematical similarity between the 45-degree line and the Point-to- Curve methods. The method of using a 45-degree line to find the closest distance between a point and line is done by parameterization of the equation for the curve into a vector in terms of x and y values. For instance, a curve denoted by the equation $y = 3x^2 - 6x + 10$ would become the vector $r = (x, 3x^2 - 6x + 10)$. The value for the point in question, $p = (x1, y1)$, is then subtracted from the vector r giving $r - p = (x-x1, 3x^2 - 6x + 10 - y1)$. Now, since the slope of a 45-degree line is exactly 1 and slope is defined as the change in y divided by the change in x, then for a 45-degree line $\Delta y = \Delta x$ and $\Delta y - \Delta x = 0$. As $r - p$ is a representation of the change in y and change in x, then the x-value of $r - p$ is subtracted from the y-value of the vector and the resulting equation is set to zero. The resulting equation is solved for x and the values given should be solutions to the 45-degree line approximation. Since several possible roots can be given as solutions, constraints can be placed on the output such that only the value within the desired range will be found. The other solutions can be discarded because the equation solved is a general equation over the entire Euclidean space. The final x-value obtained is the x location of the intersection of the curve and the 45-degree line. This value can then be used to find the y-value of intersection and then a simple distance formula, $d^2 = (x1 - 2)^2 + (y1 - y2)^2$ can be used to determine the distance between the point and the curve along a 45-degree line.

Like the 45-degree line method, Point-to-Curve uses the parameterization of the curve and the value of the point to fix $r - p$. Since $r - p$ is a measure of the deviation in x and y between the point and the curve, this value can be squared by taking the dot product $(r - p) \cdot (r - p)$. This equation is minimized yielding points on the chosen curve, one of which will be the minimum for calculating the distance between the point and curve. The minimization is done by setting the derivative of the dot product equal to zero and solving for x. These values can be both real and imaginary, but as imaginary values give non-physical results, these values can be discarded. The same location constraints from the 45-degree line method can be applied to the solutions and the one remaining solution is the x-intersection of the curve and the line drawn from the point to the curve with the smallest possible distance. This x-intersection

value can then be used to find the y-intersection value from the equation of the curve and the distance formula applied to the intersection values and the value of the point to give the actual distance between the point and the curve.

The computationally intensive step in both of these methods is in the factorization of the polynomial. Polynomial factorization has been demonstrated as an NP-complete problem, meaning that the time it takes to factor the polynomial completely scales exponentially with the size of the polynomial. This is not a problem for polynomials of order 4 or less, since these can be solved analytically using known algorithms. A problem could arise if high order functions are used to model the line. However, for the types of plots common for $\Delta E$ vs. E and CsI fast-slow data this is not prohibitive as the use of spline fits allows the order of the resulting polynomial to be kept low enough (no greater than 5 or 6) that the time to factor the polynomial is quite low. The factoring algorithm used in this case is that found in the GSL library packages linked in the ROOT [2] analysis package.

The Point-To-Curve method is more theoretically robust than the other three methods and should yield an exact analytical answer to the question of distances while the other methods give approximations. While the Point-To-Curve method could potentially use more computational time, all tests on actual data have shown that at the level the method is currently used, there is no noticeable time difference in the calculations.

[1] S. Wuenschel *et al.*, *Progress in Research*, Cyclotron Institute, Texas A&M University (2007-2008), p.II-28.
[2] Rene Brun and Fons Rademakers, ROOT - An Object Oriented Data Analysis Framework, Proceedings AIHENP'96 Workshop, Lausanne (September 1996); Nucl. Instrum. Methods Phys. Res. **A389**, 81 (1997). See also http://root.cern.ch/.

# Analysis of $^{86,78}$Kr + $^{64,58}$Ni data taken on the upgraded NIMROD-ISiS

S. Wuenschel, S. Galanopoulos, K. Hagel, Z. Kohley, L. W. May, J. B. Natowitz, D. V. Shetty,
S. N. Soisson, G. Souliotis, B. C. Stein, R. Wada, and S. J. Yennello

Projectile fragmentation data from the reaction of $^{86,78}$Kr with $^{64,58}$Ni at 35MeV/u was taken on the upgraded NIMROD-ISiS detector [1]. The data was taken with high multiplicity and downscaled minimum bias triggers as well as a pulser trigger for Neutron Ball background. A total of 209 hours of data were taken.

Data analysis started with particle identification of the delta E- E and CsI Fast-Slow plots. Linearization was chosen rather than gating as a result of its improved isotope separation and error analysis capabilities. The linearization method was based on an established method of R. Wada. Lines are chosen for each element with two chosen for Hydrogen. A graphical user interface was developed for the line picking/adjusting. The linearization method intrinsically depends on the user's ability to create a smooth line and then calculate an accurate distance between the data points and the line. A new method of distance calculation was developed and is described in [2].

Once a distance can be calculated between the data points and the chosen lines, the data can then be re-plotted as a function of element (defined from the line) and channel number (which roughly correlates to energy). This plot is then projected onto the X-axis yielding a visual and quantitative quality of the line fit (Figure 1). This plot can then be analyzed for charge and mass particle identification.
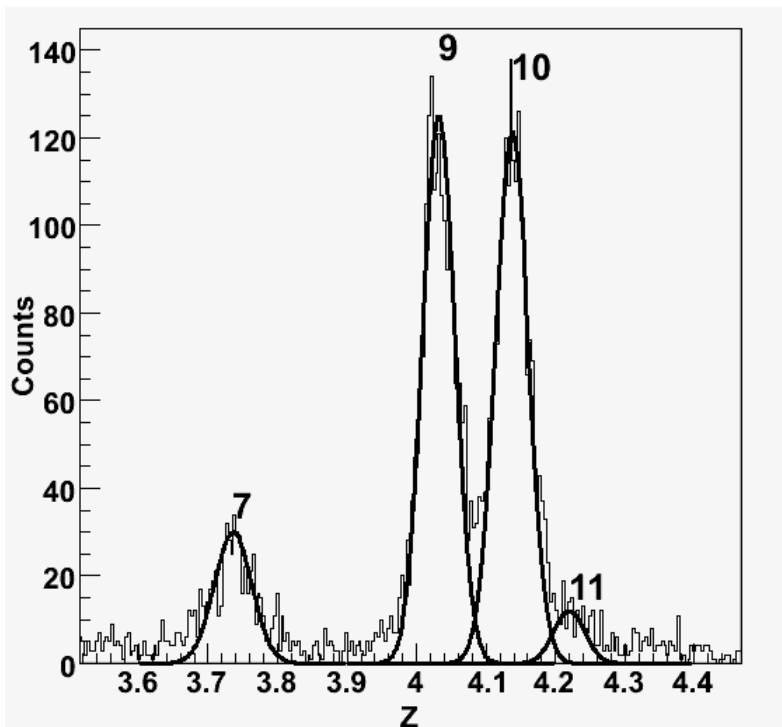


**Figure 1.** A 1D projection of linearized data with fitted Gaussian functions.

To establish a reliable estimate of mass for peaks that are not completely separated, Gaussians were fitted to the isotopes of each element in each detector. An idea of the error in mass identification can then be made from the probability of the particle belonging to the peak of a particular isotope.

Resolution can be improved by the addition of upper and lower limits on the data. Upper limits are used to cut saturated data points while low thresholds cut out low level noise inherent in the detectors.

Energy calibration of the data is underway. The silicon detectors are calibrated using a combination of punch-through points and punch-in points.  These methods have been compared and shown to agree within a few percent. The energy loss characteristic of heavy particles is dominated by the silicon signals, so they can be calibrated using an extrapolation of the silicon energy to total energy based on the Orsay energy loss tables. Intermediate mass fragments are also calibrated by this method though considerably more sensitive to minor changes in the silicon calibration.  The light charged particles (Z=1,2,3) are calibrated using the cesium iodide slow signal through the Tassan-Got [3] formula. The calibrations for the light charged particles are compared to earlier NIMROD data for which the calibration is very well established. This will ensure consistency of the current data set.

[1] S. Wuenschel *et al.*, *Progress in Research*, Cyclotron Institute, Texas A&M University (2006-2007), p. II-34.
[2] L. W. May *et al.*, *Progress in Research*, Cyclotron Institute, Texas A&M University (2007-2008), p. II-26.
[3] L. Tassan-Got, Nucl. Instrum. Methods Phys. Res. **B194**, 503 (2000).

# Calibration of the $^{32,36}$S, $^{86}$Kr on $^{112,124}$Sn, $^{197}$Au data taken on the FAUST array

B. C. Stein, S. N. Soisson, G. A. Souliotis, D. V. Shetty, S. Galanopoulos,
S. Wuenschel, Z. Kohley, L. W. May, and S. J. Yennello

Systems of 45MeV/A $^{32}$S on $^{112,124}$Sn and $^{197}$Au, 45MeV/A $^{36}$S on $^{112,124}$Sn, and 30MeV $^{86}$Kr on $^{112,124}$Sn and $^{197}$Au were measured with the Forward Array Using Silicon Technology (FAUST) [1]. Calibration of the data set, including particle identification (PID) energy calibration of the Si-CsI telescopes, is in progress.

PID has been accomplished though the use of a linearization method. In this method, the distance between a point in question and the linearization line was calculated using a recently developed point to curve distance algorithm [2]. This method combined with the updated preamps installed in FAUST before the 2005-2006 run have led to isotopic identification for elements up to Z=14. Previously, isotopic identification on the FAUST Array was not possible above Z=8. Figure 1 shows the raw Si-CsI spectrum, the full spectrum linearized, and a zoomed in view of the beryllium peaks in the linearized spectrum.

Energy Calibration of the 68 Si-CsI telescopes comprising FAUST first requires calibration of the front silicon detector using a $^{228}$Th source as well as other known points on the energy spectrum such as the energy deposited in the silicon detector from elastically scattered beam particles. Calibration of the CsI scintillator is then achieved through comparison with the Orsay energy loss tables using a formalism proposed by Larochelle which models the light output from a CsI crystal based on the energy deposited [3].



**Figure 1.** (Top) Raw Silicon-CsI spectrum for FAUST detector 52 in ring D. (Middle) Linearized raw spectrum for detector 52 plotted against raw CsI channel. (Bottom) Linearized raw spectrum zoomedin to show the isotopes of beryllium. Gaussians have been fit to the peaks. The number above each peak identifies the isotope of Beryllium.

[1] F. Gimeno-Nogues *et al.*, Nucl. Instrum. Methods Phys. Res. **A399**, 94 (1997).

[2] L. W. May *et al.*, *Progress in Research*, Cyclotron Institute, Texas A&M University (2007-2008), p II-26.

[3] Y. Larochelle *et al.,* Nucl. Instrum. Methods Phys. Res. **A348**, 167 (1994).

# A dual-axis dual-lateral position sensitive detector for the FAUST array

S. N. Soisson, B. C. Stein, L. W. May, and S. J. Yennello

In the last several years advances in silicon strip technology and continuous position sensitive detectors have allowed for more precise measurement of the emission angle of fragments from heavy-ion reactions. By achieving a greater understanding of the emission pattern of fragments from heavy-ion collisions, it is possible that the modes of disassembly of excited nuclei can be differentiated [1]. Because of the success of FAUST due to its reconstruction capabilities it is a prime candidate for a move towards greater position sensitivity to allow for a greater understanding of multifragmentation processes.

We have continued work with a dual-axis dual-lateral position sensitive detector (DADL PSD) in conjunction with Micron Semiconductor. The second prototype experienced charge leakage issues between the back guard ring and the back side [2]. This issue in manufacturing was corrected by Micron Semiconductor and a third prototype was delivered.

The third prototype of a DADL PSD delivered has been shown to function as designed. A DADL PSD is a highly uniform p-on-n silicon structure with highly uniform resistive junction and ohmic layers and equipotential channels. The readout between the two anodes is orthogonal with respect to the readout between the two cathodes. The total energy of an incident particle is determined by either the summation of the charge collected on the front contacts or the back contacts. The position of the incident particle on each axis can be easily determined using a conventional formula such as $X \propto (Q_1-Q_2) / (Q_1+Q_2)$, where Q is the charge collected from one contact.

An experiment was performed in the SEE Line to determine how a DADL PSD would perform under experimental conditions. Data was taken with $^{20}$Ne + $^{nat}$Au at 45 MeV/nucleon. A detector telescope comprised of a DADL PSD and a CsI(Tl) was placed at $30°_{lab}$ with beam on target, as well as $0°_{lab}$ with a direct dispersed beam. It has been determined that the optimal running conditions for this detector is to apply voltage to the front side to completely reverse bias the detector. The front and back guard rings receive -15 V and +5 V respectively. A 260 ohm resistor is placed between the detector and pre-amplifier to insure that complete charge splitting occurs when an incident particle hits near the charge collection strip. An amplifier shaping time of 3 μs is chosen to allow for maximum position and energy resolution.

With the detector placed at $0°_{lab}$, position measurements were taken. In Fig. 1, we see the position reconstruction of a 9 by 9 gridded mask. Each hole is 1/32 in. or ~800 μm in diameter. It is clearly seen that each
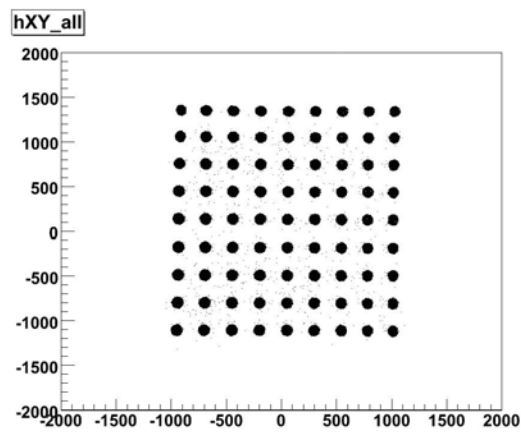


**Figure 1.** Reconstruced position for a 9 by 9 gridded mask.

hole is uniform in shape and the grid appears square.  Calculations have been performed to show that the position resolution is 200 μm.    With the detector placed at $30°_{lab}$ , the $^{20}$Ne beam was placed on a Au target.  This set up allowed for the measurement of fragments produced in the heavy-ion reaction. In Fig. 2 it is shown that clear isotopic separation can be obtained.  The DADL PSD shows particle identification on par with the current FAUST set up.  A $^{228}$Th source was used to determine the energy resolution of this detector at the end of the experiment.  It was found that the energy resolution is 80 keV [3].
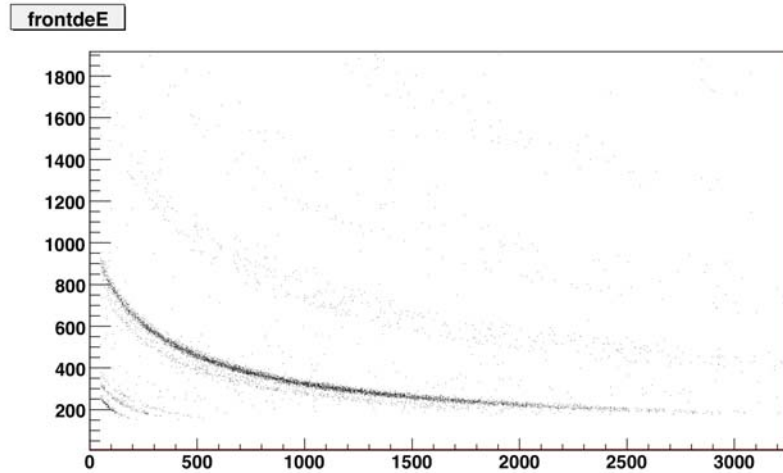


**Figure 2.** ΔE – E spectra showing clear particle identification.

The development of the DADL PSD has been completed.  It has an energy resolution of 80 keV and a position sensitivity of 200 μm under experimental conditions.

[1] R. J. Charity *et al.,* Phys. Rev. C **46**, 1951 (1992).
[2] S. N. Soisson *et al., Progress in Research,* Cyclotron Institute, Texas A&M University (2006-2007) p.
    II-23.
[3] IEEE Std 300$^{TM}$ -1988(R2006)

# SECTION III

# NUCLEAR THEORY

# The nature of the low energy isovector dipole excitations in neutron rich nuclei

E. Nica, D. C. Fuls, and S. Shlomo

We investigate the properties of the Isovector Giant Dipole Resonance (IVGDR) in neutron-rich nuclei, in particular the nature of its low-energy components. Studies of properties of the IVGDR in neutron-rich nuclei are important for the understanding of processes occurring in neutron stars and heavy-ion collisions. It is common in the literature to carry out discretized Hartree-Fock (HF)-based random phase approximation (RPA) calculations of the strength function of giant resonances by putting the nucleus in a box [1]. In this case, all single-particle states are bound and have no width. Therefore, all p-h excitations appear as bound excited states. In particular, discretized HF-RPA calculations for the strength function of the IVGDR have been carried out in the past with violations of self-consistency and employing a large smearing parameter. Because of this, small peaks in the RPA response function may have been incorrectly interpreted as low-energy resonances. It is thus important to establish whether these excitations are indeed resonances or are due to threshold effects.

The main way to establish if the small peaks seen in the IVGDR response function obtained in some discretized HF based RPA calculations represent bona-fide resonances is to perform the HF-based Continuum RPA (CRPA) calculations. The Continuum HF-RPA properly accounts for the decay of particles excited beyond the threshold energy [2], whereas the discretized version deals only with bound single particle states. Comparing the results obtained with the continuum calculations with those from the discretized calculations should indicate if these peaks are truly resonance states or not [3].

For the effective nucleon-nucleon interaction we use a simplified Skyrme-type nucleon-nucleon interaction given by

$$V_{ij} = t_0 \delta(\mathbf{r}_i - \mathbf{r}_j) + \frac{1}{6} t_3 \rho^\alpha \left( \frac{\mathbf{r}_i + \mathbf{r}_j}{2} \right) \delta(\mathbf{r}_i - \mathbf{r}_j),$$ (1)

where $t_0$=1600 MeV*fm$^3$, $t_3$=12500 MeV*fm$^4$ and $\alpha$=1/3. In our RPA calculations we use a Green's Function formalism. The RPA Green's Function is given by [2]

$$G^{RPA} = G^{(0)}(1 + V_{ph} G^{(0)})^{-1},$$ (2)

where $V_{ph}$ stands for the particle-hole (p-h) interaction and $G^{(0)}$ is the bare p-h Green's Function. The nuclear response associated with the scattering operator $F$ is given by

$$S(E) = \sum_n \left| \langle 0|F|n \rangle \right|^2 \delta(E - E_n),$$ (3)

where $|0\rangle$ and $|n\rangle$ denote the ground and excited states, respectively. In the Green's Function formalism,

$$S(E) = \frac{1}{\pi} \operatorname{Im}[Tr(fGf)]. \tag{4}$$

For a resonance $\operatorname{Im}\langle fGf \rangle$ has a peak at a resonance energy E=$E_R$, and $\operatorname{Re}\langle fGf \rangle$ decreases with E, going through zero at $E_R$.

The Figure shows the results for $\operatorname{Im}\langle fGf \rangle$ (solid line) and $\operatorname{Re}\langle fGf \rangle$ (dashed line) of the free (top) and CRPA (bottom) response functions for $^{60}$Ca. We note that: (i) The neutron and proton separation (threshold) energies are; Sn=4.674 MeV, Sp=13.591 MeV. (ii) The sharp peaks at 8.398, 8.917 and 11.676 MeV are due to proton bound to bound particle-hole excitations $\pi 0d \rightarrow \pi 0f$, $\pi 1s \rightarrow \pi 1p$ and $\pi 0d \rightarrow \pi 1p$, respectively. (iii) The neutron particle-hole excitation are all to the continuum. The threshold effects of enhancement in $\operatorname{Im}\langle fGf \rangle$ above 4.674 MeV and at around 6 MeV are clearly seen in the figure. (iv) In the RPA excitation strength ($\operatorname{Im}\langle fGf \rangle$) we observe the collective IVGDR above 11 MeV with threshold enhancement at low excitation energies.
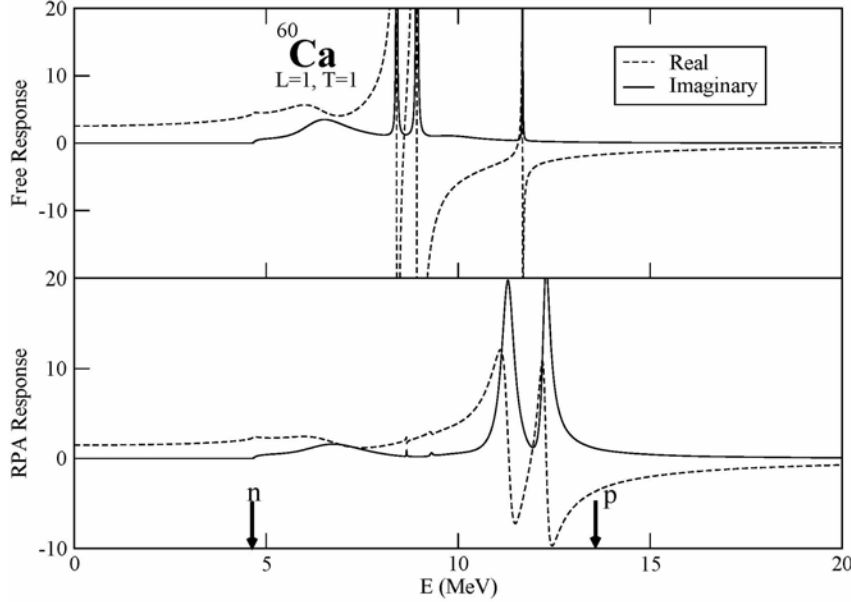
[1] N. Paar, D. Vretenar, E. Khan, and G. Colo, Rep. Prog. Phys. **70**, 691 (2007).
[2] S. Shlomo and G. F. Bertsch, Nucl. Phys. **A243**, 507 (1975).
[3] E. Nica, D. C. Fuls, and S. Shlomo (to be published).

# A modern nuclear energy density functional

D. C. Fuls, V. K. Au, and S. Shlomo

Density functional theory, which is based on a theorem for the existence of a universal energy density functional (EDF) that depends on the densities of the constituents and their derivatives, provides a powerful approach for theoretical calculations of properties of many body systems. However, the main challenge is to find the EDF. The development of a modern and more realistic nuclear EDF for accurate predictions of properties of nuclei is of the highest priority for the worldwide nuclear physics community.

Starting from the EDF associated with the Skyrme effective nucleon-nucleon interaction [1], we aim to construct a more realistic EDF with improved predictive power for properties of nuclei at and away from the valley of stability. It should be emphasized that in earlier attempts to determine a more realistic interaction, the main objective has been that the experimental data on ground state properties of nuclei be reproduced by the mean-field theory. In our approach we use the effective interaction to determine the properties of giant resonances within the RPA theory and thus introduce RPA correlations into the ground state. Therefore, for consistency, we must require that the comparison with data be made after the inclusion of the effects of RPA correlations in the ground states of nuclei, i.e. going beyond mean-field theory.

Recently, we have determined within the Hartree-Fock (HF) approximation a new and more realistic Skyrme interaction (named KDE0) by fitting [2] a set of extensive data on binding energies, "bare" single particle energies, charge radii, and radii of valence nucleon density distribution of nuclei. We have included in the fit, for the first time, the data on the energies of the isoscalar giant monopole resonances (ISGMR) of nuclei and imposed additional constraints, such as a non-negative value for the slope of the symmetry energy density at high nuclear matter (NM) density (at three times the saturation density of NM) and the Landau's stability constraints on nuclear matter. We have implemented, for the first time, the simulated annealing method together with an advanced least square method to search for the global minima. We have continued our work [3] to further improve our EDF by *addressing the following tasks:*

*(i)* Modifying the isospin dependence of the spin-orbit interaction in order to better reproduce the spin-orbit splitting of single particle orbits in neutron-rich and proton-rich nuclei.

*(ii)* Including in the fit for determining the EDF additional experimental data on ground state properties of nuclei, such as binding energies and radii.

*(iii)* Including in the fit for determining the EDF the data on giant resonances, such as the ISGMR and the isoscalar giant dipole resonance (ISGDR), which are sensitive to the NM incompressibility coefficient $K$, the isovector giant dipole resonance (IVGDR), which is sensitive to the symmetry energy density, and the isoscalar giant quadrupole resonance (ISGQR), which is sensitive to the effective mass.

[1] T. H. R. Skyrme, Phil. Mag. **1**, 1043 (1956); Nucl. Phys. **9**, 615 (1959).
[2] B. K. Agrawal, S. Shlomo and V. Kim Au, Phys. Rev. C **72**, 014310 (2005).

[3] D. C. Fuls, V. K. Au and S. Shlomo (to be published).

# The Schiff moment and the isoscalar giant dipole resonance

N. Auerbach[1]  and S. Shlomo

[1]*School of Physics and Astronomy, Tel-Aviv University, Tel-Aviv, Israel*

The theoretical determination of Schiff moments is necessary in order to relate the measured upper limits of dipole moments in atoms to the upper limits of time reversal violations. At present several experiments are planned and being performed to measure dipole moments in the radium isotopes. The Schiff operator is identical to the excitation operator associated with the isoscalar giant dipole resonance (ISGDR). It is therefore important to study the strength distribution of ISGDR and to find nuclei in which this strength is shifted to low-energies. Such low-energy strength in the even-even nucleus could couple to the single-particle states of opposite parity in the odd-even nucleus and enhance the effects of T, P-violation.

One could look for such low-energy ISGDR strength by calculating the inverse energy weighted sum rule (IEWSR):

$$IEWSR = \sum_n \left| \langle n | \hat{S} | 0 \rangle \right|^2 (E_n - E_0)^{-1} \ .$$

This sum rule can be obtained from the response function of the ISGDR, evaluated in fully self-consistent Hartree-Fock (HF)-based random phase approximation (RPA). Even better and more efficient is to perform a constrained Hartree-Fock (CHF) computation with the $\lambda \hat{S}$ operator being the constraining term. One can then obtain the IEWSR by evaluating the second derivative of the HF energy with respect to $\lambda$. A large IEWSR signals a phase transition, which in this case could mean a change in the nuclear shape. Studying nuclei away from the stability line will conceivably lead to some regions in which the enhancements of the Schiff moment due to low-lying ISGDR strength will be large. We will carry out calculations for the ISGDR for neutron-rich light and heavy nuclei.

# An improved calculation of the isospin-symmetry-breaking corrections
## to superallowed Fermi β decay

I. S. Towner and J. C. Hardy

In the determination of $V_{ud}$, an important strength of the nuclear measurements is that there are many $0^+ \rightarrow 0^+$ transitions available for study. It then becomes possible to validate the analysis procedure by checking that all transitions individually yield statistically consistent results for $V_{ud}$. Since the isospin-symmetry-breaking corrections depend on nuclear structure, they differ from transition to transition and are particularly sensitive to this consistency test. Thus the appearance of an anomalous result from any transition could signal a problem with the structure-dependent correction for that case, a problem which might have implications for other cases as well.

One disturbing development arose with the recent precise Penning-trap measurements [1, 2] of the $Q_{EC}$ value for the superallowed decay of $^{46}$V, which left the result for that transition more than two standard deviations away from the average of all other well-known transitions. This possible anomaly led us initially to reexamine the isospin-symmetry-breaking corrections for the $^{46}$V transition, but what we learned from that reexamination prompted us to a more general reevaluation of the corrections for other transitions as well. The results of this reexamination have just been published [3].

Our previous shell-model calculations for $^{46}$V considered six valence nucleons occupying the *pf*-shell orbitals outside a $^{40}$Ca closed shell. However, an important part of the charge-dependent correction depends on the radial mismatch between the decaying proton in the parent nucleus and the resulting neutron in the daughter nucleus; but both these nucleons are bound to $^{45}$Ti, so the structure of that nucleus turns out to be important too. What is most striking about $^{45}$Ti is that it has a $3/2^+$ state at an excitation energy of only 330 keV, which is strongly populated in single-nucleon pick-up reactions like (p,d) and ($^3$He, α). Such low-lying *sd*-shell states can contribute to the structural parentage of the initial and final states of the superallowed transition and consequently must affect the radial mismatch between them. This indicated to us that a complete calculation of the isospin-symmetry-breaking correction for the decay of $^{46}$V should include contributions from shells deeper than the *pf* shell.

The isospin-symmetry breaking correction, $\delta_C$, is typically broken up into two pieces, $\delta_C = \delta_{C1} + \delta_{C2}$, of which the second, $\delta_{C2}$, is the larger and more important component. It depends on the mismatch in the radial wave functions for the proton and neutron involved in the β transition. In ref. [3], this correction is evaluated from the formula

$$\delta_{C2} \approx \sum_{\pi^<,\alpha} S_\alpha^< \Omega_\alpha^< - \tfrac{1}{2} \sum_{\pi^>,\alpha} S_\alpha^> \Omega_\alpha^> \ , \tag{1}$$

where $S_\alpha$ are spectroscopic factors for neutron pick-up in orbital α from, in our example, $^{46}$Ti, while $\Omega_\alpha$ is a measure of how much the radial overlap integral between the proton and neutron radial wave functions departs from unity. The sum over π is a sum over all "parent" states in $^{45}$Ti that have significant parentage with the ground states of $^{46}$Ti and $^{46}$V. The superscripts < and > denote whether the isospin of the states in $^{45}$Ti are isospin-lesser states, with $T_\pi = 1/2$, or isospin-greater states, with $T_\pi = 3/2$.

This equation provides the key to the strategy we used in calculating $\delta_{C2}$. It demonstrates that there is a cancellation between the contributions of the isospin-lesser states and the isospin-greater states. Moreover, if the orbital $\alpha$ were completely full, then the Macfarlane and French sum rules [4] for spectroscopic factors would require $\sum_{\pi^<} S_\alpha^< = \frac{1}{2} \sum_{\pi^>} S_\alpha^>$ and the cancellation in Eq.(1) would be very strong. In fact, the cancellation would be complete if $\Omega_\alpha^< = \Omega_\alpha^>$. This cancellation is not in general complete because the radial-mismatch factors for isospin-lesser states are larger than those for isospin-greater states. Even so, cancellation is always significant, and it becomes most complete when closed-shell orbitals are involved. Thus, although the dominant contributions to $\delta_{C2}$ come from unfilled orbitals, we conclude that closed-shell orbitals must play a role, albeit one that decreases in importance as the orbitals become more deeply bound.

Based on these observations, our strategy was to use experiment to guide us in determining which closed-shell orbitals are important enough to include. Ideally, of course, one would take the spectroscopic factors determined from experiment and insert them into Eq.(1) but, especially where delicate cancellations are involved, the reliability of (forty-year-old) experimental spectroscopic factors is certainly not up to the task. Our strategy then was to use the shell model to calculate the spectroscopic factors but to limit the sum over orbitals $\alpha$ just to those for which large spectroscopic factors have been observed in neutron pick-up reactions.

Following along these lines, we have completed new calculations of $\delta_{C2}$ incorporating core orbitals in the shell model in cases where independent experimental information indicates that they are required. When combined with the other theoretical corrections and the experimental *ft* values we obtained a new set of corrected $\mathscr{F}t$ values. The agreement among the $\mathscr{F}t$ values for the thirteen well measured cases is very good and the consistency check imposed by the Conserved Vector Current hypothesis is well satisfied.

With these new corrections, the value of $V_{ud}$ is increased by 0.04%, or by one standard deviation of the previous result [5]. With the new value, the sum of squares of the top-row elements of the CKM matrix is in perfect agreement with unitarity. However, this should not be regarded as the end of the story. Although there is excellent agreement with unitarity, it is the 0.1% uncertainty on the experimental sum that actually sets the critical limit on possible new physics beyond the standard model. This uncertainty can still be reduced by new precise experiments.

[1] G. Savard, F. Buchinger, J. A. Clark, J. E. Crawford, S. Gulick, J. C. Hardy, A. A. Hecht, J. K. P. Lee, A. F. Levand, N. D. Scielzo, H. Sharma, K. S. Sharma, I. Tanihata, A. C. C. Villari, and Y. Wang, Phys. Rev. Lett. **95**, 102501 (2005).

[2] T. Eronen, V. Elomaa, U. Hager, J. Hakala, A. Jokinen, A. Kankainen, I. Moore, H. Penttila, S. Rahaman, J. Rissanen, A. Saastamoinen, T. Sonoda, J. Aysto, J. C. Hardy and V. S. Kolhinen, Phys. Rev. Lett. **97**, 232501 (2006).

[3] I. S. Towner and J. C. Hardy, Phys. Rev. C **77**, 025501 (2008).

[4] J. B. French and M. H. Macfarlane, Nucl. Phys. **26**, 168 (1961).

[5] J. C. Hardy and I. S. Towner, Phys. Rev. C **71**, 055501 (2005).

# Heavy ion collisions at LHC in a multiphase transport model

L. W. Chen,[1] C. M. Ko, B. A. Li,[2] Z. W. Lin,[3] and B. W. Zhang[4]

[1]*Institute of Theoretical Physics, Shanghai Jiao Tong University, Shanghai 200240, China*
[2]*Department of Physics, Texas A&M University-Commerce, Commerce, Texas 75429-3011*
[3]*Department of Physics, East Carolina University, Greenville, North Carolina 27858-4353*
[4]*Institute of Particle Physics, Central China Normal University, Wuhan 430079, China*

Using a multiphase transport (AMPT) model [1], we have studied heavy ion collisions at the Large Hadron Collider (LHC) at CERN [2,3]. The charged hadron pseudorapidity distribution is found to show a clear plateau structure with a value of about 2500 and 4500, respectively, with and without nuclear shadowing, which are about a factor of three larger than corresponding ones at RHIC. The inverse slope parameters of the transverse momentum spectra of identified midrapidity hadrons are larger than those at RHIC as a result of stronger final-state rescatterings at LHC. Based on a parton scattering cross section of 10 mb, which is needed to describe observed hadron elliptic flows at RHIC, the elliptic flows of light and heavy quarks at LHC display the expected mass ordering at low transverse momenta, i.e., the elliptic flow is smaller for quarks with larger masses. Compared to those at RHIC, the elliptic flow of pions at LHC is larger while that of protons is smaller. The elliptic flows of heavy mesons, which are estimated from those of quarks using the quark coalescence or recombination model, are dominated by those of heavy quarks, while those of the quarkonia $J/\psi$ and $Y$ consisting of a heavy quark and its antiquark and having certain transverse momentum are simply twice those of their constituent heavy quarks at half the momentum. The correlation functions in the longitudinally comoving frame of pions or kaons at LHC, calculated from the positions and momenta of pions or kaons at freeze out, are narrower than at RHIC. Fitting the correlation functions by Gaussian functions, extracted source radii at LHC are larger than those at RHIC. In both collisions, radii of the emission source for pions are larger than those for kaons. As at RHIC, the smaller lambda parameter for pions than for kaons is due to the large halo in the pion emission source from decays of omega mesons. Also, the emission sources are non-Gaussian and are shifted in the direction of the pion or kaon transverse momentum.

[1] Z. W. Lin, C. M. Ko, B. A. Li, B. Zhang, and S. Pal, Phys. Rev. C **72**, 064901 (2005).
[2] C. M. Ko, L. W.Chen, and B. W. Zhang, Braz. J. Phys. 37, 969 (2007).
[3] N. Armesto *et al.*, J. Phys. G **35**, 054001 (2008).

# Thermal charm production in quark-gluon plasma at LHC

B. W. Zhang,[1] C. M. Ko, and W. Liu

[1]*Institute of Particle Physics, Central China Normal University, Wuhan 430079, China*

Modeling central heavy ion collisions at the Large Hadron Collider (LHC) at CERN by a schematic longitudinally boost invariant and transversely expanding fire-cylinder of quark-gluon plasma, we have evaluated the number of thermally produced charm quark pairs at next-to-leading-order in QCD. With an initial temperature of 700 MeV for an equilibrated quark-gluon plasma at an initial proper time of 0.2 fm/c and a charm quark mass of 1.3 GeV, we have obtained about 30% enhancement in the production of charm quarks than that produced directly from initial hard collisions, which is taken to be 20 pairs at midrapidity, as shown in Fig. 1. About equal contributions are obtained from the leading order and the next-leading order processes. This result is, however, sensitive to the initial conditions for the produced quark-gluon plasma and the charm quark mass. The enhancement is increased to about 80% if the initial temperature is increased to 750 MeV, but it is reduced to about 10% if the initial temperature is 630 MeV. Delaying the proper time at which a thermalized quark-gluon plasma is formed does not affect much thermal charm quark production as the effect due to decreased initial temperature is compensated by that from the increased volume of the quark-gluon plasma. With a larger charm quark mass of $m_c = 1.5$ GeV, thermal charm quark production from the quark-gluon plasma becomes unimportant.
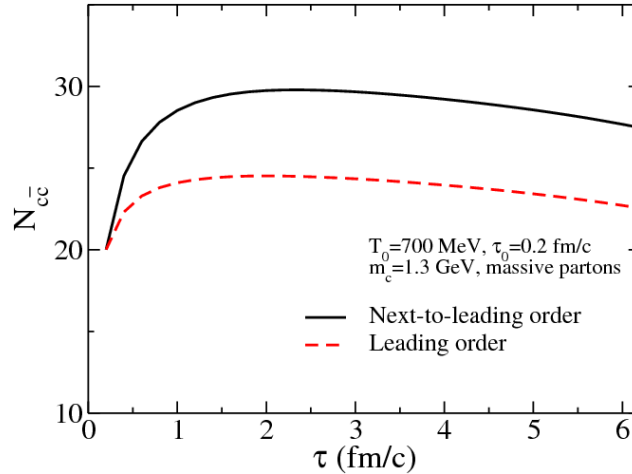


**Figure 1.** Number of charm pairs as a function of proper time in central Pb+Pb collisions at $s^{1/2}_{NN}$=5.5 TeV in the leading order (dashed line) and the next-to-leading order (solid line) in QCD.

[1] B. W. Zhang, C. M. Ko, and W. Liu, Phys. Rev. C **77**, 024901 (2008).

# Isospin-dependent properties of asymmetric nuclear matter in relativistic mean-field models

L. W. Chen,[1] C. M. Ko, and B. A. Li[2]

[1]*Institute of Theoretical Physics, Shanghai Jiao Tong University, Shanghai 200240, China*
[2]*Department of Physics, Texas A&M University-Commerce, Commerce, Texas 75429-3011*

Using various relativistic mean-field models, including the nonlinear ones with meson field self-interactions, those with density-dependent meson-nucleon couplings, and the point-coupling models without meson fields, we have studied the isospin-dependent bulk and single-particle properties of asymmetric nuclear matter [1]. In particular, we have determined the density dependence of nuclear symmetry energy from these different relativistic mean-field models and compared the results with the constraints recently extracted from analyses of experimental data on isospin diffusion and isotopic scaling in intermediate-energy heavy ion collisions as well as from measured isotopic dependence of the giant monopole resonances in even-A Sn isotopes. Among the 23 parameter sets in the relativistic mean-filed model that are commonly used for nuclear structure studies, only a few are found to give symmetry energies that are consistent with empirical constraints as shown in Fig. 1. We have also studied the nuclear symmetry potential and the isospin-splitting of the nucleon effective mass in isospin asymmetric nuclear matter. We find that both the momentum dependence of the nuclear symmetry potential at fixed baryon density and the isospin-splitting of the nucleon effective mass in neutron-rich nuclear matter
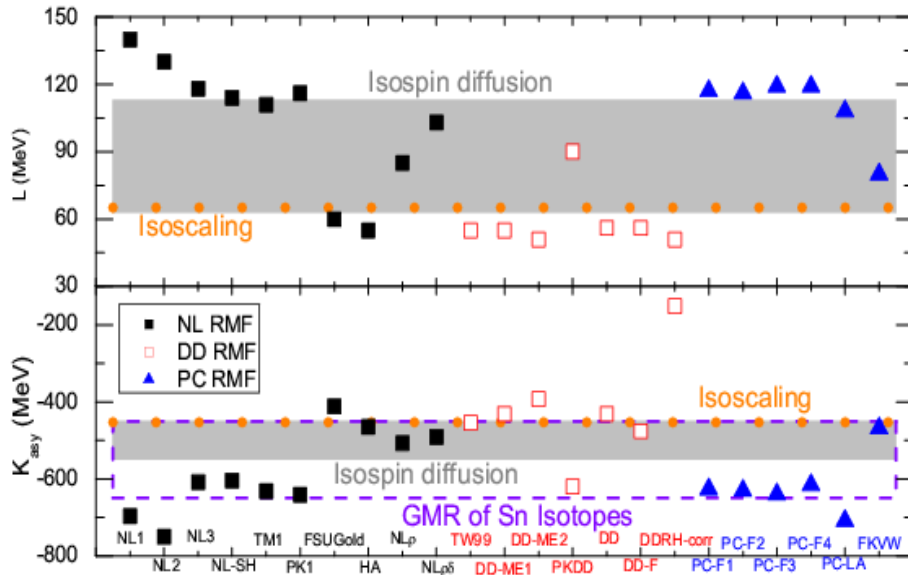


**Figure 1**. Values of the slope L and and curvature $K_{asy}$ of nuclear symmetry energy for the 23 parameter sets in the nonlinear (solid squares), density-dependent (open squares), and point-coupling (triangles) RMF models. The constraints from the isospin diffusion data (shaded band), the isoscaling data (solid circles), and the isotopic dependence of the GMR in even-A Sn isotopes (dashed rectangle) are also included.

depend not only on the nuclear interactions but also on the definition used for the nucleon optical potential.

[1] L. W.Chen, C. M. Ko, and B. A. Li, Phys. Rev. C **76**, 054316 (2007).

# $\Lambda_c$ enhancement from strongly coupled quark-gluon plasma

S. H. Lee,[1] K. Ohinish,[1] S. Yasui,[2] I. K. Yoo,[3] and C. M. Ko

[1]*Institute of Physics and Applied Physics, Yonsei University, Seoul 120-749,Korea*
[2]*Department of Physics, National Taiwan University, Taipei 10617, Taiwan*
[3]*Pusan National University, Pusan 609-735, Republic of Korea*

Because of the strong attractive color-spin interaction between two quarks in the flavor anti-triplet and color anti-triplet channel, the [ud] diquark has played an important role in the structure of hadrons. Assuming that stable bound diquarks also exist in strongly coupled quark-gluon plasma that is produced in relativistic heavy ion collisions, we have studied their effects on the yield of $\Lambda_c$ in these collisions [1]. Based on the quark coalescence model for hadron production from the quark-gluon plasma, we have calculated the contributions to $\Lambda_c$ production from both the normal three-body coalescence of independent c, u and d quarks and the two-body coalescence of the c quark and the [ud] diquark. The resulting $\Lambda_c$ to the $D^0$ yield ratio, which is the same in heavy ion collisions at the Relativistic Heavy Ion Collider (RHIC) and the Large Hadron Collider (LHC), is shown in Fig. 1 for different scenarios as a function of the temperature of the quark-gluon plasma. It is seen that the $\Lambda_c/D^0$ ratio at the critical temperature $T_C = 0.175$ GeV is about 0.11 without diquarks and increases to about 0.44 in the presence of the diquark [ud] with mass $m_{[ud]} = 0.6$ GeV (thin solid line), corresponding to a loosely bound state which can hardly exist near $T_C$. If the diquark mass has the minimum value $m_{[ud]} = 0.455$ GeV (bold solid line) due to the attractive color-spin interaction, the $\Lambda_c/D^0$ ratio becomes even larger and has a value of about
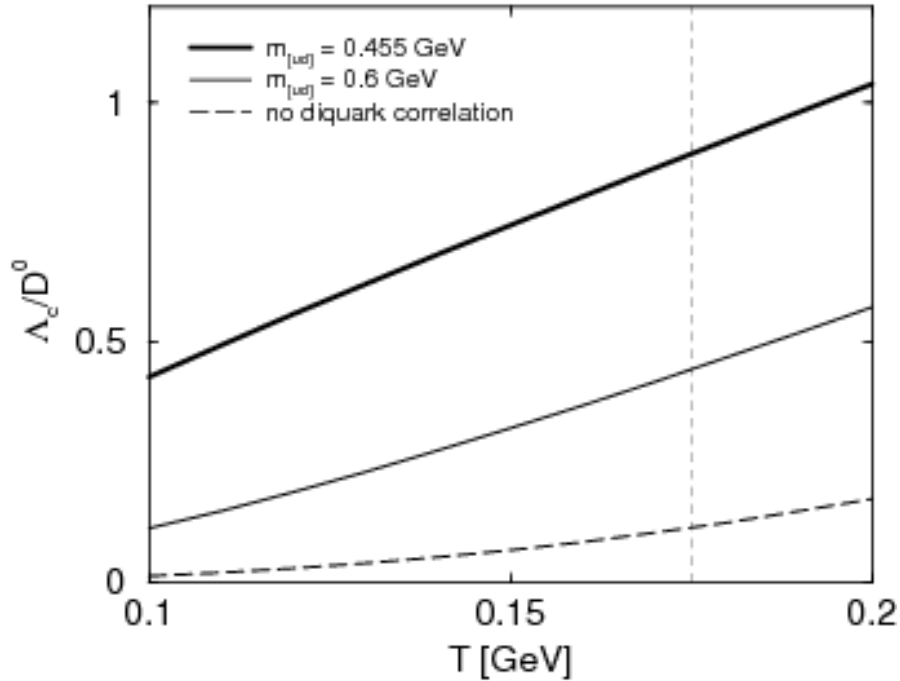


**Figure 1.** Yield ratio $\Lambda^c/D^0$ as a function of temperature.

0.89. Therefore, the diquarks in quark-gluon plasma raise the $\Lambda_c/D^0$ ratio by about a factor 4 - 8 in comparison with the case without diquarks. A similar enhancement is found for the $\Lambda_b/B^0$ ratio between bottom baryons and bottomed mesons. The study of $\Lambda_c/D^0$ and $\Lambda_b/B^0$ enhancements in relativistic heavy ion collisions would thus open a new way to find the existence of QGP in heavy ion collisions and also provide an experimental tool to probe the diquark correlation in quark-gluon plasma. This would, in turn, confirm the diquark structure in heavy baryons with a single heavy quark.

[1] S. H. Lee, K. Ohinish, S. Yasui, I. K. Yoo, and C. M. Ko, Phys. Rev. Lett. **100**, 222301 (2008).

# Charmed exotics in heavy ion collisions

S. H. Lee,[1] S. Yasui,[1] W. Liu, and C. M. Ko

[1]*Institute of Physics and Applied Physics, Yonsei University, Seoul 120-749, Korea*

Based on the consideration of the color-spin interaction between diquarks, which describes reasonably the mass splittings between many hadrons and their spin flipped partners, we have shown that tetraquark mesons and pentaquark baryons that consist of two charmed quarks could be bound. Using the quark coalescence model, their yields in heavy ion collisions at both the Relativistic Heavy Ion Collider (RHIC) and the Large Hadron Collider (LHC) are estimated [1]. Although the results depend on the oscillator frequencies used for quark wave functions as shown in Fig. 1 for the abundance of the tetraquark meson $T_{cc}$, the expected large charm quark number in central Pb+Pb collisions at LHC makes its value appreciable. For an oscillator frequency of 0.3 GeV, appropriate for charmed hadrons, the abundance of the tetraquark meson $T_{cc}$ at LHC is about $10^{-4}$, while that of pentaquark baryon $\Theta_{cs}$ is about $10^{-3}$. For the doubly charmed baryon $\Xi_{cc}$, the estimated number is about $3.2 \times 10^{-4}$ at LHC. Charmed hadrons would be more abundantly produced, particularly the $T_{cc}$, if charm quarks are produced from the quark-gluon plasma formed in these collisions. The open and hidden charmed hadron physics is expected to be an interesting subject in the forthcoming heavy ion collision experiments.
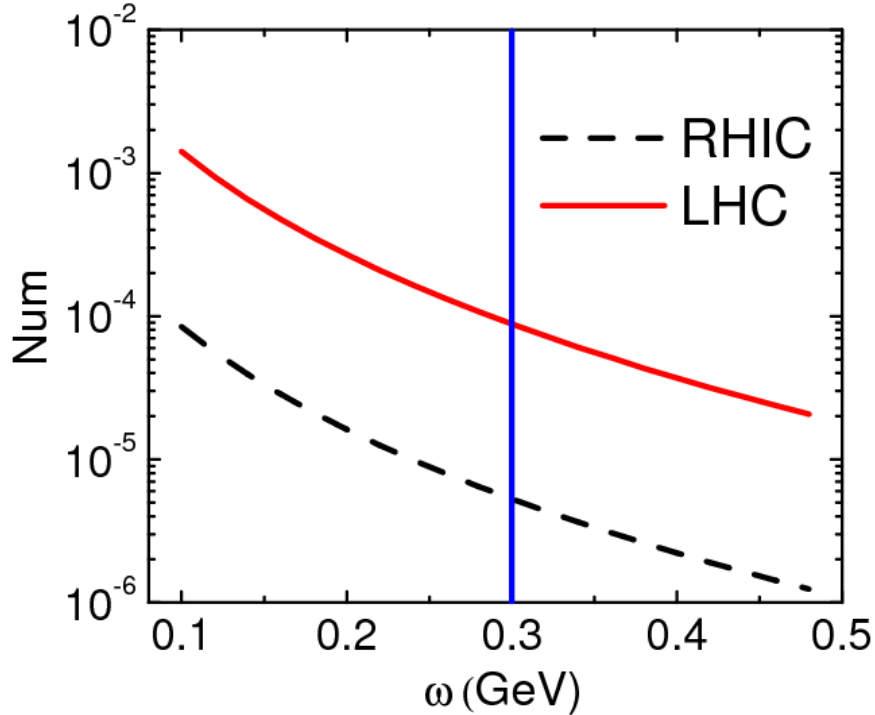


**Figure 1**. Number of $T_{cc}$ produced at RHIC and LHC as a function of the oscillator frequency used for the quark wave functions in $T_{cc}$.

[1] S. H. Lee, S. Yasui, W. Liu, and C. M. Ko, Eur. Phys. J. C **54**, 259 (2008).

# Nuclear modification factors for high transverse momentum pions and protons at LHC

W. Liu, B. W. Zhang,[1] and C. M. Ko

[1]*Institute of Particle Physics, Central China Normal University, Wuhan 430079, China*

Including conversions between quark and gluon jets in a quark-gluon plasma (QGP) via both elastic qg↔gq and inelastic qq↔gg reactions, we have predicted the nuclear modification factor for both protons and pions as well as their ratios at large transverse momenta in central Pb+Pb collisions at $s^{1/2}_{NN} =$ 5.5 TeV [1]. As shown in the left window of Fig. 1, the nuclear modification factor $R_{AA}$ for large transverse momenta pions increases from 0.18 at $p_T =$ 5 GeV to 0.4 at $p_T =$ 40 GeV due to a smaller drag coefficient at large transverse momenta. The $R_{AA}$ of protons has a similar behavior, but its value is smaller because of stronger suppression of gluon than quark jets. The resulting $p/\pi^+$ ratio shown by the solid line in the right window of Fig. 1 approaches that in p+p collisions at same energy when the transverse momenta become very large. At lower transverse momenta, the $p/\pi_+$ ratio remains, however, smaller than that in p+p collisions, which is different from that in heavy ion collisions at RHIC as a result of the larger ratio of gluon to quark jets at LHC. Without conversions between quark and gluon jets, the $p/\pi^+$ ratio decreases by a factor of two as shown by the dotted line.
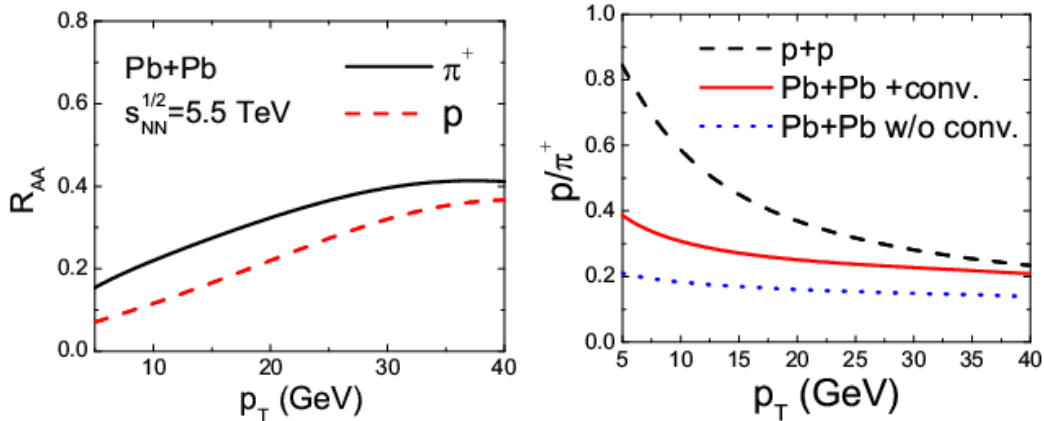


**Figure 1**. Left window: Nuclear modification factor $R_{AA}$ for $\pi^+$ (solid line) and proton (dashed line) in central Pb+Pb collisions at $s^{1/2}_{NN} =$ 5.5 TeV. Right window: $p/\pi^+$ ratio without (dotted lines) or with jet conversions (solid lines). Dashed lines correspond to p+p collisions at same energy.

[1] N. Armesto *et al.*, J. Phys. G **35**, 054001 (2008).

# Nucleon and Δ resonances in KΣ(1385)} photoproduction from nucleons

Y. Oh, C. M. Ko, and K. Nakayama[1]

[1]*Department of Physics and Astronomy, University of Georgia, Athens, GA 30602*

The reaction mechanisms for ΣK(1385) photoproduction from the reaction $\gamma p \to K^+ \Sigma^0(1385)$ in the resonance energy region are investigated in a hadronic model [1]. Both contributions from N and Δ resonances of masses around 2 GeV as given in the Review of Particle Data Group and by the quark model predictions are included. The Lagrangians for describing the decays of these resonances into KΣ(1385) are constructed with the coupling constants determined from the decay amplitudes predicted by a quark model. Comparing the resulting total cross section for the reaction $\gamma p \to K^+ \Sigma^0(1385)$ with the preliminary data from the Thomas Jefferson National Accelerator Facility, we find that the most important contributions are from the two-star rated resonances $\Delta(2000)$ $F_{35}$, $\Delta(1940)$ $D_{33}$, and $N(2080)$ $D_{13}$, as well as the missing resonance $N$ $3/2^-(2095)$ predicted in the quark model as shown in Fig. 1. We have also predicted the differential cross section and photon asymmetry in this reaction.
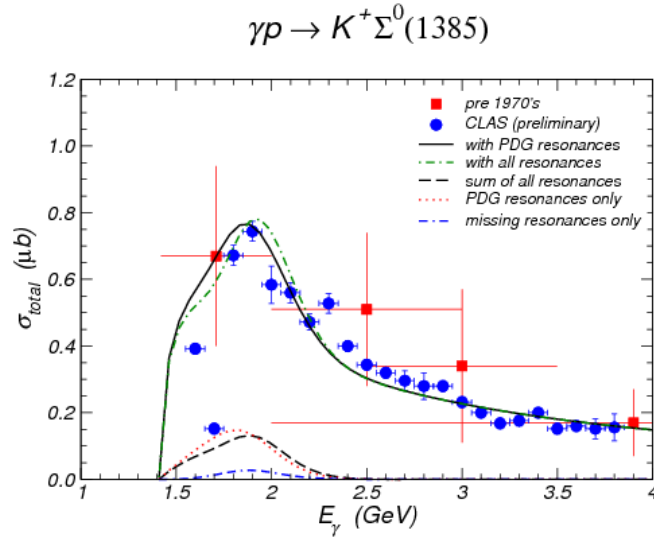


**Figure 1.** Total cross sections for the $\gamma p \to K^+ \Sigma^0(1385)$ reaction with various resonances.

[1] Y. Oh, C. M. Ko, and K. Nakayama, Phys. Rev. C **77**, 045204 (2008).

# Nonperturbative heavy-quark diffusion in the quark-gluon plasma

H. van Hees, M. Mannarelli, V. Greco, and R. Rapp

Heavy quarks (charm and bottom) are valuable probes of the hot and dense matter produced in ultrarelativistic heavy-ion collisions: they are produced in initial hard nucleon-nucleon collisions and subsequently interact with the medium consisting of light quarks and gluons. Data on light hadron spectra in 200 AGeV Au-Au collisions at the Relativistic Heavy-Ion Collider (RHIC) have shown that the produced partonic medium can be described by ideal hydrodynamics, suggestive for a strongly interacting quark-gluon plasma (sQGP) [1,2]: after the collision the medium appears to equilibrate rapidly building up pressure which is associated with the observed collective flow of hadrons. Heavy quarks, due to their large mass, $m_Q \gg T_c$ ($T_c \approx 180$ MeV: critical temperature), are particularly sensitive to the microscopic interaction mechanisms underlying the apparent rapid thermalization. At RHIC the measurement of transverse-momentum ($p_t$) spectra and elliptic flow, $v_2$, of non-photonic electrons [3,4] - originating from the decay of open-charm (D) and –bottom mesons (B) - have lead to the conclusion that heavy quarks interact surprisingly strongly with the medium, largely inheriting its collective-flow pattern via the corresponding drag within the medium. These observations indicate large momentum-diffusion coefficients which can not be accounted for in perturbative QCD (pQCD).

We have investigated the drag-diffusion processes of heavy quarks in the QGP via relativistic Langevin simulations of a Fokker-Planck equation with transport coefficients calculated from a non-perturbative evaluation of elastic heavy-quark (HQ) scatterings in the QGP [5]. We have employed static quark anti-quark potentials extracted from heavy-quark free energies computed in lattice-QCD (lQCD) within a Brueckner many-body calculation, defined by a coupled set of Bethe-Salpeter (BS) and Dyson equations. The four-dimensional BS equation has been reduced to a three-dimensional Lippmann-Schwinger (LS) equation using the Thompson scheme. The interaction kernel, $K$, is identified with the static lQCD-based potential and supplemented with a relativistic Breit (current-current) correction for finite quark velocities. The uncertainty due to different input potentials from lattice QCD is at the 40% level (here we use a parameterization of a quenched calculation [6]). The LS equation has been partial-wave expanded and solved numerically in S- and P-wave channels. All color channels (singlet and octet for quark-antiquark, as well as antitriplet and sextet for quark-quark) are included. The resulting finite-temperature T-matrices exhibit resonance states close to the quark-antiquark threshold in the attractive color-singlet (meson) and -antitriplet (diquark) channels up to temperatures of ~1.5 $T_c$. Compared to our earlier introduced effective resonance model [7], the interactions in the present approach are generated dynamically without free parameters.

The heavy-light quark T-matrices are utilized to compute drag and diffusion coefficients within a Fokker-Planck equation. The nonperturbative HQ interactions with light anti-/quarks from the medium are supplemented with elastic scattering off gluons in leading-order pQCD using a strong coupling constant, $\alpha_s = g^2/(4\pi) = 0.4$, and a Debye-screening mass, $\mu = gT$. The drag coefficients, $\gamma$ (related to the pertinent thermal relaxation time via $\tau^{eq} = 1/\gamma$), reach up to $\gamma = 1/(7\text{fm}/c)$ for c-quarks at low momenta close to $T_c$. This is comparable to the effective resonance model of Ref. [7] but a factor of ~4 larger than elastic

pQCD scattering alone. The "melting" of the resonance states toward higher temperatures leads to drag coefficients decreasing with increasing temperature, which is opposite to both pQCD and the effective resonance model [7].

HQ diffusion in semi-/central 200 AGeV Au-Au collisions has been simulated using a Langevin process in an elliptic fireball model [8]. The temperature evolution is determined by an ideal gas QGP equation of state assuming isentropic expansion, and the flow field has been adjusted to results of hydrodynamical models [9]. In particular, the elliptic flow for semicentral collisions is parameterized with confocal elliptic isobar surfaces within the fireball, with a bulk elliptic flow of 5.5% to reproduce the empirical hadron elliptic flow consistent with quark coalescence models [10]. The final HQ distributions of the Langevin simulation are hadronized into D- and B-mesons at $T_c$ in a combined coalescence/ fragmentation scheme [8]. We emphasize that the microscopically calculated resonance correlations in the meson and diquark channels of the T-matrix close to $T_c$ naturally merge into a coalescence description of hadronization [11].

Semileptonic decays of the D- and B-meson spectra provide single-electron ($e^{\pm}$) spectra which are compared to STAR [3] and PHENIX [4] data in Fig. 1. The agreement with experiment is rather remarkable in view of the essentially parameter-free calculation of the HQ-scattering rates (the uncertainty of the lQCD-based potentials amounts to ~30% at the level of observables). The increase of the HQ drag and momentum-diffusion coefficients with decreasing temperatures seems to be supported by the data since the at high-$p_t$ suppression of heavy quarks (i.e. $R_{AA}<1$) occurs mostly early in the fireball evolution, while the anisotropy of the flow, $v_2$, builds up in the later stages.
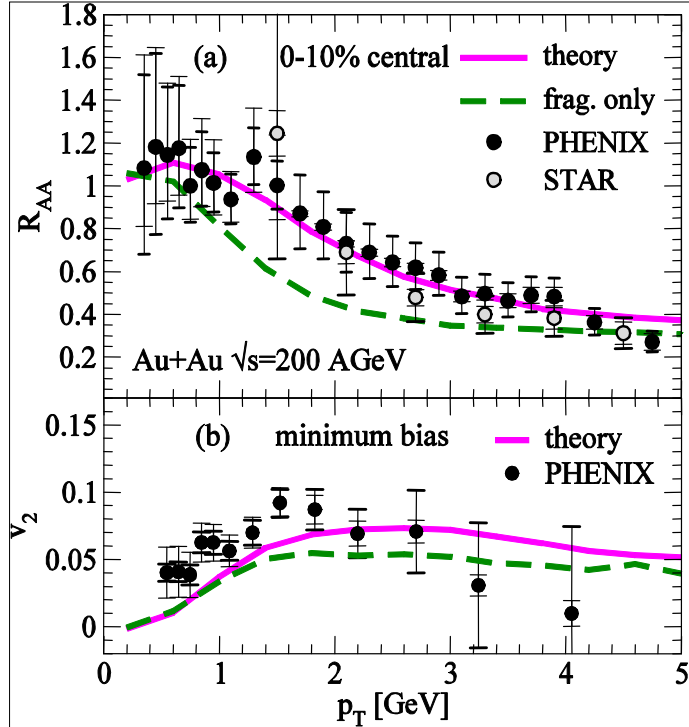


**Figure 1**. Upper panel: nuclear modification factor, $R_{AA}$, of single electrons in central 200 AGeV Au-Au collisions. The solid line represents the result of our HQ-diffusion model based on nonperturbative elastic scattering of charm and bottom quarks with light anti-/quarks evaluated using the in-medium T-matrix [5]. The dashed line shows the result when only ($\delta$-function) fragmentation is taken into account for the hadronization process. Lower panel: elliptic flow coefficient, $v_2$, within the same model applied to semi-central (b=7 fm) 200 AGeV Au-Au collisions. The data in both panels are taken from Refs. [3,4].

[1] E. V. Shuryak, Prog. Part. Nucl. Phys. **53**, 273 (2004).

[2] P. F. Kolb, U. W. Heinz, arXiv:nucl-th/0305084.

[3] B. I. Abelev *et al.* [STAR Collaboration], Phys. Rev. Lett. **98**, 192301 (2007).

[4] A. Adare *et al.* [PHENIX Collaboration], Phys. Rev. Lett. **98**, 172301 (2007).

[5] H. van Hees, M. Mannarelli, V. Greco, and R. Rapp, Phys. Rev. Lett. (in press), arXiv:0709.3444 [hep-ph].

[6] O. Kaczmarek *et al.*, Nucl. Phys. Proc. Suppl. **129**, 560 (2004); C. Y. Wong, Phys. Rev. C **72**, 034906 (2005).

[7] H. van Hees, R. Rapp, Phys. Rev. C **71**, 034907 (2005).

[8] H. van Hees, V. Greco, and R. Rapp, Phys. Rev. C **73**, 034913 (2006).

[9] P. F. Kolb, J. Sollfrank, and U. Heinz, Phys. Rev. C **62**, 054909 (2000).

[10] V. Greco, C. M. Ko, and R. Rapp, Phys. Lett. B **595**, 202 (2004).

[11] L. Ravagli and R. Rapp, Phys. Lett. B **655**, 126 (2007).

# Dilepton observables at the CERN super proton synchrotron

H. van Hees and R. Rapp

Invariant-mass ($M$) spectra of dileptons in relativistic heavy-ion collisions (HICs) provide direct information on the electromagnetic (EM) current correlation function in the hot and dense medium throughout its entire evolution.

In the vacuum, as known from $e^+e^-\rightarrow$hadrons, the EM correlator is well described by the light vector mesons (most notably the $\rho$-meson) for invariant masses $M<1.5$GeV, and by a perturbative QCD continuum at $M>1.5$ GeV. Thus, to understand the dilepton signal in HICs one has to assess the in-medium modifications of the light vector mesons. At high temperatures and densities QCD predicts a phase transition from a chirally broken to a symmetric state, at a critical temperature of $T_c$=160-190 MeV at vanishing baryon density. This implies a softening of hadronic spectral functions and a degeneracy among chiral-partner states.

Employing many-body theory based on effective hadronic models [1], we have analyzed recent high-precision NA60 data [2] on dimuon $M$ and transverse-momentum ($q_T$) spectra in 158AGeV In-In collisions [2]. Our approach includes a detailed description of the light vector mesons including mesonic and baryonic interactions in the medium and results in a massive broadening especially for the $\rho$ meson, with small mass shifts. The pertinent EM current correlator determines the dilepton emission rate which has to be integrated over the thermal evolution of the medium, which we modeled by a homogeneous thermal fireball with radial flow. The temperature evolution is extracted utilizing an equation of state for an ideal gas of light quarks and gluons above $T_c$ and for a hadron resonance gas below $T_c$. In the hadronic phase hadron-chemical potentials are introduced to conserve the particle-number ratios which are fixed at chemical freeze-out temperatures of $T_{ch}\approx$160-175 MeV (consistent with thermal-model fits to heavy-ion data).

Our earlier model predictions [3] show good agreement with inclusive NA60 dimuon $M$-spectra in semi-/central In-In collisions [4], but underpredict the experimental $q_T$ spectra (and corresponding slope parameters) above $q_T\sim$1 GeV. We therefore have conducted a systematic study of sources for hard dileptons, including radiation from (i) t-channel-meson exchange in thermal $\pi\rho\rightarrow\pi\gamma$ scattering, (ii) decays of hard $\rho$ mesons, which are produced in primordial N-N collisions, undergoing jet quenching but not equilibration, (iii) decays of $\rho$ mesons after thermal freeze-out ($T_{fo}$=120-140 MeV), which in the earlier models [1,3] were approximated by an extra 1 fm/$c$ of fireball lifetime; the spectra from a thermal source are, however, softer by a Lorentz factor $1/\gamma=M/q_0$ ($q_0$: dilepton energy) compared to the decay of freely streaming $\rho$ mesons due to relativistic time dilation [2]. We also have taken into account (iv) Drell-Yan annihilation in primordial N-N collisions, extrapolated to small $M$ using constraints from the real-photon point.

Although the t-channel-meson exchange contributions are the hardest among all thermal sources, their absolute magnitude cannot explain the observed slopes of the $q_T$ spectra above 1 GeV. The comparison improves including the other sources of hard dileptons listed above. However, to reproduce the large measured effective slopes in the low-mass region ($M<1$ GeV) an increase of the radial

acceleration of the fireball is necessary, leading to larger blue shifts of the $q_T$-spectra (especially for $\rho$ decays after thermal freeze-out). The slopes at larger invariant masses are less affected since the dominant contribution in this region mostly originates from larger temperatures, i.e., earlier stages of the fireball evolution. It is important to note that the refinements of the model concerning hard dilepton sources do not spoil the previously found agreement [3] in the description of the $M$-spectra, dominated by thermal radiation which is most relevant at lower $q_T < 1$ GeV (left panel of Fig. 1). We furthermore have verified that the (earlier and recent) dielectron spectra by CERES/AN45 [5] in central 158 AGeV Pb-Au collisions are well described within our updated approach. In particular, the large enhancement at very low $M < 2m_\pi$ is consistent with our predictions and underlines the importance of baryon effects in the medium modification of the light vector mesons (middle panel of Fig. 1).

Finally we have studied the sensitivity of the model to the equation of state (EoS) by varying (i) the critical temperature according to recent lattice-QCD results [6], $T_c$=160-190 MeV, and (ii) the chemical-freezeout temperature according to thermal-model fits to hadron data in HICs [7]. In addition to our standard scenario with $T_c = T_{ch}$=175 MeV (labelled EoS-A in Fig. 1), we studied a case with $T_c = T_{ch}$=160 MeV (EoS-B), as well as $T_c$=190 MeV and $T_{ch}$=160 MeV (EoS-C). The latter is characterized by chemical equilibrium in the hadronic phase for $T$=160-190 MeV. We find that the $M$-spectra are quite insensitive to these variations in the EoS, due to the fact that the underlying dilepton rates for QGP (hard-thermal loop improved quark-antiquark annihilation) and hadron gas (hadronic many-body vector-meson spectral functions) are very similar in the vicinity of the phase boundary, interpreted as a "quark-hadron duality" [1].

Another important observation (and direct consequence of quark-hadron duality) is that the current uncertainty in $T_c$ prevents a conclusion on whether dilepton emission for 1 GeV$<M<$1.5 GeV is predominantly of partonic or hadronic (multi-pion) origin, since both the QGP- (EoS-B) and hadron-dominated (EoS-C) scenarios describe the measured $M$-and $q_T$-spectra and effective slopes comparably well.
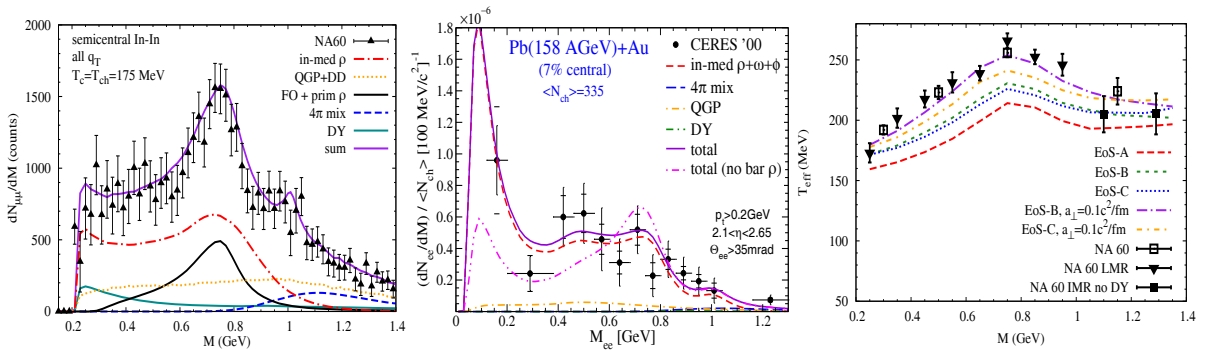


**Figure 1**. Left panel: dimuon excess spectrum of our approach [2] compared to NA60 data [4] from semicentral 158 AGeV In-In collisions; middle panel: the same model applied to compute dielectron excess spectra in 158 AGeV Pb-Au collisions confronted with CERES/NA45 data [5]; right panel: effective slope parameters of dimuon-$q_T$ spectra in semicentral 158 AGeV In-In assuming different equations of state and transverse acceleration of the thermal fireball expansion (see the text for details), compared to NA60 data [4].

[1] R. Rapp and J. Wambach, Eur. Phys. J. A **6**, 415 (1999).

[2] H. van Hees and R. Rapp, Nucl. Phys. A (in press), arXiv:0711.3444[hep-ph].

[3] H. van Hees and R. Rapp, Phys. Rev. Lett. **97**, 102301 (2006).

[4] R. Arnaldi *et al.*, (NA60 Collaboration) Phys. Rev. Lett. **100,** 022302 (2008); S. Damianovic *et al.*, (NA60 (NA60 Collaboration) Nucl. Phys. **A783**, 327 (2007).

[5] D. Adamova *et al.*, (CERES Collaboration), arXiv:nucl-ex/0611066.

[6] Z. Fodor and S. D. Katz JHEP **04**, 050 (2006); F. Karsch, J. Phys. G **34**, S627 (2007).

[7] A. Andronic, P. Braun-Munzinger and J. Stachel, Nucl. Phys. **A772**, 167 (2006); F. Becattini, J. Manninen and M. Gazdicki, Phys. Rev. C **73**, 044905 (2006).

**Transverse momentum spectra of J/ψ in heavy-ion collisions**

X. Zhao and R. Rapp

It has long been suggested [1] that the suppression of J/ψ mesons produced in primordial nucleon-nucleon collisions in ultrarelativistic heavy-ion collisions can be utilized to probe the Quark-Gluon Plasma (QGP). However, the suppression of this "direct component" can be masked by secondary J/ψ formation due to coalescence of charm and anticharm quarks (regenerated component) at the hadronization transition [2], if c-cbar pairs are produced copiously. Evidence for regeneration has been found at the Relativistic Heavy-Ion Collider (RHIC) [3], where the suppression turns out to be similar to SPS (Super Proton Synchrotron) energies although the temperature of the putative QGP at RHIC is higher.

Toward a more quantitative assessment of suppression and coalescence mechanisms, we have computed transverse momentum ($p_t$) spectra of charmonia ($\Psi = J/\psi, \chi_c, \psi'$) in a two-component approach (direct + regenerated component) [4]. For the direct component we solve a Boltzmann transport equation,

$$p^\mu \partial_\mu f_{dir}(\vec{x}_t, \vec{p}_t, \tau) = -E_\psi \cdot \Gamma(\vec{x}_t, \vec{p}_t, \tau) \cdot f_{dir}(\vec{x}_t, \vec{p}_t, \tau)$$

($f_{dir}(\vec{x}_t, \vec{p}_t, \tau)$: phase space distribution function of charmonia, $E_\psi$: energy of Ψ with 3-momentum modulus p, $\vec{x}_t$: spatial position of Ψ, $\Gamma(\vec{x}_t, \vec{p}_t, \tau)$: charmonium dissociation rates). The initial distributions, $f_{dir}(\vec{x}_t, \vec{p}_t, 0)$ incorporate nuclear absorption and Cronin effects, the latter being implemented by a Gaussian smearing of the initial $p_t$-spectra in elementary N-N collisions. The charmonium dissociation rates are evaluated using the quasi-free breakup mechanism $g(q)+\Psi \rightarrow c+cbar+g(q)$ [5] instead of the commonly employed gluo-dissociation [6], $g+\Psi \rightarrow c+cbar$, which becomes inefficient for small binding energies. The momentum dependence of the dissociation rates is shown in Fig. 1. The direct component also includes the leakage effect, i.e. charmonia exiting the fireball are not subject to suppression.
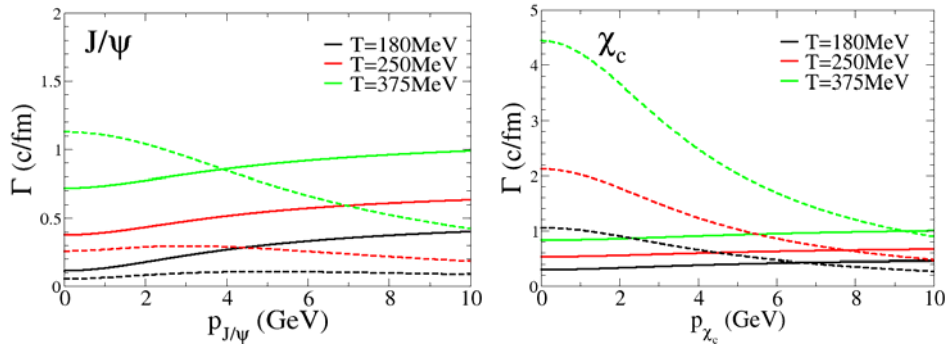


**Figure 1**. Comparison of the momentum dependence of quasifree (solid lines, in-medium binding energies) and gluo-dissociation rates (dashed lines, free binding energies) for J/ψ (left panel) and $\chi_c$ (right panel) at different temperatures.

For the regenerated charmonia we assume a local thermal distribution with $p_t$ spectra given by the blastwave expression

$$f_{bw}(p_t) \propto m_t \int_o^R rdr K_1\left(\frac{m_t \cosh y_t}{T}\right) I_0\left(\frac{p_t \sinh y_t}{T}\right)$$

(R and $y_t$: radius and transverse rapidity of the fireball); the pertinent normalization (abundance), $N_{coal}$, is determined via a momentum-independent rate equation, $dN_{coal}/d\tau = -<\Gamma>\cdot(N_{coal} - R\cdot N_\psi^{eq})$ with $<\Gamma>=\Gamma(p=0)$ and $N_\psi^{eq}$ being the charmonium equilibrium numbers from the statistical model with a correction factor $R=1-\exp(-\tau/\tau_c^{eq})$ to mimic incomplete kinetic equilibration of c-quarks in A-A collisions ( $\tau_c^{eq}$ is the thermal relaxation time for c-quarks). Our results for J/$\Psi$ transverse momentum spectra are represented by the nuclear modification factor, $R_{AA}(p_t)$ (the number of J/$\psi$'s for a given $p_t$ relative to that in p-p collisions times the number of binary collisions), for direct and regenerated components in Fig. 2 and compared to PHENIX data [3].
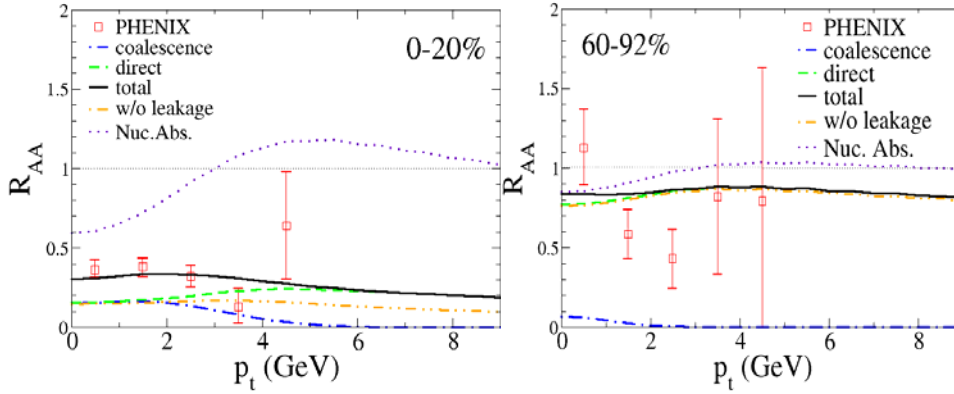


**Figure 2**. $R_{AA}$ vs. $p_t$ for central (left) and peripheral (right) Au-Au collisions at RHIC. PHENIX data [3] are compared to our calculations: initial primordial component (dotted line), including QGP and HG suppression (dashed line), and with leakage effect switched off (dash-double-dotted line); the coalescence contribution is given by the dash-dotted line.

By integrating $R_{AA}(p_t)$ over $p_t$ we obtain the centrality dependence of the inclusive J/$\psi$ yield and their average squared transverse momentum, $<p_t^2>$, in Au-Au collisions, plotted in Fig. 3 vs. the number of participant nucleons, $N_{part}$. Our results are largely consistent with PHENIX data [3]. Future studies will address the full solution of the transport equation including the gain term with microscopic input for the charm-quark distribution functions.
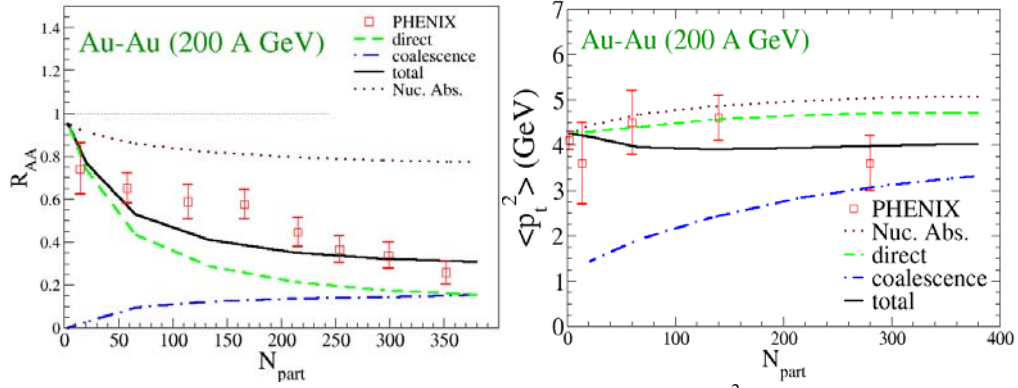
**Figure 3**. Results of the 2-component model for $R_{AA}(N_{part})$ and $<p_t^2>(N_{part})$ at RHIC, compared to PHENIX data [3]. The dotted line represnt the primordial input, while the dashed line additionally include QGP an HG suppression. The coalescence yield is represented by the dash-dotted line.

[1] T. Matsui, H. Satz, Phys. Lett. B **178**, 416 (1986).

[2] P. Braun-Munzinger and J. Stachel, Phys. Lett. B **490**, 196 (2000).

[3] A. Adare, *et al.* (PHENIX Collaboration), Phys. Rev. Lett. **98**, 232301 (2007).

[4] X. Zhao and R.Rapp, arXiv:0712.2407 [hep-ph].

[5] L. Grandchamp and R. Rapp, Phys. Lett. B **523**, 60 (2001).

[6] M. E. Peskin, Nucl. Phys. **B156**, 365 (1979); G. Bhanot and M. E. Peskin, Nucl. Phys. **B156**, 391 (1979).

# Perturbative QCD and multiple scattering in nuclear matter

R. J. Fries and A. Majumder[1]

[1]*Department of Physics, Duke University, Durham, North Carolina 27708*

Traditional factorization theorems in perturbative QCD describe only a single scattering of partons in high energy collisions of hadrons or nuclei. This is not sufficient if the mean free path of a parton is smaller than the size of the nuclear matter. A rigorous way to treat multiple scattering within a factorized pQCD framework as so-called higher twist corrections has been laid out by J. Qiu and G. Sterman. In the past R.J. Fries has successfully applied this formalism to proton-nucleus collisions. He was the first one to carry out a resummation of higher twist contributions [1]. Renewed interest in this rigorous approach comes from heavy ion physics where pQCD inspired calculations of jet energy loss have turned out to carry a dependence on model assumptions.

R.J. Fries has continued his collaboration with A. Majumder to further develop the higher-twist formalism. Their interest has turned to radiative corrections of multiple scatterings in nuclei. As a first example they studied photon emission in lepton-nucleus (e+A) scattering in the limit of small photon energies and large nuclei. This required the resummation of an arbitrary number of scatterings in the nucleus. A comprehensive paper laying out the formalism in detail will be published [2]. In the future, they plan to generalize their results to gluon emission and to apply the formalism to photon-hadron correlations.

[1] R. J. Fries, Phys. Rev. D **68**, 074013 (2003).
[2] R. J. Fries, Phys. Rev. C **77**, 065209 (2008).

# Hadro chemistry in jets as a quark gluon plasma probe

R. J. Fries and W. Liu

R. J. Fries and W. Liu have suggested to use the relative abundances of hadrons measured at high transverse momentum $p_T$ in high energy nuclear collisions as a novel and complementary probe for the quark gluon plasma. This is based on the observation that the concept of a jet of fixed flavor is ill-defined in heavy ion collisions and that the leading parton can easily change identity (or flavor) in collisions with thermal partons from the surrounding medium. Moreover, the conversion rate is directly connected to the mean free path of the parton in the medium. This idea was first worked out in Ref. [1], significantly extending several concepts that had been discussed in the literature before (e.g. induced photon radiation from jets and quark-gluon conversions).

Promising new observables have been introduced, including double ratios of hadron yields in nucleus-nucleus and proton-proton collisions. Particularly exciting is the prediction of an enhanced production of Kaons at large transverse momentum at the Relativistic Heavy Ion Collider RHIC. In the future these concepts will be applied to heavy quarks and elliptic flow at high $p_T$.

[1] R. J. Fries, Phys. Rev. C **77**, 054902 (2008).

**The initial state of high energy nuclear collisions**

R. J. Fries and collaborators

At asymptotically large energies the wave function of hadrons and nuclei exhibits a large saturated gluon density. This phenomenon has been called the color glass condensate For heavy ion collisions at RHIC and LHC this concept is believed to be very important, governing the initial state and early time dynamics of the collision. One of the main questions is how the colliding color glass evolves into a thermalized quark gluon plasma. In an ongoing effort with several collaborators R.J.Fries is working on two aspects of this question.

(a) With J. Kapusta (U of Minnesota) and Y. Li (Iowa State U) he has investigated the energy momentum tensor at early times after the collision of two nuclei in the McLerran-Venugopalan model (one model for the color glass condensate). This is based on previous work in which they investigated the classical Yang-Mills equations for the gluon field at asymptotically small times. The energy momentum tensor can be used as input for further hydrodynamic calculations of the fireball.

(b) It is believed that the fireball created in high energy nuclear collisions thermalizes after a rather short time and that ideal relativistic hydrodynamics can be used to describe the evolution of the system after equilibration. However, it becomes more and more clear that dissipative effects from shear and bulk viscosities have to be studied systematically in order to extract quantitative information about the quark gluon plasma from experiment. Together with B. Muller (Duke U) and A. Schafer (U of Regensburg), R. J. Fries started simulations of simple hydrodynamic systems using realistic bulk and shear viscosities for quark and gluon matter. The goal is to investigate off-equilibrium effects on expansion rates and entropy production. With the same collaborators R. J. Fries has also studied the decoherence time of the gluon field in leading order in the coupling constant in the McLerran-Venugopalan model. Together with the results from (a) estimates this is expected to give a complete and consistent set of initial conditions for the hydrodynamic evolution.

# The recombination model

R. J. Fries and C. Nonaka[1]

[1]*Nagoya University, Nagoya, Japan*

The recombination model has been a success story at RHIC. It describes certain features of hadron production at intermediate transverse momentum at RHIC energies by simply assuming coalescence of effective quarks into hadrons. R. J. Fries has been one of the main proponents of the recombination model in the past [1]. One remaining challenge for recombination models are RHIC data on di-hadron correlations which exhibit some features of QCD jets. Previously, R. J. Fries and collaborators showed that near-side correlations of two hadrons are compatible with a model which includes both fragmentation of jets and recombination of partons if small 2-particle correlations among partons are allowed. These correlations could emerge from quenched jets, so called hot spots.

Recently R. J. Fries started a collaboration with C. Nonaka to apply this technique to away-side correlations (i.e. hadrons that are measured with a difference of approximately 180 degrees in azimuthal angle). No such study has been carried out before. This project has the potential to finally settle open questions concerning recmbination models and di-hadron correlations. The focus will be on the baryon-to-meson ratio of away-side hadrons which can distinguish recombined hadrons from fragmented hadrons.

[1] R. J. Fries, B. Müller, C. Nonaka, and S. A. Bass, Phys. Rev. Lett. **90**, 202303 (2003).

# Determination of the nuclear vertex constants (asymptotic normalization coefficients) for the $^{7}$Be $\leftrightarrow$ $^{3}$He + $^{4}$He vertex from the N/D equations and astrophysical factor for the $^{4}$He($^{3}$He,$\gamma$)$^{7}$Be reaction

A. M. Mukhamedzhanov, L. D. Blokhintsev,[1] B. F. Irgaziev,[2] A. N. Safronov,[1] and A. A. Safronov[1]

[1]*Skobeltsyn Institute of Nuclear Physics, Moscow State University, Russia*
[2]*GIK Institute of Engineering Sciences and Technology,Topi, District Swabi, N.W.F.P.,Pakistan*

Our consideration is based on the fundamental principles of the scattering theory – analyticity and unitarity of the S matrix, i.e. the partial wave scattering amplitude is an analytical function in the momentum (energy) plane with the poles due to the bound states and cuts generated by these poles due to the unitarity conditions in all open channels. In such an approach the information abound the bound state poles and their residues ( nuclear vertex constants (NVCs) or asymptotic normalization coefficients (ANCs) ) can be obtained from the analytical continuation of the scattering amplitudes (phase shifts) from the upper part of the right (unitary) cut in the energy plane to the bound state pole. The key point here is the analytical structure of the partial Coulomb-modified nuclear scattering amplitude. On the first energy sheet this amplitude has a right (unitary) cut, the bound state poles at negative energies and the left (dynamical) cut generated by the exchange processes. At low energies the impact of the inelastic channels is small and has been neglected. Analytical structure of the Coulomb modified nuclear scattering amplitude allows one to determine the Coulomb renormalization of the ANC: $C = \Gamma(l+1+\eta)\widetilde{C}$. Here, $\eta$ is the Coulomb parameter of the bound state, $l$ is the orbital momentum of the bound state, and $\widetilde{C}$ is the renormalized ANC, which does not contain the main Coulomb effect generated by the Gamma function. We find for the ANCs $^{7}$Be $\leftrightarrow$ $^{3}$He + $^{4}$He for the ground and first excited states of $^{7}$Be $3.87\ \mathrm{fm}^{-1/2}$ and $2.95\,\mathrm{fm}^{-1/2}$, correspondingly. These ANCs determine the overall normalization of the astrophysical factor for the direct radiative capture reaction $^{4}$He($^{3}$He,$\gamma$)$^{7}$Be in the pp-chain because this reaction is totally peripheral at astrophysically relevant energies. To calculate the astrophysical factor it is sufficient to use the hard-sphere approximation with the channel radius of 4.0 fm. Our calculated astrophysical factor at zero energy is $S(0) = 0.47$ keVb.

# Benchmark on neutron capture extracted from (d,p) reaction:
## application for $^{48}$Ca(d,p)$^{49}$Ca  and $^{48}$Ca(n,γ)$^{49}$Ca

A. M. Mukhamedzhanov, P. Mohr,[1] and F. M. Nunes[2]

[1]*Strahlentherapie, Diakoniekrankenhaus Schwäbisch Hall, D-74253 Schwäbisch Hall, Germany,*
[2]*National Superconducting Cyclotron Laboratory and Department of Physics and Astronomy, Michigan State University, East Lansing, Michigan 48864*

Reaction rates of capture reactions are a crucial input to astrophysical network calculations. In particular, neutron capture reactions, which play a pivotal role in the astrophysical r-process nucleosynthesis, have to be known for nuclei between the valley of *β*-stability and the neutron-drip line. Typically the neutron capture rates for the r-process have been estimated using the statistical Hauser-Feshbach model, although this may be unreliable away from stability as the level density is low. *(n,γ)* cross sections for short-lived unstable nuclei cannot be measured experimentally and have to be taken from theory. However, the production of unstable nuclei close to the r-process path has become possible in the recent years, and neutron transfer experiments like *(d,p)* on these nuclei are becoming more and more feasible as beam intensity continues to rise. It is important to underscore that such experiments can be done also at the Cyclotron Institute, Texas A&M University. It opens a possibility to use the *(d,p)* as indirect tool to determine the direct capture *(n,γ)*.  Earlier we suggested  [1,2] a combined method to determine the spectroscopic factors (SFs) from transfer reactions using the information about the asymptotic normalization coefficients (ANCs). Introduction of the ANC will allow us to determine the parameters of the bound state potential parameters and obtain more accurate SF.  In this work we use this method to benchmark the *(d,p)* reactions to calculate the neutron radiative capture reactions. To test our method we applied it for analysis of the direct radiative capture reaction $^{48}$*Ca(n,γ)*$^{49}$*Ca*. We note that $^{48}$*Ca* is considered to be a double magic nucleus, hence the $^{49}$*Ca*  ground state is well described as a single-particle  neutron wave function bound to the core.  To apply our method first we determine the ANC for $^{49}$*Ca* → $^{48}$*Ca* + n from the sub-Coulomb transfer reaction $^{48}$*Ca(d,p)*$^{49}$*Ca* [3]**.**  After that we determine the SF for the configuration $^{48}$*Ca + n*.  Fortunately in the case under consideration direct measurements for $^{48}$*Ca(n,γ)*$^{49}$*Ca*  are available [4] and we can compare the SF and ANC determined from the radiative capture process with the ones obtained from the $^{48}$*Ca(d,p)*$^{49}$*Ca*  reaction**.**  Results for the ground state of $^{49}$*Ca* are shown in Fig. 1  for  the SF   $S(b)$  and ANC $C^2(b)$, respectively, where b is the single-particle ANC. As expected,  the sub-Coulomb reaction is totally peripheral  and provides the ANC $C^2 = 32.1 \pm 3.2 \, \mathrm{fm}^{-1}$  for the $^{49}$*Ca* (0.00 MeV) → $^{48}$*Ca* (0.00 MeV) + n. $^{48}$*Ca(d,p)*$^{49}$*Ca*  reactions at 13 and 19 MeV deuteron energies are also peripheral and provide only the information about the ANC. However, the $^{48}$*Ca(d,p)*$^{49}$*Ca*   reactions at energies 30 and 56 MeV are not peripheral and, by comparing the  $C^2(b)$  with the ANC  $C^2$, one can determine (from their intersection)  the single-particle ANC b and the SF   $S = C^2 / b^2$.  In Fig. 1  we also show   $S(b)$  and $C^2(b)$  obtained for the  direct radiative capture reaction $^{48}$*Ca(n,γ)*$^{49}$*Ca***.**
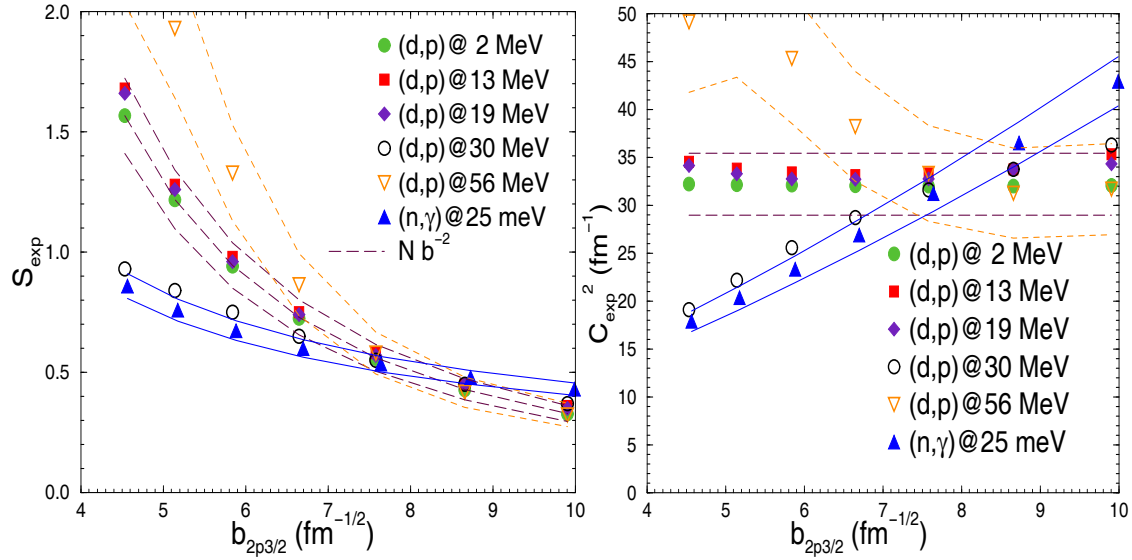
**Figure 1**. $S(b)$ and $C^2(b)$ from the $^{48}Ca(d,p)^{49}Ca$ reaction at $E_d$ = 1.99 MeV (green dots), $E_d$ = 13MeV (red squares), $E_d$ = 19 MeV (purple diamonds), $E_d$ = 30 MeV (open circles) $E_d$ = 56 MeV (open triangles), and from $^{48}Ca(n,\gamma)^{49}Ca$ at 25 meV (blue triangles). Also shown are the experimental uncertainties in the *(d,p)* reaction at 1.99 MeV (dashed lines), at 56 MeV (long-dashed lines) and the *(n,γ)* reaction (solid lines).

As we can see the curves for *(n,γ)* and *(d,p)* reactions intersect with the sub-Coulomb curves at $b \approx 7.8$ fm$^{-1/2}$ confirming that the *(d,p)* and *(n,γ)* provide a consistent information about the SFs. Thus we can conclude that for $^{49}Ca$ both *(n,γ)* and *(d,p)* provide very close SF, i.e. *(d,p)* reactions can be used to determine the SF and calculate direct radiative *(n,γ)* reaction cross sections. The paper has been published in Phys. Rev. C **77**, 051601 (R) 2008.

[1] S. A. Goncharov *et al.*, Sov. J. Nucl. Phys. **35**, 383 (1982).

[2] A. M. Mukhamedzhanov and F. M. Nunes,, Phys. Rev. C **72**, 017602 (2005).

[3] J. Rapaport , A. Sperduto, and M. Salomaa, Nucl. Phys. **A197**, 337 (1972).

[4] H. Beer *et al.*, Phys. Rev. C **54**, 2014 (1996).

# A new astrophysical S factor for the $^{15}$N(p,γ)$^{16}$O reaction via the ANC method

A. M. Mukhamedzhanov, P. Bem,[1] V. Burjan,[1] C. A. Gagliardi, V. Z. Goldberg, Z. Hons,[1]
M. La Cognata,[2] V. Kroha,[1] J. Mrazek,[1] J. Novak,[1] S. Piskor,[1] R. G. Pizzone,[2] A. Plunkett,
S. Romano,[2] E. Simeckova,[1] C. Spitaleri,[2] L. Trache, R. E. Tribble, F. Vesely,[1] and J. Vincour[1]

[1]*Nuclear Physics Institute, Czech Academy of Sciences, Rez, Czech Republic*
[2]*Universita di Catania and INFN Laboratori Nazionali del Sud, Catania, Italy*

The $^{15}$N(p,γ)$^{16}$O reaction provides a path from the CN cycle to the CNO bi-cycle and CNO tri-cycle. The measured astrophysical factor for this reaction is dominated by resonant capture through two strong $1^-$ resonances at $E_R$ = 312 and 962 keV and direct capture to the ground state. Asymptotic normalization coefficients (ANCs) for the ground and 7 excited states in $^{16}$O were extracted from the comparison of experimental differential cross sections for the $^{15}$N($^3$He,d)$^{16}$O reaction with distorted-wave Born approximation calculations. Using these ANCs and proton and resonance widths determined from an R matrix fit to the data from the $^{15}$N(p,α)$^{12}$C reaction, we have carried out an two-level, two channel R matrix calculation to obtain the astrophysical factor for the $^{15}$N(p,γ)$^{16}$O reaction shown in Fig. 1. The results indicate that the direct capture contribution was previously overestimated. We find the astrophysical factor to be S(0) = 36.0 ± 6.0 keVb, which is about a factor of two lower than the presently accepted value. Our astrophysical factor in the energy interval 150 − 300 keV goes along the lower limit of data reported in [1], agreeing with the data from [2]. We conclude that for every 2200±300 cycles of the main CN cycle, one CN catalyst is lost due to this reaction.
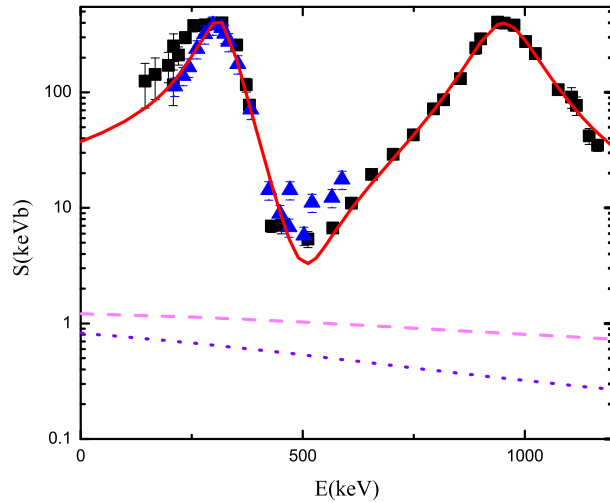


**Figure 1.** The astrophysical factor for the $^{15}$N(p,γ)$^{16}$O reaction. The black squares are data from [1], the blue triangles are data from [2], solid red line is our total S factor, magenta dotted line is the nonresonant S factor for direct captures to 8 bound states and violet dotted line is the nonresonant S factor for capture to the ground state.

[1] C. Rolfs and W. S. Rodney, Nucl. Phys. **A235**, 450 (1974).
[2] D. F. Hebbard, Nucl. Phys. **15**, 289 (1960).

# Indirect measurement of the $^{18}$O(p,α)$^{15}$N reaction rate through the Trojan horse method

M. La Cognata,[1] C. Spitaleri,[1] R. E. Tribble, T. Al-Abdullah, A. Banu, S. Cherubini,[1]
V. Crucilla,[1] C. Fu, V. Z. Goldberg, M. Gulino,[1] L. Lamia,[1] A. M. Mukhamedzhanov,
R. G. Pizzone,[1] S. M .R. Puglia,[1] G. G. Rapisarda,[1] S. Romano,[1] M. L. Sergi,[1]
G . Tabacaru, L. Trache, S. Tudisco,[1] A. Tumino,[1] and Y. Zhai.

[1] *INFN - Laboratori Nazionali del Sud, Dipartimento di Metodologie Chimiche e Fisiche per l'Ingegneria, Universita di Catania, Catania, Italy*

$^{19}$F is one of the few naturally occurring isotopes whose nucleosynthesis is still uncertain. SNe, AGB and WR stars are its most likely sources. In particular fluorine abundances observed in giants can constrain AGB star models since they are sensitive to the environmental conditions in the intershell region and to the dynamics of the mixing phenomena taking place in such stars. The $^{18}$O(p,α)$^{15}$N reaction can affect fluorine yield from AGB stars since it produces $^{15}$N nuclei which are later burnt to $^{19}$F through the $^{15}$N(α,γ)$^{19}$F capture reaction during a thermal pulse. Large uncertainties characterize $^{19}$F nucleosynthesis since experimental $^{19}$F abundances are not reproduced by current AGB models.

A possible solution of these experimental problems can come from nuclear physics studies. Indeed the measurement of nuclear cross sections at ultra-low energies is a very difficult task because of the presence of the Coulomb barrier exponentially suppressing the cross section. Therefore extrapolation is necessary when data at astrophysical energies are unavailable. Even when measurements are available inside the Gamow window, electron screening makes the bare-nucleus cross section inaccessible. Thus indirect techniques such as the Trojan Horse Method (THM) have been developed to extract low-energy cross sections with no need of extrapolation.

In the present work the THM is applied to the $^{2}H(^{18}O,^{15}N \; \alpha)n$ ($2 \rightarrow 3$ particles process) to deduce the sub-Coulomb astrophysical S(E)-factor for the $^{18}O(p,\alpha)^{15}N$ reaction.
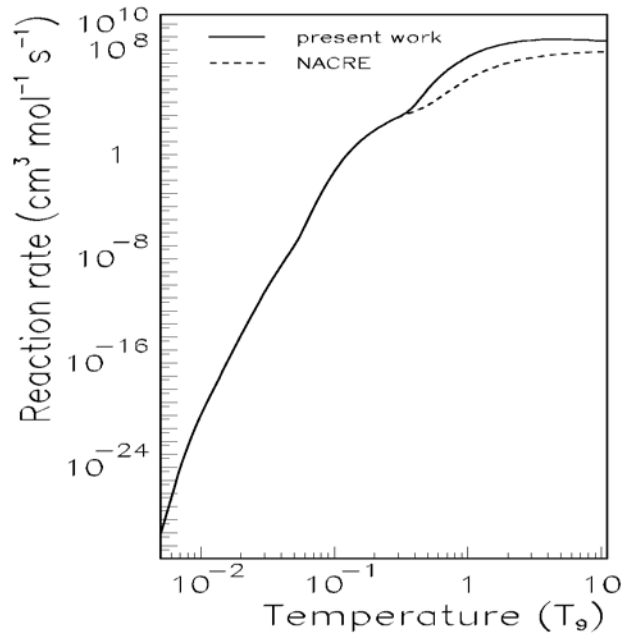


**Figure 1.** Reaction rate for $^{18}$O(p,α)$^{15}$N as function of temperature.

The experiment was performed at the Texas A&M University Cyclotron Institute, with a 54 MeV, 5~enA $^{18}$O beam impinging onto a 100 $\mu g / cm^2$ thick CD$_2$ target.

The second stage of the experiment with better resolution has been performed at Catania National Laboratory,. The results of the experiments are being analyzed and new theoretical approach developed at Texas A&M University is applied to determine the astrophysical factor for the $^{18}$O$(p, \alpha)^{15}$N reaction from the THM data. New reactions rates calculated using the data obtained from these measurements are shown in Fig. 1. The paper has been submitted to Phys. Rev. Lett.

# S-matrix poles and determination of the bound, virtual and resonance parameters for the light nuclei

B. F. Irgaziev,[1] V. Z. Goldberg, A. M. Mukhamedzhanov, Yu. V. Orlov,[2] and I. Qazi[1]

[1]*GIK Institute of Engineering Sciences and Technology,Topi, District Swabi, N.W.F.P.,Pakistan*

[2] *Skobeltsyn Institute of Nuclear Physics, Moscow State Universit, Moscow, Russia*

A general method is developed for determination of the *S*-matrix pole parameters for bound, virtual and resonance states based on numerical solutions with high precision of the Schrödinger equation. This method is well-known for the bound state. In this work we generalize it for the case of the Gamov resonance and virtual states in spite of the fact that the corresponding solutions increase exponentially at $r \to \infty$. The specific calculations are performed for the virtual states of the $^2$He and triton. The results obtained for the virtual $^2$H and triton are in good agreement with those found using the Lippmann−Schwinger integral equations analytically continued to the unphysical energy sheet. The normalization method for the Gamov state wave function is also considered.

Using the developed method we investigated the resonance states $(1/2^+, 5/2^+)$ in $^{15}$F and its ground state which is the subthreshold resonance. We analyzed also the bound $3/2^+$ state of $^{14}$N, the low-lying states $1/2^+$ (gr.st.) and the excited states $1/2^-$ and doublet $(5/2^+, 3/2^-)$ in mirror nuclei $^{11}$Be and $^{11}$N. Our two-body (nucleon-target) approach allows one to treat on the equal foot both bound and virtual states and resonances. In particular, we are able to determine the pole of the S matrix for the broad resonance $s^+_{1/2}$ in $^{11}$N, when the phase shift does not reveal resonance behavior.

# Surface-integral approach to scattering theory

A. S. Kadyrov,[1]  A. M. Mukhamedzhanov,  I. Bray, [1] and A. T. Stelbovics[1]

[1]*Curtin University of Technology, GPO Box U1987, Perth, WA 6845, Australia*

It is customary to define the scattering amplitude in terms of the scattering wavefunction and the potential of interaction. Despite the fact that the Coulomb wave function and the Coulomb potential are both known analytically, the conventional theory is not able to provide a standard definition for the amplitude of scattering of two charged particles, which yields the Rutherford cross section. Such a definition has been given only recently [1] in a so-called surface-integral approach. Consider now breakup of a bound state of two particles in collisions with a third particle when all particles are charged. Here again the conventional theory fails to give a formal definition for calculating the breakup amplitude in post form in terms of the total wavefunction with outgoing scattered-wave boundary conditions describing this breakup process. For the atomic three-body problem such a form of the breakup amplitude has also been given recently [2,3] in the same approach.

The goal of our work is to extend the general formalism of scattering theory to cover two-body and three-body systems with long range interactions with Coulombic tails. The extension is based on a surface-integral approach. New definitions for the potential scattering amplitude valid for arbitrary interactions are presented. For the Coulomb potential the generalized amplitude gives the physical on-shell amplitude without recourse to a renormalization procedure. New representations for the breakup amplitude in a three-body system are derived. This is shown to resolve a long-standing problem about the missing conventional *post* form of the breakup amplitude for the long-range Coulombic  interactions. The new forms are found to have equivalent surface-integral forms well suited for practical calculations. Finally, we derive the surface-integral representations for amplitudes for all other possible scattering processes taking place in an arbitrary three-body system.

[1] A. S. Kadyrov, I. Bray, A. M. Mukhamedzhanov, and A. T. Stelbovics, Phys. Rev. A **72**, 032712 (2005).
[2] A. S. Kadyrov, A. M. Mukhamedzhanov, A. T. Stelbovics, and I. Bray, Phys. Rev. A **70**, 062703 (2004).
[3] A. S. Kadyrov, I. Bray, A. T. Stelbovics, and A. M. Mukhamedzhanov, (submitted)

# SECTION IV

# ATOMIC, MOLECULAR
# AND MATERIALS SCIENCE

**Systematics of *K* and *L* x-ray satellite spectra**

V. Horvat and R. L. Watson

Multiple inner-shell ionization of an atom in a heavy-ion collision and the vacancy rearrangement that follows are fundamental processes that so far have not been adequately described theoretically. The only fundamental theory of multiple inner-shell ionization whose results are widely available is the geometrical model [1]. It predicts that in central collisions (i.e. collisions restricted to small impact parameters) the average fraction of vacancies produced in the shell having principal quantum number $n$ is given by [1]

$$p_n = X_n /[4.2624 + X_n^2 (1 + 0.5 \exp(-X_n^2 /16))] , \tag{1}$$

where

$$X_n = 4V[G(V)]^{1/2} Z_1 \alpha c /(n v_1) \tag{2}$$

is referred to as a universal variable. In eq. (2), $Z_1$ is the projectile atomic number, $\alpha$ is the fine structure constant $c$ is the speed of light in vacuum, $v_1$ is the projectile speed, $n$ is the principal quantum number of the spectator vacancies, $V = v_1 /v_2$ is the scaled projectile speed ($v_2$ is the average speed of an electron having principal quantum number $n$), and $G(V)$ is the binary encounter approximation (BEA) scaling function [2].

However, we found [3] that this result greatly overestimates the measured average number of $L$- and $M$-shell vacancies produced in central heavy-ion collisions and, therefore, cannot be relied upon for accurate predictions. Nevertheless, based on measurements of $K\alpha$ x-ray spectra involving a large variety of thick solid targets, projectiles, and collision energies, we have established [3] that the measured values of the apparent average fraction of $L$ vacancies at the time of $K$ x-ray emission ($p_L^x$) define a "universal" curve when plotted as a function of $X_2$. Furthermore, it was found [3] that the available data can be well represented by

$$p_L^x = a_2 /[1 + (b_2 / X_2)^{c_2}], \tag{3}$$

using $a_2 = 0.537 \pm 0.006$, $b_2 = 2.11 \pm 0.08$, $c_2 = 2.02 \pm 0.03$.

This analysis was subsequently applied to the spectra of target $L$ x rays [4]. It was found that a formula similar to eq.(3) can be used to describe the apparent average fraction of $M$ vacancies at the time of $L$ x-ray emission;

$$p_M^x = a_3 /[1 + (b_3 / X_3)^{c_3}], \tag{4}$$

where $a_3 = 0.530 \pm 0.012$, $b_3 = 1.507 \pm 0.044$, and $c_3 = 2.15 \pm 0.12$. This finding adds considerable weight to the significant role the geometrical model variable plays in the description of multiple ionization by

heavy ion impact. These results are important because they provide a means of accurately predicting the characteristics of $K$ and $L$ x-ray satellite distributions for other collision systems, regardless of projectile energy, projectile atomic number, and target atomic number.

The two curves defined by eqs.(3,4) are shown in Figure 1. The one representing $p_M{}^x$ as a function of $X_3$ [eq. (4)] lies above the one representing $p_L{}^x$ as a function of $X_2$ [eq. (3)]. The difference between the two sets of values reaches a maximum of $0.089 \pm 0.017$ at $X = 1.9$. However, at large $X$ the difference is statistically insignificant ($a_3 - a_2 = 0.007 \pm 0.013$). The maximum difference is significantly larger than the standard deviation of the residuals (0.013) obtained in the fit to the measured data points. This indicates that there may be some deviation from the universal scaling predicted by the geometrical model at the intermediate values of the universal variable. However, if the two curves are plotted as a function of $X/b$ (as shown in Figure 2), the maximum difference between them is less than 0.009.
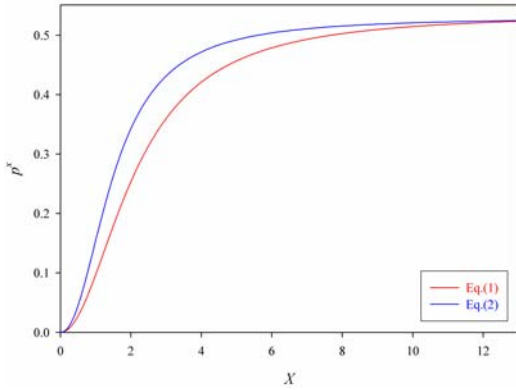


**Figure 1.** Apparent average fraction of $L$-shell [eq.(3)] and $M$-shell vacancies [eq.(4)] at the time of $L$ and $M$ x-ray emission, respectively, as a function of the universal variable.
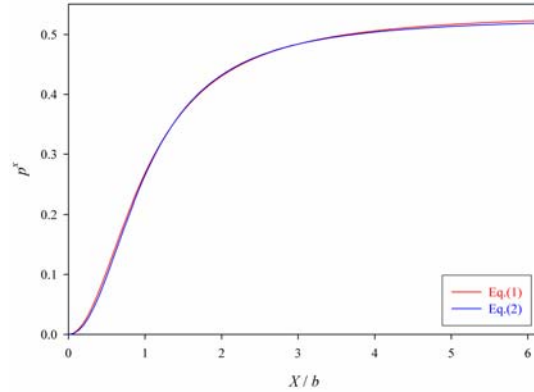


**Figure 2.** Apparent average fraction of $L$-shell [eq.(3)] and $M$-shell vacancies [eq.(4)] at the time of $L$ and $M$ x-ray emission, respectively, as a function of the universal variable divided by the empirical parameter $b$.

[1] B. Sulik, I. Kadar, S. Ricz, D. Varga, J. Vegh, G. Hock, and D. Berenyi, Nucl. Instrum. Methods Phys. Res. **B28**, 509 (1987).
[2] J. H. McGuire and P. Richard, Phys. Rev. A **9**, 1374 (1973).
[3] V. Horvat, R. L. Watson, and Y. Peng, Phys. Rev. A **74**, 022718 (2006).
[4] V. Horvat, R. L. Watson, and J. M. Blackadar, Phys. Rev. A **76**, 032724 (2008).

# $K\alpha$ x-ray satellite distribution of Ar produced in heavy ion collisions

V. Horvat, R. L. Watson, and Y. Peng

Spectra of $K\alpha$ x rays emitted from Ar gas at atmospheric pressure under bombardment by 10 MeV/amu heavy ions (atomic number $Z_1 = 6$ to 79) were measured in high resolution using a curved crystal spectrometer. The results are shown in Figure 1. Energies of the $K\alpha_{1,2}$ and $K\beta_1$ diagram transitions are indicated by the vertical dashed lines. The $K\alpha_{1,2}$ peak includes unresolved contributions of $2p\rightarrow 1s$ transitions from ions with a single vacancy and $2p\rightarrow 1s$ transitions from ions with additional $M$-shell vacancies. The former are known as $K\alpha$ diagram transitions, while the latter will be referred to as $K\alpha L^0$ satellites. Additional $i$ spectator vacancies in the $L$ shell give rise to the peaks that are shifted up in energy and, consequently, resolved from each other and from the previously described $K\alpha_{1,2}$ peak. They will be referred to as $K\alpha L^i$ satellite peaks. Most of the $K\alpha L^i$ satellite transitions ($i = 0$ to 7) are due to $K$-shell ionization by the projectiles, while most of the diagram



**Figure 1.** Measured spectra of x rays emitted from Ar gas at the pressure of 1 atm under bombardment by 10 MeV/amu ions (as labeled).

transitions are due to secondary $K$-shell ionization [1,2]. Figure 1 shows that the distribution of $K\alpha$ satellites shifts to higher average values of $i$ as the projectile atomic number increases.

The distribution of $M$-shell vacancies associated with $K\alpha L^i$ satellite transitions affects the widths and centroids of the corresponding peaks. Typically, this effect is small enough so that the $K\alpha L^i$ satellite peaks still can be resolved from each other, but large enough to obliterate any structure that might arise due to the various ways in which the electronic angular momenta can be coupled (i.e., multiplet splitting), although, in most cases, such a structure cannot be observed due to the complexity of multiplet splitting alone. However, there are two notable exceptions. One corresponds to the case in which $i = 0$ and the average number of $M$-shell vacancies is much less than one, while the other corresponds to the case in which $i = 7$ and the average number of $M$-shell vacancies is very close to the maximum (i.e., 8 for Ar). In the former case it may be possible to resolve the $K\alpha_{1,2}$ doublet (provided that the resolution of the

spectrometer is adequate, which is not the case here), while in the latter case it may be possible to resolve the $K\alpha L^7$ doublet (which is the case here). The latter effect is obvious in the spectra induced by Kr, Xe, Ho, Ta, and Au projectiles, in which the two $K\alpha L^7$ peaks are prominent.

In the absence of any $M$-shell electrons, the $K\alpha L^7$ doublet consists of a lower energy peak, corresponding to the $1s2p(^3P)\rightarrow 1s^2(^1S)$ transition, and a higher energy peak, corresponding to the $1s2p(^1P)\rightarrow 1s^2(^1S)$ transition. The predominant contribution to the $^3P$ peak is expected to originate from the $^3P_1$ state, which should be formed with the same statistical probability as the $^1P_1$ state, but its decay is delayed because $^3P\rightarrow{}^1S$ transitions are spin forbidden. Therefore, there is a larger probability for the $^3P$ state to decay by non-radiative means, such as collisional quenching. The probability for collisional quenching increases with increasing gas pressure, which leads to the reduction in intensity of the $^3P\rightarrow{}^1S$ peak relative to the $^1P\rightarrow{}^1S$ peak [3].

An additional $K$ vacancy gives rise to peaks that are shifted even higher up in energy. They are referred to as $K^2\alpha L^i$ satellite peaks (or $K\alpha$ hypersatellites). In the case of Ar, $K\alpha$ hypersatellites start somewhere between the $K\alpha L^7$ satellite and the $K\beta_1$ diagram peak. As illustrated by Figure 1, their distribution also shifts to higher average values of $i$ as the projectile atomic number increases. In the spectra induced by C and Ne projectiles, the hypersatellite peaks are buried in the background.
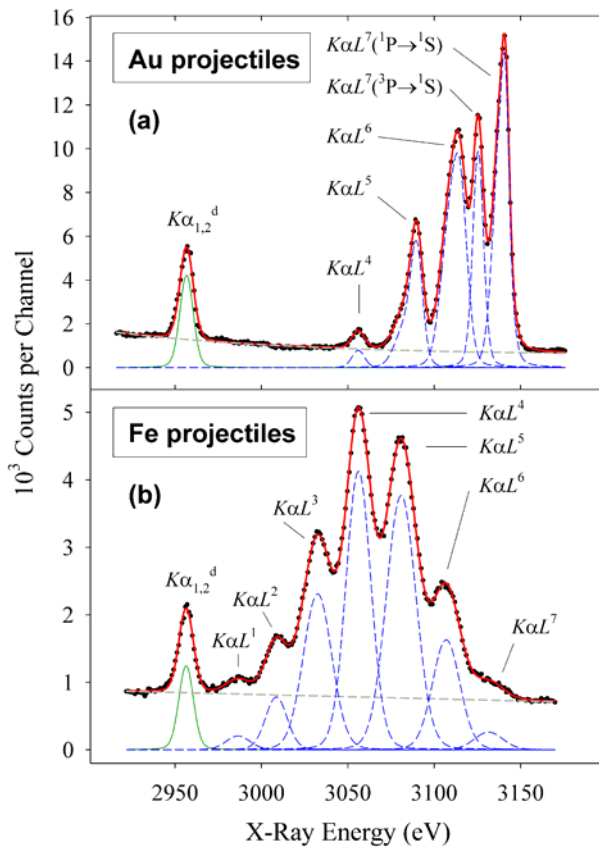


**Figure 2.** Fitted $K\alpha$ satellite spectra of Ar induced by (a) Au and (b) Fe projectiles at 10 MeV/amu.

The measured x-ray spectrum induced by sulfur ions contains significant contributions from the projectile $K\beta_1$ transitions. Their contribution overlaps with that of the Ar $K\alpha L^5$ satellite. The red circles in Figure 1 show the uncorrected (normalized) spectrum, while the red line shows the spectrum in which the contribution from sulfur $3p\rightarrow 1s$ transitions has been subtracted. Additionally, iron projectile $K\alpha$ x rays from second order diffraction may contribute to the Ar $K$ x-ray spectra in the hypersatellite region. Therefore, the peaks in the Ar $K\alpha$ hypersatellite region were analyzed only for the spectra induced by Kr, Xe, Ho, Ta, and Au projectiles.

The $K\alpha$ satellite and hypersatellite intensity can be described quantitatively in terms of the apparent average fraction of $L$ vacancies ($p_L^x$), defined as

$$p_L^x = \tfrac{1}{8}\sum_{i=1}^{8}(iI_i)/I_{tot} , \qquad (1)$$

where

$$I_{tot} = \sum_{i=0}^{8} I_i \; , \tag{2}$$

In the expressions above, $I_i$ are the intensities of the $K\alpha L^i$ peaks. For selected cases (listed above), $p_L^x$ was also determined from the intensities of $K^2\alpha L^i$ peaks.

Two examples of the fitted $K\alpha$ satellite spectra (those obtained with Au and Fe projectiles) are shown in Figure 2. The measured data points are shown as solid black circles, while the thick solid (red) line represents the overall fit. The background is shown as a thick dashed (gray) line, while the thin solid (green) line outlines the contributions from the diagram x rays. The thin dashed (blue) lines represent the contributions from individual peaks.

The values of $p_L^x$ determined using Eqs.(1,2) based on the results from least-squares curve-fitting of the collected spectra are shown in Figure 3, in which the open circles show the results obtained using the intensities of the $K\alpha$ satellite peaks, while the filled circles show those obtained using the intensities of the $K\alpha$ hypersatellite peaks. The thin solid (red) line is the best-fit logistic curve for the "satellite" data points, while



**Figure 3.** The apparent average fraction of $L$-shell vacancies at the time of $K$ x-ray emission ($p_L^x$) as a function of the universal variable.

the thin dashed (green) line is the best-fit logistic curve for the "hypersatellite" data points. The thick solid (blue) line represents the result from Ref.[4], which was obtained from the satellite peak intensities in measurements with various *solid* targets (atomic numbers $Z_2 = 6$ to 92). The thick dashed (black) line represents the geometrical model prediction of the average fraction of $L$ vacancies at the time of collision, according to Eq.(21) from Ref.[5].

The magnitude of the difference between the red and the blue curve in Figure 3 at any given value of $X_2$ is a measure of the (negative) contribution of interatomic transitions to the values of $p_L^x$ in solids. Apparently, interatomic transitions play an increasingly significant role as the number of atomic vacancies increases (i.e. when the rate of intraatomic transitions is reduced due to the reduced availability of atomic electrons). Actually, the differences between the red and the blue curves in Figure 3 are more likely to represent lower limits to the contributions from interatomic transitions. This is because projectiles traveling in solids have more inner-shell vacancies than those traveling in gas due to the higher collision frequency. Therefore, ionization of solid targets should initially be enhanced over that of gas targets.

The green curve in Figure 3 shows the results obtained for the $K\alpha$ hypersatellites. It lies above the red curve for all values of $X_2$, which reflects the fact that an increased degree of $K$-shell ionization also leads to an increased degree of $L$-shell ionization. Apparently, collisions between a target atom and a heavy ion at smaller impact parameters (i.e., those that are more likely to result in double $K$-shell ionization) also reduce the $L$-shell electron population more effectively.

[1] R. L. Watson, J. M. Blackadar, and V. Horvat, Phys. Rev. A **60**, 2959 (1999).
[2] V. Horvat and R. L. Watson, J. Phys. B **34**, 777 (2001).
[3] H. F. Beyer, R. Mann, and F. Folkmann, J. Phys. B **14**, L377 (1981), H. F. Beyer, R. Mann, and F. Folkmann, J. Phys. B **15**, 1083 (1982).
[4] V. Horvat, R. L. Watson, and Y. Peng, Phys. Rev. A **74**, 022718 (2006).
[5] B. Sulik, I. Kadar, S. Ricz, D. Varga, J. Vegh, G. Hock, and D. Berenyi, Nucl. Instrum. Methods Phys. Res. **B28**, 509 (1987).

# Kα x-ray satellite and hypersatellite intensity distributions
## of vanadium metal and oxides excited in heavy ion collisions

R. L. Watson, V. Horvat, and Y. Peng

Previous work has shown that the intensity distributions of Kα x-ray satellites arising from the decay of collision-produced excited states containing single K- plus additional L-shell vacancies are sensitive to the chemical environment for elements in the third row of the periodic table [1,2]. The origin of this chemical effect has been attributed to L vacancy transfer processes occurring between the time of collision and the time of x ray emission. In particular, fast transitions from higher levels to the L shell can change the number of L vacancies present when a K x ray is emitted. Furthermore, inter-atomic transitions from neighboring atoms can significantly contribute to the L-vacancy quenching process. For third row elements, transitions to the L shell must involve valence electrons and hence the chemical environment can be expected to have a direct influence on the rates of both intra-atomic and inter-atomic vacancy transfer.

So far, similar chemical effects have not been reported for fourth row elements. The valence shell of these elements is the N shell, which implies that inner shell x-ray transitions will be less sensitive to the chemical environment. However, chemical bonding in the fourth row transition elements involves the 3d electrons and this fact has led to extensive investigations of the dependence on oxidation state of their Kβ x-ray structure excited by electrons, photons, and protons (see for example Refs. 3 and 4). These studies have revealed significant changes in the relative intensities of the various Kβ components.

Recently we have measured the Kα x-ray spectra of vanadium metal and three of its oxides (VO, $V_2O_4$, and $V_2O_5$), excited by 15 MeV/amu Ne, Ar, Kr, Ag, and Ho ions, in order to examine the Kα x-ray satellite and hypersatellite intensity distributions for evidence of a chemical dependence. Vanadium was chosen as the target element because the energy region covered by its K x-ray spectrum could be accessed with good resolution by second order diffraction using a LiF crystal. In addition, its Kα satellites and hypersatellites are well separated from each other and from the Kβ diagram/satellite peaks. A spectrum obtained with 15 MeV/amu Kr ions incident on vanadium metal is shown in Fig. 1. The $K\alpha_{1,2}$ (or $KL^0$) and $K\beta_{1,3}$ diagram peaks (solid green lines) are predominately excited by secondary electrons and x-rays, while the major features of interest here, the satellite and hypersatellite distributions (dashed blue lines), are produced by heavy ion collisions in which single and double K plus additional L vacancies are created, respectively.

The spectra were corrected for absorption and detector efficiency, and fit with Voigt functions as shown in Fig. 1. The apparent average L-vacancy fractions, $p_L^x$, (defined in the preceding report) were calculated directly from the measured satellite and hypersatellite intensities. In the case of the satellites, it was necessary to estimate the intensity of the collision-produced component of the $KL^0$ peak by fitting the satellite intensities to a binomial distribution. Since the vanadium oxide targets were thick compressed pellets, care was taken to accurately account for the x-ray production and absorption cross sections in calculating the average projectile energy associated with the measured x-ray spectra.
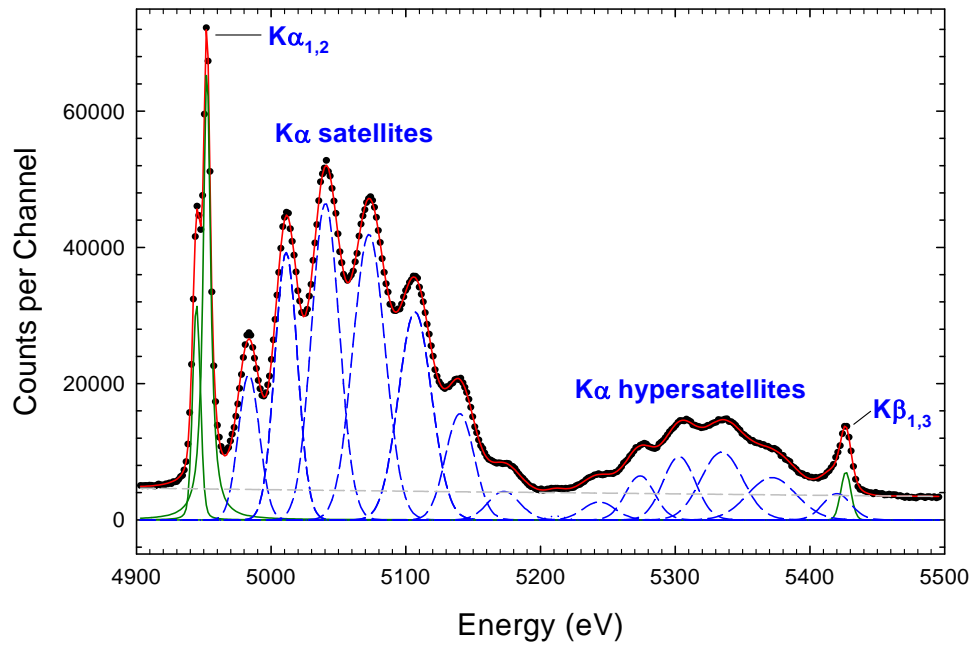
**Figure 1**. Spectrum of vanadium Kα x rays excited by 15 MeV/amu Kr ions incident on a vanadium metal target. The solid (red) curve through the data points shows the overall fit to the data.
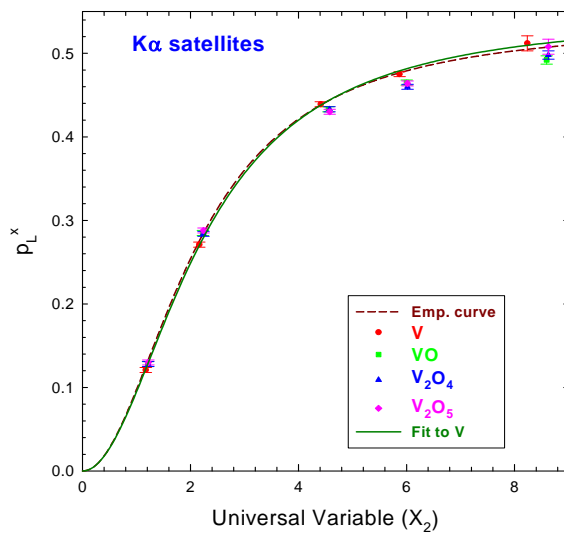


**Figure 2**. Comparison of the apparent average L-vacancy fractions for the satellites of vanadium metal and oxides as a function of the geometric model parameter. The solid (green) curve shows a fit to the vanadium metal points and the dashed (brown) curve shows the empirical curve determined previously [5] for a variety of metal targets.

The Kα x-ray satellite results are shown in Fig. 2 in the form of a plot of $p_L^x$ as a function of the geometric model variable $X_2$ (see preceding report). Based on our previous work with metal targets [5], we expect the vanadium metal values to lie on an empirical curve shown by the dashed (brown) line. The solid (green) line was fit to the vanadium metal points and shows very good agreement with the empirical curve. The relatively low $p_L^x$ value data points for the vanadium oxides (obtained using Ne and Ar projectiles) are displaced from the corresponding vanadium metal points due to projectile energy loss, but they fall on the same curve. This indicates that their satellite distributions are identical to those that would be obtained for vanadium metal using projectiles of the same average energy. However, the oxide $p_L^x$ values obtained with the higher atomic number projectiles fall significantly and systematically below the curve defined by the metal data points. (It should be noted that the data points for Ho projectiles have much larger error bars than the rest due to low counting statistics caused by the limited beam intensity that was available). Although the effect is small, it may be concluded that, as the L-vacancy fraction increases, the oxides become somewhat more efficient at filling L vacancies than the metal

The results obtained for the Kα x-ray hypersatellites are shown in Fig. 3. Unfortunately, the low
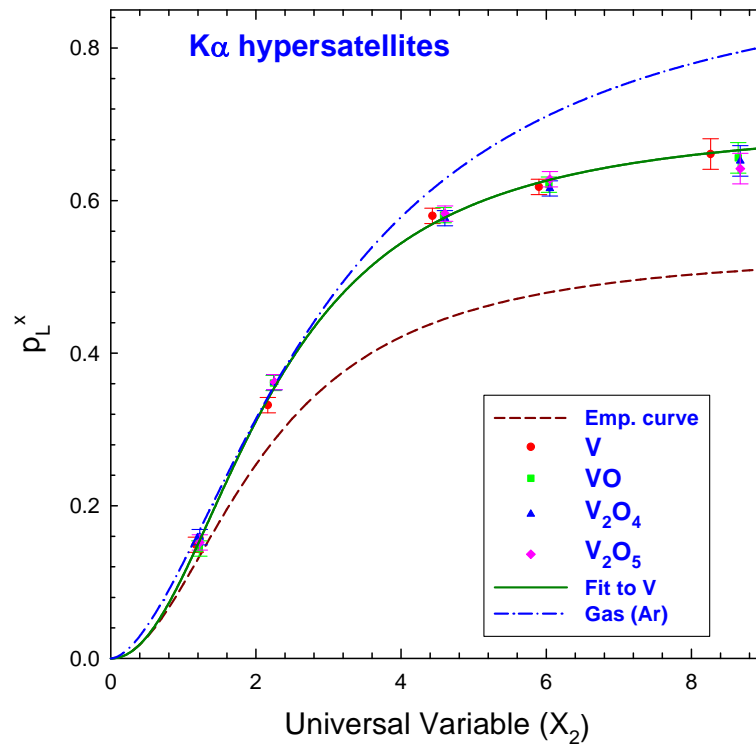


**Figure 3**. Comparison of the apparent average L-vacancy fractions for the hypersatellites of vanadium metal and oxides as a function of the geometric model parameter. The solid (green) curve shows a fit to the vanadium metal points, the dashed (brown) curve shows the empirical satellite curve, and the dot-dashed (blue) curve is a fit to the Ar (gas) hypersatellite data from the preceding report.

intensities of the hypersatellites and the accompanying larger error bars prevent as sensitive a test as was possible for the satellites.  Considering the experimental error, it must be concluded that there is no evidence of a chemical effect for the hypersatellite intensity distributions.  However, it is apparent from a comparison of the fitted hypersatellite curve (green) with the empirical satellite curve (brown) that, for solid targets, the $p_L^x$ values of the hypersatellites are much larger than those of the satellites.  Furthermore, comparison of the solid (green) curve  with the dot-dashed (blue) curve in Fig. 3 (from the Ar data discussed in the preceding report) shows there is an even larger increase in the $p_L^x$ values for the higher atomic number projectiles going from solid targets to gaseous targets, in which inter-atomic transitions cannot occur.

[1] R. L. Watson, A. K. Leeper, B. I. Sonobe, T. Chiao, and F. E. Jenson, Phys. Rev. A **15**, 914 (1977).
[2] J. A. Demarest and R. L. Watson, Phys. Rev. A **17**, 1302 (1978).
[3] S. D. Gamblin and D. S. Urch, J. Elect. Spectrosc. And Rel. Phenom. **113**, 179 (2001).
[4] S. Fazinić, M. Jaskšić, L. Mandić, and J. Dobrinić, Phys. Rev. A **74**, 062501 (2006).
[5] V. Horvat, R. L. Watson, and Y. Peng, Phys. Rev. A **74**, 022718 (2006).

# SECTION V

# SUPERCONDUCTING CYCLOTRON, INSTRUMENTATION, AND RIB UPGRADE

# K500 operations and development

D. P. May, G. J. Kim, H. L. Clark, and F. P. Abegglen

## Introduction

During the 2007-2008 reporting period a total of 34 different beams, including 14 newly developed beams, were used for experiments. There were a total of 42 beam tunings not counting multiple tunes of beams for the SEE program. The SEE program will be treated separately.

## Ion Sources

During the January shut-down ECR1 was opened for examination and cleaning, and it was discovered that another small spot of damage had developed in the aluminum wall of the plasma chamber directly on a plasma flute. The plasma flutes overlap the poles of the hexapole, so the damage likely occurred at a weak place in the magnetic field of the hexapole. Over time this process accelerated as the excess plasma-heating of the spot heated the weak area of the underlying permanent magnet material causing its field to become even weaker in this region.

Measuring the field at the wall at the position of the damage and comparing it to the value measured after the hexapole was assembled revealed that there was an original field minimum at this position located at the joint between two blocks of permanent magnet material and that this minimum was now lower. The damaged area is almost identical to another spot noted in 2002 and repaired by replacing a hexapole bar in January of 2004. The new spot is not at the midpoint of the hexapole as before, but 4.0" closer to the injection end of the source.

Because the axial confinement field reinforces three of the poles of the hexapole at each end of the ion source, the plasma flutes of an ECR ion source form a three-pointed star on the injection end and a three-pointed star on the extraction end. The two stars are rotated by 60° with respect to one another, and they extend along the cylindrical walls of the plasma chamber and overlap by a few inches at the midpoint. In order to spare the hexapole further heating at the damaged position the axial magnetic field of ECR1 was reversed. This rotates the three flutes of each plasma star by 60°. To match the star on the injection end, the injection end plate with its microwave feed and the steel plug, which accommodates this feed, were both rotated by 60°. After this field reversal ECR1 has continued to perform well.

In March of 2007 ECR2 had been moved to a position above the K150 cyclotron so that it could provide beams for the K150. During the summer ECR2 was turned on again but without the power supply for the biased plate or lead shielding and only supplied low charge state beams.

## Cyclotron Beams

New beams of $^{12}$C at 10 AMeV, $^{14}$C at 12 AMeV, $^{19}$F at 26 AMeV, $^{27}$Al at 30 AMeV, $^{32}$S at 10 and 40 AMeV, $^{47}$Ti at 30 AMeV, $^{56}$Fe at 10 AMeV, $^{63}$Cu at 10 AMeV, $^{78}$Kr at 35 AMeV, $^{86}$Kr at 15

AMeV and at 35 AMeV and $^{124}$Sn at 26 AMeV were developed. For $^{47}$Ti a foil of the isotopic material was spot-welded onto the flat side (facing into the source) of a non-isotopic titanium sputter target. Later in a source-only trial an isotopic foil was folded and spot-welded to a stainless-steel wire support. This worked well, but the sputtering occurred on only one side of the material. A vacuum feed-through capable of 360º rotation will be tried next with this isotopic target.

**Operations**

For the period April 1, 2007 through March 31, 2008, the operational time is summarized in Table I, while Table II lists how the scheduled time was divided. There were three major repairs that

**Table I.** 2007-2008 Operational Time

| Time | Hrs. | %Time |
|------|------|-------|
| Beam on target | 5967.25 | 76.5 |
| Tuning, optics, set-up | 77.00 | 1.0 |
| Beam development | 345.50 | 4.4 |
| Scheduled maint. | 440.50 | 5.6 |
| Unscheduled maint. | 967.75 | 12.5 |
| Idle time | 1.00 | 0.0 |
| Total | 7801.00 | 100.0 |

**Table II**. 2007-2008 Scheduled Beam Time.

| Time | Hrs. | %Time |
|------|------|-------|
| Nuclear physics | 1690.00 | 25.7 |
| Nuclear chemistry | 1253.50 | 19.1 |
| Atomic physics | 308.00 | 4.7 |
| Outside collaboration | 0.00 | 0.0 |
| Outside users | 3131.50 | 47.7 |
| Beam development | 181.50 | 2.8 |
| Total | 6564.50 | 100.0 |

caused significant loss of time. In August helium-refrigerator problems caused a loss of over four days of beam time, followed in September by a water leak of a dee stem internal to the K500 that resulted in 3.5 days of lost beam time. Finally, after the January shut-down the helium refrigerator did not perform up to specification and finally failed in the last days of February. The entire month of March was lost to what has been determined to be contamination of the helium with moisture. As a consequence the unscheduled maintenance for this year represents a much higher percentage of time than for previous years.

# Radiation effects facility

H. L. Clark, J. Brinkley, G. Chubarian, V. Horvat, B. Hyman, G. Souliotis, and G. Tabacaru

In this reporting period, the Radiation Effects Facility (REF) was used for 2,373 hours, which is a ~5% decrease over the 2,498 hours used in the 2006-2007 reporting period. ~350 scheduled hours were lost during unscheduled maintenance in February - March 2008. Users of the facility (and hours used) over the past year were: Boeing Satellite Systems (378), SEAKR (259), Xilinx Corporation (218.25), NASA JPL (197.75), Aeroflex (177.25), NAVSEA (174), NASA GSFC (306.25), Sandia National Laboratory (87), Air Force Research Laboratory (77.5), International Rectifier (63), Northrop Grumman (59), Ball Aerospace (56.5), PVAMU (40), General Dynamics (35), Radiation Assured Devices (35), BAE Systems (32), Lockheed Martin (28), Intel Corporation (23.25), Honeywell (21.25), Maxwell Technologies (19.5), Intersil (16), SOREQ NRC (16), Medtronics (14.5), ST Micro (11.5), VPT Incorporated (11), NASA JSC (8) and Harris Corporation (8). New users included SOREQ NRC, Medtronics, ST Micro and VPT Incorporated.

Table I compares the facility usage by commercial and government customers. The ratio from this reporting year (62% to 38%) is similar to the trend seen in previous reporting periods and commercial hours still dominate. Commercial hours decreased by 8% and government hours increased by 1% over hours from 2006-2007. Much of the testing conducted at the facility continues to be for defense systems by both government and commercial agencies. It is expected that the facility will continue to be as active in future years.

**Table I.** Radiation Effects Facility usage by commercial and government customers for this and previous reporting years.

| Reporting Year | Total Hours | Commercial Hours (%) | Government Hours (%) |
|---|---|---|---|
| 2007-2008 | 2,373 | 1,482 (62%) | 891 (38%) |
| 2006-2007 | 2,498 | 1,608 (64%) | 890 (36%) |
| 2005-2006 | 2,314 | 1,314 (57%) | 1,000 (43%) |
| 2004-2005 | 2,012 | 1,421 (71%) | 591 (29%) |
| 2003-2004 | 1,474 | 785 (53%) | 689 (47%) |
| 2002-2003 | 1,851 | 1,242 (67%) | 609 (33%) |
| 2001-2002 | 1,327 | 757 (57%) | 570 (43%) |
| 2000-2001 | 1,500 | 941 (63%) | 559 (37%) |
| 1999-2000 | 548 | 418 (76%) | 131 (24%) |
| 1998-1999 | 389 | 171 (44%) | 218 (56%) |
| 1997-1998 | 434 | 210 (48%) | 224 (52%) |
| 1996-1997 | 560 | 276 (49%) | 284 (51%) |
| 1995-1996 | 141 | 58 (41%) | 83 (59%) |

Table II lists the beams used this year and the number of times each was requested. In total, 550 beams were run this year which is identical to the previous year. 15 and 25 MeV/u Kr and Xe were most utilized as well as 15 MeV/u Au. A new beam of 40A MeV $^{14}$N was added to SEELine users list.

**Table II.** Beams used and the number of times requested for this reporting year and previous years. 550 beams were run this year.

| Particle Type | A MeV | Requests 2000-01 | Requests 2001-02 | Requests 2002-03 | Requests 2003-04 | Requests 2004-05 | Requests 2005-06 | Requests 2006-07 | Requests 2007-08 |
|---|---|---|---|---|---|---|---|---|---|
| $^{20}$Ne | 15 | 1 | 13 | 19 | 15 | 23 | 36 | 39 | 37 |
| $^{40}$Ar | " | 4 | 24 | 43 | 46 | 51 | 56 | 60 | 57 |
| $^{63}$Cu | " | N/A | N/A | 5 | 14 | 22 | 23 | 25 | 24 |
| $^{84}$Kr | " | 6 | 26 | 55 | 47 | 49 | 75 | 81 | 77 |
| $^{109}$Ag | " | N/A | N/A | 6 | 18 | 15 | 26 | 28 | 28 |
| $^{129}$Xe | " | 5 | 18 | 43 | 51 | 50 | 78 | 84 | 84 |
| $^{141}$Pr | " | N/A | N/A | 2 | 2 | 1 | 4 | 4 | 4 |
| $^{165}$Ho | " | 3 | 11 | 17 | 7 | 8 | 22 | 24 | 24 |
| $^{181}$Ta | " | 4 | 5 | 4 | 3 | 5 | 3 | 3 | 3 |
| $^{197}$Au | " | 12 | 9 | 23 | 34 | 34 | 46 | 50 | 49 |
| $^{22}$Ne | 25 | 27 | 13 | 19 | 6 | 15 | 21 | 23 | 20 |
| $^{40}$Ar | " | 31 | 20 | 32 | 16 | 25 | 31 | 33 | 35 |
| $^{84}$Kr | " | 32 | 20 | 35 | 26 | 33 | 40 | 43 | 45 |
| $^{129}$Xe | " | 25 | 18 | 24 | 15 | 25 | 34 | 37 | 40 |
| H-D | 40 | 1 | 8 | 10 | 4 | 7 | 4 | 4 | 5 |
| $^{14}$N | " | N/A | N/A | N/A | N/A | N/A | N/A | N/A | 3 |
| $^{20}$Ne | " | 5 | 3 | 5 | 6 | 11 | 2 | 2 | 3 |
| $^{40}$Ar | " | 12 | 8 | 10 | 7 | 13 | 7 | 8 | 9 |
| $^{78}$Kr | " | 13 | 9 | 6 | 5 | 10 | 3 | 3 | 3 |
| Total | | 192 | 207 | 360 | 324 | 399 | 511 | 552 | 550 |

**Cyclotron computing**


R. Burch and K. Hagel


This past year we continued to enhance the Cyclotron Institute's computing capacity and infrastructure. The primary improvements were: operating system upgrades, increased file and backup server capacity, new computational server, data acquisition (DAQ) server enhancements, new DAQ network infrastructure, and wireless access. These enhancements are an important part of the services we provide the Institute's personnel, empowering them to carry out their research programs and the Institute's mission.

In the past we maintained several flavors of Linux for the servers we manage. We have now standardized on Scientific Linux (SL). We retired Red Hat Linux as our primary operating system. This was an important change in operating systems for servers which we manage. When Red Hat discontinued support for the free Red Hat Linux and offered a subscription based service (RHEL), we switched to Fermi Linux and then to Scientific Linux (SL) as our primary operating system for computational, data analysis, and administrative services. Scientific Linux is a free, stable and capable operating system which uniquely fits the needs and mission of our Institute. This past year we finished the migration of all computational servers to SL 4. We plan to continue running SL 4 on all current and new computational and data analysis servers until necessity requires that we migrate to SL 5. DAQ frontend servers will continue to run Red Hat Linux 7, as required by their hardware configuration, until drivers for hardware are rewritten. We plan to run SL 5 on all current and new administrative servers and so gain experience and expertise useful in upgrading our computational servers from SL 4 to SL 5 when required. We started the migration of current administrative servers to SL 5 and so far migrated the lab's ssh gateway, web, backup, syslog, and radius servers to SL 5.

In an effort to satisfy the Institute's growing demand for data storage and computational power, the previous year we had upgraded the file server with eight SATA drive slots [1], four of which were populated with 2TBytes of data storage capacity. In the past year we populated the remaining four slots, maxing out our data storage capacity at 5TBytes. We also added a 300GByte SCSI disk to the file server for expanding user's home directories as needed. In order to maintain adequate backups of our expanding home directory structure and critical files on our servers, we upgraded the new backup server [1] by increasing internal storage to 2TByte and increasing our offsite storage to 700GBytes. We also added one new computational server, a Dell PowerEdge 1950 with two Xeon 2.66GHz Quad Core processors and 8GBytes of RAM and brought it on-line with SL 4. We now have a total of 12 computational servers available for general lab usage where Condor feeds these servers with jobs on demand.

The DAQ Backend server was upgraded with extended capabilities and a significant increase in data storage capacity to satisfy the ever growing demands of the experiments preformed at the Institute. We also upgraded the data acquisition network, replacing the 10Mbit Fiber hubs and converters with 100Mbit Fiber switches.

This past year we added secure (WPA) wireless to the Institute. Authentication, authorization, and accounting is granted and logged via a stand-alone SL 5 radius server as required by the university's security regulations.

In an effort to supply the Institute with the resources it needs in a secure and cost effective environment, we chose a free operation system maintained by the national labs Fermi Lab and CERN which uniquely fits our Institute's needs and mission. We significantly increased our Institute's storage capacity augmented with computational power. We enhanced the capabilities of the DAQ Backend server, rebuilt its network infrastructure and added wireless to the Institute.

[1] R. Burch, K. Hagel, Progress in Research, Cyclotron Institute, Texas A&M University (2006-2007), p.V-7.

# Cyclotron institute upgrade project

H. L. Clark, F. P. Abegglen, G. J. Kim and D. P. May

On January 3, 2005 the Cyclotron Institute Upgrade Project (CIUP) began with the approval of the CIUP management plan by the Department of Energy Nuclear Physics Office. The project will extend to the first quarter of calendar year 2011. When completed, the upgraded facility will provide high-quality re-accelerated secondary beams in a unique energy range in the world. Funding for the upgrade comes from several sources: the Department of Energy, matching support from TAMU, the Robert A. Welch Foundation and beam-time sales for testing electronics components at the Cyclotron Institute.

The CIUP is divided into three major tasks: (1) Re-commission the existing K150 (88") cyclotron and refurbish beam lines; (2) Construct light-ion and heavy-ion guides and produce 1+ radioactive ions; (3) Transport and charge boost radioactive ions and accelerate in the K500 cyclotron.

Most of the effort during this reporting period focused on Task 1, restoring the K150 cyclotron major equipment. This included commissioning the K150 RF system and K150 ECR ion source & injection line and accelerating first beams from the K150 cyclotron. Progress was also made on the beam lines with installation of three large dipole magnets and coring the passageway through the K150 vault wall into cave 2. It is anticipated that the K150 beam lines will be completed by the end of summer 2008 with an anticipated first experiment in the fall. Progress was also made on Tasks 2 and included development of a 2m long SPIG to connect the light ion guide to the CB ECR ion source. A radioactive $^{228}$Th source has been procured and will be used to further develop the light ion guide system. Development of the heavy ion guide gas cell system with the collaboration of ANL still continues. First pieces of the gas cell are now under construction. Task 3 progress includes the delivery and assembly of the CB-ECR ion source constructed through a DOE SBIR project. All items to complete the CB-ECR ion source have been procured. Construction of the n+ transport system has begun and the power supplies for the magnets and cryogenic vacuum systems have been procured.

In October 2007, first beams of 20 MeV protons were accelerated and extracted from the K150 cyclotron. Values from the cyclotron log book from 1987 were used as the starting values for the RF system, deflector system and cyclotron main, trim and valley coils. After some optimization, the main coil was set to 612 A for a 6.7 kG magnetic filed, the RF system was tuned to 10.1051 MHz with the dee voltage set to 73 kV and the extraction deflector voltage set to 51 kV. Table 2 compares the final operating parameters to those from 1987 and shows excellent agreement with previous operation. In 1987, protons were introduced from an internal filament source; therefore the currents for the first few trim coils are understandably different. Table I shows the beam current values measured by the refurbished beam probe at various extraction radii. The internal beam transmission from 10" to 38" was ~34% and the extraction efficiency was only 10%. Ultimately, 25 nA was extracted and measured on the first Faraday cup (FC-01) outside the cyclotron. This first test showed that the vital components of the cyclotron have been restored. For the production of radioactive ions, much higher intensity is required. However, two key items were not installed for the test: dee inserts and axial Glaser lens in the upper yoke. Due to their absence the shape of the beam in the center region could not be optimized.

**Table I**. Comparison of K150 cyclotron operating parameters from 1987 to 2007 for 20 MeV protons. All values are in good agreement except for trim coils 1 and 2 which shape the magnet field of the central region of the cyclotron. However in 1987, protons were introduced from an internal filament ion source and in 2007 from ECR2 through the vertical injection line.

| K150 Cyclotron Parameters | 1987 | 2007 |
|---|---|---|
| RF Frequency (MHz) | 10.1051 | 10.1051 |
| Dee Voltage (kVolts) | 63 | 73 |
| Main Coil (Amps) | 611.9 | 612.22 |
| Trim Coil 1 (Amps) | -449 | 0.22 |
| Trim Coil 2 (Amps) | -335 | -110.00 |
| Trim Coil 3 (Amps) | -218 | -216.12 |
| Trim Coil 4 (Amps) | -66 | -82.64 |
| Trim Coil 5 (Amps) | -33 | -33.09 |
| Trim Coil 6 (Amps) | 68 | 68.86 |
| Trim Coil 7,8 (Amps) | 0 | 0 |
| Trim Coil 9 (Amps) | -20 | -20.10 |
| Trim Coil 10 (Amps) | 94 | 94.29 |
| Trim Coil 11 (Amps) | 48 | 48.04 |
| Trim Coil 12 (Amps) | 191 | 191.04 |
| Trim Coil 13 (Amps) | 257 | 239.90 |
| Trim Coil 14 (Amps) | -174 | -174.23 |
| Trim Coil 15 (Amps) | -4 | -4.03 |
| Trim Coil 16 (Amps) | -783 | -781.68 |
| Trim Coil 17 (Amps) | 612.9 | 652.86 |
| Deflector Voltage (kV) | 46 | 50.89 |
| Deflector Position 1 | 50600 | 50600 |
| Deflector Position 3 | 50600 | 50600 |
| Deflector Position 6 | 49500 | 49500 |
| Deflector Position 2 | 48740 | 48716 |
| Deflector Position 4 | 52484 | 52440 |
| Deflector Position 5 | 50100 | 50100 |
| Deflector Position 7 | 50500 | 50500 |

**Table II**. Beam probe current readings for 20 MeV protons at various distances from the center of the K150 cyclotron.

| Beam Probe Radius (inches) | Beam Probe Current (nA) |
|---|---|
| 10 | 650 |
| 15 | 510 |
| 20 | 340 |
| 25 | 270 |
| 30 | 250 |
| 35 | 220 |
| 38 (Deflector Entrance) | 220 |

In order to better understand the particle orbits in the central region of the cyclotron, electric field and magnetic field maps are needed. Since no actual mappings exist, theoretical maps may be created from sophisticated software programs. For magnetic field maps, Vector Fields' TOSCA program was purchased. The geometry of the poles, hills and valleys and center plug are entered into the program (as shown in Fig 1). To reduce computation time, whenever possible a simplified geometry is used to describe the actual shapes of the cyclotron (as shown in Fig 2).
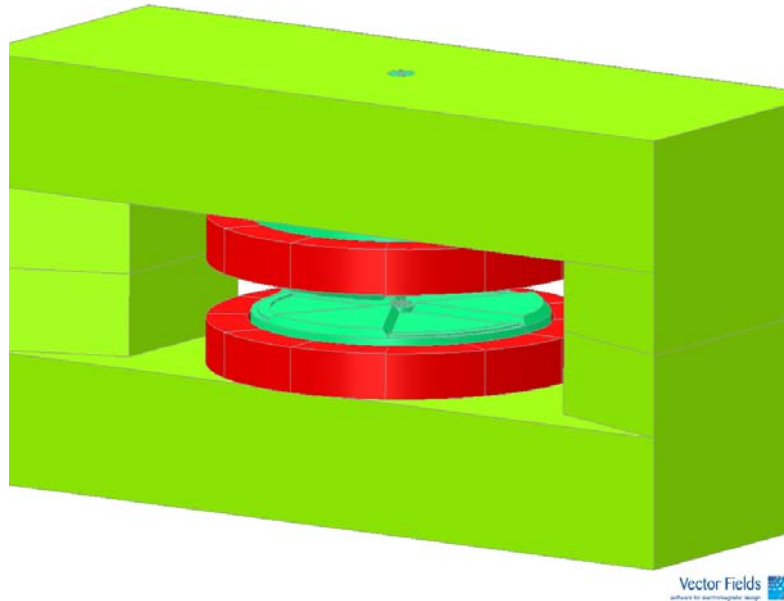


**Figure 1.** Initial TOSCA modeling of the K150 cyclotron.
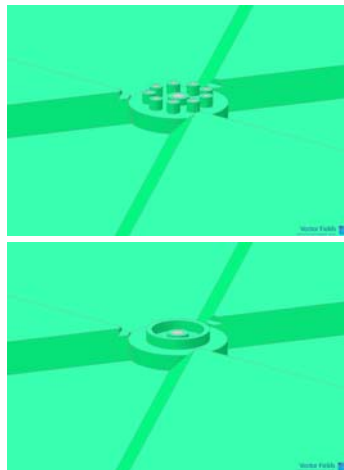


**Figure 2**. (top) View of the cyclotron center region with nine buttons around the center plug. (bottom) A simplified model with a ring instead of the nine buttons.

First calculations with TOSCA at 1120 A are shown in Fig. 3 along with an equivalent POISSON calculation and the field map data from the Berkeley 88" cyclotron. The TOSCA and POISSON calculations are in agreement. The TOSCA and Berkeley calculations agree to within 10%, however the form of the average B field versus radius is well produced by both programs. At the outer edge of the pole face, the "Rose" shim has been incorporated but does not account for all the rise of the magnetic field. The trim coils, which are series of concentric circular conductors, are modeled well by TOSCA and POISSON and agree well with the Berkeley field maps (shown in Fig. 4).
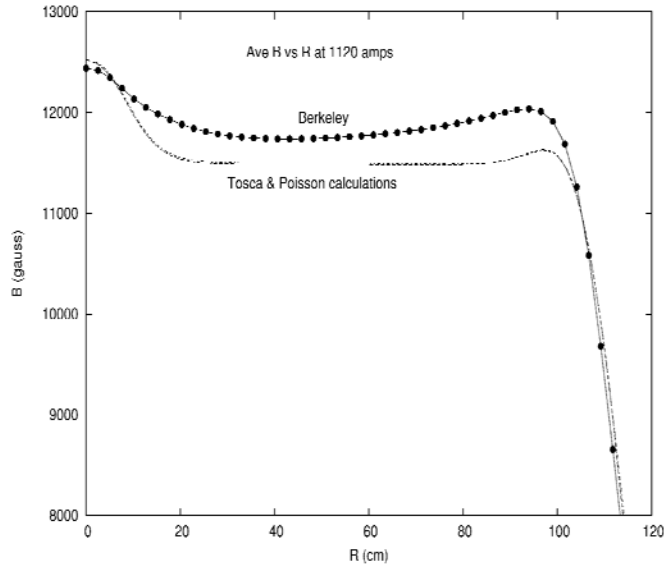


**Figure 3**. Comparison of the Berkeley field map data with TOSCA and POISSON calculations at 1120 A.
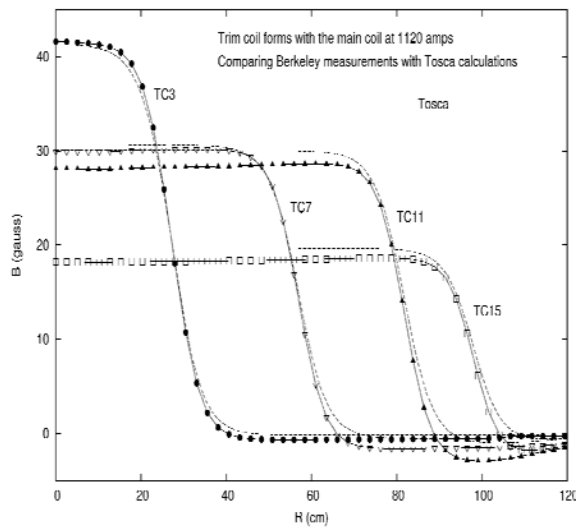


**Figure 4**. Comparison of the B field forms for 4 of the 15 trim coils at 1120 A on the main coil.

# The charge-breeding ECR ion source

D. P. May and W. D. Cornelius[1]

[1]*Scientific Solutions, San Diego, California*

Before radioactive ions can be injected into the K500 cyclotron, they must have the proper charge-state for acceleration. The boosting of a singly charged ion to higher charge-states is termed "charge breeding". The ECR ion source (CB-ECRIS) that will be devoted to charge breeding the radioactive ions produced by the ion guides was delivered in August. It was designed and built by Scientific Solutions of San Diego, California with a Phase I and a Phase II Small Business Innovative Research grant from the U.S. Department of Energy. The Cyclotron Institute is supplying the axial-coil power supplies, the vacuum pumps and the 14.5 GHz transmitter for the source.

The source was designed to enable a minimum of contamination and a high degree of efficiency. The efficiency in injection is made possible by an open path through the injection plate and by external electrostatic Einzel lenses. The efficiency of capture and charge breeding is provided for by high magnetic containment fields and the plasma-chamber cooling protection that allows high microwave power input. Two large coils supply the axial mirror magnetic field, and a surrounding Halbach type hexapole, assembled with Nd-Fe-B permanent magnets, provides the radial mirror field. The plasma chamber is formed by a water-cooled aluminum liner. The source is of medium volume and will operate at 14.5 GHz with the possibility of adding a lower second frequency later.

Scientific Solutions assembled the ion source in October. After pumping on the source the vacuum achieved on both the injection and extraction end was in the middle $10^{-8}$ torr range. CB-ECRIS will be commissioned after the transmitter and remaining axial-coil power supply are delivered and the analysis line is assembled.

**Progress on the light ion guide facility**

G. Tabacaru, J. Arje, and H. L. Clark

The construction of the light ion guide is part of the Cyclotron Institute Upgrade Project. In the previous report [1] we have briefly described its principle.

In the last year extensive tests were performed for developing a transport system using a sextupole resonant structure. The sextupole consist in an assembly of six metallic rods (in our case, brass) connected to an RF generator. The sextupole has only one resonant frequency fixed by its length, and there is no mass selection involved. The rods are 2 mm diameter and are placed on a circular pattern of 4 mm diameter. We have tested a sextupole of 30 cm length and a longer one of 100 cm. Tests were performed also with the 100 cm long sextupole together with the 30 cm long sextupole, using only one RF generator. As ion sources, a spark chamber and an ion gun were used. Figure 1 shows a view of the spark chamber coupled with the 100 cm long sextupole and the vacuum chamber.
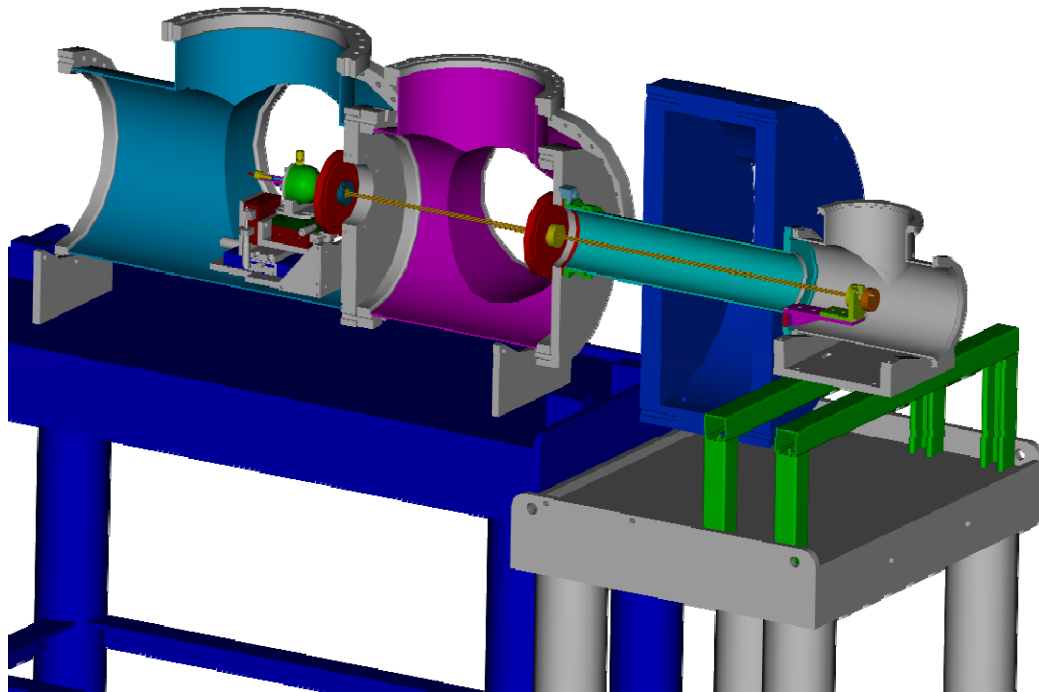


**Figure 1.** View of the spark chamber, 100 cm sextupole and the vacuum chambers.

The measurements were performed in various conditions and we found: 1) we are able to transport $1^+$ ions from the source to long distances (130 cm); 2) the efficiency is relatively constant for a range of pressures in the target chamber ($P_{tc}$ on the Figure 2); 3) absolute efficiency is impossible to verify due to the impossibility of estimation in the impurities level; 4) using the ion gun we can transport $^{24}$Mg and $^{85}$Rb without changing the resonant frequency of the sextupole, so as expected there is no selection in

mass involved. We have to mention here that the ion gun measurements are made in vacuum; Helium gas cannot be used due to its high cooling capacity. In the Figure 2 we present an example of measurement using the spark chamber and the 100 cm sextupole for different pressures of helium in the target chamber.
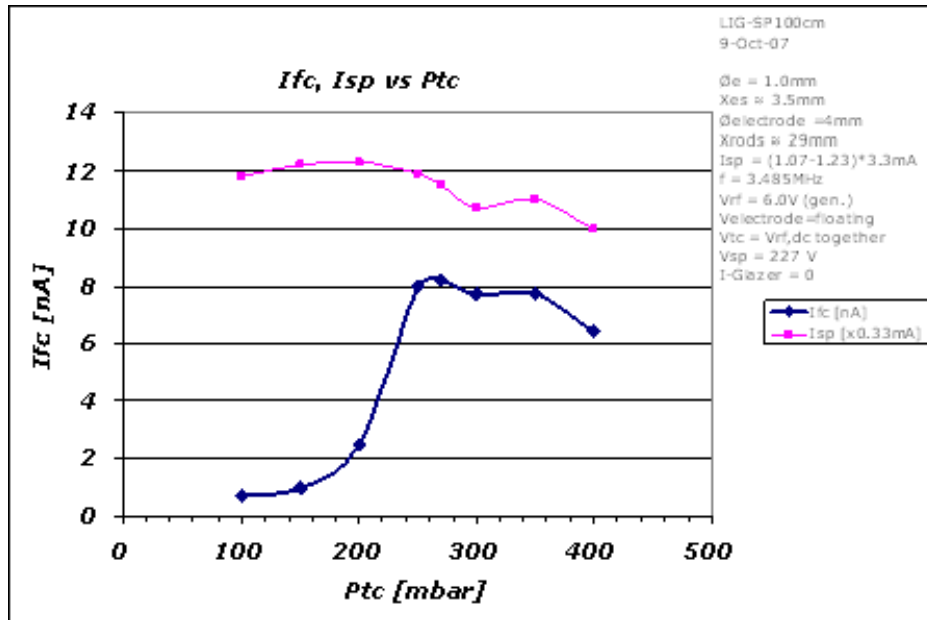


**Figure 2.** Current vs. pressure measurements with 100 cm long sextupole.

The next challenge in this project will be the coupling of the sextupole into the Charge Breeding ECR source [2]. But for this development a radioactive source is needed. It is known that the background current out of the ECR source is big compared with the injected current. Only using a radioactive source we can identify charge boosted ions (from $1^+$ to higher charge state) and diagnose the coupling of the sextupole with the ECR source. We already have acquired a [228]Th open source and at the time when this report is being written, the experiments are in progress. We hope that next year will have a successful report on making highly charged radioactive ions using the light ion guide in conjunction with the Charge Breeding ECR.

[1] G. Tabacaru, J. Arje, and H. L. Clark, *Progress in Research*, Cyclotron Institute, Texas A&M University (2006-2007), p.V-20; http://cyclotron.tamu.edu/publication.html.
[2] H. L. Clark, Progress in Research, Cyclotron Institute, Texas A&M University (2006-2007), p.V-8; http://cyclotron.tamu.edu/publication.html.

# Heavy ion guide: beam transport and diagnostics

G. Chubarian, F. P. Abegglen, H. L. Clark, G. Derrig, G. J. Kim, D. P. May, G. A. Souliotis,
G. Tabacaru, and R. E. Tribble

Our present plans for a heavy-ion guide system are based on developments at Argonne National Laboratory (ANL) [1]. For the heavy-ion guide, preselection of ions will be done using a superconducting solenoid similar to that being used now in the BigSol spectrometer. Earlier tests with a 1 m long gas cell at low input intensities (below $10^7$ ion/sec) have been carried out at ANL with beams up to 4 MeV/A and at GSI with initial beams of 280 MeV/A to check the stopping efficiency. Consistent results with stopping and extraction efficiencies close to 40% have been obtained in both tests with realistic pressures of 100 to 200 mbar and helium pumping speeds less than 3000 m$^3$/hr. Similar results, but with significantly higher load, up to $10^9$ ion/sec, were obtained on a modified ANL gas catcher (RIA gas catcher prototype) [2]. This is very important result, since using deep inelastic collisions, we expect high production rates for a large range of secondary ions [3]. Currently complete set of parts for two similar gas catchers are being manufactured for ANL and TAMU.

After extraction from the gas cell 1+ ions will be delivered to the charge breeding ECR source where they will be stripped to a high charge state and then the highly charged ions will be injected into and accelerated by the K500 cyclotron. Starting from the original production of radioactive species and after, including collection, extraction and transport to the injection point, we need to control the efficiencies of each stage.
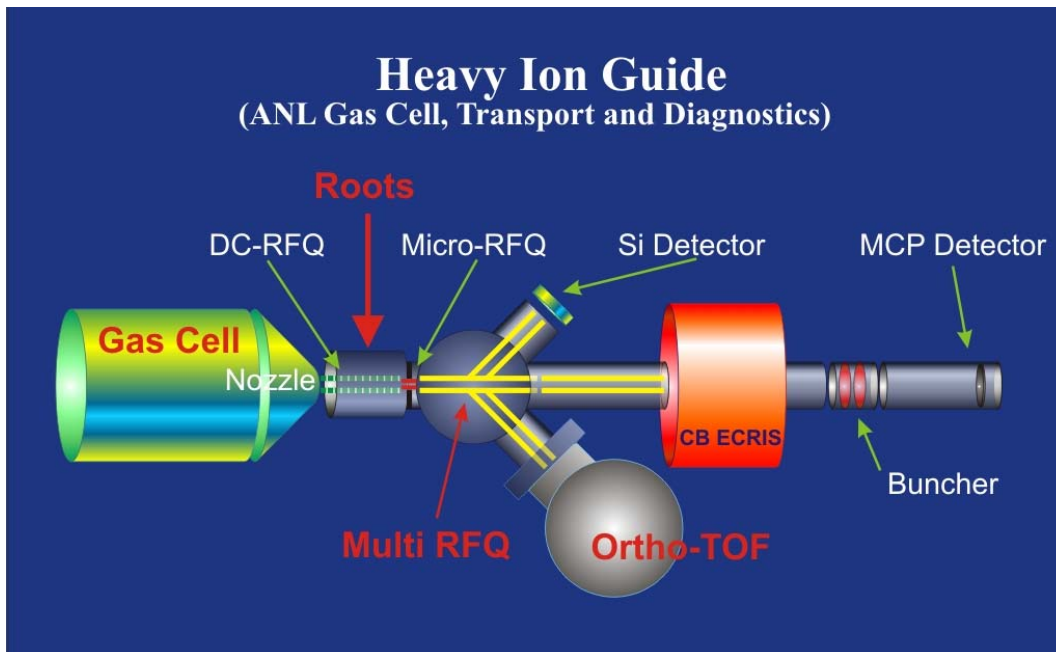


**Figure 1.** Schematic of heavy ion guide (ANL gas cell, transport and diagnostics).

Fig. 1 schematically shows a suggested secondary beam transport and diagnostic system. After extraction the secondary beam enters a Multi-RFQ beam transport system where the exit direction is defined with the help of three mobile central branching segments of the RFQ (see Fig.2) [4]. The beam can go straight or be deflected 45° relative to the central axis. There are two curved and one straight segment and their position can be adjusted with the help of a remotely controlled elevator. One of 45° branches will be connected with the orthogonal electrostatic time-of-flight mass spectrometer (Ortho-TOF) shown in Fig. 3.
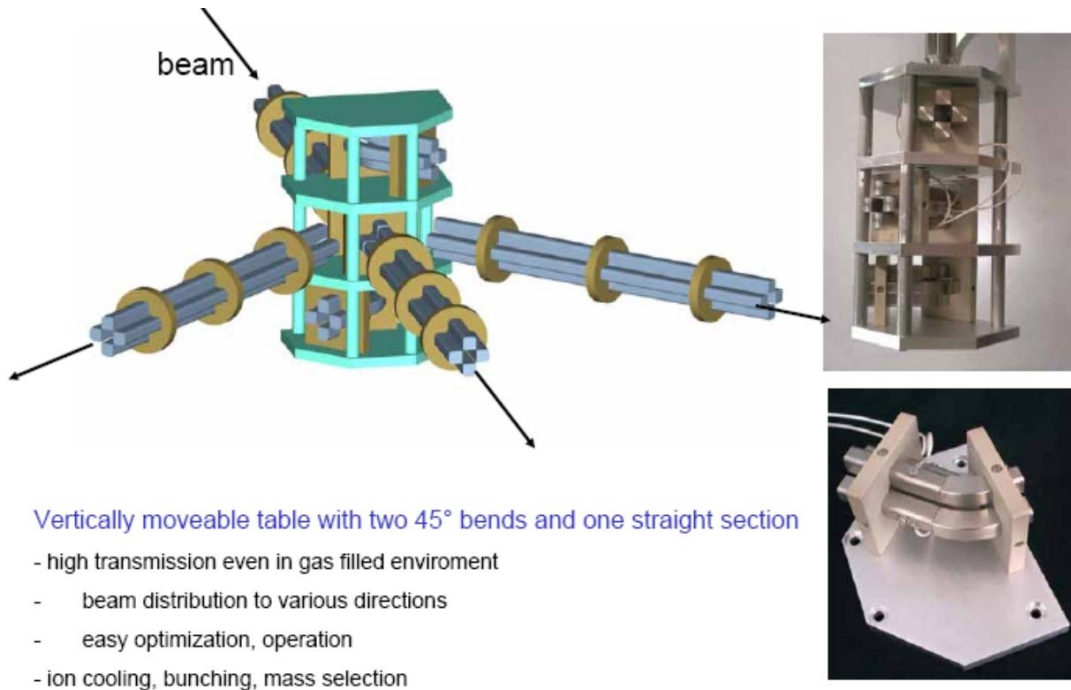


**Figure 2.** Multi-RFQ beam transport system.

After entering the Ortho-TOF, 1+ ions will be accelerated up to 6 keV energy via a pulsed electrostatic accelerator and will travel towards the bottom of the 1.7 m long cylinder. At the bottom of the cylinder, using double stage electrostatic reflector, ions will make a U-turn and move up to the microchannel plate (MCP) timing detector located in the same plane as the accelerator. By measuring time-of-flight we can determine the masses of the ions. The Ortho-TOF has a resolution of one part in 5000 at ,inimum, which is more then enough to determine masses of the ions with an accuracy of better then 1 a.e.m. On the other 45 degree branch a solid state Si detector will be mounted, which also allows to define the yield of the radioactive ions by measuring decay curves of short lived ß activities. Ortho-TOF coupled with Multi-RFQ system was earlier designed at Giessen University and experimentally proved itself as a precise and easy to operate tool [5].
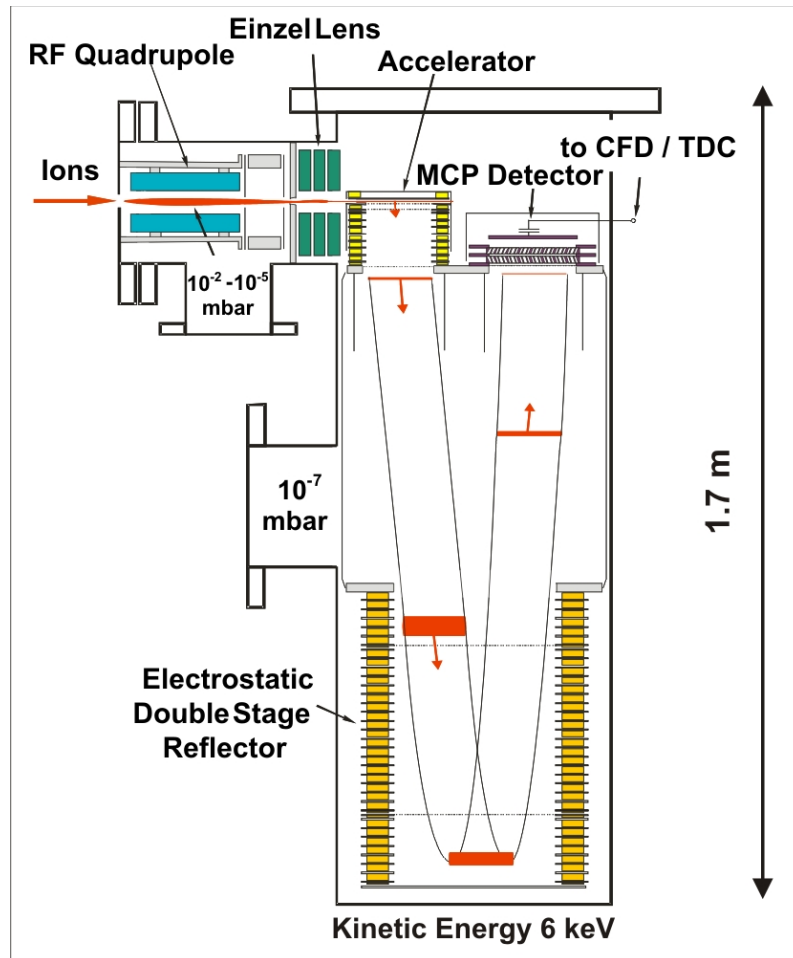
**Figure 3.** Layout of the orthogonal electrostatic time-of-flight mass spectrometer.

It is also very important to find out final number of recharged secondary radioactive ions after the Charge Breeder. Due to the long flight path from the Charge Breeder to the injection point and very low velocity of the radioactive ions time-of-flight system may be used. This is possible to achieve by placing beam buncher right after the Charge Breeder and removable MCP timing detector close to the injection point.

The Heavy Ion Guide is a product of close collaboration between TAMU Cyclotron Institute, Argonne National Laboratory, Giessen University-GSI and NSCL Michigan State University.

1. G. Savard *et al.*, Nucl. Instrum. Methos Phys. Res. **B204**, 582586 (2003).
2. G. Savard (private communication).
3. G. A. Souliotis *et al.,* Nucl. Instrum. Methods Phys. Res. **B204**, 166 (2003).
4. W. R. Plass (private communication).
5. S. Eliseev, PhD Thesis, Justus-Liebig University, Giessen, 2004.

**Upgrades to the cyclotron computer control system**

T. Cowden, F. P. Abegglen, R. Burch, and T. O'Berski

The Rabbit based microcontroller and base card have been designed to control Alpha power supplies configured with two sixteen bit ports, one to drive a DAC and the other to read an ADC. Since the introduction of the Rabbit embedded controller into the cyclotron computer control system, several benchmarks and improvements have occurred. Beam has been extracted from the K150 under computer control with only minor glitches. The Rabbit controller has been incorporated into parts of the K500 control system with prospects for replacing aging components and obsolete systems. The base board the embedded controller plugs into has been improved with buffered outputs and more inputs. A variation of the base board has been built to handle serial I/O, handling up to six serial ports. The infrastructure to support the embedded controllers has begun to be put into place.

Serial Rabbits have been put into use as remote vacuum readouts throughout the beam-line system. They have improved reliability and eased expansion over the old system. Some of the ion-gauge controllers have direct serial outputs and only require a serial line to the vacuum microcontroller. Older ion gauge controllers require a small parallel to serial card designed to imitate the serial ion gauge controller protocol. The system has been in operation for a year. The adapter card is useful in other applications as a bit status indicator. New power supplies with serial ports can be controlled with the serial embedded microcontroller with the addition of a relay card and a parallel to serial adapter card.

The standard model Rabbit controller base board used in the K150 trimcoil supplies has been improved with the addition of buffers to the parallel DAC outputs and a multiplexed status input to increase the number of status inputs from five to eight. This was necessary with the retrofit of a Rabbit controller in a large dipole power supply that is switched between several magnets. The microcontroller can now read what load it has been switched to. The DAC outputs are buffered for improved drive capability in future applications. A separate external multiplexer attached to the standard embedded controller allows one Rabbit to read and write to the Alpha quadrupole power supplies that consist of one supply and two separate outputs.

Other variations on the standard base board include some test models with the parallel DAC output replaced by an on board digital to analog converter, an isolated sixteen bit serial DAC that can swing from 0 to 10 volts. As the ADC input can be adapted to read a meter, this configuration can replace the STD Bus crate system that controls a majority of the power supplies currently in use. The use of an opto-isolated meter readback completes the electrical isolation of the controller.

Ethernet switches and the electrical boxes to hold them are being installed as needed to provide the network connections for the embedded controllers. The electrical boxes also contain a regulated power supply for the controllers. The central control nexus in the K500 control room has been upgraded with a 24 port ethernet switch to handle the extra ethernet connections. The improved connectivity allows some troubleshooting to include a laptop version of the control console to be plugged in where needed.

Upgrades to the rest of the system are in progress. A new wide screen flat panel display added to the control panel improves the look and feel of the control screens, but highlights the age of the workstation computers. A system to test the workstation upgrade is on order, with the need to bridge several computer generations of hardware and software of greatest concern. It is hoped that the hardware upgrade will pave the way for a general software upgrade at a later date.

**Improved control over the source-detector distance in β-γ coincidence measurements**

V. E. Iacob, V. V. Golovko, and J. C. Hardy

The precision of branching ratios extracted from simultaneous measurements of $\beta$-$\gamma$ coincidences and $\beta$ singles depends most on how well the absolute efficiency of the $\gamma$ detector is known. For a decay scheme like that of $^{34}$Ar, in which each excited level populated in the $\beta$-decay daughter subsequently $\gamma$ decays directly to the ground state, the branching ratio can be expressed to a first approximation as

$$BR_\gamma = \frac{N_{\beta-\gamma}}{N_\beta \times \varepsilon_\gamma} \qquad (1)$$

where $N_{\beta-\gamma}$ and $N_\beta$ are the total numbers of observed $\beta$-$\gamma$ coincidences and $\beta$-singles respectively, and $\varepsilon_\gamma$ is the absolute efficiency for detection of the $\gamma$ ray. We have already calibrated the absolute efficiency of our HPGe detector to a precision of 0.2% in the energy range 50 keV to 1800 keV and 0.5% up to 3.5 MeV using long-lived sources [1]. However, in the calibration measurements the source-to-detector distance could be controlled to ±0.1 mm, while in a real experiment the source is implanted in a mylar tape, which is positioned in front of the $\beta$ and $\gamma$ detectors by our fast tape-transport system (see, for example, ref. [2]). Being a mechanical system, the tape-transport system positions the activity to a lower accuracy. To overcome this limitation, we have upgraded our measurement system by adding a laser-based position sensor, *AccuRange 600-4* [3], which is able to determine a distance to ±0.1 mm for distances in the range from 9 to 19 cm. The distribution of the tape-to-detector distances as observed in our recent $^{34}$Ar experiment [4] is given in Fig. 1. Before this upgrade we could use only the average source-detector
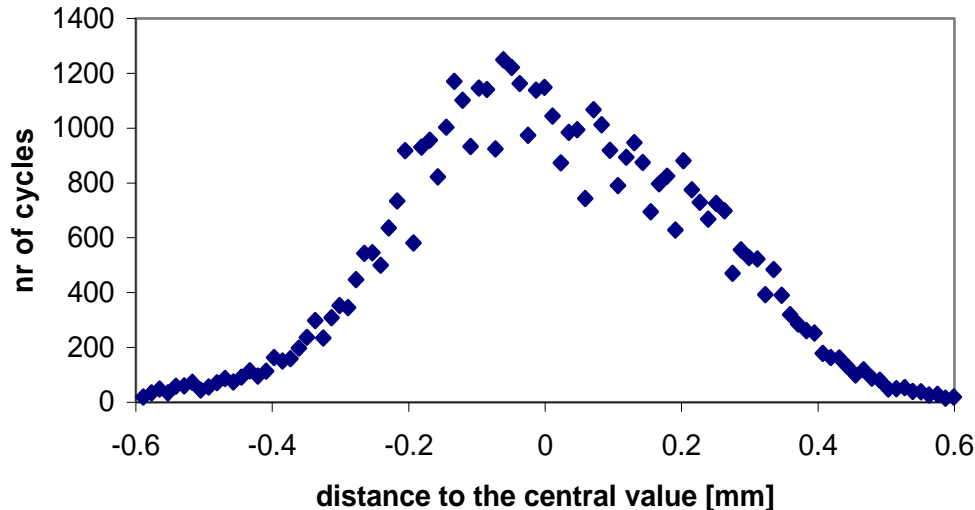


**Figure 1**. Distribution of the source-to-HPGe-detector distance relative to the central value (15.1 mm) as measured in the $^{34}$Ar experiment [4].

distance, which we assumed – and have now verified – had an spread, FWHM, of 0.5 mm. Thus, the absolute efficiency, $\varepsilon_\gamma$, in equation (1) had to carry a higher uncertainty, which in turn increased the

uncertainty in the extracted branching ratios. In the upgraded system, every detection cycle is now tagged with its own source-detector distance, accurate to 0.1 mm. This increases the precision we can achieve in a branching-ratio measurement to the limit defined by the precision of the absolute efficiency of the $\gamma$-ray detector.

[1] J. C. Hardy, *et al.*, Int. J. Appl. Radiat. Isot. **56**, 65 (2002), R. G. Helmer, *et al.*, Nucl. Instrum. Methods Phys. Res., **A511**, 360 (2003). R. G. Helmer, *et al.*, Int. J. Appl. Radiat. Isot. **60**, 173 (2004).
[2] V. E. Iacob, *et al.*, Phys. Rev. C **74**, 015501 (2006).
[3] http://www.acuityresearch.com/AR600/
[4] V. E. Iacob, *et al.*, *Progress in Research*, Cyclotron Institute, Texas A&M University (2007-2008), p. I-29.

# Application of Geant4 for efficiency calculations of a scintillating plastic β-detector

V. V. Golovko, V. E. Iacob and J. C. Hardy

In a separate report [1], we describe Monte Carlo (MC) studies of the efficiency of a 1-mm-thick plastic detector to few-MeV positrons with three MC programs: Geant4 [2], EGSnrc [3] and Penelope [4]. Simulated results have previously been compared with measured data from standard conversion-electron sources: $^{133}$Ba, $^{137}$Cs and $^{207}$Bi [5]. These MC studies of our β-detector efficiency are important for the measurement of precise β$^+$-branching-ratios since there is a slight difference in the efficiency of the β-detector for different β-branches. This has an effect on the number of observed β-γ coincidences, over and above the well known efficiency of our γ-ray detector. We report here the final comparison between Geant4 MC simulations and experiment for the three sources, including an absolute efficiency measurement for the $^{207}$Bi β-source. A manuscript describing this work has been submitted for publication [6].

The realistic geometric model that was chosen for the simulation is shown in Figure 1 of Ref. [5]; the material composition is also described there. Figure 1 of this report shows the energy deposition into the β-detector generated by the radioactive decay module (RDM) of Geant4 in the case of the decay of $^{137}$Cs. Three different electromagnetic (EM) packages were used: standard, low-energy and Penelope (see ref. [1] for more details); normalized residuals in standard-deviation units also shown in the lower panel of the figure for the differences between the low-energy EM package and the other two packages. The resulting total β-efficiencies for three EM physics packages are 15.18(3)%, 15.16(3)%, and 15.11(3)%, respectively, for the low-energy, standard, and Penelope packages, with a low-energy threshold of 50 keV and at a distance of 13 mm from the surface of the radioactive source to the front face of the β-detector. For our superallowed β-decay measurements, our low-energy threshold is set at about 75 keV. Under these conditions, the total β-detector efficiency is 13.80(3)% in all three models. Obviously, it makes no
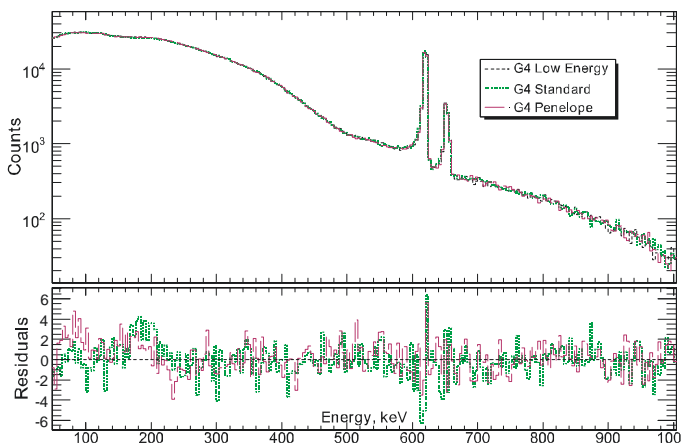


**Figure 1**. Geant4 MC-generated energy deposition into the β-detector for the decay of $^{137}$Cs. Three different EM physics models are used: standard, low-energy and Penelope.
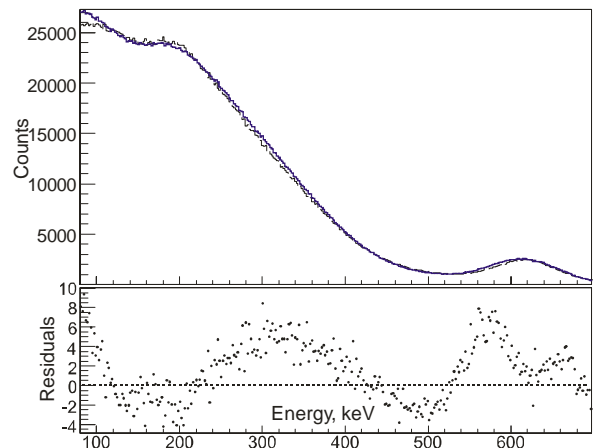


**Figure 2**. Measured spectrum for the decay of $^{137}$Cs, compared to the Geant4 result simulated with the low-energy EM package (thin dashed line – Geant4; thick solid line - experiment).

difference which EM physics model we choose in making our Geant4 MC simulations. For all further simulations reported here, we used the low-energy EM package.

To generate the MC emission spectra we began by programming Geant4 based on the RDM. Although the primary electron spectrum generated by the RDM for [207]Bi showed no obvious problems, when we repeated the procedure for [133]Ba, to our surprise we found that the electron spectrum produced by the RDM was simply not correct, yielding relative conversion-electron intensities in significant disagreement with ENSDF data. The emission spectrum from ^{137}Cs also turned out to be incorrect, but here the main problem was more subtle: there are two β-decay branches from ^{137}Cs, which are both treated by Geant4 as allowed. In fact both transitions are forbidden, with shape-correction factors that have been determined experimentally by Behrens and Christmas [7]. In addition, the RDM gave the incorrect intensity for one of the conversion electron lines of [137]Cs. In both decays - of [133]Ba and [137]Cs - we bypassed the RDM and inserted each decay mode and transition individually, with the correct intensities for the conversion electrons and the correct shape for the forbidden β-transitions. We did this with the General Particle Source module available in Geant4, which allows the user to define standard energy, angle and space distributions of the primary particle.

Based on a primary spectrum thus generated for each source, the MC code then determined the total energy deposited into the scintillator. However, before this result could be compared with the experimental spectrum, it was necessary to add the effects of statistical fluctuations introduced by the processes of light production and transmission, as well as by photo-multiplication and electronic pulse analysis. For this purpose, we looked to a published study of the response of a plastic scintillator to mono-energetic beams of positrons and electrons [8], which tabulated the width of the full-energy Gaussian peak as a function of energy between 0.8 and 3.8 MeV. Since we also needed to deal with energies lower than that, we made a linear extrapolation to β-energies below 0.8 MeV. All MC spectra were corrected for the resolution of the plastic scintillator by applying this resolution function to the MC data.

In comparing the experimental data with the MC results, we treated two energy-calibration coefficients (*y*-intercept and slope) in each measured spectrum as adjustable fit parameters. For this purpose we used a special C++ ROOT program to fit the shape of the MC results to the experimental data. For all three cases the low-energy cut-off threshold was also chosen as a free parameter in the fit, and from all three fits we obtained the same low-energy threshold, 80±3 keV. The resulting comparisons for our three sources as well as the normalized residuals, for ^{137}Cs, [133]Ba, and [207]Bi, appear in Figures 2, 3 and 4 respectively.

The agreement between the Geant4 simulations and experiment is good for all three sources, although for [207]Bi the normalized $\chi^2$ of 8.9 is less impressive than for the other two (0.4 for [133]Ba and 4.0 for ^{137}Cs). In this case, the discrepancy comes partly from the fact that the energy range of the fit, 80 – 1143 keV, was much wider than for the others. It is also possible that the higher $\chi^2$ is caused by our simple linear extrapolation of the results in [8] to describe the peak width in our simulated response function. If the resolution were in fact somewhat worse than this extrapolation indicates - a not unreasonable possibility - then the agreement with experiment could be considerably improved. It is also worth noting that the slight discrepancies in the peak positions evident in all three spectra could be explained by small non-linearities in the experimental energy calibration.
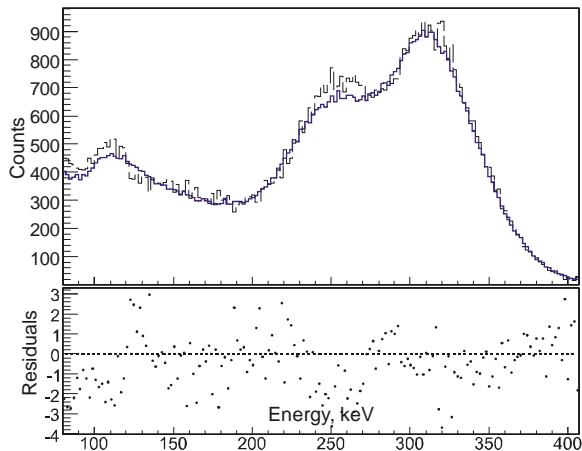
**Figure 3**. Measured spectrum for the decay of $^{133}$Ba, compared to the Geant4 result simulated with the low-energy EM package (thin dashed line – Geant4; thick solid line - experiment).
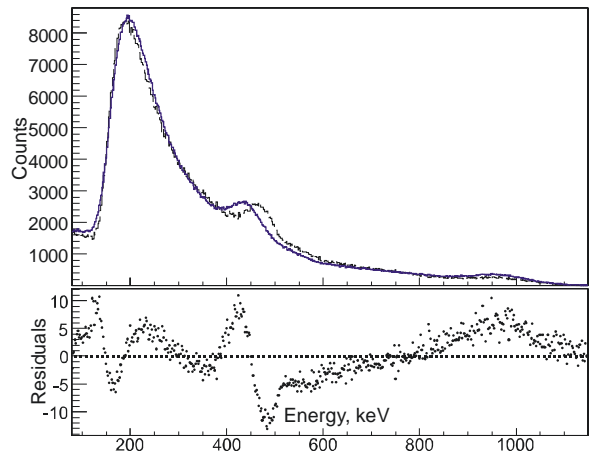


**Figure 4**. Measured spectrum for the decay of $^{207}$Bi, compared to the Geant4 result simulated with the low-energy EM package (thin dashed line – Geant4; thick solid line - experiment).

Although the activities of the radioactive sources that we used for this work are nominally 1 μCi (37 kBq), the accuracy of this value was quoted to an approximate ±15% by the supplier, Isotope Products Laboratory. So that we could get a more precise value for our β-detector efficiency, we made our own measurement of the $^{207}$Bi source activity using our well-calibrated HPGe γ-detector [9] to detect the known γ rays from the decay. In this way we established the source activity to be of 1.31(1) μCi as of 16 January, 2008. Now, knowing the activity of the source as well as the low-energy threshold already obtained from our fit, we could deduce from our experimental data the absolute efficiency of the β-detector to be 3.48(2)% at the distance of 13.2(1) mm (as determined with an AccuRange 600$^{TM}$ Laser Displacement Sensor, which has an absolute precision better than 0.1 mm). With exactly this geometry, the Geant4 simulation yielded an absolute efficiency of 3.50(1)%, in excellent agreement with experiment.

We now consider that the quality of the simulations for our plastic β detector is quite sufficient to provide the precision we require for our superallowed β-decay studies.

[1] V. V. Golovko, V. E. Iacob, J. C. Hardy and D. Melconian, *Progress in Research*, Cyclotron Institute, Texas A&M University (2007-2008), p. V-25.

[2] S. Agostinelliae, J. Allisonas, K. Amakoe, *et. al.*, Nucl. Instrum. Methods Phys. Res. **A506**, 250 (2003).

[3] I. Kawrakow, Med. Phys. **27**, 485 (2000).

[4] J. Baro *et al*., Nucl. Instrum. Methods Phys. Res. **B100**, 31 (1995).

[5] V. V. Golovko, V. E. Iacob, and J. C. Hardy, *Progress in Research*, Cyclotron Institute, Texas A&M University (2005-2006), p.I-43; (2006-2007), p. V-23.

[6] V. V. Golovko *et al*., Nucl. Instrum. Methods Phys. Res. A (accepted).

[7] H. Behrens and P. Christmas, Nucl. Phys. **A399**, 1310 (1983).

[8] E. T. H. Clifford *et al.*, Nucl. Instrum. Methods **224**, 440 (1984).

[9] J. C. Hardy *et al*., Appl. Rad. Isotopes **56**, 65 (2002).

# A comparative study of three Monte Carlo codes for β-detector simulations

V. V. Golovko, V. E. Iacob, J. C. Hardy and D. Melconian

In order to determine the vector coupling constant and to test the unitarity of the Cabibbo-Kobayashi-Maskawa (CKM) matrix, one has to make precise measurements of nuclear masses, β-branching ratios and half-lives [1]. The measurements of half-lives and branching ratios are performed in a simple, but very precise counting station at our institute. A typical "on-line" branching ratio experiment (see, for example Ref. [2, 3]) involves collection of the accelerator-produced radioactive nuclei on the tape of a tape-transport system that rapidly moves the collected sample to a position located between a scintillaton detector and a well-calibrated 70% HPGe γ-detector. Coincident β-γ events are collected and recorded. In order to completely understand all systematic effects contributing to the branching ratio measurements, one must determine the relative efficiency of the scintillator as a function of β-particle energy because the various γ-ray peaks follow β-transitions with different end-point energies and their observed relative intensities are affected by the small differences in β -detection efficiency. The work reported here continues an investigation, previously reported [4], of the response function of β-particles from standard open β-sources (*eg.* $^{207}$Bi). Here we are concerned with the question of which Monte Carlo (MC) code is more suitable for simulations of low-energy electron transport. We present a comparison of Monte Carlo simulations with three general purpose codes: Geant4 (version 4.9.0), Penelope and EGSnrc.

The completely realistic geometric model for Geant4 [5], which was chosen for MC simulation, is shown in Figure 1 of Ref. [4]. The β-detector consists of a 1-mm thick BC404 scintillator material coupled via a plastic optical pad made from lucite to a photomultiplier. The scintillator-optical-pad assembly is enclosed in an opaque cylindrical shield made from 1.5-mm-thick PVC. The opening in the scintillator end of the PVC shield is covered with a pin-hole-free, 5-μm-thick havar foil. The β-particles enter the detector assembly through this foil with essentially negligible energy loss.

The Geant4 Simulation Toolkit includes a series of packages for the simulation of the electromagnetic (EM) interactions [6], specialized for different particle types, energy range or approach in physics modeling. In this work, we considered only positrons and used the low-energy and standard EM physics models in Geant4. The Penelope package is an alternative
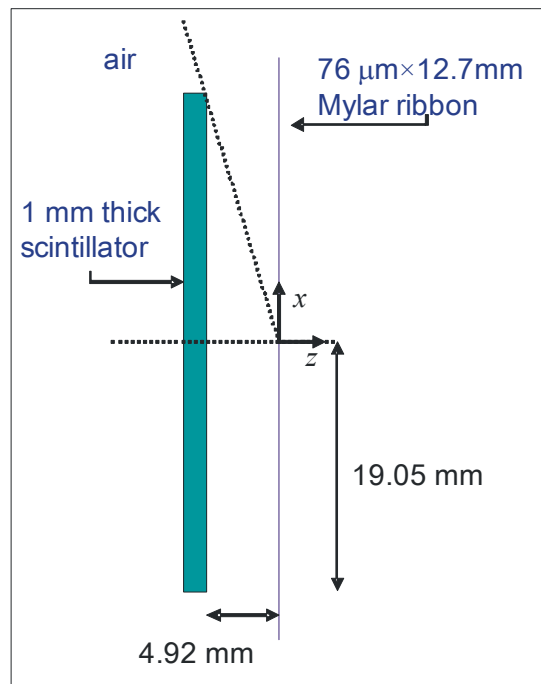


**Figure 1**. Simplified geometry used for MC simulations of a scintillating β-detector efficiency with three general purpose codes: Geant4, EGSnrc and Penelope.

low-energy implementation in Geant4; it is a re-engineered version [7] of the original stand alone Penelope MC code [8, 9]. EGSnrc is a general purpose package designed for the MC simulation of the coupled transport of electrons and photons in arbitrary geometries [10]. EGSnrc utilizes versions of Moliere theory that describe the global effect of many small-angle scattering interactions. The multiple scattering (MSC) model used in Geant4 belongs to the class of condensed simulations that use model functions to determine the angular and spatial distributions after a step. The stand-alone Penelope code inherently differs in how it handles MSC by additionally including hard collisions (such as large-angle Mott scattering). As this may be significant for a proper description of back-scattering of low-energy betas, it is important to compare the results of the different codes in our specific geometry and energy range of interest.

In order to compare the codes, a simple MC experiment was performed. First, all materials in the simulated geometry were replaced by vacuum, except for the plastic detector. As a source, we took a point-like mono-energetic positron source that emitted isotropically. Under these conditions, the total efficiency of the detector was approximately the same as its geometrical efficiency, which could be calculated from the fractional solid angle subtended by the scintillator relative to the source. The total (geometrical) efficiency was calculated by the formula

$$\varepsilon = \frac{\Omega}{4\pi} = \frac{1}{2}\left(1 - \frac{H}{\sqrt{R^2 + H^2}}\right),$$

where $H$ is the distance between the detector and source, $R$ is the radius of the scintillator, and $\Omega$ is the solid angle of the cone. See Figure 1. In our case, this leads to an efficiency of 37.5 %. Figure 2(a) shows the simulated results – obtained with the Geant4 low-energy EM package – for mono-energetic $\beta^+$-particles with energies in the range of 200 keV to 20 MeV. All MC-simulated results show very good agreement with the prediction based on the geometrical model. In the MC calculations we included all $\beta$-
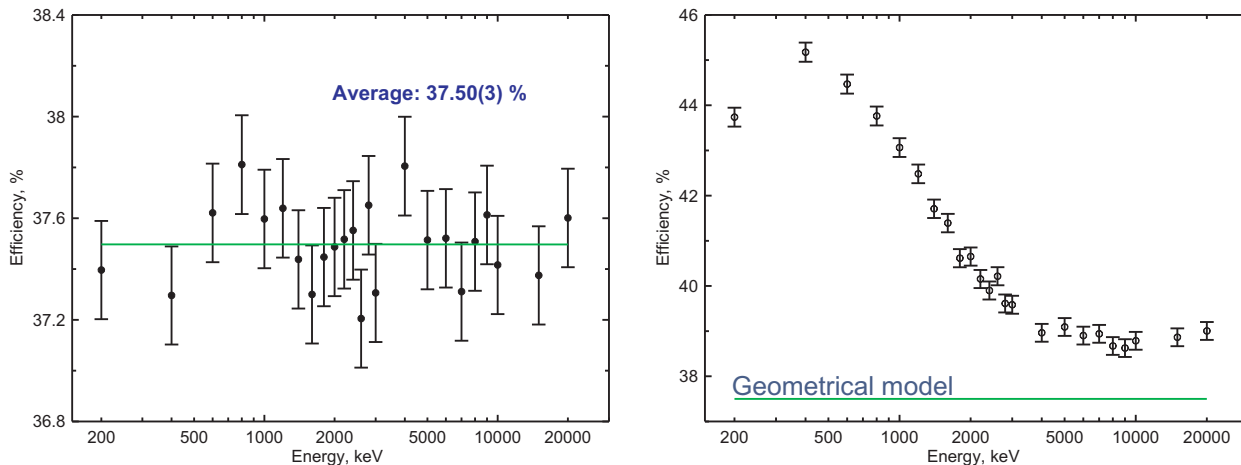


**Figure 2**. (a) Efficiencies calculated for a point-like $\beta$-source at 4.92 mm from the front of the scintillator in vacuum. Results are shown for monoenergetic $\beta$-particles emitted at various energies in the range from 200 keV to 20 MeV. (b) Efficiencies calculated for the same scintillator but with the point-like $\beta$-source placed in the center of a 76 $\mu$m thick aluminized mylar tape, also in vacuum.

particles that lost non-zero energy in the scintillator (*i.e.* no "cut-off" energy was used). Naturally, the introduction of a "cut-off" energy would shift the absolute efficiency to a lower value.

To our surprise, when the same point-like source was placed into the center of a 76 $\mu$m-thick aluminized mylar tape – the condition that applies to our actual on-line $\beta$-decay measurements –the total efficiency of the $\beta$-detector changes drastically throughout the whole energy range, but especially for $\beta$-particles energies below 4 MeV. See Figure 2(b). Although the mylar tape is very thin, it causes enough (back)scattering to increase the total efficiency of the detector by up to 20%. Even for betas at energies above 4 MeV, although the total efficiency remains more or less constant, it is still 4% higher than the result obtained by the simple geometrical estimation.

Figure 3(a) shows a comparison of the results from the Penelope code with the results from three different Geant4 EM physics models: low-energy EM model, standard EM model and a model that claims to emulate the Penelope code. (The EGSnrc results are not shown since they were virtually indistinguishable from the Penelope results.) Although we expected the results from the stand-alone Penelope to be the same as those from the Geant4 Penelope EM model, that was not what we found. This apparently is a consequence of the fact that the reengineered Penelope EM model contained in Geant4 uses a different method to describe the multiple scattering of beta particles than did the original Penelope code.
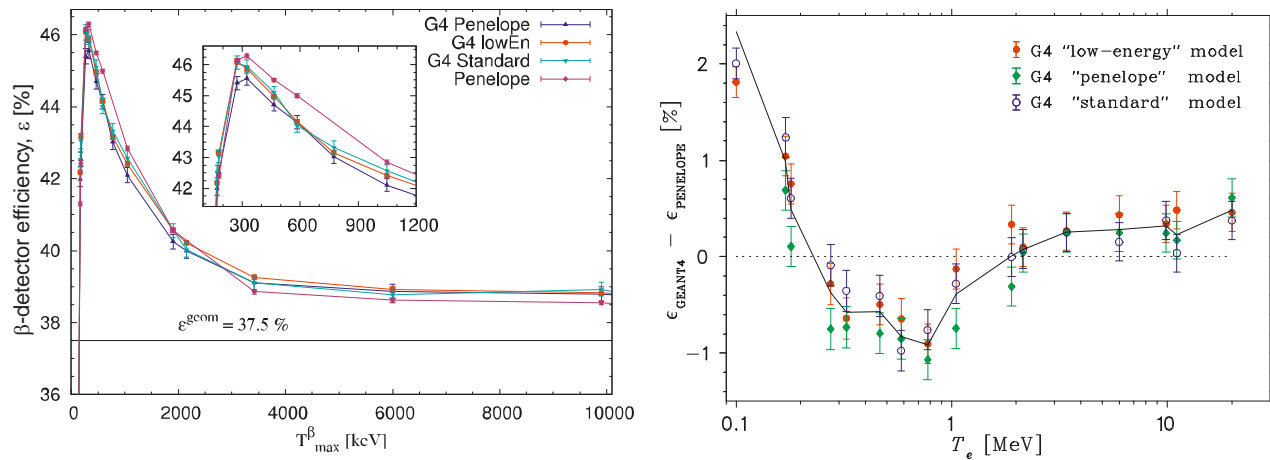


**Figure 3**. (a): $\beta$-detector efficiency of the plastic scintillator placed in air at a distance of 4.92 mm from a point-like source of mono-energetic positrons located at the center of aluminized mylar tape with thickness 76 μm; four different MC calculations are shown. The horizontal line is the geometrical efficiency. (b): The difference in efficiencies between Penelope and Geant4 with various EM physics models. The horizontal dotted line represents the stand-alone Penelope MC results.

Figure 3(b) shows the difference between the results for the efficiency calculations performed with the stand-alone Penelope program versus the three different EM physics models available in Geant4. Above 300 keV the difference in the efficiencies between the various Geant4 EM models and Penelope is less than 1%, with even better agreement above 1 MeV. The biggest discrepancies are in the energy region from 100 keV up to 1 MeV, although even there it is never larger than 2%.

The differences in MC codes that we have observed in these thin materials with very simplified geometry appear not to be entirely negligible. However, the resulting absolute efficiencies for monoenergetic positrons from point-like sources placed in the center of the aluminized mylar tape do not exceed 2% for the energies below 1 MeV and are well below 1% for energies between 1 MeV and 12 MeV. A comparison of Monte Carlo simulations for realistic sources – $^{207}$Bi, $^{22}$Na and $^{60}$Co – is described in a separate report [11].

[1] J. C. Hardy and I. S. Towner, Phys. Rev. C **71**, 055501 (2005); I. S. Towner and J. C. Hardy, Phys. Rev. C **77**, 025501 (2008).

[2] V. E. Iacob, J. C. Hardy, C. A. Gagliardi, et. al., Phys. Rev. C **74**, 015501 (2006).

[3] J. C. Hardy, V. E. Iacob, M. Sanchez-Vega, et. al., Phys. Rev. Lett. **91**, 082501 (2003).

[4] V. V. Golovko, V. E. Iacob, and J. C. Hardy, *Progress in Research*, Cyclotron Institute, Texas A&M University (2005-2006), p. I-43.

[5] S. Agostinelliae *et. al.*, Nucl. Instrum. Methods Phys. Res. **A506**, 250 (2003).

[6] GEANT4 Colaboration, Physics Reference Manual, CERN (2005).

[7] K. Amako *et. al.*, IEEE Trans. Nucl. Sci. **52**, 910 (2005).

[8] J. Baro *et. al.*, Nucl. Instrum. Methods Phys. Res. **B100**, 31 (1995).

[9] J. Sempau, J. M. Fernandez-Varea, E. Acosta, F. Salvat, Nucl. Instrum. Methods Phys. Res. **B207**, 107 (2003).

[10] I. Kawrakow, D. W. O. Rogers, NRCC Report PIRS-701, NRC, Otawa, (2003).

[11] V. V. Golovko, V. E. Iacob, J. C. Hardy, *Progress in Research*, Cyclotron Institute, Texas A&M University (2007-2008), p. V-21.

# Response function to low energy β particles in a thin plastic scintillator

V. E. Iacob, V. V. Golovko, and J. C. Hardy

Our β-decay measurements require extremely accurate half-life and branching-ratio measurements in order to be competitive in testing the unitarity of the Cabibbo-Kobayashi-Maskawa (CKM) matrix [1]. While the measurements themselves are simple in principle, the required precision makes them very demanding.

The measurement of a branching ratio requires the simultaneous measurement of β-γ coincidences and β singles. The set-up we use in these measurements includes a 70% HPGe detector 15 cm from the source, and a 1 mm thick plastic scintillator 4 mm from the source on the opposite side. The measuring cycle has been described, for example, in ref. [2]. If the efficiency of the β-detector, $\varepsilon_\beta$, did not depend on the energy of the incoming particle, then the branching ratio could be extracted directly from the β-γ coincidences and β singles: denoting the total number of observed β-γ coincidences and β-singles by $N_{\beta-\gamma}$ and $N_\beta$ we can write

$$\left.\begin{array}{l} N_\beta = N_{decays} \times \varepsilon_\beta \\ N_{\beta-\gamma} = N_{decays} \times \varepsilon_\beta \times BR_\gamma \times \varepsilon_\gamma \end{array}\right\} \Rightarrow \quad BR_\gamma = \frac{N_{\beta-\gamma}}{N_\beta \times \varepsilon_\gamma} \qquad (1)$$

where $\varepsilon_\gamma$ is the efficiency of the γ-ray detector and $BR_\gamma$ is the branching ratio for the γ ray of interest. This equation demonstrates the critical role played by the absolute efficiency of the HPGe detector and puts tough demands on its precision, since it is this precision that ultimately limits what can be achieved for the branching ratio. We already know the absolute efficiency of our detector to very high precision [2] having performed a complex series of source measurements along with corresponding Monte Carlo (MC) simulations, the later allowing us to make a reliable interpolation between measured values.

However, there is another factor that affects the result. Equation (1) must be corrected to account for the energy dependence of the response function of the β-detector. In general, any β decay includes several branches, each populating a different state in the daughter nucleus. Each branch has a different end-point energy and consequently has a slightly different probability for detection in the β detector. As a result, the $\varepsilon_\beta$ in the equation for $N_\beta$ does not exactly cancel with the $\varepsilon_\beta$ in the equation for $N_{\beta-\gamma}$. This situation becomes even more important in our measurements because of two important factors: (1) as with any detection system, noise must be rejected by a low-energy threshold, which also rejects some low-energy betas; and (2) the nuclei we study have quite high Q-values and decay via branches with a wide range of different end-point energies. To account for these factors, it is important that the numerator in eq. (1) should contain the β-detection efficiency specific to the branch of interest, while the denominator should include the overall β-detection efficiency for all branches. In the case of $^{34}$Ar, where $Q_{EC}$ = 6063 keV, the decay populates excited levels in $^{34}$Cl ranging from 461 keV to 3129 keV. Thus the end-point energies span a range of more than 2.6 MeV, enough to make variation in the β efficiency quite significant.

As there is no easy experimental access to mono-energetic electrons and even less to mono-energetic positrons, we have opted to examine the experimental efficiency of our detector based on measurements of total spectra, compared with MC calculations that mimic the experimental geometries

and materials. While for the calibration of the HPGe detector we used the CYLTRAN code from the "Integrated Tiger Series" [3], in our study of the $\beta$-detector we used the EGSnrc code [4], since CYLTRAN does not distinguish positron from electron interactions, and ignores higher-order effects such as in-flight annihilation. Our initial source measurements and MC calculations revealed the importance of the correct description of the composition and geometry of the source [5]. This prompted us to use in the present measurements only those sources for which we knew the exact geometry and material used in the source, its backing and supporting frame.

In a first series of experiments, we used a home-made $^{60}$Co source. It had been prepared from a 10-mm-diameter, 3-µm-thick foil of 99.9% pure $^{59}$Co, activated at the Texas A&M TRIGA reactor. After activation, the foil was sandwiched between two 4-µm-thick mylar foils, the whole system being held by a frame whose inner diameter was 15.5 mm with inner edges tapered to minimize electron scattering. Measurements were then made with the source located at distances ranging from 3 mm to 15 mm from the plastic scintillator. Fig. 1 presents an inter-comparison of the experimental and MC-simulated spectra for a source-scintillator distance of 3 mm. The MC simulation was performed with the EGSnrc package [4]. The numerical effort to simulate electron and positron spectra is significantly higher – and more time consuming – than that required to model a gamma spectrum because the slowing down process in the case of the $\beta$ particles involves thousands of elementary interactions. Thus, when generating a MC spectrum, we used enough computer time to obtain the statistics necessary to define the energy range below about 500 keV and then scaled the spectrum up to match the experimental number of counts. As can be seen from Fig. 1, the MC and experimental spectra are almost identical although for higher energies the MC data show more statistical scatter than the experimental data.
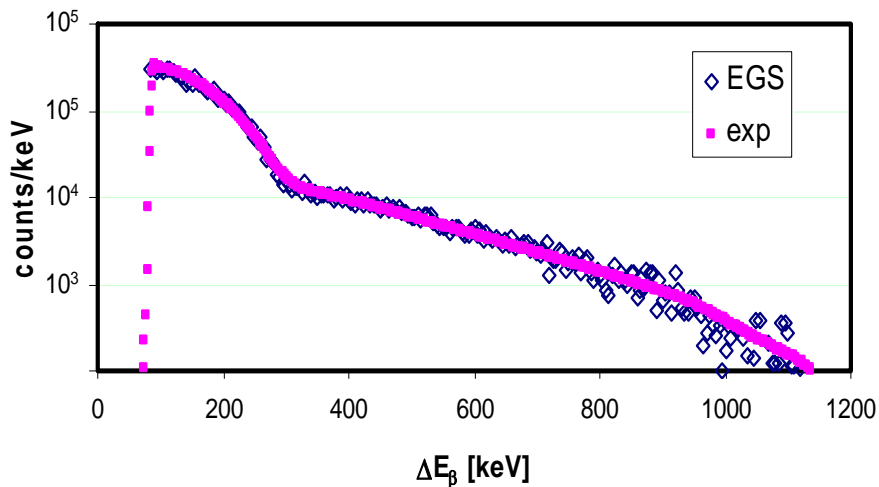


**Figure 1**. Experimental (solid squares) versus Monte-Carlo [4] (open diamonds) data for the β- spectrum from a $^{60}$Co source as recorded by a 1-mm-thick ΔE plastic scintillator.

Since Eq. 1 includes the $\beta$-efficiency in both numerator and denominator, only the relative changes in $\beta$ efficiency are required for a full analysis. However, as a further validation of our MC simulation, we compared the experimental and MC-predicted absolute efficiencies. In the case of $^{60}Co$, with a threshold energy of 80 keV we found the experimental efficiency to be 14.5% vs. 14.7% for the MC calculation, which is very satisfactory agreement.

Since $^{60}Co$ emits electrons and the superallowed decays of interest to us are actually positron emitters, we undertook a second series of experiments, in which we measured a $^{22}Na$ source, commercially available from Amersham. As with the $^{60}Co$ source, we measured total spectra at various source-detector distances and compared them with the corresponding MC simulations. Fig. 2 compares the experimental and MC spectra obtained for the $^{22}Na$ source located 4 mm from the scintillator.
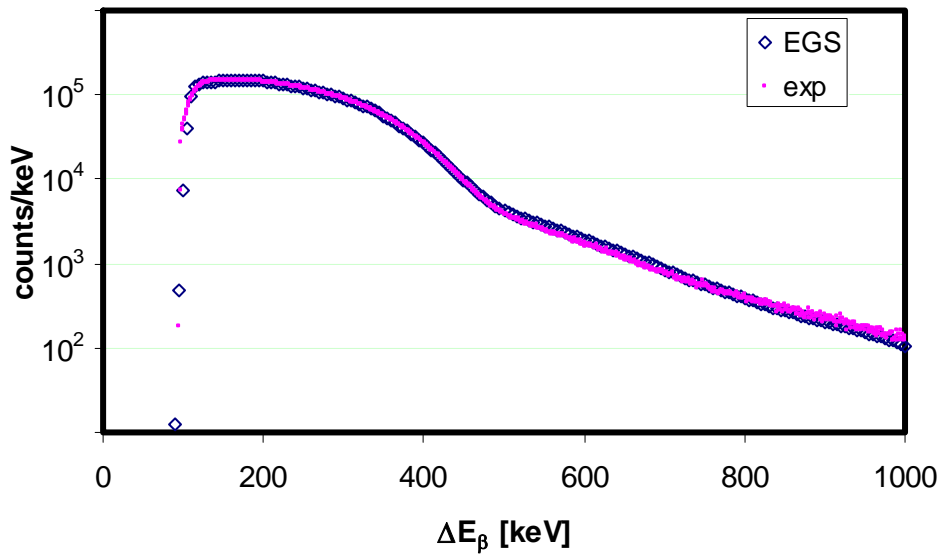


**Figure 2.** Experimental (solid squares) versus Monte-Carlo [4] (open diamonds). $\beta^+$ spectra in the 1mm thick $\Delta E$ plastic scintillator as generated by a $^{22}Na$ source

As this case is closer to our experimental conditions, the MC spectrum was calculated with significantly higher statistics than in the $^{60}Co$ case. Obviously the MC simulation gives a very good description of the experimental spectrum. We would like to have compared the absolute efficiencies as we had done for $^{60}Co$ but unfortunately the supplier's information regarding the source dimensions and strength was inadequate. This prompted us to order a new source, specifically designed to suit our purposes with a very thin cover and backing. Measurements on the new source are expected to improve even further our characterization of the response function of our $\beta$ detector to positrons.

[1] I. S. Towner, J. C.Hardy, Phys. Rev. C **77**, 025501 (2008)
[2] V. E. Iacob *et al.*, *Progress in Research*, Cyclotron Institute, Texas A&M University (2005-2006), p. I-31.

[3] J. A. Halbleib, T. A. Mehlhorn, 1986, The Integrated Tiger Series (ITS) of coupled electron/photon Monte Carlo transport codes. Nucl. Sci. Eng. 92, 338–339.

[4] http://www.irs.inms.nrc.ca/inms/irs/EGSnrc/EGSnrc.html

[5] V. V. Golovko *et al.*, *Progress in Research*, Cyclotron Institute, Texas A&M University (2006-2007), p. V-23.

# SECTION VI

# PUBLICATIONS

**Folding model analysis of 240 MeV $^6$Li elastic scattering on $^{116}$Sn and inelastic scattering to low-lying states of $^{116}$Sn,** X. Chen, Y.-W. Lui, H.L. Clark, Y. Tokimoto, and D.H. Youngblood, Phys. Rev. C **76**, 054606 (2007).

**Isoscalar giant resonance strength in $^{28}$Si,** D.H. Youngblood, Y.-W. Lui, and H.L. Clark, Phys. Rev. C **76**, 027304 (2007).

**Decay of $^{10}$C excited states above the 2p+2α threshold and the contribution from democratic two-proton emission**, R.J. Charity, K. Mercurio, L.G. Sobotka, J.M. Elson, M. Famiano, A. Banu, C. Fu, L. Trache, and R.E. Tribble**,** Phys. Rev. C **75**, 051304(R) (2007).

**Radii of halo states in light nuclei deduced from ANC**, F. Carstoiu, L. Trache, C.A. Gagliardi, A.M. Mukhamedzhanov and R.E. Tribble, Rom. Rep. Phys. **59**, 357 (2007).

**Nuclear astrophysics with radioactive nuclear beams: indirect methods**, L. Trache, Rom. J. Phys. **52**, 823 (2007).

**pp collisions at RHIC**, C.A. Gagliardi, *Carpathian Summer School of Physics 2007*, AIP Conference Proceedings, **972**, 177 (2008).

**Fundamental interactions, nuclear masses, astrophysics, and QCD**, C.A. Gagliardi, *Carpathian Summer School of Physics 2007*, AIP Conference Proceedings, **972**, 5 (2008).

**Reaction rates for H-burning in stars from experiments with radioactive nuclear beams**, Livius Trache, *Carpathian Summer School of Physics 2007*, AIP Conference Proceedings, **972**, 230 (2008).

**Recent astrophysical experiments on cyclotron of NPI at Rez in collaboration with Texas A&M University**,V. Kroha, V. Burjan, Z. Hons, J. Mrazek, S. Piskor, C.A. Gagliardi, A.M. Mukhamedzhanov, L. Trache, R.E. Tribble, G. Pizzone, S. Romano and C. Spitaleri, *Carpathian Summer School of Physics 2007*, AIP Conference Proceedings, **972**, 279 (2008).

**Extracting the asymptotic normalization coefficients in neutron transfer reactions to determine the astrophysical reaction rates for $^{22}$Mg(p,γ)$^{23}$Al and $^{17}$F(p,γ)$^{18}$Ne**, T. Al-Abdullah, F. Carstoiu, X. Chen, H. Clark, C. Fu, C.A. Gagliardi, Y.-W. Lui, A.M. Mukhamedzhanov, G. Tabacaru, Y. Tokimoto, L. Trache, R.E. Tribble and Y. Zhai, *Carpathian Summer School of Physics 2007*, AIP Conference Proceedings, **972**, 439 (2008).

**Recent applications of the THM to the AGB star nucleosynthesis**, M. LaCognata, C. Spitaleri, R.E. Tribble, T. Al-Abdullah, A. Banu, S. Cherubini, V. Crucilla, C. Fu, V. Goldberg, M. Gulino, L. Lamia, A.M. Mukhamedzhanov, R.G. Pizzone, S.M.R. Puglia, G.G. Rapisarda, S. Romano, M.L. Sergi, G. Tabacaru, L. Trache, A. Tumino and Y. Zhai, *Carpathian Summer School of Physics 2007*, AIP Conference Proceedings, **972**, 485 (2008).

**Exotic nuclei and nuclear/particle astrophysics (II)**, edited by Livius Trache and Sabin Stoica**,** *Proceedings of the Carpathian Summer School of Physics 2007,* American Institute of Physics Conference Proceedings, **972** (2008).

**Indirect measurement of the $^{18}$O(p, $\alpha$)$^{15}$N reaction rate through the THM**, M.La Cognata, C. Spitaleri, R.E. Tribble, T.Al-Abdullah, A. Banu, S. Cherubini, V. Crucilla, C. Fu, V.Z. Goldberg, M. Gulino, L. Lamia, A.M. Mukhamedzhanov, R.G. Pizzone, S.M.R. Puglia, G.G. Rapisarda, S. Romano, M.L. Sergi, G. Tabacaru, L. Trache, S. Tudisco, A. Tumino, S. Typel, Y. Zhai   J. Phys. G **35**, 014014 (2008).

**Single and double proton emissions from the $^{14}$O+$^{4}$He interaction**, C.Fu, V.Z. Goldberg, A.M. Mukhamedzhanov, G.G. Chubarian, G.V. Rogachev, B. Skorodumov, M. McCleskey, Y. Zhai, T. Al-Abdullah, G. Tabacaru, L. Trache, R.E. Tribble   Phys. Rev. C **76**, 021603 (2007).

**Astrophysical S(E) factor of the $^{15}$N(p, $\alpha$)$^{12}$C reaction at sub-Coulomb energies via the Trojan horse method**, M.La Cognata, S. Romano, C. Spitaleri, S. Cherubini, V. Crucilla, M. Gulino, L. Lamia, R.G. Pizzone, A. Tumino, R.E. Tribble, C. Fu, V.Z. Goldberg, A.M. Mukhamedzhanov, D. Schmidt, G. Tabacaru, L. Trache, B.F. Irgaziev   Phys. Rev. C **76**, 065804 (2007).

**The Trojan horse method in nuclear astrophysics: recent results**, S. Romano, C. Spitaleri, S. Cherubini, V. Crucilla, M. Gulino, M. La Cognata, L. Lamia, R.G. Pizzone, S.M.R. Puglia, G.G. Rapisarda, M.L. Sergi, S. Tudisco, A. Tumino, R.E. Tribble, V. Goldberg, A. Mukhamedzhanov, G. Tabacaru, L. Trache, V. Kroha, V. Burjan, Z. Hons, J. Novac, J. Vincour, E. Somorjai, Z. Elekes, Z. Fulop, G. Gyurky, G. Kiss, A. Szanto de Toledo, N. Carlin, M.M. De Moura, M.G. Del Santo, M.G. Munhoz, R. Liguori Neto, F.A. Souza, A.A.P. Suaide, E. Szanto, J. Phys. G **35**, 014008 (2008).

**Low-lying resonant states in $^{16}$F using a $^{15}$O radioactive ion beam**, D.W. Lee, K. Perajarvi, J. Powell, J.P. O'Neil, D.M. Moltz, V.Z. Goldberg, J. Cerny  Phys. Rev. C **76**, 024314 (2007).

**Lowest excited states of $^{13}$O**, B.B. Skorodumov, G.V. Rogachev, P. Boutachkov, A. Aprahamian, V.Z. Goldberg, A.M. Mukhamedzhanov, S. Almaraz, H. Amro, F.D. Becchetti, S. Brown, Y. Chen, H. Jiang, J.J. Kolata, L.O. Lamm, M. Quinn, A. Woehr  Phys. Rev. C **75**, 024607 (2007).

**Lowest proton decay of $^{20}$Ne states populated in the $^{14}$O+α reaction**, C. Fu, V.Z. Goldberg, A.M. Mukhamedzhanov, G.G. Chubarian, G.V. Rogachev, B.B. Skorodumov, M. McCleskey, Y. Zhai, T. Al-Adullah, G. Tabacaru, L. Trache, R.E. Tribble, AIP Conference Proceedings, **1005**, 144 (2008).

**Astrophysical S-factor of the $^{12}$N(p,γ)$^{13}$O reaction determined from the ($^{12}$N,$^{13}$O) proton transfer reaction**, A. Banu, T. Al-Abdullah, V. Burjan, F. Carstoiu, C. Fu, C.A. Gagliardi, M. McCleskey, G. Tabacaru, L. Trache, R.E. Tribble, Y. Zhai, *Carpathian Summer School of Physics 2007*, AIP Conference Proceedings, **972**, 444 (2008).

**Astrophysical S-factor of the $^{12}$N(p,γ)$^{13}$O reaction in relation to Population III stars**, A. Banu, T. Al-Abdullah, V. Burjan, F. Carstoiu, C. Fu, C. A. Gagliardi, M. McCleskey, G. Tabacaru, L. Trache, R.E. Tribble, Y. Zhai, *Proceedings of "First Stars III"*, AIP Conference Proceedings, 990, 347 (2007).

**A facility upgrade at Texas A&M University for accelerated radioactive beams**, R.E. Tribble, F. Abegglen, G. Chubarian, H.L. Clark, G. Derrig, G. Kim, D. May, G.A. Souliotis, G. Tabacaru, Eur. J. Phys. ST **150**, 255 (2007).

**The half-life of $^{198}$Au: high-precision measurement shows no temperature dependence**, J.R. Goodwin, V.V. Golovko, V.E. Iacob and J.C. Hardy, Eur. Phys J. A **34**, 271 (2008).

**Improved calculation of the isospin-symmetry-breaking corrections to superallowed Fermi β decay**, I.S. Towner and J.C. Hardy, Phys. Rev. C **77**, 025501 (2008).

**Internal conversion coefficients in $^{134}$Cs, $^{137}$Ba and $^{139}$La: a precise test of theory**, N. Nica, J.C. Hardy, V.E. Iacob, C. Balonek and M.B. Trzhaskovskaya, Phys. Rev. C **77**, 034306 (2008).

**$Q_{EC}$ values of the superallowed β emitters $^{50}$Mn and $^{54}$Co**, T. Eronen, V.-V Elomaa, U. Hager, J. Hakala, J.C. Hardy, A. Jokinen, A. Kankainen, I.D. Moore, H. Pentilla, S. Rahaman, S. Rinta-Antila, J. Rissanen, A. Saastamoinen, T. Sonoda, C. Weber and J. Aysto, Phys. Rev. Lett. **100**, 132502 (2008).

**Precise half-life measurement of the superallowed β$^+$ emitter $^{10}$C**, V.E. Iacob, J.C. Hardy, V. Golovko, J. Goodwin, N. Nica, H.I. Park, L. Trache and R.E. Tribble, Phys. Rev. C **77**, 045501 (2008).

**Superallowed nuclear beta decay: a window on the weak interaction**, J.C. Hardy, *Carpathian Summer School of Physics 2007*, AIP Conference Proceedings, **972**, 119 (2008).

**Nuclear data sheets for A = 140**, N. Nica, Nucl. Data Sheets **108**, 1287 (2007).

**A pulsed drift cavity to capture 30 keV ion bunches at ground potential**, S. Coeck, B. Delaure, M. Herbane, M. Beck, V.V. Golovko, S. Kopecky, V. Yu. Koslov, I.S. Kraev, A. Lindroth, T. Phalet, D. Beck, P. Delahaye, A. Her;ert, F. Wenander and N. Severijns, Nucl. Instrum. Methods Phys. Res. **A572**, 585 (2007).

**Alpha-decay half-life of $^{253}$Es in metallic Fe at temperature between 4 K and 50mK**, N. Severijns, A.A. Belyaev, A.L. Erzinkyan, P.-D. Eversheim, V.T. Filimonov, V.V. Golovko, G.M. Gurevich, P. Herzog, I.S. Kraev, A.A. Lukhanin, V.I. Noga, V.P. Parfenova, T. Phalet, A.V. Rusakov, Yu. G. Toporov, C. Tramm, V.N. Vyachin, F. Wauters, D. Zakoucky and E. Zotov, Phys. Rev. C **76**, 024304 (2007).

**The quenching of nucleon yields in the nonmesonic weak decay of Λ-hypernuclei and the three-body weak decay process**, H. Bhang, S. Ajimura, K. Aoki, A. Banu, T. Fukuda, O. Hashimoto, J.I. Hwang, S. Kameoka, B.H. Kang, E.H. Kim *et al.*, Eur. Phys. J. A **33**, 259 (2007).

**Sub-barrier Coulomb excitation of $^{110}$Sn and its implications for the $^{100}$Sn shell closure**, J. Cederkall, A. Ekstrom, C. Fahlander, A.M. Hurst, M. Hjorth-Jensen, F. Ames, A. Banu, P.A. Butler, T. Davinson, U. Datta Pramanik *et al.*, Phys. Rev. Lett. **98**, 172501 (2007).

**Decay asymmetry in non-mesonic weak decay of light Λ-hypernuclei**, T. Maruta, S. Ajimura, K. Aoki, A. Banu, T. Fukuda, O. Hashimoto, J.I. Hwang, S. Kameoka, B.H. Kang, E.H. Kim *et al.*, Eur. Phys. J. A **33**, 255 (2007).

**Observation of the 7 MeV excited spin-flip and non-spin-flip partners in $^{16}_{Λ}$O by γ-ray spectroscopy**, M. Ukai, S. Ajimura, H. Akikawa, D. E. Alburger, <u>A. Banu</u>, R. E. Chrien, G. B. Franklin, J. Franz, O. Hashimoto, T. Hayakawa *et al.*, Eur. Phys. J. A **33**, 247 (2007).

**The detector system of the BigSol spectrometer at Texas A&M,** M Barbui, S. Pesente, G. Nebbia *et al.*, Nucl. Instrum. Methods Phys. Res. **B265**, 605 (2007).

**Clustering and symmetry energy in a low density nuclear gas**, S. Kowalski, J.B. Natowitz, S. Shlomo *et al.*, Nucl. Phys. **A787**, 619c (2007).

**Experimental determination of the symmetry energy of a low density nuclear gas**, S. Kowalski, J.B. Natowitz, S. Shlomo *et al.*, Phys. Rev. C **75**, 014601 (2007).

**Properties of the initial participant matter interaction zonein near –Fermi-energy heavy-ion collisions**, J. Wang, T. Keutgen, R. Wada *et al.*, Phys. Rev. C **75**, 014604 (2007).

**Density dependence of the symmetry energy and the nuclear equation of state: A dynamical and statistical model perspective,** D.V. Shetty, S.J. Yennello, and G.A. Souliotis, Phys. Rev. C **76**, 024606 (2007).

**Constraining the density dependence of the symmetry energy in the nuclear equation of state using heavy ion beams,** D.V. Shetty, S.J. Yennello, and G.A. Souliotis, Nucl. Instrum. Methods Phys. Res. B **261**, 990 (2007).

**Properties of hot nuclear fragments formed in multifragmentation and their astrophysical implications,** G.A. Souliotis, A.S. Botvina, D.V. Shetty, A.L. Keksis, M. Jandel, M. Veselsky, and S.J. Yennello, Nucl. Instrum. Methods Phys. Res. **B261**, 996 (2007).

**Rare isotope production in the Fermi energy regime and application to the Texas A&M RIB upgrade,** G.A. Souliotis, A.L. Keksis, B.C. Stein, M. Veselsky, M. Jandel, D.V. Shetty, S.N. Soisson, S. Wuenschel, and S.J. Yennello, Nucl. Instrum. Methods Phys. Res. **B261**, 1094 (2007).

**Investigating the nuclear equation of state through N/Z equilibration,** S. Yennello, A. Keksis, and E. Bell, AIP Conference Proceedings, **947**, 321 (2007).

**Multifragmentation, phase transitions and the nuclear equation of state**, S.J. Yennello, *Proceedings of the Predeal International Summer School in Nuclear Physics*, (World Scientific, Singapore, 2007) p. 418.

**Effects of multiple ionization on the spectra of *L* x rays excited in heavy-ion collisions,** V. Horvat, R.L. Watson, J.M. Blackadar, Phys. Rev. A **77**, 032724 (2008).
**The equation of symmetric and asymmetric nuclear matter**, S. Shlomo, Nucl. Phys. At. Energy 3(21)7 (2007).

**Equation of state of symmetric and asymmetric nuclear matter**, S. Shlomo and Tapas Sil, AIP Conference Proceedings **884**, 340 (2007).

**Bulk properties of nuclear matter from excitations of nuclei**, Shalom Shlomo, AIP Conference Proceedings **947**, 371 (2007).

**Hartree-Fock based random phase approximation description of giant resonances and the nuclear equation of state**, Shalom Shlomo, AIP Conference Proceedings **972**, 137 (2008).

**Trojan horse as an indirect technique in nuclear astrophysics**, A.M. Mukhamedzhanov, L.D. Blokhintsev, B.F. Irgaziev, A.S. Kadyrov, M. La Cognata, C. Spitaleri and R.E. Tribble, J. Phys. G **35**, 014016 (2008).

**Indirect techniques in nuclear astrophysics. asymptotic normalization coefficient and Trojan Hors**e, A. M. Mukhamedzhanov, L.D. Blokhintsev, S. Brown, V. Burjan, S. Cherubini, V.Z. Goldberg, M. Gulino, B.F. Irgaziev, E. Johnson, K. Kemper *et al.*, Nucl. Phys. **A787** , 321c (2007).

**No signature of nuclear-Coulomb interference in the proton-proton elastic scattering via the Trojan horse method**, A. Tumino, C. Spitaleri, G.G. Rapisarda, S. Cherubini, S. Blagus, M. Bogovać, V. Crucillá, Z. Elekes, Z. Fülöp, M. Gulino *et al.*, Nucl. Phys. **A787**, 337c (2007)

**Deuteron elastic scattering and stripping processes off $^{12}$C as a three-body problem**, E.O. Alt, L.D. Blokhintsev, A.M. Mukhamedzhanov, and A.I. Sattarov, Phys. Rev. C **75**, 054003 (2007).

**Suppression of the Coulomb interaction in the Off-Energy-Shell p-p scattering from the p+d → p+p+n reaction**, A. Tumino, C. Spitaleri, A.M. Mukhamedzhanov, G.G. Rapisarda, S. Cherubini, V. Crucillá, Z. Elekes, Z. Fülöp, M. Gulino, G. Gyürky, G. Kiss, M. La Cognata, L. Lamia, F. Mudó, R.G. Pizzone, S. Romano, M.L. Sergi, and E. Somorjai, Phys. Rev. Lett. **98**, 252502 (2007).

**Jet conversions in a quark-gluon plasma**, W. Liu, C.M. Ko, and B.W. Zhang, Phys. Rev. C **75**, 051901 (R) (2007).

**J/Ψ absorption by nucleons in the meson-cxchange model**, Y. Oh, W. Liu, and C.M. Ko, Phys. Rev. C **75**, 064903 (2007).

**Partonic transport description of heavy ion collisions**, C.M. Ko, L.W. Chen, and B.W. Zhang, J. Phys. G **34**, S413 (2007).
**Jet conversions in a quark-gluon plasma**, C.M. Ko, W. Liu, and B.W. Zhang, Braz. J. Phys. **37**, 855 (2007).

**Heavy quark three-body collisional energy loss in QGP**, W. Liu and C.M. Ko, J. Phys. G **34**, S775 (2007).

**Heavy-ion collisions at LHC in a multiphase transport model**, C.M. Ko, L.W. Chen, and B.W. Zhang, Braz. J. Phys. **37**, 969 (2007).

**$D_{sJ}$ (2317) meson production in ultrarelativistic heavy ion collisions,** L.W. Chen, C.M. Ko, W. Liu, and M. Nielsen, Phys. Rev. C **76**, 014906 (2007).

**Jet conversions in QGP and suppression of identified hadrons**, W. Liu, C.M. Ko, and B.W. Zhang, Int. J. Mod. Phys. E **16**, 1930 (2007).

**Probing the nuclear symmetry energy with heavy-ion reactions induced by neutron-rich nuclei**, L. W. Chen, C.M. Ko, B.A. Li, and G.C. Yong, Front. Phys. China **3**, 327 (2007).

**Isospin-dependent properties of asymmetric nuclear matter in relativistic mean-field models**, L.W. Chen, C.M. Ko, and B.A. Li, Phys. Rev. C **76**, 054316 (2007).

**Elliptic flow of deuterons in relativistic heavy ion collisions,** Y. Oh and C.M. Ko,  Phys. Rev. C **76**, 054910 (2007).

**Jet flavor conversions in the quark-gluon plasma**, C.M. Ko, W. Liu, and B.W. Zhang, Few Body Sys. **41**, 63 (2007).

**Constraining properties of neutron stars with heavy-ion reactions in terrestrial laboratories**, B.A. Li, L.W. Chen, C.M. Ko, P.G. Krastev, A.W. Steiner, and G.C. Yong, J. Phys. G **35**, 014044 (2008).

**Thermal charm quark production in a quark-gluon plasma in Pb-Pb Collisions at $s^{1/2}_{NN}$=5.5 TeV**, B. W. Zhang, C.M. Ko, and W. Liu, Phys. Rev. C **77**, 024901 (2008).

**Charmed exotics in heavy ion collisions**, S.H. Lee, S. Yasui, W. Liu, and C.M. Ko, Eur. Phys. J. C **54**, 259 (2008).

**Evolution of the bulk properties of the hot dense matter in relativistic heavy ion collisions**, B. Zhang, L.W. Chen, and C.M. Ko, J. Phys. G 35, 065103 (2008).

**Xi and Omega baryons in the Skyrme model**, Yongseok Oh, Phys. Rev. D **75**, 074002 (2007).

**Low-energy thermal photons from meson-meson bremsstrahlung**, W. Liu and R. Rapp, Nucl. Phys. **A796**, 101 (2007).

**Q-anti-Q modes in the quark-gluon plasma**, D. Cabrera and R. Rapp, Eur. Phys. J. A **31**, 858 (2007).

**Hot and dense QCD matter and heavy-ion collisions**, R. Rapp, Nucl. Instrum. Methods Phys. Res. **B261**, 1053 (2007).

**T-matrix approach to quarkonium correlation functions in the quark-gluon plasma**, D. Cabrera and R. Rapp, Phys. Rev. D **76**, 114506 (2007).

**Melting rho meson and thermal dileptons**, R. Rapp, H. van Hees and T. Strong, Braz. J. Phys. **37**, 779 (2007).

**Interpretation of recent SPS dilepton data**, H. van Hees and R. Rapp, J. Phys. G **34**, S1051 (2007).

**Theory and phenomenology of vector mesons in medium**, R. Rapp, J. Phys. G **34**, S405 (2007).

**Quark coalescence based on a transport equation**, L. Ravagli and R. Rapp, Phys. Lett. B **655**, 126 (2007).

**Early time evolution of high energy heavy ion collisions**, R.J. Fries, J. Phys. G **34**, S851 (2007).

**Nuclear modification factor for charged pions and protons at forward rapidity in central Au + Au collisions at 200 GeV**, I. Arsene, I.G. Bearden, D. Beavis *et al.*, Phys. Lett. B **650**, 219 (2007).

**Production of mesons and baryons at high rapidity and high p(T) in proton-proton collisions at $\sqrt{s} =$ 200 GeV**, I. Arsene, I.G. Bearden, D. Beavis *et al.*, Phys. Rev. Lett. **98**, 252001 (2007).

**An introduction to high $p_T$ physics at RHIC**, Saskia Mioduszewski, AIP Conference Proceedings, **972**, 185 (2008).

**Cold nuclear matter effects on J/Psi as constrained by deuteron-gold measurements at $\sqrt{s_{NN}} =$ 200-GeV**, A. Adare *et al.* (PHENIX Collaboration), Phys. Rev. C **77**, 024912 (2008).

**Centrality dependence of charged hadron production in deuteron + gold and nucleon + gold collisions at $\sqrt{s_{NN}} =$ 200-GeV**, S.S. Adler *et al.* (PHENIX Collaboration), Phys. Rev. C **77**, 014905 (2008).

**Pion production by protons on a thin beryllium target at 6.4-Ge, 12.3-GeV/c, and 17.5-GeV/c incident proton momenta**, I. Chemakin *et al.* (E910 Collaboration), Phys. Rev. C **77**, 015209 (2008), Erratum-ibid. C**77**, 049903 (2008).

**Transverse momentum and centrality dependence of dihadron correlations in Au+Au collisions at $\sqrt{s_{NN}} =$ 200-GeV: Jet-quenching and the response of partonic matter**, A. Adare *et al.* (PHENIX Collaboration), Phys. Rev. C **77**, 011901 (2008).

**Results from RHIC and a look to the future**, S. Mioduszewski, Nucl. Instrum. Methods Phys. Res. **B261**, 1058 (2007).

**Forward lambda production and nuclear stopping power in d + Au collisions at $\sqrt{s_{NN}} =$ 200-GeV**, B.I. Abelev *et al.* (STAR Collaboration), Phys. Rev. C **76**, 064904 (2007).

**Strangelet search in Au+Au collisions at $\sqrt{s_{NN}} =$ 200 GeV**, B.I. Abelev *et al.* (STAR Collaboration), Phys. Rev. C, **76**, 011901(R) (2007).

**Global polarization measurement in Au+Au collisions**, B.I. Abelev *et al.* (STAR Collaboration), Phys. Rev. C **76**, 024915 (2007).

**Measurement of transverse single-spin asymmetries for di-jet production in proton-proton collisions at** $\sqrt{s_{NN}}$ **= 200-GeV**, B.I. Abelev *et al.* (STAR Collaboration), Phys. Rev. Lett. **99**, 142003 (2007).

**Energy dependence of pi$^{\pm}$, p and anti-p transverse momentum spectra for Au+Au collisions at** $\sqrt{s_{NN}}$ **= 62.4 and 200-GeV**, B.I. Abelev *et al.* (STAR Collaboration), Phys. Lett. B **655**, 104(2007).

**Measurement of density correlations in pseudorapidity via charged particle multiplicity fluctuations in Au+Au collisions at** $\sqrt{s_{NN}}$ **= 200-GeV**, S.S. Adler *et al.* (PHENIX Collaboration), Phys. Rev. C **76**, 034903 (2007).

**Inclusive cross-section and double helicity asymmetry for pi$^{0}$ production in p + p collisions at** $\sqrt{s_{NN}}$ **= 200-GeV: Implications for the polarized gluon distribution in the proton**, A. Adare *et al.* (PHENIX Collaboration), Phys. Rev. D **76**, 051106 (2007).

**Elliptic flow for phi mesons and (anti) deuterons in Au + Au collisions at** $\sqrt{s_{NN}}$ **= 200-GeV**, S. Afanasiev *et al.* (PHENIX Collaboration), Phys. Rev. Lett. **99**, 052301 (2007).

**Partonic flow and phi-meson production in Au + Au collisions at** $\sqrt{s_{NN}}$ **= 200-GeV**, B.I. Abelev *et al.* (STAR Collaboration), Phys. Rev. Lett. **99**, 112301 (2007).

**Mass, quark-number, and** $\sqrt{s_{NN}}$ **dependence of the second and fourth flow harmonics in ultra-relativistic nucleus-nucleus collisions**, B.I. Abelev *et al.* (STAR Collaboration), Phys. Rev. C **75**, 054906 (2007).

**A detailed study of high-p(T) neutral pion suppression and azimuthal anisotropy in Au+Au collisions at** $\sqrt{s_{NN}}$ **= 200-GeV**, S.S. Adler *et al.* (PHENIX Collaboration), Phys. Rev. C **76**, 034904 (2007).

**J/psi production versus transverse momentum and rapidity in p+p collisions at** $\sqrt{s_{NN}}$ **= 200-GeV**, A. Adare *et al.* (PHENIX Collaboration), Phys. Rev. Lett. **98**, 232002 (2007).

**Correlated production of p and anti-p in Au+Au collisions at** $\sqrt{s_{NN}}$ **= 200-GeV**, A. Adare *et al.* (PHENIX Collaboration), Phys. Lett. B **649**, 359 (2007).

**Energy loss and flow of heavy quarks in Au+Au collisions at** $\sqrt{s_{NN}}$ **= 200-GeV**, A. Adare *et al.* (PHENIX Collaboration), Phys. Rev. Lett. **98**, 172301 (2007).

**System size and energy dependence of jet-induced hadron pair correlation shapes in Cu+Cu and Au+Au collisions at** $\sqrt{s_{NN}}$ **= 200 and 62.4-GeV**, A. Adare *et al.* (PHENIX Collaboration), Phys. Rev. Lett. **98**, 232302 (2007).

**J/psi production vs centrality, transverse momentum, and rapidity in Au+Au collisions at $\sqrt{s_{NN}}$ = 200-GeV**, A. Adare *et al.* (PHENIX Collaboration), Phys. Rev. Lett. **98**, 232301 (2007).

**Production of omega mesons at large transverse momenta in p + p and d + Au collisions at $\sqrt{s_{NN}}$ = 200-GeV**, S.S. Adler *et al.* (PHENIX Collaboration), Phys. Rev. C **75**, 051902 (2007).

**Centrality dependence of pi$^0$ and eta production at large transverse momentum in $\sqrt{s_{NN}}$ = 200-GeV d+Au collisions**, S.S. Adler *et al.* (PHENIX Collaboration), Phys. Rev. Lett. **98**, 172302 (2007).
**Rapidity and species dependence of particle production at large transverse momentum for d+Au collisions at $\sqrt{s_{NN}}$ = 200-GeV,** B.I. Abelev *et al.* (STAR Collaboration), Phys. Rev. C **76**, 054903 (2007).

**Measurement of single muons at forward rapidity in p+p collisions at $\sqrt{s_{NN}}$ = 200-GeV and Implications for charm production**, S.S. Adler *et al.* (PHENIX Collaboration), Phys. Rev. D **76**, 092002 (2007).

**Scaling properties of azimuthal anisotropy in Au+Au and Cu+Cu collisions at $\sqrt{s_{NN}}$ = 200-GeV**, A. Adare *et al.* (PHENIX Collaboration), Phys. Rev. Lett. **98**: 162301 (2007).

**Transverse momentum and centrality dependence of high-p(T) non-photonic electron suppression in Au+Au collisions at $\sqrt{s_{NN}}$ = 200-GeV**, B.I. Abelev *et al.* (STAR Collaboration), Phys. Rev. Lett. **98**, 192301 (2007).

**Strange particle production in p+p collisions at $\sqrt{s_{NN}}$ = 200-GeV**, B.I. Abelev *et al.* (STAR Collaboration), Phys. Rev. C **75**, 064901 (2007).

**$\rho_0$ photoproduction in ultra-peripheral relativistic heavy ion collisions at $\sqrt{s_{NN}}$ = 200 GeV**, B.I. Abelev *et al.* (STAR Collaboration), Phys. Rev. C **77**, 034910 (2008).

**Centrality dependence of charged hadron and strange hadron elliptic flow form $\sqrt{s_{NN}}$ = 200 GeV Au+Au collissions**, B.I. Abelev *et al.* (STAR Collaboration), Phys. Rev. C **77**, 054901 (2008).

**Forward $\Lambda$ production and nuclear stopping power in $d$ + Au collisions at $\sqrt{s_{NN}}$ = 200 GeV**, B.I. Abelev *et al.* (STAR Collaboration), Phys. Rev. C **76**, 064904 (2007).

**Enhanced strange baryon production in Au+Au collisions compared to p+p at $\sqrt{s_{NN}}$ = 200 GeV**, B.I. Abelev *et al.* (STAR Collaboration), Phys. Rev. C **77**, 44908 (2008).

**Measurement of Y production in $p$ + $p$ and $p$ + $d$ interactions at 800 GeV/c**, L.Y. Zhu, P.E. Reimer, B. Mueller, T.C. Awes, M.L. Brooks, C.N. Brown, J.D. Bush, T.A. Carey, T.H. Chang, W.E. Cooper, C.A. Gagliardi, G.T. Garvey, D.F. Gesaman, E.A. Hawker, X.C. He, D.E. Howell, L.D. Isenhower, D.M.

Kaplan, S.B. Kaufman, S.A. Kinksiek, D.D. Koetke, D.M. Lee, W.M. Lee, M.J. Leitch, N. Makins, P.L McGaughey, J.M. Moss, P.M. Nord, V. Papavassiliou, B.K. Park, G. Petit, J.C. Peng, M.E. Salder, W.E. Sondheim, P.W. Stankus, T.N. Thompson, R.S. Towell, R.E. Tribble, M.A. Vasiliev, J.C. Webb, J.L. Willis, P. Winter, D.K. Wise, Y. Yin, G.R. Young, Phys. Rev. Lett. **100**, 062301 (2008).

**Global polarization measurement in Au+Au collisions**, B.I. Abelev *et al.* (STAR Collaboration), Phys. Rev. C **76**, 024915(2007).

**Measurement of transverse single-spin asymmetries for dijet production in proton-proton collisions at $\sqrt{s_{NN}}$ = 200 GeV**, B.I. Abelev *et al.* (STAR Collaboration), Phys. Rev. Lett. **99**, 142003 (2007).

**The energy dependence of $p_t$ angular correlations inferred from mean-$p_t$ fluctuation scale dependence in heavy ion collisions at the SPS and RHIC**, J. Adams *et al.* (STAR Collaboration), J. Phys. G **34**, 451 (2007).

**Measurement of angular distributions of Drell-Yan dimuons in $p + d$ interaction at 800 GeV/c**, L.Y. Zhu, J.C. Peng, P.E. Reimer, T.C. Awes, M.L. Brooks, C.N. Brown, J.D. Bush, T.A. Carey, T.H. Chang, W.E. Cooper, C.A. Gagliardi, G.T. Garvey, D.F. Gesaman, E.A. Hawker, X.C. He, L.D. Isenhower, D.M. Kaplan, S.B. Kaufman, S.A. Kinksiek, D.D. Koetke, D.M. Lee, W.M. Lee, M.J. Leitch, N. Makins, P.L McGaughey, J.M. Moss, B.A. Mueller, P.M. Nord, V. Papavassiliou, B.K. Park, G. Petit, M.E. Salder, W.E. Sondheim, P.W. Stankus, T.N. Thompson, R.S. Towell, R.E. Tribble, M.A. Vasiliev, J.C. Webb, J.L. Willis, D.K. Wise, G.R. Young, Phys. Rev. Lett. **99**, 082301 (2007).

**Two-particle correlations on transverse momentum and momentum dissipation in Au-Au collisions at at $\sqrt{s_{NN}}$ = 130 GeV**, J. Adams *et al.* (STAR Collaboration), J. Phys. G **34**, 799 (2007).

**Strange particle production in p+p collisions at $\sqrt{s_{NN}}$ = 200 GeV**, B.I. Abelev *et al.* (STAR Collaboration), Phys. Rev. C **75**, 064901 (2007).

**Scaling properties of hyperon production in Au+Au collisions at $\sqrt{s_{NN}}$ = 200 GeV**, J. Adams *et al.* (STAR Collaboration), Phys. Rev. Lett. **98**, 062301 (2007).

# SECTION VII

# APPENDIX

*Introductory Remarks at the Long Range Plan Working Group Meeting*, **R.E. Tribble**, Galveston, Texas (April, 2007).

*Tokyo Meeting Report: New Initiatives*, **R.E. Tribble**, **Invited Talk**, OECD Meeting, Tokyo, Japan (May, 2007).

*Report to IUPAP WG9: NSAC Long Range Plan and the RIB Task Force,* **R.E. Tribble**, **Invited Talk**, IUPAP Meeting, Tokyo, Japan (May, 2007).

*Radioactive Beams for Nuclear Spectroscopy and Nuclear Astrophysics*, **R.E. Tribble**, **Invited Talk**, Direct Reaction with Exotic Beams, Tokyo, Japan (May, 2007).

*A Facility for Rare Isotope Beams in the U.S.*, **R.E. Tribble**, **Invited Talk**, International Nuclear Physics Conference, Tokyo, Japan (June, 2007).

*A New Long Range Plan for Nuclear Science*, **R.E. Tribble**, **Invited Talk**, Carpathian Summer School, Sinia, Romania (August, 2007).

*Nuclear Science and U.S. Education*, **R.E. Tribble**, **Invited Talk**, Carpathian Summer School, Sinia, Romania (August, 2007).

*Indirect Methods in Nuclear Astrophysics: Asymptotic Normalization Coefficients*, **R.E. Tribble**, **Invited Talk**, Fourth European Summer School on Experimental Nuclear Astrophysics, Catania, Italy (September, 2007).

*Latest Results on Muon Decay from the TWIST Collaboration*, **R.E. Tribble**, **Invited Talk**, 2007 APS Division of Nuclear Physics Annual Meeting, Newport New, Virginia (October 2007).

*Report to NuPECC on NSAC Activities*, **R.E. Tribble**, NuPECC Meeting, Bucharest, Romania (October, 2007).

*Electron-Ion Collider and the NSAC Long Range Plan*, **R.E. Tribble**, **Invited Talk**, EIC workshop, Stony Brook University, Stony Brook, New York (December, 2007).

*pp Collisions at RHIC*, **C.A. Gagliardi**, **Invited Talk**, Carpathian Summer School, Sinia, Romania (August, 2007).

*Hard QCD in pp Collisions at RHIC*, **C.A. Gagliardi**, **Invited Talk**, International Workshop Hard QCD with Antiprotons at GSI FAIR, Trento, Italy (July, 2007).

*Phases of QCD Matter*, **C.A. Gagliardi**, **Invited Talk**, 2007 Jefferson Lab Users Group Meeting, Newport News, Virginia (June, 2007).

*Cross Sections for Reactions in Explosive H-burning from Reactions at 10 MeV/u*, **L. Trache**, T. Al-Abdullah, A. Banu, C. Fu, C.A. Gagliardi, A.M. Mukhamedzhanov, G. Tabacaru, R.E. Tribble, Y. Zhai, F. Carstoiu, V. Burjan, **Invited Talk**, Minisymposium on Transfer reactions in Nuclear Astrophysics, APS April meeting, Jacksonville, Florida (April 2007).

*Reaction Rates for H-burning in Stars*, **L. Trache, Invited Talk**, "Horia Hulubei" Institute for Physics and Nuclear Engineering, Bucharest-Magurele, Romania, (June 2007).

*Reaction Rates for H-burning in Stars from Experiments with Radioactive Nuclear Beam*, **L. Trache**, **Invited Lecture**, The 22$^{nd}$ Carpathian Summer School in Physics, Sinaia, Romania (August 2007).

*Technique and Study of Beta-Delayed p-Decay of Proton-Rich Nuclei*. **L. Trache**, T. Al-Abdullah, A Banu, C. Fu, V. Golovko, J.C. Hardy, V.E. Iacob, H.I. Park, G.Tabacaru, R.E. Tribble, Y. Zhai, J. Aysto, A. Saastamoinen, P.J. Wood, T. Davidson, M.A. Bentley and J.D. Jenkins, 2007 APS Division of Nuclear Physics Annual Meeting, Newport New, Virginia (October 2007).

*Breakup of Radioactive Nuclear Beams at Intermediate Energies as Indirect Method for Nuclear Astrophysics*, **L. Trache,** F. Carstoiu, C.A. Gagliardi, R.E. Tribble, A. Banu, 10$^{th}$ International Symposium on Origin of Matter and Evolution of Galaxies ( OMEG07), Sapporo, Japan (December 2007).

*Beta-Delayed proton-Decay for Nuclear Astrophysics*, **L. Trache**, EURISOL User Group Workshop, Florence, Italy (January 2008).

*Astrophysical S-factor of the $^{12}N(p,\gamma)^{13}O$ Reaction Determined from the $(^{12}N,^{13}O)$ Proton Transfer Reaction*, **A. Banu**, The 22$^{nd}$ Carpathian Summer School in Physics, Sinaia, Romania (August 2007).

*Alchemy of the Universe: Nucleosynthesis of Chemical Elements*, **A. Banu**, Saturday Morning Physics at Texas A&M University, College Station, Texas (February 2008).

*Determination of the Astrophysical S-factor for the $^{12}N(p,\gamma)^{13}O$ Reaction from $(^{12}N,^{13}O)$ Proton Transfer*, **A. Banu**, 2007 APS Division of Nuclear Physics Annual Meeting, Newport New, Virginia (October 2007).

*Performance Evaluation of Novel Square-Bordered Position-Sensitive Silicon Detectors with Four-Corner Readout*, **A. Banu**, 2007 APS Division of Nuclear Physics Annual Meeting, Newport New, Virginia (October 2007).

*Interaction of Low Energy Radioactive Beams with Helium and Hydrogen. Research Goals and Experimental Approaches*, **V.Z. Goldberg**, **Invited Talk,** 6$^{th}$ International Conference on Nuclear and Radiation Physics, Almaty, Kazakhstan (June 2007).

*Some Unsolved Problems in the Structure of the Light Exotic Nuclei*, **V.Z. Goldberg**, **Invited Talk**, 57$^{th}$ International Conference on Problems on Nuclear Spectroscopy and Nuclear Structure, Voronezh, Russia (June 2007).

*Compound Nuclear Reactions Induced by Radioactive Beams*, **V.Z. Goldberg**, International Conference on Compound Nuclear Reactions (CNR2007), Tenaya Lodge, California (October 2007).

*The Nearest Goals in the Studies of Exotic Nuclei by the Resonance Scattering*, **V.Z. Goldberg**, **Invited Seminar**, Joint Institute for Nuclear Research, Dubna, Russia (June 2007).

*Resonance Reactions Induced by Radioactive Beams: Studies of Exotic Nuclei and Applications to Nuclear Astrophysics*, **V.Z. Goldberg**, **Invited Seminar**, CENPA, University of Washington, Seattle, Washington (October 2007).

*Superallowed Nuclear Beta Decay: Recent Results and Their Impact on $V_{ud}$*, **J.C. Hardy**, **Invited Talk**, Fundamental Neutron Physics Program (INT-07-1), Institute for Nuclear Theory, University of Washington, Seattle, Washington (March 2007).

*Superallowed Nuclear Beta Decay: Testing CVC and CKM Unitarity,* **J.C. Hardy**, **Invited Talk**, The International Workshop on "Fundamental Symmetries: From Nuclei and Neutrinos to the Universe," European Center for Theoretical Studies in Nuclear Physics and Related Areas (ECT*), Trento, Italy (June 2007).

*Superallowed Nuclear Beta Decay: A Window on the Weak Interaction*, **J.C. Hardy**, **Invited Talk**, Carpathian Summer School of Physics 2007, Exotic Nuclei and Nuclear/Particle Astrophysics, Sinaia, Romania (August 2007).

*Precise Tests of Internal-Conversion Theory*, **J.C. Hardy**, **Invited Talk,** 16th International Conference on Radionuclide Metrology and its Applications, Cape Town, South Africa (September 2007).

*Superallowed Nuclear Beta Decay: Recent Results and Their Impact on $V_{ud}$*, **J.C. Hardy**, **Invited Talk,** Fourth Argonne/INT/MSU/JINA RIA Theory Workshop on Rare Isotopes and Fundamental Symmetries, Institute for Nuclear Theory, University of Washington, Seattle, Washington (September 2007).

*New Calculations of the Isospin-Symmetry-Breaking Correction to Superallowed Beta Decay*, **I.S. Towner**, **Invited Talk**, Fourth Argonne/INT/MSU/JINA RIA Theory Workshop on Rare Isotopes and Fundamental Symmetries, Institute for Nuclear Theory, University of Washington, Seattle, Washington (September 2007).

*Overview of Precision Internal Conversion Measurements as Tests of Internal Conversion Theory*, **N. Nica**, **Invited Talk,** 17th Meeting of the International Network of Nuclear Structure and Decay Data Evaluators (NSDD), Saint Petersburg, Russia (June 2007).

*How Idiosyncratic is the Weak Force?* **J.C. Hardy**, Lecture to REU students, Cyclotron Institute, Texas A&M University, College Station, Texas (July 2007).

*The Weak Force: Dancing to Its Own Tune*, **J.C. Hardy**, Popular Lecture at Saturday Morning Physics at Texas A&M University, College Station, Texas (January 2008).

*Mass-Chain Evaluation for ENSDF*, **N. Nica**, Brookhaven National Laboratory, Upton, New York (April 2007).

*Evaluated Nuclear Structure Data File*, **N. Nica**, Brookhaven National Laboratory, Upton, New York (April 2007).

*Precise Branching Ratios from $\beta$-$\gamma$ Coincidences: The Case of $^{34}Ar$*, **V.E. Iacob**, J.C. Hardy and V.V. Golovko, APS Meeting, Jacksonville, Florida (April 2007).

*Use of the GEANT4 Code in Precise Measurements of $\beta^{+}$-Branching-Ratios*, **V.V. Golovko**, V.E. Iacob and J.C. Hardy, APS Meeting, Jacksonville, Florida (April 2007).

*The Structure of $^{23}$Al and Consequences on the Depletion of $^{22}$Na from O-Ne Novae*, **Y. Zhai**, L. Trache, V.E. Iacob, J.C. Hardy, C. Fu, T. Al-Abdullah, N. Nica, M. McCleskey, V.V. Golovko, H.I. Park, G. Tabacaru, A. Banu, R.E. Tribble, APS Meeting, Jacksonville, Florida (April 2007).

*Comparison of Various Monte Carlo Codes for Response Function Studies of a Plastic β-Detector Used in Precise β$^+$-Branching-Ratios Experiments*, **V.V. Golovko**, V.E. Iacob and J.C. Hardy, 2007 APS Division of Nuclear Physics Annual Meeting, Newport News, Virginia (October 2007).

*Precision Measurement of $^{23}$Al Beta-Decay*, **Y. Zhai**, V.E. Iacob, J.C. Hardy, T. Al-Abdullah, A. Banu, C. Fu, V.V. Golovko, M. McCleskey, N. Nica, H.I. Park, G. Tabacaru, R.E. Tribble and L. Trache, 2007 APS Division of Nuclear Physics Annual Meeting, Newport News, Virginia (October 2007).

*Confirmation of Precise Branching-Ratio Measurement in the β Decay of $^{34}$Ar*, **V.E. Iacob**, J.C. Hardy and V.V. Golovko, 2007 APS Division of Nuclear Physics Annual Meeting, Newport News, Virginia (October 2007).

*Test of Internal-Conversion Theory with Precise γ- and x-Ray Spectroscopy*, **N. Nica**, J.C. Hardy, C. Balonek, V.E. Iacob, J. Goodwin, H.I. Park, W.E. Rockwell and M.B. Trzhaskovskaya, 2007 APS Division of Nuclear Physics Annual Meeting, Newport News, Virginia (October 2007).

*Recent Precision ICC Measurements at TAMU*, **N. Nica**, US Nuclear Data Program Meeting (USNDP), Brookhaven National Laboratory, Upton, New York (November 2007).

*ENSDF Evaluation at Texas A&M University*, **N. Nica**, US Nuclear Data Program Meeting (USNDP), Brookhaven National Laboratory, Upton, New York (November 2007).

*Hard Probes at RHIC*, **Saskia Mioduszewski**, **Invited Talk**, The Winter Workshop on Nuclear Dynamics, South Padre Island, Texas (April 2008).

*Hard Probes and Heavy Flavor from STAR*, **Saskia Mioduszewski** (for the STAR Collaboration), **Invited talk**, The Recontres de Moriond: QCD and High-Energy Interactions, La Thuile, Italy (March 2008).

*Photon-Jet Correlations at RHIC*, **Saskia Mioduszewski**, **Invited Talk**, The High-$p_T$ Workshop at RHIC-AGS Users' Meeting, Brookhaven National Laboratory, Upton, New York (June 2007).

*Photon-Jet Correlations at RHIC*, **Saskia Mioduszewski**, **Invited Talk**, Conference on Early Time Dynamics in Heavy Ion Collisions, Montreal, Canada (July 2007).

*Overview of RHIC with a Look to the Future*, **Saskia Mioduszewski**, **Invited Lecture**, The Carpathian Summer School of Physics, Sinaia, Romania (August 2007).

*Using the Calorimeter Pre-Shower Detector in STAR*, **Rory Clarke** (for the STAR collaboration), 2007 APS Division of Nuclear Physics Annual Meeting, Newport News, Virginia (October 2007).

*Probing the Medium with Photons*, **Ahmed Hamed** (for the STAR Collaboration), School of Collective Dynamics in High-Energy Collisions, Berkeley, California (May, 2007).

*Probing the Medium with -Jet Correlation Measurements in STAR*, **Ahmed Hamed** (for the STAR Collaboration), 20th International Conference on Ultrarelativistic Nucleus-Nucleus Collisions (Quark Matter 2008), Jaipur, India (February 2008).

*Gamma-Jet Analysis in $\sqrt{s_{NN}}$ = 200 GeV Au + Au Collisions with the Solenoidal Tracker at the Relativistic Heavy Ion Collider (STAR)*, **Martin Codrington**, The Industry-University Cooperative Chemistry Program (IUCCP), Texas A&M University, College Station, Texas (October, 2007).

*Gamma-Jet Analysis in $\sqrt{s_{NN}}$ = 200 GeV Au + Au Collisions with the Solenoidal Tracker at the Relativistic Heavy Ion Collider (STAR)*, **Martin Codrington** (for the STAR Collaboration), 2007 APS Division of Nuclear Physics Annual Meeting, Newport News, Virginia (October 2007).

*Probing the Matter Created at the Relativistic Heavy Ion Collider (RHIC)*, **Martin Codrington**, **Invited Semina,** Florida Memorial University, College of Natural Science, Miami Gardens, Florida (April, 2007).

*Electron Identification at STAR and the Barrel Pre-Shower Detector*, **Matthew Cervantes** (for the STAR Collaboration), 2007 APS Division of Nuclear Physics Annual Meeting, Newport News, Virginia (October 2007).

*Electron Identification at STAR and the Barrel Pre-Shower Detector*, **Matthew Cervantes** (for the STAR Collaboration), Joint Texas Meeting of the APS, Texas A&M University, College Station, Texas (October, 2007).

*Nuclear Symmetry Energies at Low Density*, **J.B. Natowitz**, **Invited Talk**, Department of Physics, University of Padova, Padova, Italy (May 2007).

*Nuclear Collisions, Metastable Nuclei and the Nuclear Equation of State*, **J.B. Natowitz**, **Invited Talk**, Workshop on f7/2 to the Quark Gluon Plasma, Legnaro National Laboratory, Italy (May 2007).

*Agitated Nuclei and the Nuclear Equation of State*, **J.B. Natowitz**, **Invited Talk**, Symposium Celebrating the 50th Anniversary of the Flerov Laboratory of Nuclear Reactions, Dubna, Russia (May 2007).

*Heavy Ion Reactions: Metastable Nuclei and the Nuclear Equation of State*, **J.B. Natowitz**, **Invited Talk**, Department of Physics, Texas A&M university – Commerce, Commerce, Texas (February 2008).

*Probing Very Low Density Nuclear Matter in Heavy Ion Collisions*, **J.B. Natowitz**, **Invited Talk**, ACS National Meeting, New Orleans, Louisiana (April 2008).

*Produced Proton and Anti-proton in p+p Collisions at 62 and 200 GeV*, **K. Hagel**, 2007 APS Division of Nuclear Physics Annual Meeting, Newport New, Virginia (October 2007).

*Investigating the Nuclear Equation of State through N/Z Equilibration,* **S.J. Yennello**, **Invited Talk**, VII Latin American Symposium on Nuclear Physics and Applications, Cusco, Peru (June 2007).

*Neutron-Rich Rare Isotope Production in the Fermi Energy Domain and Application to the Texas A&M Radioactive Beam Upgrade*, **G.A. Souliotis**, International Conference on Electromagnetic Isotope Separators and Techniques Related to their Applications (EMIS-2007), Deauville, France (June 2007).

*Large Acceptance Spectrograph Design and Deep-Inelastic Scattering,* **G.A. Souliotis, Invited Talk**, S3 (Super-Separator-Spectrometer) Collaboration Meeting, GANIL, Caen, France (July 2007).

*Study of Projectile Multi-Fragmentation in $^{24}Mg + ^{112,124}Sn$ Reactions at 32 MeV/A,* **S. Galanopoulos,** 6th Summer School on Exotic Beam Physics, East Lansing, Michigan (August 2007).

*Using Light Cluster Production to Probe the Density Dependence of Nuclear Symmetry Energy,* **S.N. Soisson,** 6th Summer School on Exotic Beam Physics, East Lansing, Michigan (August 2007).

*Fragment Emission in Projectile Fragmentation Reactions,* **B.C. Stein,** 6th Summer School on Exotic Beam Physics, East Lansing, Michigan (August 2007).

*Density Dependence of the Symmetry Energy and the Nuclear Equation of State,* **S.J. Yennello, Invited Talk,** 234th ACS National meeting, Boston, Massachusetts (August 2007).

*Heavy Residue Studies below the Fermi Energy and the Role of the Nuclear Symmetry Energy,* **G.A. Souliotis, Invited Talk,** 234th ACS National meeting, Boston, Massachusetts (August 2007).

*Heavy Residue Studies near the Fermi Energy and the role of the Nuclear Symmetry Energy,* **G.A. Souliotis, Invited Talk,** International Conference on Nuclear Fragmentation (NUFRA2007), Kemer (Antalya), Turkey (September 2007).

*Insights into the Density Dependence of the Symmetry Energy through Nuclear Reactions,* **S.J. Yennello, Invited Talk,** International Conference on Nuclear Fragmentation (NUFRA2007), Kemer (Antalya), Turkey (September 2007).

*Constraining the Density Dependence of the Symmetry Energy and the Nuclear Equation of State: A Dynamical and Statistical Model Approach,* **D.V. Shetty,** 2007 APS Division of Nuclear Physics Annual Meeting, Newport New, Virginia (October 2007).

*Nucleon Transfer Calculations Using the HIPSE Model,* **Z. Kohley,** 2007 APS Division of Nuclear Physics Annual Meeting, Newport New, Virginia (October 2007).

*Microscopic Calculations of Heavy-Residue Formation in Quasielastic and Deep-Inelastic Collisions below the Fermi Energy,* **G.A. Souliotis,** 2007 APS Division of Nuclear Physics Annual Meeting, Newport New, Virginia (October 2007).

*N/Z Equilibration in Deep Inelastic Collisions and the Fragmentation of the Resulting Quasiprojectiles,* **A.L. Keksis,** 2007 APS Division of Nuclear Physics Annual Meeting, Newport New, Virginia (October 2007).

*NIMROD Upgrade,* **S. Wuenschel,** 2007 APS Division of Nuclear Physics Annual Meeting, Newport New, Virginia (October 2007).

*Dual-Axis, Duo-Lateral Position Sensitive Detector,* **R. Dienhoffer,** 2007 APS Division of Nuclear Physics Annual Meeting, Newport New, Virginia (October 2007).

*A Dual-Axis, Duo-Lateral Position Sensitive Detector Upgrade to the FAUST Detector Array,* **S. Soisson,** Joint Texas Meeting of APS, SPS, NHSP,AAPT, NSBP and FIAP, Texas A&M University, College Station, Texas (October 2007).

*Nuclear Reactions: Exploring Phase Transitions in Nuclear Material,* **S.J. Yennello**, Arkansas Tech University, Russellville, Arkansas (October 2007)

*Novel Approaches in Rare Isotope Production and Nuclear Reaction Dynamics,* **G.A. Souliotis,** Department of Chemistry, Texas A&M University, College Station, Texas (February 2008).

*The Nuclear Matter Equation of State and Properties of Finite Nuclei*, **Shalom Shlomo**, Vuong Kim Au, and Tapes Sil, **Invited Talk**, International Nuclear Physics conference – INPC2007, Tokyo, Japan (June 2007).

*Bulk Properties of Nuclear Matter from Excitation of Nuclei*, **Shalom Shlomo**, **Invited Talk**, Seventh Latin American Symposium on Nuclear Physics and Applications Conference, Cusco, Peru (June 2007).

*Hartree-Fock Based Random Phase Approximation Description of Giant Resonances and the Nuclear Equation of State,* **Shalom Shlomo**, **Invited Talk**, Carpathian Summer School of Physics – 2007 (CSSP07), Sinaia, Romania (August 2007).

*Properties of Nuclear Matter from Excitations of Nuclei*, **S. Shlomo**, **Invited Talk**, Ben-Gurion University, Beer Sheva, Israel (September 2007).

*The Incompressibility Coefficient in the Non-Relativistic and Relativistic Models,* **V. Kim Au**, The International Symposium on Physics of Unstable Nuclei, Hoian, Vietnam (July 2007).

*The New Skyrme Type Effective Nucleon-Nucleon Interaction,* **V. Kim Au**, Nishina Center, RIKEN, Japan (September 2007).

*Indirect Techniques in Nuclear Astrophysics*, **A.M. Mukhamedzhanov**, INPC 2007, Tokyo, Japan (June 2007).

*Trojan Horse as Indirect Technique in Nuclear Astrophysics*, **A.M. Mukhamedzhanov**, **Invited Lecture**, The 4th European School in "Experimental methods in Nuclear Astrophysics", Santa Tecla, Sicily, Italy (September 2007).

*Elastic Scattering and Stripping Processes of $^{12}C$ as a Three-body Problem*, **A.M. Mukhamedzhanov**, **Invited Talk**, University of Surrey, Guildford, United Kingdom (October 2007).

*Benchmark of Neutron Direct Capture Reactions Extracted from (d,p) Reactions*, **A.M. Mukhamedzhanov**, **Invited Talk**, NNSA Symposium, Washington DC (January 2008).

*Predictions of the AMPT Model for LHC*, **C.M. Ko**, **Invited Talk**, International Workshop on Predictions for Heavy Ion Collisions at LHC, CERN, Geneva, Switzerland (May 2007).

*Jet Conversions in QGP*, **C.M. Ko**, **Invited Talk**, 7th International Workshop on Particle Physics Phenomenology, Taipei, Taiwan (June 2007).

*Jet Conversions in QGP*, **C.M. Ko**, **Invited Talk**, 10th International Workshop on Relativistic Nuclear Physics from Hundreds MeV to TeV, Kiev, Ukrain (June 2007).

*Partonic Effects in Heavy Ion Collisions at FAIR*, **C.M. Ko**, **Invited Talk**, 4th International Workshop on Critical Point and the Onset of Deconfinement, Darmstadt, Germany (July 2007).

*Jet Conversions in QGP*, **C.M. Ko**, **Invited Talk**, International Conference on Early Time Dynamics in Heavy Ion Collisions, Montreal, Canada (July 2007).

*Recent Results from the AMPT Model*, **C.M. Ko**, **Invited Talk**, International Workshop on Particle Correlations and Fluctuations, Sonona, California (August 2007).

*Thermal Charm Production at LHC*, **C.M. Ko**, **Invited Talk**, International Symposium on Multiparticle Dynamics, Berkeley, California (August 2007).

*Charm Production in Relativistic Heavy Ion Collisions*, **C.M. Ko**, **Invited Talk**, Asian Pacific Center for Theoretical Physics Focus Program on Hadronic Physics at RHIC, Seoul, Korea (December 2007).

*Hyperon Spectrum in the Skyrme Model*, **Y. Oh**, Asian Pacific Center for Theoretical Physics Focus Program on Hadronic Physics at RHIC, Seoul, Korea (December 2007).

*Nucleon Resonances in KS(1385) Photoproduction*, **Y. Oh**, Asian Pacific Center for Theoretical Physics Focus Program on Hadronic Physics at RHIC, Seoul, Korea (December 2007).

*Charm Deuteron Elliptic Flow in Relativistic Heavy Ion Collisions*, **Y. Oh**, Asian Pacific Center for Theoretical Physics Focus Program on Hadronic Physics at RHIC, Seoul, Korea (December 2007).

*Heavy-Quark Diffusion in Heavy-Ion Collisions*, **R. Rapp**, **Invited Talk**, International Conference on Early Time Dynamics in  Heavy Ion Collisions, Montreal, Canada (July 2007).

*Phase Transitions with Subnucleonic Degrees of Freedom*, **R. Rapp**, **Invited Lecture**, Carpathian Summer School of Physics – 2007 (CSSP07), Sinaia, Romania (August 2007).

*Phenomenology Quarkonium Correlators in Medium*, **R. Rapp**, **Invited Talk**, Quarkonium Working Group Workshop (QWG07), DESY, Hamburg, Germany (October 2007).

*Thermal Dileptons at LHC*, **H. van Hees**, International Workshop on "Heavy-Ion Collisions at the LHC: Last Call for Predictions", CERN, Geneva, Switzerland (May 2007).

*Heavy-Quark Kinetics in the QGP at LHC*, **H. van Hees**, International Workshop on "Heavy-Ion Collisions at the LHC: Last Call for Predictions", CERN, Geneva, Switzerland (May 2007).

*Heavy Quarks and Vector Mesons in Medium*, **R. Rapp**, **Invited Lecture**, School of Collective Dynamics in High-Energy Collisions in Honor of Prof. G. E. Brown on "Medium Properties, Chiral Symmetry and Astrophysical Phenomena", Lawrence Berkeley National Laboratory, Berkeley, California (May 2007).

*An Improved Coalescence Formalism Based on a Transport Equation*, **L. Ravagli**, School of Collective Dynamics in High-Energy Collisions in Honor of Prof. G. E. Brown on "Medium Properties, Chiral Symmetry and Astrophysical Phenomena", Lawrence Berkeley National Laboratory, Berkeley, California (May 2007).

*Electromagnetic Spectra at CERN SPS and the QCD Phase Diagram*, **H. van Hees**, **Invited Talk**, ECT* Workshop on "Electromagnetic Probes of Strongly Interacting Matter: The Quest for Medium Modification of Hadrons", Trento, Italy (June 2007).

*Omega and Phi Mesons in Hot/Dense Matter: Nuclear Production Reactions and Heavy-Ion Collisions*, **D. Cabrera**, **Invited Talk**, ECT* Workshop on "Electromagnetic Probes of Strongly Interacting Matter: The Quest for Medium Modification of Hadrons", Trento, Italy (June 2007).

*Transverse Momentum Dependence of J/psi in Heavy-Ion Collisions*, **X. Zhao**, 2007 APS Division of Nuclear Physics Annual Meeting, Newport New, Virginia (October 2007).

*Heavy-Quark Diffusion in the Quark-Gluon Plasma*, **H. van Hees**, Joint Texas Meeting of APS, SPS, NHSP,AAPT, NSBP and FIAP, Texas A&M University, College Station, Texas (October 2007).

*Transverse Momentum Dependence of J/psi in Heavy-Ion Collisions*, **X. Zhao**, Joint Texas Meeting of APS, SPS, NHSP,AAPT, NSBP and FIAP, Texas A&M University, College Station, Texas (October 2007).

*Heavy Quarks in sQGP and Observables at RHIC and LHC*, **R. Rapp**, **Invited Talk**, International Heavy Quark Workshop, Lawrence Berkeley National Laboratory, Berkeley, California (November 2007).

*Dilepton Production at SPS Energies*, **H. van Hees**, **Invited Talk**, CERN- Theory Workshop on " Electromagnetic Radiation in Nuclear Collisions", Geneva, Switzerland (December 2007).

*In-Medium Vector Mesons from Hadronic Many-Body Theory*, **R. Rapp, Invited Talk**, CERN- Theory Workshop on " Electromagnetic Radiation in Nuclear Collisions", Geneva, Switzerland (December 2007).

*Theoretical Review of Dileptons from Heavy-Ion Collisions,* **H. van Hees**, **Invited Plenary Talk**, 20th International Conference on Ultrarelativistic Nucleus-Nucleus Collisions (Quark Matter 2008), Jaipur, India (February 2008).

*Heavy-Quark Diffusion in the sQGP*, **H. van Hees**, **Invited Talk**, International Workshop on "Hot and Dense Matter in the RHIC-LHC Era", Tata Institute of Fundamental Research, Mumbai, India (February 2008).

*Initial Energy Density, Momentum and Flow in Heavy Ion Collisions*, **R.J. Fries**, CERN, Geneva, Switzarland (May 2007).

*Photons and Dileptons at LHC*, **R.J. Fries**, Workshop on Heavy Ion Collisions at the LHC: Last Call for Predictions, CERN, Heneva, Switzerland (May 2007).

*Quark and Gluon Degrees of Freedom in High-Energy Heavy Ion Collisions*, **R.J. Fries**, **Invited Plenary Talk**, International Nuclear Physics Conference (INPC 2007), Tokyo, Japan (June 2007).

*Early Time Evolution of High Energy Nuclear Collisions*, **R.J. Fries**, **Invited Talk**, Workshop on Early Time Dynamics in Heavy Ion Collisions, McGill University, Montreal, Canada (July 2007).

*Initial Energy Density and Flow in Heavy Ion Collisions from Classical Gluon Fields*, **R.J. Fries**, RIKEN and Brookhaven Nuclear Theory Group, Brookhaven National Laboratory, Upton, New York (September 2007).

# RESEARCH PERSONNEL AND ENGINEERING STAFF

April 1, 2007 - March 31, 2008

## Faculty and Research Group Leaders

Rainer Fries, Assist. Prof. of Physics
Carl A. Gagliardi, Professor of Physics
John C. Hardy, Professor of Physics
Che Ming Ko, Professor of Physics
Dan Melconian, Assist. Prof. of Physics – From
           11/1/07
Saskia Mioduszewski, Assist. Prof. of Physics
J. B. Natowitz, Professor of Chemistry, Bright Chair
Ralf Rapp Associate Prof. of Physics
Shalom Shlomo, Senior Scientist
Robert E. Tribble, Professor of Physics, Director
Rand L. Watson, Professor of Chemistry
Sherry J. Yennello, Professor of Chemistry
Dave H. Youngblood, Professor of Physics
Akram M. Zhanov, Senior Scientist

## Research Staff

Henry Clark, Accelerator Physicist (50%)
Grigor Chubaryan, Research Scientist
John C. Hagel, Research Scientist (50%)
Vladimir Horvat, Research Scientist (50%)
Victor Iacob, Associate Research Scientist
Yiu-Wing Lui, Research Scientist
Ninel Nica, Assist. Research Scientist
George Souliotis, Associate Research Scientist
Livius Trache, Research Scientist
Ryoichi Wada, Research Scientist

## Visiting Scientists

Aldo Bonasara – From 6/25/07 To 9/18/07
Daniel Cabrera-Urban – To 10/31/07
Vladilen Goldberg
Ian Towner – From 6/20/07 To 8/22/07

## Accelerator Physics and Radiation Line Staff

Juha Arje, Research Scientist
Joseph Brinkley, Research Associate – From
           12/1/07
Henry Clark, Accelerator Physicist (50%)
Vladimir Horvat, Research Scientist (50%)
Bruce Hyman, Research Associate

George Kim, Accelerator Physicist
Don May, Accelerator Physicist
Gabriel Tabacaru, Accelerator Physicist

## Computer Systems Staff

Robert Burch, Jr., Systems Analyst/Sr.
    Microcomputer/LAN Administrator
John C. Hagel, Research Scientist (50%)

## Engineering Staff

Greg Derrig, Senior Mechanical Engineer
Robert Olsen, Senior Mechanical Engineer

## Postdoctoral Research Associates

Adriana Banu
Zhiqiang Chen
Rory Clarke
Changbo Fu – From 7/21/07 To 10/15/07
Stratos Galanopoulous
Victor Golovko
Ahmed Hamed
Krishichayan – From 10/19/07
Wei Liu
Yong S. Oh
Yong Peng – To 2/1/08
Lorenzo Ravagli – To 12/31/07
Prakash Sahu – To 12/31/07
Murad G. Sarsour
Dinesh Shetty
Hendrik van Hees
Au Kim Vuong
Yongjun Zhai – From 12/16/07
Benwei Zhang – To 1/31/08

**STUDENTS**

April 1, 2007 - March 31, 2008

**Graduate Students**

Tariq Al-Abdullah – To 6/30/07
Jonathan Button – From 9/1/07
Matthew Cervantes
Xinfeng Chen
Martin Codrington
James Drachenberg
Changbo Fu – To 7/21/07
David Carson Fuls – From 6/1/07
John Goodwin
Ting He – From 6/1/07 To 8/31/07
Liaoyuan Huo – From 1/16/08
August Keksis – To 5/3/07
Zach Kohley
Yun Li – To 8/10/07
Matthew McCleskey
Hyo-In Park
Li Jun Qin
Ellen Simmons – From 5/31/07
Sarah Soisson
Alexandria Spiridon – From 1/16/08
Brian Stein
Trent Strong – From 9/1/07
Sara Wuenschel
Yongjun Zhai – To 12/16/07
Xingbo Zhao

**Undergraduates and Student Technicians**

Giacomo Bonasera – From 7/20/07 To 8/31/07
Hannah Childress – From 10/8/07
Alfredo J. Echeverria
Vedia Ebru Gonulal – From 7/11/07 To
                                    10/31/07
Anthony Grupp – From 8/27/07
Katie Huseman
Joshua Kammer – To 7/18/07
Jennifer Jeffress – To 12/21/07
Toby Martin
Larry May – To 8/31/07
Thomas Merket – From 11/4/07
John Murray – From 6/27/07 To 8/31/07
Ashley Noack – From 1/10/08
Kara Peek – From 8/27/07
Robert Polis
Wade Ben Smith – From 9/27/07
Derek Wilson – To 9/17/07
Shauna Yow – To 9/6/07

# ORGANIZATIONAL CHART - CYCLOTRON INSTITUTE

**DIRECTOR**
Tribble

**SEE Line**
**Proj. Manager**
H. Clark

Brinkley
Chubaryan
Horvat
Hyman

**Senior ME**
**Derrig**

**Sr.**
**Mechanical**
**Engineer**
Olsen

**Designer II**
Molitor

**Machine Shop**
**Supervisor**
Norris

Bielamowicz
A. Clark
Raines
Whiteley

**Operations Chief**
Abegglen

**Electrical Shop**
Black
Cowden
Eisenmann
Gathings
LaPoint
Malave
Morgan
O'Berski
Peeler
Russell
Sherman
Yendrey
Zajicek

**Building**
**Maint.**
Gallegos
Kingsbury
Mynar
Piolet

**Senior Accelerator**
**Physicist**
May

**Accelerator**
**Physicists**
Kim
H. Clark
G. Tabacaru

**Computer**
**Systems**
Hagel
Burch

**Administration/**
**Accounting**
Jeske

Deason
Hodges
Munsey
Speikes

Research
Group Leaders

Research
Scientists

Research
Associates

Graduate
Students

**STUDENTS WHO RECEIVED GRADUATE DEGREES**
**FROM THESIS WORK CONDUCTED**
**AT**
**THE CYCLOTRON INSTITUTE**

**April 1, 2007 – March 31, 2008**

| Name | Year | Thesis Title | Advisor | First Position | Present Position |
|------|------|-------------|---------|---------------|------------------|
| Jennifer Ann Iglio | 2007 | *Symmetry Energy and the Isoscaling Properties of the Fragments in Multifragmentation of $^{40}Ca + ^{58}Ni$, $^{40}Ar + ^{58}Ni$ and $^{40}Ar + ^{58}Fe$ Reactions* | S. J. Yennello | Graduate Research Assistant | Invensys Process Systems |
| Thomas Henry | 2007 | *Reconstruction and Attributes of Jets Observed in $\sqrt{s} = 200$ GeV Proton-Proton and Deuteron-Gold Collisions* | C. A. Gagliardi | Graduate Research Assistant | |
| Yong Peng | 2007 | *Systematics of Cross Sections for Target K-vacancyProduction in Heavy Ion Collisions* | R. L. Watson | Graduate Research Assistant | Post Doc., M. D. Anderson Hospital, Houston, Texas |
| August Keksis | 2007 | *N/Z Equilibration in Deep Inelastic Collisions and the Fragmentation of the Resulting Quasiprojectiles* | S. J. Yennello | Graduate Research Assistant | Post Doc. , Los Alamos National Laboratory |
| Changbo Fu | 2007 | *One-Proton, Two-Protons and Alpha Emission from $^{14}O+\alpha$ Resonance Interactions* | R. E. Tribble | Graduate Research Assistant | Post Doc., National Institute of Standards and Technology, Gaithersburg, Maryland |
| Tariq Al-Abdullah | 2007 | *Extracting the Asymptotic Normalization Coefficients in Neutron Transfer Reactions to Determine the Reaction Rates of $^{22}Mg(p,\gamma)^{23}Al$ and $^{17}F(p,\gamma)^{18}Ne$* | C. A. Gagliardi | Graduate Research Assistant | Faculty Position at Hashemite University, Jordan |
| Au Kim Vuong | 2007 | *New Skyrme Nucleon-Nucleon Interaction for the Mean-field Approximation* | S. Shlomo | Graduate Research Assistant | Nishina Fellowship at Cyclotron Center, RIKEN, Japan |
| Yongjun Zhai | 2007 | *The Structure of $^{23}Al$ and Astrophysical Consequences* | R. E. Tribble | Graduate Research Assistant | Medical Postdoctoral Fellow, Cancer Therapy & Research Center, University of Texas Health Science Center, San Antonio, Texas |

<u>**2007**</u>

| | | |
|---|---|---|
| April 5 | Dr. Nigel Orr, Laboratoire de Physique Corpusculaire, Universite de Caen Basse-Normandie, France | *Probing Nuclear Structure Far from Stability: from Breakup to Knockout* |
| April 10 | Dr. Lie-wen Chen, Institute of Theoretical Physics, Shanghai Jiao Tong University, Shanghai, China | *Probing the Nuclear Symmetry Energy with Heavy-Ion Reactions Induced by Neutron-Rich Nuclei* |
| April 11 | Dr. Nigel Orr, Laboratoire de Physique Corpusculaire, Universite de Caen Basse-Normandie, France | *Neutron Correlations in the Breakup of Halo Nuclei* |
| April 17 | Dr. Denis Lacroix, LPC-Caen, France/NSCL-MSU, Michigan | *Direct Description of Cluster Formation in Heavy-Ion Collisions Photon Production at RHIC* |
| April 20 | Professor G. Röpke, University of Rostock, FB Physik, Rostock, Germany | *Low-Density Nuclear Matter Equation of State and Symmetry Energy: Cluster Formation and Condensates* |
| April 26 | Professor D. G. Jenkins, Department of Physics, University of York, York, United Kingdom | *New Techniques for Probing Nuclear Shape and Isobaric Symmetry Around* |
| April 27 | Dr. Smarajit Triambak, University of Washington, Seattle, Washington | *Test of Isospin Symmetry Breaking, the Standard Model and Beyond* |
| May 2 | Dr. Abhijit Majumder, Duke University, Durham, North Carolina | *Probing the QGP with Jets and Jet Correlations* |
| May 8 | Professor Michael A. Bentley, University of York, York, United Kingdom | *Coulomb Shifts between Isobaric Analogue State* |
| June 21 | Professor Claudio Dorso, University of Buenos Aires, Buenos Aires, Argentina | *Isoscaling: a General Property of Multicomponent System* |
| June 26 | Dr. Jiansong Wang, Institute of Modern Physics, Lanzhou, China | *The Status of Hadronic Physics at HIRFL-CSR* |
| July 5 | Professor R. K. Choudhury, Nuclear Physics Division, BhaBha Atomic Research Center, Mumbai, India | *The Structure Aspects in Heavy Ion Nuclear Reactions* |

| July 6 | Professor Lee G. Sobotka, Washington University, St. Louis, Missouri | *The Mononuclear Caloric Curve and Other Stories from St. Louis* |
| September 4 | Dr. Gianfranco Prete, Labratori Nazionale di Legnaro, Italy | *The SPES Project at the Laboratori Nazionale di Legnaro* |
| September 25 | Professor N. Auerbach, Tel-Aviv University, Tel-Aviv, Israel | *The Super-Radiant Mechanism: from Nuclei to Quarks* |
| October 23 | Dr. Chiho Nonaka, Nagoya University, Nagoya, Japan | *Bulk QCD Dynamics in Relativistic Heavy Ion Collisions-3D Hydro+Micro Approach at RHIC* |
| November 14 | Professor G. Roepke, University of Rostock, FB Physik, Rostock, Germany | *Abundances of Light Clusters in Asymmetric Nuclear Matter* |
| November 19 | Dr. Aldo Bonasara, INFN Laboratori Nazionali del Sud, Catania, Italy | *The Quantum Nature of a Nuclear Phase Transition* |
| November 26 | Dr. Anna V. Unzkakova, St. Petersburg State University, St. Petersburg, Russia | *Potential-Energy Calculations in Ten-Dimensional Deformation Space* |
| November 26 | Dr. Serban Misicu, Theoretical Physics Division, NIPNE-HH, Bucharest-Magurele, Romania | *Unified Treatment of Clusterization and Cold Fission – a Path to the Understanding of the Heaviest Elements Formation* |
| December 4 | Professor C. R. Praharaj, Institute of Physics, Bhubaneswar, India | *Band Structures and High Spin States in Nuclei* |
| December 11 | Dr. Yu-Gang Ma, Shanghai Institute of Applied Physics, Chinese Academy of Science, Shanghai, China | *Anisotropic Flows of Light Nuclear Clusters and Direct Hard Photons in Intermediate Energy Heavy Ion Collisions* |

## **2008**

| March 4 | Dr. Ron Soltz, Lawrence Livermore National Laboratory, Livermore, Califonia | *Measuring the Size and Thermodynamics of a Quark Drop* |
| March 5 | Mr. Robert Cooper, University of Michigan, Ann Arbor, Michigan | *The Radiative Decay Mode of the Free Neutron* |
| March 6 | Dr. Mihai Horoi, Central Michigan University, Mount Pleasant, Michigan | *Shell Model Spectroscopic Factors and Modern Effective Interaction* |

| March 18 | Professor G. Roepke, University of Rostock, FB Physik, Rostock, Germany | *Cluster Formation and Nuclear Matter Symmetry Energy* |
| March 18 | Dr. Tibor Kibédi, Australian National University, Canberra, Australia | *Conversion Coefficients for Nuclear Structure Research and Beyond* |
| March 20 | Dr. Andrey Shirokov, Moscow State University, Moscow, Russia | *Abinitio Calculations of Light Nuclei with JISP16NN Interaction* |
| March 31 | Professor Bruce R. Barrett, Department of Physics, University of Arizona, Tucson, Arizona | *The Abinitio No Core Shell Model for Nuclear Structure and Reactions* |